DEVELOPMENT AND PRECLINICAL EVALUATION OF A NOVEL AAV VECTOR-BASED GENE THERAPY TO TREAT *RETINITIS PIGMENTOSA* TYPE 45

Johanna Elisabeth Wagner
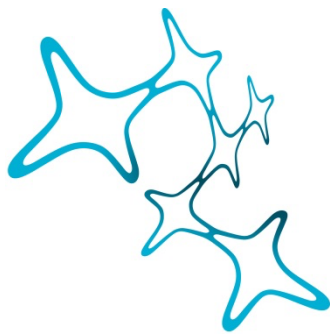
Graduate School of Systemic Neurosciences

LMU Munich

Dissertation at the
Graduate School of Systemic Neurosciences
Ludwig-Maximilians-Universität München

June, 2020

Supervisor

Prof. Dr. Stylianos Michalakis

Department of Ophthalmology

Ludwig-Maximilians-Universität München

First Reviewer:	Prof. Dr. Stylianos Michalakis
Second Reviewer:	Prof. Dr. Martin Biel
External Reviewer:	Prof. Dr. Dirk Grimm

Date of Submission:	26/06/2020
Date of Defense:	03/03/2021

Content

List of Abbreviations

°C	degree Celsius
μ	micro (10^{-6})
μg	microgram
μL	microliter
aa	amino acid
AAP	assembly-activating protein
AAV	adeno-associated virus
Ad	adenovirus
ADA	adenosine deaminase
adRP	autosomal dominant *Retinitis pigmentosa*
AmpR	ampicillin resistance gene
ANOVA	analysis of variance
APC	antigen-presenting cell
arRP	autosomal recessive *Retinitis pigmentosa*
BMSC	bone marrow-derived stem cell
bp	base pair
c	canine
c	centi (10^{-2})
C-	carboxy-
Ca^{2+}	calcium
Cap	capsid gene
CAR	cone arrestin
CB	ChemiBlocker
CBA	chicken β-actin
cd	candela

cDNA	complementary deoxyribonucleic acid
cGMP	cyclic guanosine monophosphate
CMV	immediate-early cytomegalovirus
CNBD	cyclic nucleotide-binding domain
CNG	cyclic nucleotide-gated
Cngb1	cyclic nucleotide-gated channel beta 1 gene
hCNGB1	human cyclic nucleotide-gated channel beta 1 gene
CNGB1	cyclic nucleotide-gated channel beta 1 subunit
CO_2	carbon dioxide
CRISPR	Clustered Regularly Interspaced Short Palindromic Repeat
cSLO	confocal Scanning Laser Ophthalmoscopy
C_t	cycle threshold
Da	Dalton
DMEM	Dulbecco's modified Eagle medium
DNA	deoxyribonucleic acid
dNTP	deoxyribonucleotide triphosphate
ds	double-stranded
E. coli	*Escherichia coli*
EMA	European Medicines Agency
ERG	Electroretinogram, Electroretinography
eGFP	enhanced green fluorescent protein
ESC	embryonic stem cell
EU	endotoxin units
FBS	fetal bovine serum
FDA	Food and Drug Administration
FITC	fluorescein isothiocyanate
g	gram
g	gravitational acceleration

	$1\ g \approx 9.81\ \mathrm{m\ s^{-2}}$
	$1\ g = 1.12\ \mathrm{r\ (rpm\ 1000^{-2})^2}$
GARP	glutamic acid-rich protein
GC	guanylyl cyclase
GCAP1/2	rod-type guanylyl cyclase potential protein 1/2
GCL	ganglion cell layer
G_{t1}	rod-type G-protein transducin
GDP	guanosine diphosphate
GFAP	glial fibrillary acidic protein
GLP	Good Laboratory Practice
GMP	guanosine monophosphate
GMP	Good Manufacturing Practice
GTP	guanosine triphosphate
h	hour
h	human
H_2O	water
HDR	homology directed-repair
HEK293T	human embryonic kidney cell line 293T
hPSC	human pluripotent stem cell
HPV	human papilloma virus
hRHO194	short human rhodopsin promoter (194 bp)
Hz	Hertz
IBA-1	ionized calcium-binding adaptor molecule 1
IHC	immunohistochemistry
ILM	inner limiting membrane
INL	inner nuclear layer
IPL	inner plexiform layer
IPSC	induced pluripotent stem cell

IS	inner segments
ITR	inverted terminal repeat
IV	intravitreal
k	kilo (10^3)
K	kelvin
KanR	kanamycin resistance gene
kb	kilo bases
KO	knockout
L	liter
LB	lysogeny broth medium
LCA	Leber's congenital amaurosis
Lot#	lot number
LPLD	lipoprotein lipase deficiency
LV	lentivirus
m	murine
m	meter
m	milli (10^{-3})
m^2	square meter
min	minute/s
M	molar mass
mRNA	messenger ribonucleic acid
n	nano (10^{-9})
N-	amino-
N°	number
Na^+	sodium
NAb	neutralizing antibody
NCKX1	$Na^{2+}/Ca^{2+}/K^+$-exchanger
NHEJ	non-homologous end-joining

NHP	non-human primates
NRL	neural retina leucine zipper
nt	nucleotide
OD	*oculus dexter*
ON	optic nerve
ONL	outer nuclear layer
OPL	outer plexiform layer
ORF	open reading frame
ori	origin of replication
OS	outer segments
OS	*oculus sinister*
p	pico (10^{-12})
pAd helper	Adenovirus helper plasmid
PB	phosphate buffer
PBS	phosphate buffered saline
PCL	producer cell line
PCR	polymerase chain reaction
PDE6A/B	rod specific cGMP phosphodiesterase A/B
PFA	paraformaldehyde
pH	*Potentia hydrogenii*
pi	*post injection*
pn	*postnatal*
PNA	peanut agglutinin
qPCR	quantitative real-time PCR
rAAV	recombinant AAV
RdCVF	rod-derived cone viability factor
Rep	replication gene
REP	replication protein

Rh	rhodopsin gene
Rho	rhodopsin promoter
RNA	ribonucleic acid
RNAi	ribonucleic acid interference
ROS	rod outer segments
RP	*Retinitis pigmentosa*
RP45	*Retinitis pigmentosa* type 45
RPE	retinal pigment epithelium
RPGR	*Retinitis pigmentosa* GTPase Regulator
rpm	rounds per minute
RT	room temperature
s	second
sc	self-complementary
SD-OCT	Spectral-Domain Optical Coherence Tomography
SEM	standard error of the mean
SR	subretinal injection
ss	single-stranded
SV40	simian virus 40
TBE	Tris-Borate-EDTA
TRIS	tris(hydroxymethyl)aminomethane
TF	transcription factor
TLR	Toll-like receptor
UV	ultraviolet
V	Volt $1\,V = m^2\,kg\,s^{-3}\,A^{-1}$
vg	vector genomes
VP	viral protein

WPRE	woodchuck hepatitis virus posttranscriptional regulatory element
WT	wildtype

List of Tables

List of Figures

Abstract

Loss-of-function mutations in the cyclic nucleotide-gated channel beta 1 subunit (*Cngb1*) gene are known to cause *Retinitis pigmentosa* type 45 (RP45), an incurable retinal disorder characterized by primary functional loss and degeneration of rod photoreceptors, followed by a non-cell autonomous cone death, often resulting in legal blindness. Here, a novel recombinant adeno-associated virus vector for gene supplementation therapy of *Cngb1*-linked RP was developed and tested for its efficacy in two preclinical *Cngb1* knockout (KO) animal models of RP45.

The full-length human *CNGB1* coding sequence was packaged in recombinant AAV5 under the control of a short human rhodopsin promoter, as *CNGB1* is expressed natively in rod photoreceptors. Due to the limited cargo capacity of the AAV, an optimized shortened rhodopsin promoter was designed (*hRHO194*) in order to produce the entire expression cassette in *cis* and to ensure rod-specific expression of hCNGB1. The resulting viral vector (rAAV5.hCNGB1) was produced by triple-transfection in HEK293 cells as well as in HeLa cells as a producer cell line.

For the preclinical validation of the therapy, the efficacy of rAAV5.hCNGB1 was assessed in a *Cngb1* KO mouse model as well as in a *Cngb1* KO dog model. The animals were treated with rAAV5.CNGB1 delivered via subretinal injection to assess transgene expression as well as biological activity. The effect of the treatment was read out with multiple outcome measures. Proper availability, integrity, and localization of the introduced gene product was assessed by immunohistochemistry. Retinal function was examined via ERG measurements and morphological effects on photoreceptor degeneration were monitored *in vivo* by OCT imaging. Behavioral tests were implemented to validate visual function. Additionally, critical aspects including studies on long-term efficacy, biologically active dose range, time window for a therapeutic intervention, as well as on potential toxicities were addressed, to provide further insights on the feasibility and safety of the drug administration.

The study demonstrated efficient, specific, and long-term hCNGB1 expression in murine and canine rod photoreceptors driven by the short *hRHO194* promoter. By treatment with rAAV5.hCNGB1, a substantial preservation of rod and cone photoreceptors was achieved in both *Cngb1* KO mice and dogs. Furthermore, the efficacy of rAAV5.hCNGB1 was dose-dependent manifesting itself as an increasing expression level with ascending dose, resulting in enhanced biological efficacy in both animal models. In addition, a toxic side effect was identified for the vector produced in HeLa cells emerging in a dose-dependent manner, which was not observed for the vector produced in HEK293 cells. It was further shown, that the viral vector-introduced human CNGB1 subunit was capable of forming functional chimeric rod-specific CNG channels together with the endogenous murine or canine CNGA1 subunits

leading to a recovery of rod photoreceptor function as well as markedly improved vision-guided behavior in both animal models. Furthermore, retinal stress in the *Cngb1* KO mouse, manifesting as Müller cell gliosis, was reduced by rAAV5.hCNGB1, even beyond the treated region of the retina. Finally, it was shown that a degeneration-induced inflammation was diminished by the treatment in the *Cngb1* KO dog model, shown as reduced microglia activation, while in one treated dog an increased immune reaction was observed, manifesting as increase activation of microglia within the retina.

These results demonstrated the efficacy of the rAAV5.hCNGB1 gene supplementation therapy in small and large animals and thus showed the transferability of this approach to human application. Thereby, the work covered a major part of the preclinical phase and proved that rAAV5.hCNGB1 is a suitable candidate for a clinical application. The results of this study provided novel insights into the transferability of a gene therapy from mouse to man and will serve as a basis for a design of preclinical toxicology studies and early-phase clinical application of rAAV5.hCNGB1.

1 Introduction

1.1 Gene Therapy

The prospect of curing inherited monogenic disorders by genetic modifications using exogenous DNA currently harbors one of the most challenging tasks in biomedical research, the corresponding product development, and its therapeutic application. In fact, the first strategy on this gene therapy approach was already published in 1972 by Friedman and Roblin (Friedman and Roblin, 1972). The fixation of a mutated gene or the normalization of gene expression with a once-only medication, ideally even curing the disease, has since aroused great interest in this concept. Previous protein-based treatments required repeated infusions, whereas gene therapeutics delivered to long-lived cells enabled the sustainable production of endogenous proteins. The virus was one of the first vectors studied to insert DNA into the target tissue, since this naturally occurring biological agent has been optimized the insertion of its genome for replication in a host cell throughout the evolution. Various types of viruses have already been selected for this purpose; one of the most intensively studied viruses today is the adeno-associated virus (AAV; Naso et al., 2017).

However, due to unenlightened disease mechanisms as well as the lack of knowledge about viral vectors, target cells, and tissues, it was still a long journey from concept to clinical application. In 1990, a four-year-old girl received the first drug as part of the very first clinical gene therapy trial for the treatment of adenosine deaminase (ADA) deficiency (Blaese, 1993). This opened the door for a series of further clinical gene therapy studies, although initially, there was no clinical benefit in many cases. The turn of the millennium then brought considerable improvements in gene transfer efficiencies, but this also led to novel toxic side effects. In 1999, gene therapy was set back by many years when 18-year-old Jesse Gelsinger was treated with recombinant adenoviruses against inherited ornithine transcarbamylase (OTC) deficiency by James Wilson at the University Hospital of Philadelphia. Four days after the treatment, the patient died as a consequence of multi-organ failure caused by uncontrolled immune reaction (Jenks, 2000; Branca, 2005; Wilson, 2009). This forced scientists to carefully study immune responses to virus administration and to implement appropriate modifications to keep these reactions under control. Continuous improvement of safety and specificity of the gene therapy vectors finally led to outstanding clinical success in the following years (Fischer and Cavazzana-Calvo, 2008; Wilson, 2009; Mingozzi and High, 2011; Kaufmann et al., 2013). The approval of the therapy of lipoprotein lipase deficiency (LPLD) in 2012, offered under the brand name Glybera®, finally represented a breakthrough in medicine (Gaudet et al., 2013; Bryant et al., 2013). Today, approximately 3000 clinical trials on gene therapy drugs are being conducted with the virus as by far the most widely used vector. The AAV

accounts for about 8 % of all vectors used in current studies (http://www.abedia.com/wiley/index.html; see figure 1).
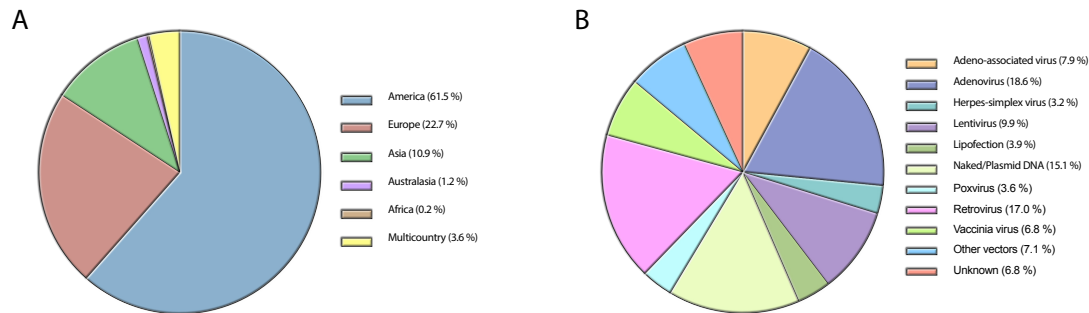
Figure 1: Geographical distribution of conducted gene therapy clinical trials (A) and the respective vectors applied (B) in 2019. A. Approximately two thirds of all clinical trials are currently being conducted in America and about one quarter in Europe. B. The virus is the most frequently used vector in clinical gene therapy studies. With 18.5 % of all clinical trials, the adenovirus is the most commonly applied vector. The AAV accounts for about 8 % of all conducted gene therapy trials. (Adapted from The Journal of Gene Medicine, 2018, John Wiley and Sons Ltd.)

1.2   The Adeno-Associated Virus as a Vector for Gene Therapy

1.2.1   The Adeno-Associated Virus

Adeno-associated viruses (AAVs) are able to infect a broad spectrum of dividing and non-dividing cell types, and have thus become a favored instrument for gene therapy. AAVs are dependoparvoviruses belonging to the *Parvoviridae* family. They were first discovered in 1965 as contaminants of cell cultures infected with adenoviruses, giving rise to their name (Atchison et al., 1965). They are not able to replicate themselves; replication and a productive infection require a co-infection with a helper virus such as adenovirus or herpes virus (Atchison et al., 1965; Buller et al., 1981). In the absence of a helper virus, the AAV genome usually persists within the infected cell in an extrachromosomal state as a double-stranded circular episome, without being integrated into the host genome. (Mishra and Rose, 1990; Bertran et al., 1996; Geoffroy and Salvetti, 2005; Alazard-Dany et al., 2009; Deyle and Russell, 2009). In non-dividing cells, this latent infection enables long-term expression of the introduced gene. Thereby, the episomes develop into multimeric and high molecular weight concatemers (Duan et al., 1998; Russell and Kay, 1999; Nakai et al., 2000; McCarty et al., 2004; Penaud-Budloo et al., 2008). However, about 0.1 % of the infecting AAV vectors integrate as single-proviruses or concatemers at non-homologous sites in the host-genome (Flotte et al., 1994; Bertran et al., 1996; Rutledge and Russell, 1997; Yang et al., 1997; Russell

and Kay, 1999; Deyle and Russell, 2009; Salganik et al., 2015). In 0.1 to 1.0 % of all cases AAVs can also integrate by homologous recombination (Hirata et al., 2002).

The AAV is a small, non-enveloped virus (approximately 20 nm) and its genome is composed of single-stranded (ss) DNA with a length of about 4.7 kb (see figure 2). It possesses two open reading frames flanked at each end by an inverted terminal repeat (ITR). These sequences self-assemble to T-shaped hairpin structures serving as the origin of replication (Linden et al., 1996; Grimm et al., 2005; Vance et al., 2015). The *Rep* open reading frame (ORF) codes for the non-structural proteins REP78, REP68, REP52, and REP40. The REP proteins are responsible for genome replication as well as for transcriptional control and packaging. The *Cap* ORF encodes the structural proteins VP1 (90 kDa), VP2 (72 kDa), and VP3 (62 kDa) assembling to the viral capsid (the given molecular weights are for AAV2; the sizes vary between the different stereotypes). One viral particle consists of 60 proteins organized in an icosahedral structure, in which the capsid proteins are present in a molar ratio of 1:1:10 (VP1:VP2:VP3) (Daya and Berns, 2008; Samulski and Muzyczka, 2014; Salganik et al., 2015; Naso et al., 2017; Büning and Srivastava, 2019). The assembly-activating protein (AAP) is also encoded by the *Cap* gene. It is required for efficient capsid assembly (Sonntag et al., 2011; Maurer et al., 2018). The *X* gene, expressed by its own promoter (p81), is located at the 3' end of the genome within the *Cap* gene. The encoded X protein is thought to be involved in the AAV life cycle and to influence viral replication (Cao et al., 2014; Büning and Srivastava, 2019). A frameshifted ORF within the VP1 region of the *Cap* gene encodes for the membrane-associated accessory protein (MAAP), that was found to limit AAV production by competitive exclusion (Ogden et al., 2019).
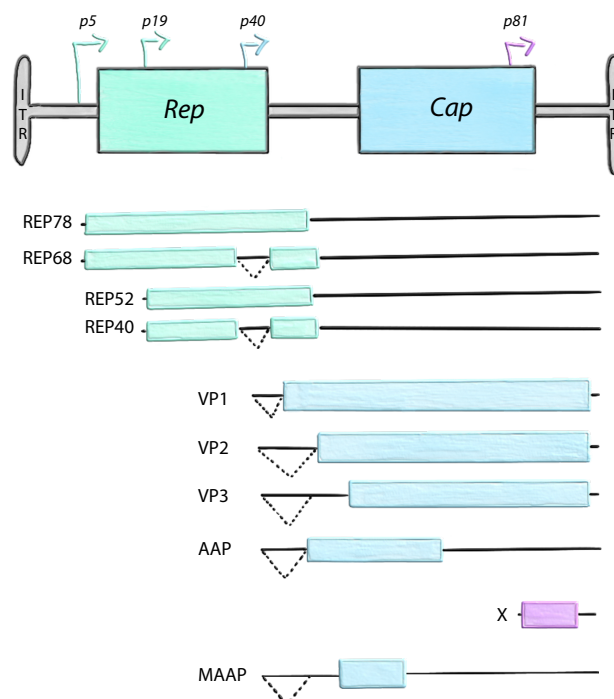
Figure 2: The genome of AAV serotype 2. The AAV2 viral genome is flanked by two Inverted Terminal Repeats (ITRs), serving as packaging signals and origins of replication. The replication gene encodes the four replication proteins that control viral transcription, replication, packaging and integration. The expression of REP78 and REP68 is controlled by the p5 promoter, while REP52 and REP40 are under control of p19. REP68 and REP40 are splice variants of REP78 and REP52, respectively (the numbers indicate molecular weight). The *p40* promoter controls the expression of all proteins encoded in the *Cap* gene, including AAP and the viral capsid proteins VP1 (90 kDa), VP2 (72 kDa) and VP3 (60 kDa). The *X* gene possesses its own promoter (p81) and is located at the 3' end of the AAV genome within the *Cap* gene. The membrane-associated accessory protein (MAAP) is encoded by a frameshift ORF within the VP1 region of the *Cap* gene. AAP is important for capsid assembly, the X protein impacts viral replication, MAAP limits AAV production by competitive exclusion, and the VPs constitute the icosahedral AAV2 capsid.

AAVs are non-pathogenic and trigger only little or even no immune response (Sun et al., 2003; Mueller and Flotte, 2008). They can be easily manipulated by replacing the viral *Rep* and *Cap* with the desired gene expression cassette. Since a recombinant AAV (rAAV) does not possess a *Rep* gene, an uncontrolled multiplication is largely excluded, even if the host cell is pre-infected with a helper virus. In addition, they show broad and specific tropism as well as stable and efficient gene expression *in vivo*. All these features contribute to their status as a valuable vector for gene therapy (Flannery et al., 1997; Bennett et al., 1999; Rabinowitz et al., 2002; Yang et al., 2002).

1.2.2   Adeno-Associated Virus Infection

Several serotypes (AAV1-12) exist among the wild-type AAVs, possessing different transduction efficiencies and tissue tropisms (the preference for entry into cells of a particular tissue). This is defined by the amino acid structure of the AAV, mediating cell surface attachment and entry mechanisms (Gao et al., 2002; Vance et al., 2015). The AAV interacts with the potential host cell via attaching to serotype-specific glycans on the cell surface. So far, several associations with heparan sulfate proteoglycans (AAV2, AAV3, AAV6) and N-linked sialic acids (AAV1, AAV5, AAV6) have been identified (Summerford and Samulski, 1998; Walters et al., 2001; Di Pasquale et al., 2003). Furthermore, a universal receptor was recently discovered recognizing almost all known serotypes (KIAA0319L; Pillay et al., 2016). After attachment to the cell, the AAV undergoes endocytosis (Duan et al., 1999; Bartlett et al., 2000; Sanlioglu et al., 2000; Nonnenmacher and Weber, 2011; Uhrig et al., 2012; Dudek et al., 2018) and microtubule-dependent trafficking to the nucleus ("endosomal trafficking"; Xiao and Samulski, 2012). Endosomal escape is achieved by a conformational change of the capsid triggered by acidification of the compartment (Sonntag et al., 2006). Following nuclear import and capsid uncoating, the single-stranded (ss) DNA is finally converted to double-stranded (ds) DNA (second-strand synthesis) so that gene expression can proceed (Ding et al., 2005; Xiao and Samulski, 2012; Nonnenmacher and Weber, 2012; Balakrishnan and Jayandharan, 2014; Salganik et al., 2015; Berry and Asokan, 2016).

1.2.3   Recombinant AAVs (rAAVs)

The most important aspect to be considered for the design of an rAAV vector is the packaging size of the AAV (including the ITRs), which is limited to about 5.2 kb (Grieger and Samulski, 2005; Dong et al., 2010; Lai et al., 2010; Wu et al., 2010). A substantial reduction in viral production yield or even plasmid truncations are results of AAV capsid size excision (Dong et al., 2010; Wu et al., 2010). Typically, a recombinant AAV plasmid for eukaryotic cell transduction contains two ITRs enclosing a mammalian promoter, the cDNA of the gene of interest, as well as a terminator, usually a polyadenylation signal (see figure 3). In order to obtain high-level gene expression in various cell types, constitutively active promoters are used including the immediate-early cytomegalovirus (CMV) or the chicken beta-actin (CBA) promoter. Cell- or tissue-specific expression, however, is achieved by using promoters being active in particular cell types (Powell et al., 2015). Most frequently, the expression cassette is cloned between the ITRs of AAV2, since AAV2 is the best characterized serotype. Therefore, also the helper plasmid usually contains the *Rep* gene of AAV2. In order to combine the advantages of AAV2 with the desired tissue tropism, most studies use the cross-packaging strategy (see also section 1.2.5 and figure 4) to produce "pseudotyped" AAV vectors using the AAV2 *Rep* gene in combination with the *Cap* gene of a distinct more appropriate serotype (Rabinowitz, 2002; Auricchio, 2003; Grimm et al., 2003; Burger et al., 2004; Wu et al., 2006; Daya and Berns, 2008).
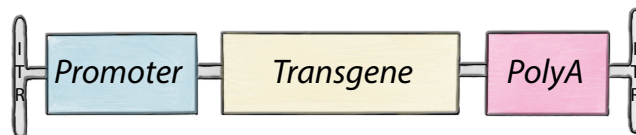
Figure 3: The typical rAAV expression cassette. A recombinant AAV plasmid for eukaryotic cell transduction is usually comprised of a mammalian promoter, the gene of interest, as well as of a terminator, usually a polyadenylation signal. The transgene expression cassette is enclosed by two ITRs, which are mostly originated from AAV2.

1.2.4   Immunogenicity of AAVs

In the past, the AAV has been shown to be less immunogenic than other viruses (Naso et al., 2017). A fully-packaged AAV possesses no engineered lipids or other chemical components that might contribute to unexpected and undesired toxicity or immunogenicity. Antigen-presenting cells (APCs) are not efficiently transduced by the AAV and furthermore, the rAAV lacks any viral genes that would contribute to an enhanced immune response (Basner-Tschakarjan et al., 2014; Basner-Tschakarjan and Mingozzi, 2014; Naso et al., 2017). Nevertheless, AAV capsid proteins as well as the delivered nucleic acid sequence can trigger several functional elements of the human immune system. The innate immune

response can be activated by pattern recognition receptors, most likely via Toll-like receptors (Hensley and Amalfitano, 2007; Zhu et al., 2009; Martino et al., 2011; Hösel et al., 2012; Basner-Tschakarjan et al., 2014; Rogers et al., 2015; Rabinowitz et al., 2019; Martino and Markusic, 2020). In addition, some patients show an activated adaptive immune response (e.g. due to previous contact to AAVs) manifesting as neutralizing antibodies (NAbs) or as activated cytotoxic T cells. This results in elimination of AAV-transduced cells ending in a reduction of the clinical effectiveness (Erles et al., 1999; Mingozzi et al., 2007; Mays and Wilson, 2011; Li et al., 2012; Louis Jeune et al., 2013; Salganik et al., 2015; Martino and Markusic, 2020). Thus, one challenge is to determine the therapeutically effective dose for each therapy that can be successfully administered to a patient who already carries a significant amount of circulating NAbs as well as an immunological memory against the corresponding virus (Louis Jeune et al., 2013).

1.2.5 Manufacturing of rAAVs for Clinical Use

As for the majority of biotherapeutics, also an rAAV has to be manufactured in a biological system. Two common procedures involve the helper virus-free transient transfection method, baculovirus or herpes simplex virus-based production systems, and packaging or producer cell lines (Clément et al., 2009; Ayuso, 2010; Clément and Grieger, 2016; Sandro et al., 2019). Triple-transfection uses three plasmids harboring the genes of interest, the *Rep* and *Cap* genes, and the helper genes of either adeno- or herpesvirus. Mostly, the HEK293 (or 293T) cell line is used as common host system for the production of rAAV (shown in figure 4A; Xiao et al., 1998; Wright, 2009; Grieger et al., 2016). However, this procedure is not the most suitable for producing large quantities of rAAVs, since a huge amount of DNA is required for virus production. In order to further scale up the manufacturing process, people often use packaging or producer cell lines containing the *Rep* and *Cap* genes integrated in their genome. Different from packaging cell lines, producer cell lines additionally include the recombinant vector sequence for the desired rAAV. The HeLa cell line is commonly used for this method. After an adenoviral infection, the cell line produces the rAAV in high quantities (displayed in figure 4B; Clark et al., 1995; Thorne et al., 2009; Martin et al., 2013; Clément and Grieger, 2016).
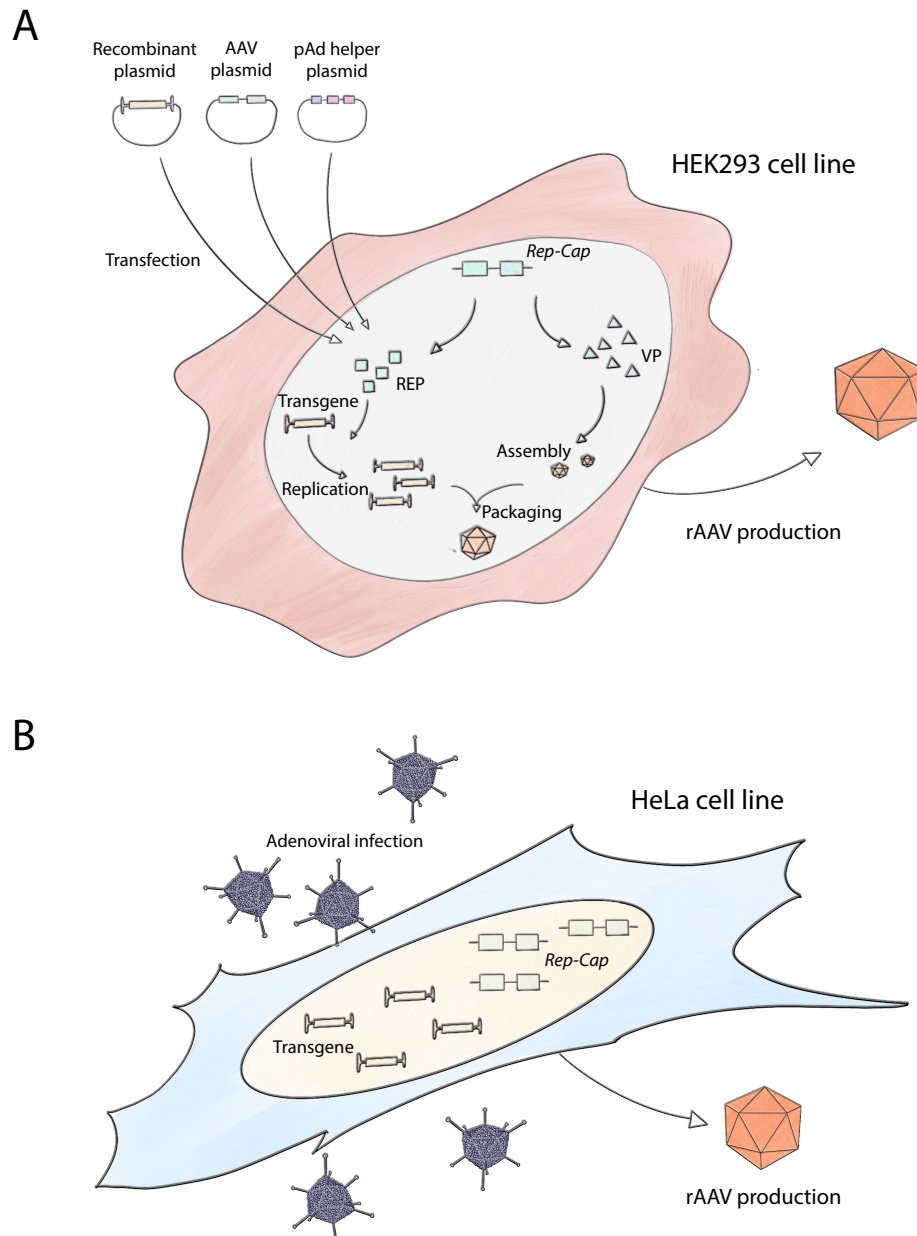
Figure 4: Two common methods for rAAV manufacturing. A. For the rAAV production via triple transfection, the recombinant plasmid carrying the respective transgene, the AAV plasmid consisting of the *Rep* and *Cap* gene, as well as the pAd helper plasmid containing the necessary adenoviral genes (E2A, E4, VA) have to be transfected to HEK293 (or 293T) cells. Within the cell, the *Rep* and *Cap* genes are translated to the replication and capsid proteins leading to the replication of the integrated transgene and to the capsid assembly, followed by viral vector packaging. Finally, the produced rAAV can be purified from the cell suspension. B. Large-scale rAAV manufacturing process based on a producer cell line. In order to generate a stable cell line, HeLa cells are transfected with a single plasmid usually containing the AAV *Rep* genes (usually AAV2) as well as the *Cap* genes of the desired serotype, the vector genome flanked by the ITRs, and a resistance gene (e.g. puromycin). Stable clones are obtained by culturing the cells in the presence of the respective antibiotic (puromycin). After screening the generated cell line for AAV productivity it is infected with a helper virus (usually adenovirus 5). After the infection, the rAAV is produced in high quantities by the cells.

1.2.6   Preclinical Evaluation of a Gene Therapy Product

Before a developed gene therapy product can be launched on the market, it must pass several preclinical and clinical phases. In the preclinical stage, the drug is not yet applied to human and does not necessarily have to be produced under good manufacturing practice (GMP) conditions. In this period, researchers usually use small as well as large animal models to test the efficiency and safety of the drug. Small animal models can be very useful in the earlier stages, usually requiring a larger number of subjects. The mouse is a commonly-used small animal primarily due to the ease of genetic manipulation and the resulting large number of available models. Further advantages are a close phylogenetic relationship and physiological similarity to humans. It has been extensively studied, allows relatively cost-effective breeding, a rapid reproduction, and manageable handling (Chader, 2002; Rosenthal and Brown, 2007). Furthermore, each strain is genetically homogeneous due to inbreeding, which leads to a relatively low variance of the experimental results. However, mice often react to experimental interventions in a way significantly different from humans (Seok et al., 2013). Therefore, it is often desired to also involve larger animals such as cats, dogs, pigs, or sheep in the advanced preclinical phases. Anatomically and physiologically, large animals are much more similar to humans in terms of, for example, organ size, life span, or the immune system. The fact that these animals are genetically more heterogeneous can become very important in the later preclinical stages, since a large genetic variance also exists in humans. Consequently, the approaches that can be used to overcome difficulties in large animal studies can be transferred more easily to humans (Casal and Haskins, 2006; Wolfe, 2009; Winkler et al., 2013; Volland et al, 2015).

1.3   The Eye as a Target for Gene Therapy

About 20-30 % of the human cortex is involved in the processing of visual information (Van Essen et al., 2001). Thus, vision is the most important sensory function and its decline causes a profound impact on the quality of life of the affected patient. Numerous inherited eye diseases exist that cause severe visual impairment, including glaucoma, *Achromatopsia*, *Retinitis pigmentosa*, Stargardt's disease, or *Chorioderemia* (Mathebula, 2012). The eye as a target organ of gene therapy offers a number of advantages and is therefore one of the most commonly targeted organs in translational gene therapy research (Dalkara et al., 2016; Dias et al., 2018). At first, it is an easily accessible organ for surgery (Bennett et al., 2012). It is small in size and compartmentalized, allowing for even small amounts of viral vectors to be sufficient for an effective therapy (Surace and Auricchio, 2003; Dinculescu et al., 2005; Buch et al., 2008). As a consequence of the blood-retina barrier and a unique intraocular microenvironment, vectors are unable to spread systemically and the global immune system barely

responds to any vector components or transgene products (Caspi, 2006; McKenna and Kapp, 2004; Willett and Bennett, 2013). Retinal cells, such as photoreceptors, are mature cells that no longer undergo proliferation after birth. This allows for an infinitely long-lasting expression of the transgene after only a single injection of the rAAV vector. Finally, well established non-invasive imaging techniques and functional tests already exist to monitor the therapeutic effect, which can be easily evaluated within preclinical and clinical studies by using the contralateral eye as an internal control (see section 1.5.2).

The human eye has a size of 23.9 mm and relatively to that, a small and thin lens (see figure 5). This is an advantage for diurnal species, as light can be deflected and refracted easily, which enables high acuity vision. Rodents, such as mice, are usually nocturnal species. They possess larger and thicker lenses relative to the eyeball. The distance from the lens to the retina (focal length) is short, allowing light to reach only a small area of the photoreceptors at a time. This results in a less sharp and smaller, but also in a brighter image (Schmitz and Motani, 2010). The eye of a mouse is only 3.5 mm in size (figure 5), almost seven times smaller than that of a human. The substantial dimensional discrepancies of the eyes have to be considered in ocular gene therapy. Therefore, much larger quantities of the therapeutic agent are required for the human eye and alternative application methods can be chosen.

Standard intraocular ophthalmic drug delivery techniques are the intravitreal and the subretinal injection. To date, scientists and clinicians have considered the subretinal administration of gene and cell therapeutics to treat retinal diseases as a more appropriate and efficient route of administration. Thereby, the drug is applied in a way to detach the neuroretina at the level between the photoreceptors and the retinal pigment epithelium (RPE); this generates a temporal artificial, so called "subretinal", compartment (Bennett et al. 2012; Peng et al., 2017). In humans, the lens occupies little space in the eye, which allows anterior insertion of the injection needle under direct monitoring (Maguire et al., 2008; Bennett et al., 2012). In the mouse, a relatively large part of the eye is filled by the lens. An anterior approach would therefore have a high potential for lens damage. For this reason, the needle is inserted from posterior through sclera and choroid (Bennett et al., 1996; Mühlfriedel et al., 2013). The large anatomical discrepancies between the eyes of mice and humans can be overcome by using large animals such as dogs. With 20.8 mm, the dog eye has a similar size as the human eye and although the dog is a crepuscular animal also the ratio lens to vitreous does not differ much from the human eye (Mutti et al., 1999; figure 5). Therefore, an anterior approach can be performed in dogs similar to that in humans and also a similar volume of the drug can be administered (Acland et al., 2001; Amado et al., 2010; Winkler et al., 2013; Bennett et al., 2012).
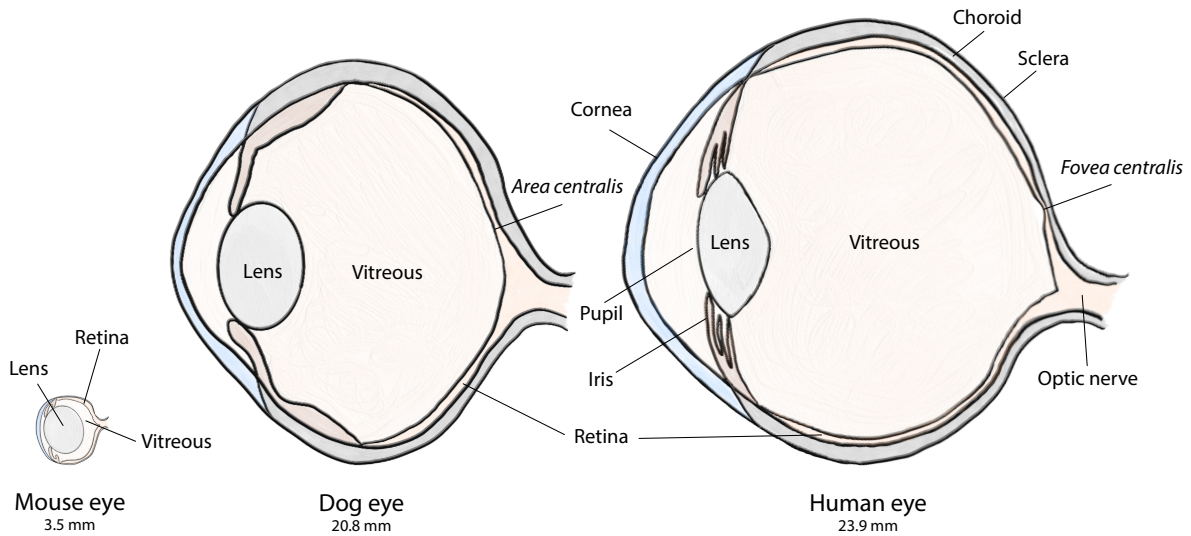
Figure 5: Comparative illustration of the eyes of mouse, dog, and human. The human eye is 23.9 mm in size and possesses a small thin lens relative to the vitreous. Light can be deflected and refracted easily, which enables sharp vision. Mice have larger and thicker lenses relative to the size of the eyeball. Furthermore, the distance from lens to retina is short (focal length) resulting in a less sharp and smaller, but also in a brighter image. The eye of a mouse is only 3.5 mm in size, almost seven times smaller than that of a human. With 20.8 mm, the dog eye has a similar size as the human eye and also the ratio lens to vitreous does not differ much from the human eye. The human retina comprises a *fovea centralis*, an excavation of the inner retinal cells in the central posterior part of the retina. In this region, cone photoreceptors are highly concentrated. This area is absent in mice. The dog eye comprises a fovea-like region where cones are accumulated, but the inner retinal cells are not excavated (*area centralis*).

1.4   Physiology and Anatomy of the Retina

The mammalian retina is located in the back of the eye and is basically arranged in layers of neuronal cells. It consists of three layers of nerve cell bodies each separated by synapses and dendrites (Kolb, 1995; Hoon et al., 2014). Its thickness is approximately 0.5 mm. In all vertebrates, the retina has an inverse organization, which means that the photoreceptors, the photosensitive cells converting the light into electric signals, are reached last by the incoming light. The nuclei of the photoreceptors form the outer nuclear layer (ONL) and their outer segments (OS) are embedded in the retinal pigment epithelium (RPE), involved in the regeneration of the visual pigment, digestion of necrotic photoreceptors, and absorption of light. It also contributes to the blood-retina barrier. The bipolar cells, being part of the inner nuclear layer (INL), receive the electric signals from the photoreceptors and further transmit it to the retinal ganglion cells (RGCs). Horizontal and amacrine cells are responsible for combining different information from specific regions of the retina in order to send specific bundled and amplified information to the RGCs. Finally, the information containing the visual image is transmitted to the brain via the ganglion cells along the optic nerve (ON). A detailed retinal structure is displayed in figure 6.
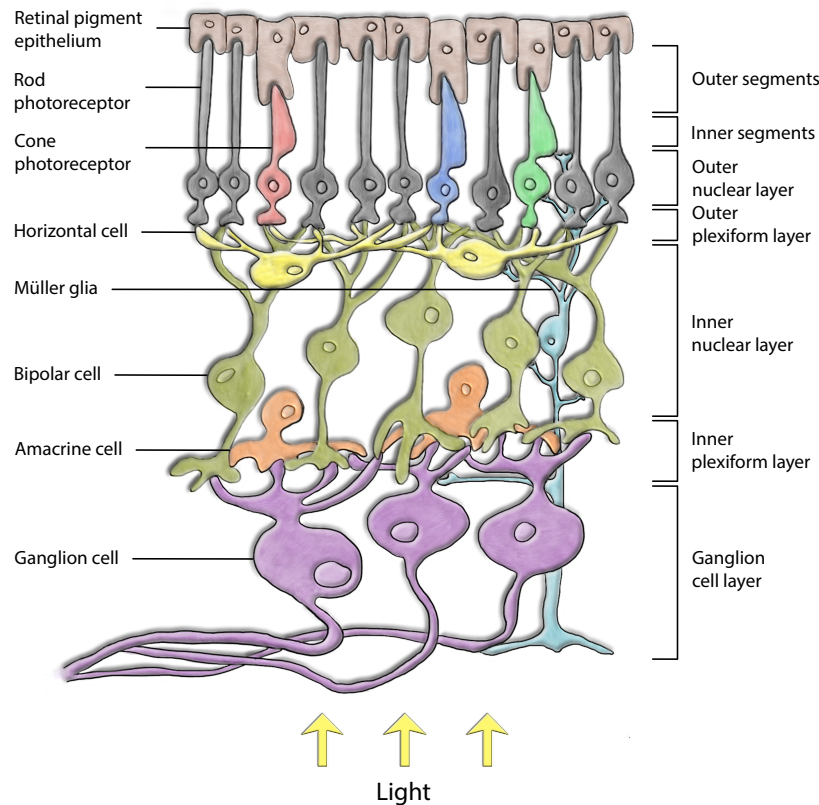
Figure 6: The inverse organization of a mammalian retina. It consists of three layers of neurons connected by synapses and dendrites. The retina has an inverse organization, which means that the cell type, that is reached last by the incoming light, are the photosensitive cells converting the light into electric signals. The nuclei of the photoreceptors form the outer nuclear layer (ONL) and their outer segments (OS) are embedded in the retinal pigment epithelium (RPE). The inner nuclear layer (INL) houses bipolar cells, horizontal cells, and amacrine cells. The electric signal is transmitted from photoreceptors to bipolar cells, passing the signal further to the retinal ganglion cells (RGCs). The electric signals are bundled and amplified at the outer and inner plexiform layer (OPL and IPL) The synaptic connections of photoreceptors, bipolar cells, and horizontal cells, expanding parallel to the retinal layers, make up the outer plexiform layer (OPL). Bipolar cells and the RGCs are connected by the amacrine cells at the inner plexiform layer (INL). The cell bodies of bipolar, horizontal, and amacrine cells form the inner nuclear layer (INL) and the ganglion cells represent the ganglion cell layer (GCL). The axons of the RGCs spread across the retinal surface, accumulate at the optic disc, and leave the eye as the optic nerve (ON) (Kolb, 1995; Hoon et al., 2014).

1.4.1   The Photoreceptors

Rod and cone photoreceptors represent the light sensitive cells of the retina (Bowmaker and Dartnall, 1979; Mustafi et al., 2009; Perkins and Fadool, 2010; Hoon et al., 2014; Molday and Moritz, 2015). Cone photoreceptors mediate color vision within daylight conditions. Different cone types are present in the vertebrate retina that possess different pigment spectra sensitivities (Rieke and Baylor, 2000; Haverkamp et al., 2005; Nikonov et al., 2006). The human retina comprises about 6 million cone cells, mainly L- (long wavelength) and M- (medium wavelength) cones, which are enriched in the central – foveomacular – area of the retina. The highest concentration is found in the foveal pit (*fovea centralis*, see

figure 5). This area, where the inner retinal cells are excavated, is located at the central posterior part of the retina where the visual axis is passing through (Kostic and Arsenijevic, 2016). Cone cells have a high resolution but are less sensitive to light, whereas rod photoreceptors are specialized for dim-light vision. 120 million rods are scattered throughout the retina while being much less present in the fovea (Molday and Moritz, 2015). They are able to detect even single photons, making them the most sensitive light detectors in nature (Hecht et al., 1942; Rieke and Baylor, 1998). In the mouse, a fovea is absent, although there is still a slight concentration of photoreceptors in the central region. The photoreceptor density is higher but the rod/cone ratio is similar to the peripheral retina humans (Volland et al., 2015). Furthermore, the human retina (and some non-human primate retinas) is the only retina among mammals comprising three types of cones (Ahnelt and Kolb, 2000; Yokoyama, 2000; Michalakis et al., 2018). All other mammalian retinas lack the L-cone being responsible for red color vision. However, cone-rich areas are found in the retina of some larger diurnal animals. A primate fovea-like region, termed *area centralis*, is for example present in the canine retina. Within this area, the cone photoreceptor density is high (M- and S- (short wavelength) cones), but an excavation of the inner retinal cells does not exist (Mowat et al., 2008; Beltran et al., 2014; Kostic and Arsenijevic, 2016; Baden and Osorio, 2019).

The structure of both rods and cones (illustrated in figure 7), being very similar within mammals, is structurally compartmentalized and can be divided into five main functional regions: outer segment (OS), connecting cilium (CC), inner segment (IS), cell body and synaptic terminal (Mustafi et al., 2009; Perkins and Fadool, 2010; Molday and Moritz, 2015). The OS of a rods is filled with tightly packed membrane discs carrying the photopigments. This very specialized morphology allows for a high density of photon absorbing molecules (rhodopsin). As a result, each rod contains 150 million rhodopsin molecules and each of them has the potential to initiate the vision cascade. In contrast, cones lack such completely internalized discs in their OS. In order to achieve a similar morphology with expanded surface for the photopigments cones have evolved multiple OS plasma membrane folds – the cone-specific lamellae – bearing the opsin molecules. This allows for faster fluxes of substances required for pigment regeneration and light adaptation (Sjostrand, 1953; Cohen, 1961). The IS contains the biosynthetic machinery where proteins are produced and subsequently trafficked to the OS through the narrow CC. The cell body harbors the nucleus and the synaptic terminal realizes the light signal transmission via the neurotransmitter glutamate to the bipolar cells and other secondary neurons (Molday and Moritz, 2015).
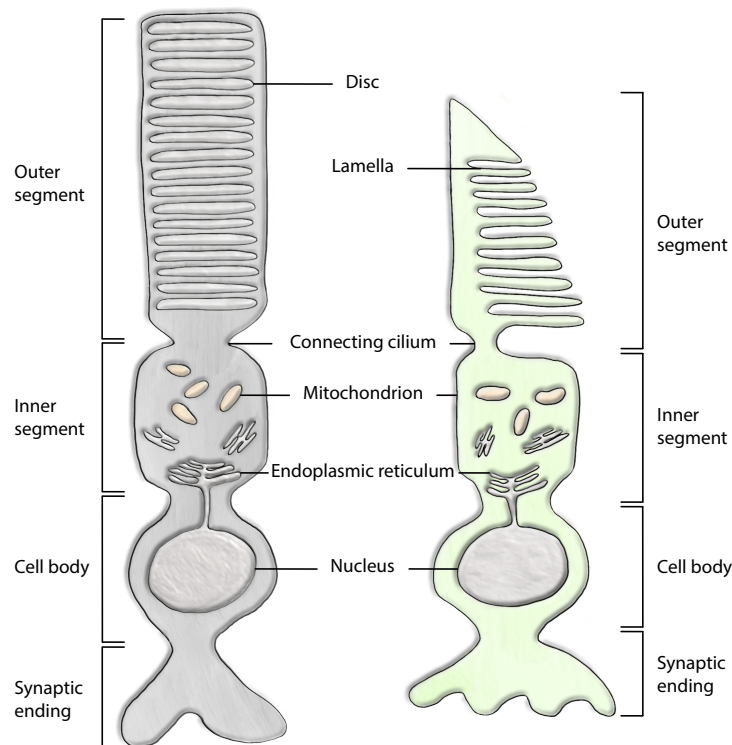
Figure 7: The rod (left) and the cone (right) photoreceptor. Rods are able to detect single photons and therefore mediate the dim-light vision. Cones are less sensitive to light, but possess a high resolution. Both rod and cone photoreceptors consist of outer segments (OS), connecting cilium (CC), inner segment (IS), nucleus, and synaptic terminal. The phototransduction takes place in the OS of the photoreceptors. The photopigment rhodopsin is present in the completely internalized discs of the rods, while the opsins are localized in the lamellae of the cones. Phototransduction proteins are folded in the IS and transported through the narrow CC to the OS. Electric signals coming from the OS are forwarded to the synaptic terminal transmitting the light signal to the inner retinal cells.

1.5   *Retinitis Pigmentosa* (RP)

Retinitis pigmentosa (RP) is a hereditary blinding disease characterized by progressive retinal degeneration affecting approximately 1 in 4000 individuals (Ammann et al., 1965; Boughman et al., 1980; Jay, 1982; Bunker et al., 1984; Grondahl, 1987; Pagon, 1988, Haim, 2002; Hartong et al., 2006, Ayuso and Millan, 2010; Sahel et al., 2010; Verbakel et al., 2018; Dias et al., 2018; Rodríguez-Muñoz, 2020). Currently, more than 1.5 million cases are known worldwide. Approximately 50 - 60 % of the RP variants are inherited autosomal recessively, but also autosomal dominant (30-40 %) or X-chromosomal forms (5-15 %) are known. The prevalence of the disease as well as the different manifestations vary enormously between the different ethnic groups from 1:9000 in Korea up to 1:750 in India (Nangia et al., 2012; Sorrentino et al., 2016; Na et al., 2017; Huang et al., 2017; Bravo-Gil et al., 2017; Birtel et al., 2018). In many cases, RP is non-syndromic, but there are also manifestations that are associated with extraretinal disease symptoms (syndromic), such as hearing loss (Usher syndrome), polydactyly and

renal dysfunction (Bardet-Biedl syndrome), bone disease (Refsum syndrome), muscle weakness, obesity, or mental retardation (Boughman et al., 1983; Weinstein, 1999; Koenig, 2003; Forsythe and Beales, 2013). To date, more than 80 different genes involved in non-syndromic RP have already been identified (https://sph.uth.edu/retnet/home.htm), making this disease highly heterogeneous. Among the different manifestations, the main symptoms are similar, but the age of onset, as well as the course and severity of vision loss are dependent on the genetic defect.

1.5.1   Pathophysiology, Symptoms, and Clinical Course

In most cases of non-syndromic RP, the disease is characterized by a primary degeneration of rods followed by the death of cone cells in the advanced stages of the disease (Hartong et al., 2006; Hamel et al., 2006; Verbakel et al., 2018). Rod degeneration manifests in night blindness and in a constricted peripheral vision which is termed as the characteristic "tunnel vision" (figure 8). Many patients do not notice or ignore difficulties in dark adaptation and are also able to compensate peripheral vision loss, which makes it difficult to generally determine the exact age of disease onset. The function at the fovea is relatively well preserved until later disease stages. Therefore, most patients need a lot of aids to orientate in the surroundings but are still able to read a book. One side effect of the rod degeneration is a higher sensitivity to bright light (glare sensitivity). Due to a dependency between rod and cone photoreceptors, a time-shifted, non-cell autonomous cone death is triggered in the advanced disease stage resulting in constriction of the visual field, followed by a decline of visual acuity, as well as the development of a dyschromatopsia. Particularly blue color vision is diminished, since blue cones are only sparsely distributed at the fovea (Kolb, 1995; Kostic and Arsenijevic, 2016). A deterioration of visual acuity is not noticed by the patients until the final stage of the disease, as the brain is able to compensate a loss of about 90 % of the cones (Geller and Sieving, 1993). Depending on the disease progression, RP can result in legal blindness, although most patients preserve the ability to perceive light, ensured by residual retinal islands or retained function at the fovea (Hamel, 2006).

Figure 8: Visual field loss with RP disease progression. Due to functionless rod photoreceptors, patients suffer from night blindness in the early stage of the disease. Furthermore, rods start to degenerate resulting in a constricted peripheral vision. As disease progresses (intermediate stage), the characteristic "tunnel vision" develops, caused by a further reduction of the visual field. One side effect of the rod degeneration is light sensitivity. In the advanced stage of the disease, the mutation-independent death of cone photoreceptors results in a further visual field constriction followed by a decline of visual acuity and dyschromatopsia, eventually resulting in legal blindness.

About 50 % of all RP cases develop posterior subcapsular cataracts (Berson et al., 1980; Pruett, 1983; Fishman et al., 1995). Common fundus abnormalities involve attenuated superficial retinal blood vessels as well as the characteristic intraretinal pigmentation ("bone spicules"), predominantly found in the periphery resulting from migrating retinal pigment epithelial cells into the neural retina (Berson et al., 1980; Li et al., 1995; Hartong et al., 2006; Hamel, 2006; see figure 9). With disease progression, patients further develop a waxy pallor in the optic discs, which is another hallmark sign of RP (Szamier, 1981; Hartong et al., 2006; Hamel, 2006; Hwang et al., 2012; Verbakel et al., 2018).

Figure 9: Fundus images of an RP patient (adapted from Hamel, 2006). Common fundus abnormalities involve attenuated retinal blood vessels as well as the characteristic "bone spicules" predominantly found in the periphery. The macula is relatively well preserved at the intermediate stage. In the advanced stage, pigment deposits are spread over the entire retina. Further clinical hallmarks are optic disc pallor and retinal atrophy.

1.5.2   Diagnosis and Disease Progression Monitoring

Since there is a large number of inherited retinal diseases which initially appear very similar, it is not sufficient to make a diagnosis based on the symptoms. In order to determine the disease unambiguously as well as to monitor disease progression, several well-established non-invasive imaging techniques and functional tests are available for physicians and scientists (Hartong et al., 2006; Verbakel et al., 2018). Electroretinography (ERG; Marmor, 1989) is used to analyze retinal function and in order to obtain information about the retinal morphology several imaging methods exist such as fundus imaging or confocal scanning laser ophthalmoscopy (cSLO; Witmer and Kiss, 2013), spectral-domain optical coherence tomography (SD-OCT; Huang et al., 1991; Chen et al., 2005; Yaqoob et al., 2005), fluorescein angiography or optical coherence tomography angiography (OCTA; Gao et al., 2016), fundus autofluorescence (FAF; Delori et al., 1995; Keilhauer and Delori; 2006), as well as adaptive optics scanning laser ophthalmoscopy (AOSLO; Georgiou et al., 2017).

SD-OCT images show retinal cross-sections providing information about the individual layers of the retina. With a weak laser light, the retina is scanned *in vivo* and the light reflections on the different

retinal structures are measured (Fujimoto, 2003). The earliest histopathological alteration occurring within RP disease progression, is a disorganization of the outer retinal layers referring to the shrinkage of photoreceptor outer segments (Milam et al., 1998; Liu et al., 2016; Goldberg et al., 2016; Verbakel et al., 2018). Disease progression results in a degeneration of photoreceptor cells which is recognizable in the OCT as a decrease of the outer nuclear layer (ONL) thickness. In late disease stages, the ONL is completely absent, whereas the inner retinal layers remain largely unchanged (Hood et al., 2011). Hyperreflective foci indicating migrating RPE or microglial cells are further pathologic attributes (Kuroda et al., 2014; Nagasaka et a., 2018).

Retinal function is determined by electroretinograms (ERGs) that measure the electric signal of the retina in response to emitted light flashes (Berson et al., 1969; Marmor, 1989; Marmor et al., 1995; McCulloch et al., 2015). RP patients show aberrant ERG signals even before they notice any night blindness symptoms. Rod-specific measurements under scotopic conditions (under exclusion of light) point out delayed electric responses as well as markedly decreased a- and b-wave amplitudes (for details see sections 2.7.4 and 3.9). Cone responses (measured via photopic ERG) are less affected but also distinctly reduced in the advanced disease stages (Marmor, 1979; Berson et al., 1993; Iannaccone et al., 1995; Sandberg et al., 1996; Holopigian et al., 1996).

1.5.3   Treatment Options for *Retinitis Pigmentosa*

Due to the enormous heterogeneity, there are only limited generally applicable treatment options for RP (Musarella and McDonald, 2011; Lin et al., 2015; Dias et al., 2018). Supplementation with antioxidants, such as vitamin A palmitate, fish oil (docosahexaenoic acid (DHA)), and lutein (Cuenca et al., 2014; Guadagni et al., 2015) as well as avoiding vitamin E can delay but not prevent the degeneration. Further pharmacological treatment intended to slow disease progression includes neuroprotection agents such as neurotrophic or growth factors (Harvey et al., 2006; Buch et al., 2007; Trifunovic et al., 2012), anti-apoptotic agents (Doonan et al., 2011; Fernandez-Sanchez et al., 2012; Cuenca et al., 2014; Guadagni et al., 2015), or anti-inflammatory agents (Glybina et al., 2009; Yoshida et al., 2013a and b). One pharmacological option for types of RP caused by mutations affecting the retinoid cycle is the continuous oral administration of a synthetic retinoid (9 cis-retinyl acetate), shown to achieve a significant improvement in vision in several RP patients (Koenekoop et al., 2014; Scholl et al., 2015; Kenna et al., 2020). For a few patients in the terminal stage of the disease, the option of an electronic retinal implant has recently become available to restore some basic visual perception by inducing neural activity in remaining retinal cells (Weiland and Humayun, 2014). In a growing number of preclinical studies, delayed degeneration or restored vision was already demonstrated via gene therapy using

different viral vectors. Adeno-associated viruses (AAVs), lentiviruses (LV), and adenoviruses (Ad), have been already used to target RPE or photoreceptors (Vollrath et al., 2001; Pang et al., 2004; Tschernutter et al., 2005; Chen et al., 2006; Trapani et al., 2014; Dalkara et al., 2016; Dias et al., 2018). Among the AAVs, serotype 1, 2, 4, and 6 demonstrated a tropism for the RPE (Auricchio et al., 2001; Weber et al., 2003; Bainbridge et al., 2008), while AAV5, 7, 8, and 9 showed photoreceptor transduction (Alloca et al., 2007; Auricchio et al, 2001; Lebherz et al., 2008; Lotery et al, 2003). While most RP gene therapy programs are still in the preclinical or early clinical stage of development, a first approved gene therapy drug already exists for RPE65-linked Leber's congenital amaurosis (LCA), a severe juvenile form of RP (Bainbridge at al., 2008 and 2015; Bennett et al., 2016; Russell et al., 2017). The gene therapy product voretigene neparvovec-rzyl (AAV2-hRPE65v2), commercialized under the brand name LUXTURNA™, is available to patients since late 2018. Further gene therapy approaches targeting different gene mutations (e.g. PDE6B or the *Retinitis pigmentosa* GTPase Regulator (RPGR)) are currently being tested in clinical trials (Petit et al., 2012; Beltran et al., 2012; Pichard et al., 2016; Cideciyan et al., 2018; Garafalo et al., 2019). In addition, there are also cell-based strategies aiming to treat advanced stage RP patients by transplantion of allogeneic healthy cells to compensate for lost photoreceptors (Jones et al., 2017; Dias et al., 2018). Currently, main sources for such allogeneic cell transplants include adult or fetal retinal cells, bone marrow-derived stem cells (BMSCs), as well as human pluripotent stem cells (hPSCs; Di Foggia et al., 2016; Javed and Cayouette, 2017; Liu et al., 2017; Jones et al., 2017; Park et al., 2017; Stern et al., 2018; Singh and MacLaren, 2018; Singh et al., 2019; Singh et al., 2020; Foltz and Clegg, 2019; M'Barek and Monville, 2019).

1.6 *Retinitis Pigmentosa* Type 45 (RP45)

Retinitis pigmentosa (RP) type 45 is caused by mutations in the cyclic nucleotide gated channel beta 1 subunit (*Cngb1*) gene, being responsible for about 4 % of all autosomal recessive RP cases (Hartong et al., 2006). To date, about 30 disease-causing mutations within the *Cngb1* gene are published (Bareil et al., 2001; Kondo et al., 2004; Simpson et al., 2011; Song et al., 2011; Azam et al., 2011; Schorderet et al., 2013; Bocquet et al., 2013; Fu et al., 2013; Nishiguchi et al.; 2013; Xu et al., 2015; Maria et al., 2015; Saqib et al., 2015; Lingao et al., 2016; Fradin et al., 2016; Perez-Carro et al., 2016; Habibi et al., 2017; Hull et al., 2017; Banerjee et al., 2017; Xiang et al., 2018; Ba-Abbad et al., 2019; Fuster-García et al., 2019; Dan et al., 2020; Rodríguez-Muñoz et al., 2020). The *Cngb1* gene encodes for the beta subunit of the rod-specific cyclic nucleotide-gated channel, which is responsible for the "dark current" of the rod outer segments (ROS).

1.6.1   The Role of the CNG Channel in Rod Phototransduction

In the dark, high levels of cyclic guanosine monophosphate (cGMP) are consistently produced by guanylyl cyclases (GCs). Cytosolic cGMP binds to the cyclic nucleotide binding domain (CNBD) of the CNG channel keeping it in its open state. This allows for the influx of sodium (Na^+) and calcium (Ca^{2+}) ions, leading to glutamate release at the synapse of the rod (Yau, 1994; Pugh et al., 1997; Michalakis et al., 2018). Incoming light causes a conformational change in the photo pigment rhodopsin, which subsequently activates a phosphodiesterase (PDE6A/B) (Kaupp and Seifert, 2002; Lamb and Pugh, 2006; Luo et al., 2008; Ashavsky and Burns, 2012; Ashavsky and Burns, 2014; Palczewski, 2014). In its active form, PDE hydrolyzes the second messenger cGMP, resulting in a reduction of the intracellular cGMP level, consequently leading to the closing of the CNG channel. The resulting hyperpolarization of the rod leads to a reduction of the glutamate release at the synaptic terminal (Hodgkin et al., 1985; Yau and Nakatani, 1985; Vinberg et al., 2017). Depending on the bipolar cell type, a decreased glutamate release initiates either a depolarization or a hyperpolarization of the respective bipolar cell. Finally, the electric signal is passed on to the retinal ganglion cells (RGCs) and transmitted via the optic nerve to the visual cortex for processing by the brain (Wässle, 2004). A detailed description of the phototransduction process is given in figure 10.

A mutation-caused deficiency of the rod CNG channel consequently leads to functionless rod photoreceptors resulting in photoreceptor degeneration. RP45 is inherited autosomal-recessively, which means that the altered allele must be present on both homologous chromosomes for phenotypic manifestation of the disease. Affected patients develop the characteristic night blindness already in early childhood, but the further course of the disease proceeds comparatively slowly. RP45 in most cases manifests at about 30 years of age when peripheral vision gets lost. The mutation-independent death of cones during disease progression leads to legal blindness at an age of about 60 years (Bareil et al., 2001; Kondo et al., 2004; Hartong et al., 2006; Simpson et al., 2011; Nishiguchi et al., 2013; Bocquet et al., 2013; Schorderet et al., 2013; Fu et al., 2013; Maranhao et al., 2015; Maria et al., 2015; Saquib et al., 2015; Fradin et al., 2016; Hull et al. 2017). Currently, there are no curative options for this type of RP.
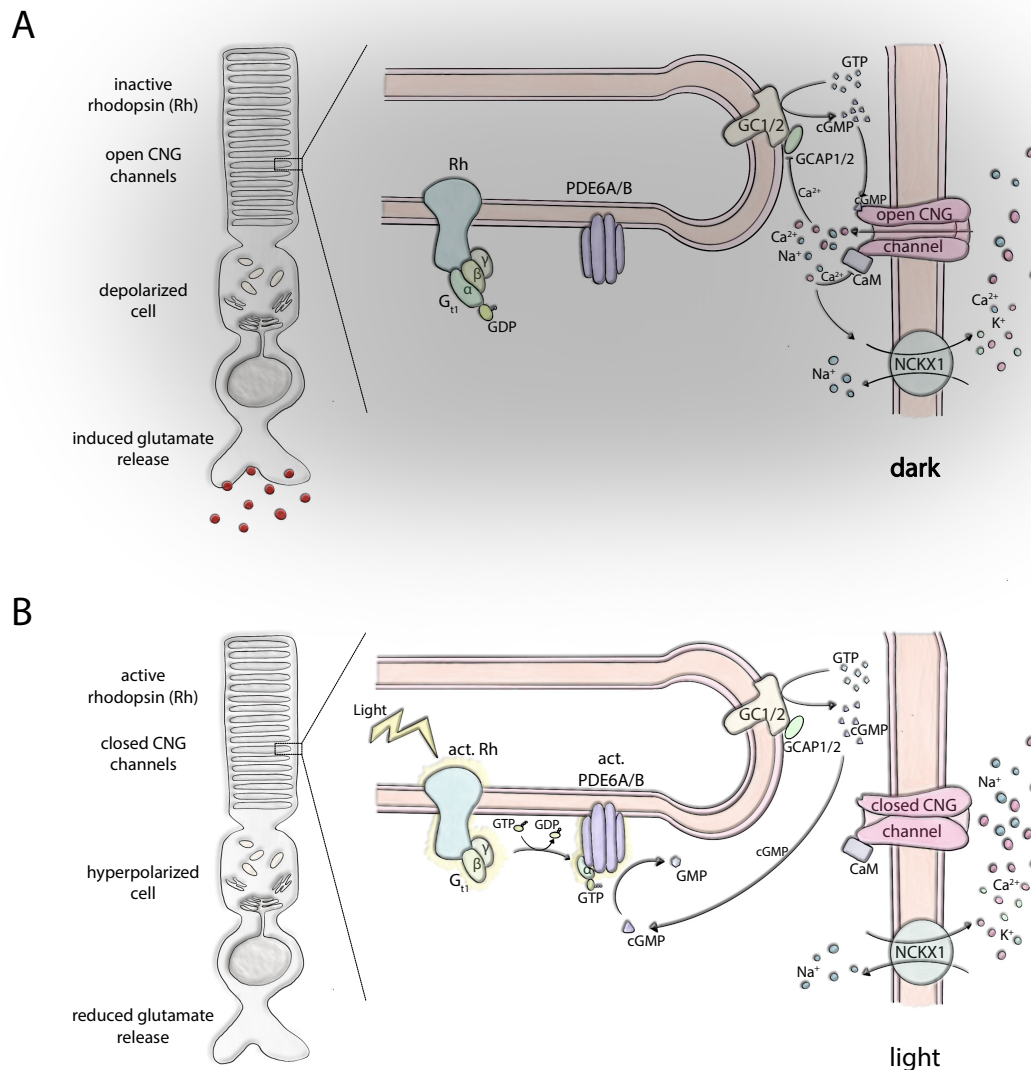
Figure 10: The phototransduction process in rod photoreceptors. In the dark, guanylyl cyclases (GCs) consistently produce high levels of cGMP that bind to the cyclic nucleotide binding domain (CNBD) of the CNG channel resulting in an open channel confirmation and a constant influx of Na^+ and Ca^{2+}. This "dark current" leads to the depolarization of the cell and further to the glutamate release at the synapse (Pugh et al., 1997; Biel and Michalakis, 2009; Michalakis et al., 2018). When a photon of light is absorbed by one of the 10^8 rhodopsin (Rh) molecules in the OS, its chromophore is isomerized to its all-trans configuration and the rhodopsin molecule is activated (Kaupp and Seifert, 2002; Lamb and Pugh, 2006; Luo et al., 2008; Ashavsky and Burns, 2012; Ashavsky and Burns, 2014; Palczewski, 2014). The stimulated rhodopsin triggers a conformational change of the trimeric G-protein transducin (G_{t1}) leading to the dissociation of its α-subunit (after binding GTP) and to the activation of a cGMP phosphodiesterase (PDE6A/B). cGMP is hydrolyzed by the PDE, resulting in a reduction of the intracellular cGMP level which consequently leads to CNG channel closing. The Ca^{2+}-influx can be only conducted by a CNG channel and since the $Na^{2+}/Ca^{2+}/K^+$-exchanger (NCKX1) continues to efflux Ca^{2+} from the cytosol, the intracellular Ca^{2+}-level decreases (Hodgkin et al., 1985; Yau and Nakatani, 1985; Vinberg et al., 2017). The ensuing photoreceptor hyperpolarization leads to a reduction of the glutamate release at the synaptic terminal. Depending on the bipolar cell type, a decreased glutamate release initiates either a depolarization or a hyperpolarization of the respective bipolar cell and also of the other secondary neurons. The resulting electric signals are finally transmitted to the visual cortex for processing (Wässle, 2004). Numerous negative feedback loops interact with the rods to allow the rod cell to quickly return to its resting state after a flash of light and to support its adaptability by lowering its responsiveness. One mediator is the intracellular Ca^{2+}-decrease leading to activation

of GCs via GC-activating proteins (GCAPs) and to the increase of the cGMP affinity of the CNG channel via calmodulin (CaM; Weitz et al., 1998; Bradley et al., 2004; Palczewski et al., 2004; Tolone et al., 2019). Rh. rhodopsin, act. Rh. activated rhodopsin, PDE6A/B. phosphodiesterase 6A/B, act. PDE6A/B. activated phosphodiesterase 6A/B, G_{t1}. G-protein transducing. GC1/2. guanylyl cyclase 1/2, CNG channel. cyclic nucleotide-gated channel, CNBD. cyclic nucleotide binding domain, GDP. guanosine diphosphate, GTP. guanosine triphosphate, NCKX1. $Na^{2+}/Ca^{2+}/K^+$-exchanger, cGMP. Cyclic guanosine monophosphate. GMP. Guanosine monophosphate, GCAP1/2. GC-activating protein ½, CaM. Calmodulin, Ca^{2+}. calcium-ions, Na^{2+}. sodium ions. K^+. potassium ions

1.6.2 The Cyclic Nucleotide-Gated Channel Beta Subunit 1 (CNGB1)

The *Cngb1* gene is located on human chromosome 16 on the long arm at position 21 (16q21; figure 11A). In mice it is present on chromosome 8 and in dogs on chromosome 2. The gene consists of 33 exons, that can be spliced into different isoforms (Ardell et al., 1996 and 2000). The CNGB1b isoform is expressed in olfactory neurons (Bönigk et al., 1999; Sautter et al., 1998), whereas CNGB1a is the rod-specific variant (Körschen et al., 1995; Ardell et al., 2000). In contrast to CNGB1b, the longer CNGB1a-isoform (240 kDa) additionally possesses a cytosolic N-terminus encoding for the glutamic acid–rich protein (GARP) important for rod outer segment (ROS) morphogenesis and structural integrity (figure 11A; Körschen et al., 1995; Ardell et al., 2000; Kaupp and Seifert; 2002; Biel et al., 2009; Zhang et al., 2009). The rod-specific CNG channel is a heterotetramer consisting of three CNGA1 subunits and one CNGB1 subunit (figure 11C), both indispensable for the functionality of the CNG channel (Weitz et al., 2002; Zheng et al., 2002; Zhong et al., 2002; Kaupp and Seifert, 2002; Biel and Michalakis, 2009). The CNGA1 subunits possess the principal channel properties. It has been shown that CNGA1 subunits are able to form functional homomeric channels in HEK293 cells as well as in xenopus oocytes. However, these channels are physiologically different from native CNG channels and are virtually non-existent *in vivo* (Körschen et al., 1995). The CNGB1 subunit contributes to the biophysical status of the CNG channel and is essential for the channel trafficking to the rod outer segment membrane (Biel et al., 1999a; Hüttl et al., 2005; Kaupp and Seifert, 2002; Trudeau and Zagotta, 2002; Matulef and Zagotta, 2003; Jenkins et al., 2006; Michalakis et al., 2006; Kizhatil et al., 2009; Michalakis et al., 2018). Each subunit consists of 6 alpha-helical transmembrane segments (1-6) forming a pore between segments 4 and 5 (figure 11B). The CNBD is connected to segment 6 via a C-linker in the carboxy (C)-terminal region. Both amino (N)- and carboxy (C)-terminus are located on the intracellular side. The binding of cGMP to the CNBD leads to a conformational change of the CNG channel. This results in the opening of the pore, enabling the influx of calcium (Ca^{2+})- and sodium (Na^+)- ions into the cell (Biel and Michalakis, 2009).
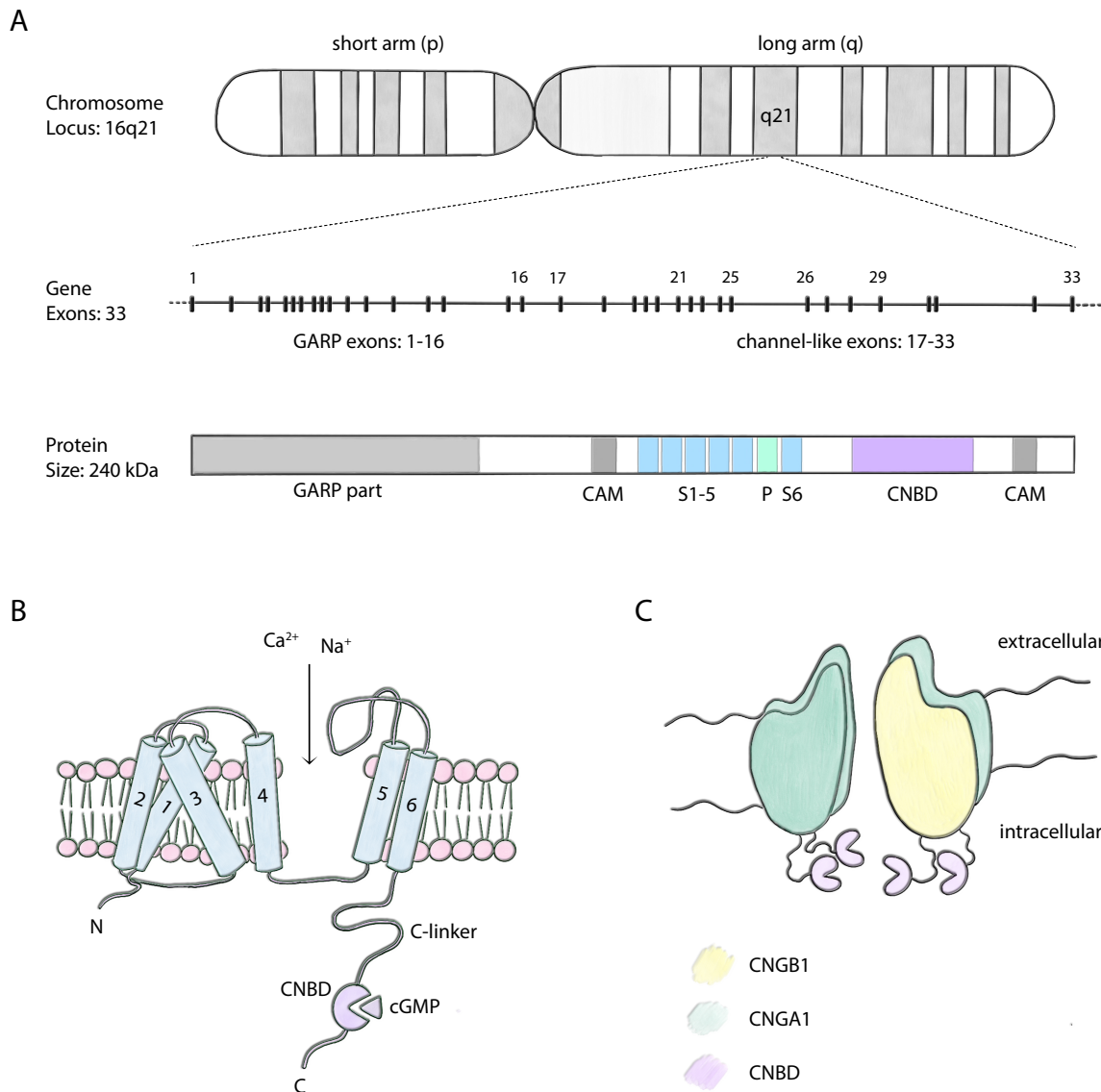
Figure 11: The human *CNGB1* gene encodes for the beta subunit of the human rod specific CNG channel. A. The human *CNGB1* gene is located on chromosome 16 on the long arm (position 16q21). It consists of 33 exons, of which the first 16 exons encode the GARP part, while exons 17-33 constitute the channel. The functional domains are two calmodulin domains (CAM), the 6 transmembrane segments (S 1-6), the pore (P), and the cyclic nucleotide binding domain (CNBD) B. Representative topology of a CNG subunit comprising six alpha-helical segments (segment 1-6) forming a pore between segments 4 and 5. N- and C-terminus are located on the intracellular side. The CNBD is connected to segment 6 via a C-linker in the C-terminal region. Binding of cGMP to the CNBD leads to a conformational change of the CNG channel, causing an opening of the pore and allowing the influx of calcium (Ca^{2+})- and sodium (Na^+)- ions. C. The rod-type CNG channel is a heterotetrametric protein complex consisting of three CNGA1 subunits and one CNGB1 subunit. S1-6 / 1-6. transmembrane segments 1-6; P. pore; N. amino terminus; CNBD. cyclic nucleotide binding domain; C. carboxy terminus. cGMP. cyclic guanosine monophosphate. GARP. glutamic acid–rich protein; CAM. Calmodulin (Adapted from Ardell et al., 2000 and Biel and Michalakis, 2009)

1.6.3   Animal Models for RP45

One form of RP45 is developed by a *Cngb1* knockout (KO; *Cngb1$^{-/-}$*) mouse model. It was generated by directed genetic manipulation to delete exon 26 of the *Cngb1* gene, which encodes the sixth transmembrane domain and is involved in pore formation. The deletion causes a shift of the reading frame, creating a stop codon at the first triplet of exon 27, which terminates the translation (Hüttl et al., 2005). Consequently, none of the ion channel CNG channel subunits are produced. In this mouse model, RP45 manifest with early onset and a slow disease progression. The rod outer segments start to degenerate already at the age of 15 days, resulting in markedly shortened OS at the age of 4 months. Cone photoreceptors start to degenerate at the age of 6 months, while about 50 % of the rods have been died. At about 1 year, only 10-20 % of the photoreceptors remain in the retina. (Hüttl et al., 2005). In addition, the *Cngb1* KO mouse model exhibits an olfactory dysfunction (Hüttl et al., 2005), as it has already been observed in CNGB1-deficient patients manifesting as anosmia and hyposmia (Charbel Issa et al., 2018; Afshar et al., 2020). Previous studies demonstrated an AAV-mediated supplementation of the murine *Cngb1* gene to this mouse model, resulting in deceleration of disease progression (Koch et al., 2012).

In previous years, a spontaneous mutation was identified within exon 26 of the canine *Cngb1* gene leading to loss of full-length CNGB1 (Winkler et al., 2013; Petersen-Jones et al., 2018). Exome sequencing revealed a 1-bp deletion and a 6-bp insertion (c.2387delA;2389_2390insAGCTAC), resulting in a frameshift and a premature stop codon. The affected *Cngb1* KO dogs develop progressive retinal degeneration manifesting as early loss of rod vision and slow photoreceptor degeneration (Winkler et al., 2013; Petersen-Jones et al., 2018). Thus, both animal models represent a majority of the so far reported RP45 cases.

1.7   Aim of the Study

Retinitis pigmentosa (RP), a group of hereditary eye diseases resulting in blindness, severely limits the life of the affected person and has a profound impact on the society. As there has been no curative treatment available for autosomal recessive human RP45 (*CNGB1*-linked RP) a gene supplementation therapy of *hCNGB1* to treat this form of retinal degeneration is the therapy of choice.

The aim of the following study is to develop a novel recombinant AAV vector optimized to enable the expression of human CNGB1 in rod photoreceptors and to evaluate its efficacy treating RP45 in two different preclinical models.

To this end, an rAAV vector expressing the *hCNGB1* gene under the control of a rod-specific promoter should be generated and produced, possessing a gene expression cassette that does not exceed the cargo capacity of an AAV. For the preclinical development of the drug, its treatment efficacy should be examined by evaluating the transspecies efficacy in small as well as in large animal models of RP45. Therefore, the generated vector should be administered to CNGB1-deficient animals and the therapeutic outcome of the gene supplementation therapy should be evaluated at the cellular, histological and functional level to address the following aspects:

- Is the *hCNGB1* gene, introduced by the rAAV vector, expressed in rod photoreceptors?

- Is a functional CNG channel formed in the rods as a result of the introduction of *hCNGB1*?

- Is the retinal degeneration in the *Cngb1* KO animals decelerated by the *hCNGB1* gene supplementation?

- Do *Cngb1* KO animals regain vision in the dark after treatment with *hCNGB1*?

- Is the efficacy of the *hCNGB1* gene supplementation dose dependent?

2   Materials and Methods

2.1   Chemicals, Solutions and Buffers

If not mentioned otherwise, all used chemicals were obtained from VWR, Sigma-Aldrich, Merck, Fluka, Roche, Bio-Rad or Roth and had the quality "*pro analysi*" or "for molecular biological use". All solutions were prepared using deionized water (Milli-Q Plus System, Millipore, Burlington, MA, USA) and subsequently autoclaved (Sterilisator, Münchener Medizin Mechanik, Munich, Germany).

2.2   Animals

The *Cngb1* KO mouse line (*Cngb1$^{-/-}$*; Hüttl et al., 2005) was generated and maintained at the mouse facility of the Department of Pharmacy Center for Drug Research, Ludwig-Maximilians-Universität Munich. The corresponding *Cngb1* wildtype mice (*Cngb1$^{+/+}$*) were used as wildtype controls. The *Cngb1* mutation was generated previously by removing exon 26 via Cre-mediated excision (Hüttl et al., 2005). Using a BAC clone (Genome Systems, St. Louis, MO, USA) isolated from a genomic 129SvJ library, a targeting vector was constructed such that exon 26 of the *Cngb1* gene was flanked in upstream direction by a loxP-neo/tk-loxP cassette and in downstream direction by a single loxP site. Cre-mediated recombination resulted in the deletion of exon 26, causing a frame shift and the introduction of a stop codon in the first triplet of exon 27 (Hüttl et al., 2005). Mouse keeping was carried out according to the legal guidelines. The mice were bred with a genetically mixed background of the strains 129SvJ and C57-Bl6/N. The rd8 mutation within the *Crb1* gene, previously detected in different North American and Asian laboratory mouse lines (Mattapallil et al., 2012) and significantly influencing the course of retinal degeneration, was not detectable in the *Cngb1* KO mouse line used in this work.

All mice received food (Ssniff; regular feed: R/M-H autoclavable V1534/35-3; balanced nutrient concentration with an average energy density and low nitrosamine concentration - well adapted for being a basis food during long-term studies; breeding feed: M-Z Extrudat, autoclavable V1124/25-3; protein concentration and quality as well as energy density is adapted to a high performance and high energy needs) and water *ad libitum* and were maintained in a 12 h light/dark cycle (lights on at 7 am). Five female or four male siblings were kept together at maximum. The inside temperature hovered around 22 °C and the relative air humidity was 60 %. For the purpose of environmental enrichment, the cages were equipped with tissue paper and, in case of breeding cages, nesting material. Ear punctures were used for identification.

The *Cngb1* KO dogs were descended from a small Papillon breeding colony, which was derived from a *Cngb1* KO female and her offspring, diagnosed with a form of progressive retinal atrophy (Winkler et al., 2013). The papillon female was donated to the Laboratory of Comparative Ophthalmology at Michigan State University. Sequencing identified a deletion of one base pair and a 6-base-pair insertion within the *Cngb1* gene (c.2387delA;2389_2390insAGCTAC), resulting in a frameshift and a premature stop codon (Winkler et al., 2013). The dogs were housed in standard laboratory accommodation in the AAALAC approved vivarium at the MSU College of Veterinary Medicine. They were maintained in a 12-hour light-dark regimen and fed a commercial laboratory dog diet with a light-dark cycle of 12:12 hours.

2.3   Genotyping

2.3.1   Genomic DNA Isolation

To obtain genomic DNA for genotyping, mouse ear biopsies were digested in 600 μL of 50 mM NaOH for 10 min at 95 °C. Subsequently, samples were mixed by vortexing and 50 μL of 1 M Tris-HCl (pH 8.5) were added for neutralization. The samples were centrifuged for 6 minutes at 13000 rpm and the DNA remaining in the supernatant was then used for amplification via polymerase chain reaction (PCR).

2.3.2   Polymerase Chain Reaction (PCR)

The PCR reaction mix using the GoTaq® DNA polymerase together with the 5× Green GoTaq® buffer (Promega, Madison, Wis, USA) was set according to the manufacturer's instructions. Annealing temperatures were adjusted to the corresponding primers that were used. The number of cycles and the duration of denaturation and elongation were dependent on the fragment to be amplified. The primers used for genotyping of *Cngb1* KO and *Cngb1* WT mice the (genomic *Cngb1*), the reaction mixture, as well as the corresponding PCR protocol are listed below. All primers have been produced by Eurofins Genomics (Ebersberg, Germany). The PCR reaction was run using the ProFlex PCR system (Thermo Fisher Scientific, Waltham MA, USA).

Primer name	Sequence 5'-3'
PSHV6bR (rev)	GCC CAG ACT AGA ACA CAA GTC
PSHV9R (rev)	CAC AGC CAT TAC ACA TAG CAG TG
PSHV8F (for)	CCT CAT GCA TGC GAC CTG AAA T

PCR reaction mixture	Volume
Template DNA	2 µL
Primer 1 (10 µM)	1.25 µL
Primer 2 (10 µM)	1.25 µL
Primer 3 (10 µM)	1.25 µL
dNTP's	0.5 µL
5× Green GoTaq® buffer	5 µL
GoTaq® DNA polymerase	0.125 µL
H_2O	ad 25 µL

PCR reaction protocol	Temperature	Duration	Cycles
Initial denaturation	95 °C	5 min	1 cycle
Denaturation	95 °C	30 s	
Annealing	57 °C	30 s	30 cycles
Elongation	72 °C	30 s	
Final elongation	72 °C	7 min	1 cycle

2.3.3 Agarose Gel Electrophoresis

DNA fragments smaller than 700 bp were separated using agarose gels in a concentration of 2 % agarose in TBE. The gels were prepared by boiling the corresponding amount of agarose (peqGOLD Universal Agarose, Peqlab Biotechnologie GmbH, Erlangen, Deutschland) in 200 mL 1× TBE in a laboratory microwave. After cooling the agarose to about 50 °C, PeqGreen (Peqlab Biotechnologie GmbH, Erlangen, Germany) was added at a final concentration of 0.025 µL mL^{-2} for the visualization under UV light and was allowed to get solid in a specialized chamber. The solid gel was placed in a horizontal electrophoresis chamber filled with the respective running buffer (1× TBE) and loaded with the PCR samples by filling them into small gel pockets. An additional molecular weight marker (Gene Ruler 1 kb plus DNA ladder, Thermo Fisher Scientific) was applied as a DNA size reference. The DNA fragments were separated at about 135-150 V. Finally, the DNA was visualized under UV light (Gel Doc 2000, Biorad, Hercules, CA, USA). A gene product of 480 bp was amplified in case of a wild-type sample and a *Cngb1* KO mouse was identified by a gene product of 415 bp.

1 × TBE buffer	Volume
0.5 M EDTA pH 8.0	20 mL
Boric acid	27.5 g
Tris	54.0 g
H$_2$O	ad 5 L

2.4 Cloning of the *pGL-hRHO194-hCNGB1a-SV40* Plasmid

The full-length transcription variant 1 of *hCNGB1* (NM_001297.4; 3.75 kb) was cloned between the inverted terminal repeats (ITRs) of serotype 2 originating from the pSub201 cis-plasmid (131 bp each; Samulski et al., 1987; Schön et al., 2017) together with the short *hRHO* (194 bp) and a previously used short polyadenylation signal (221 bp; Koch et al., 2012) acting as an effective termination and polyadenylation enhancer (Schambach et al., 2007). The plasmid backbone used contained a pUC18 (Clontech Laboratories, Mountain View, CA, USA) origin of replication, a kanamycin resistance gene (KanR), and randomized synthetic DNA fragments (pGL2.0; Schön et al., 2017). Finally, the size of the designed vector construct was 4.66 kb from 5'ITR to 3'ITR and thus did not exceed the packaging capacity of rAAV vectors. The plasmid map of *pGL2.0-hRHO194-hCNGB1a-SV40* is shown in figure 12.
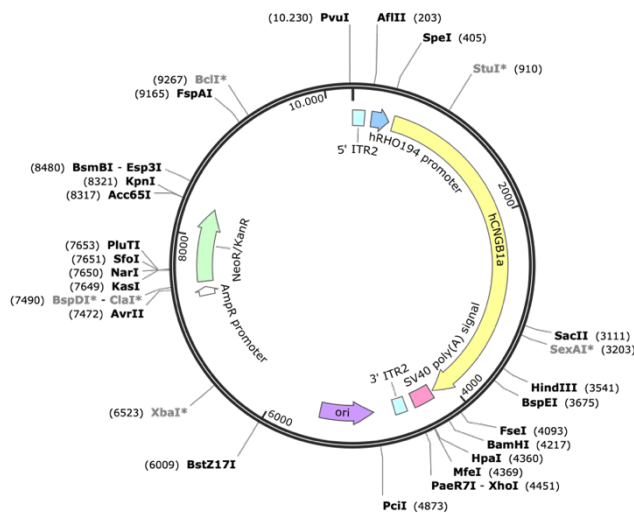
Figure 12: Plasmid map of *pGL2.0-hRHO194-hCNGB1a-SV40*. The coding sequence of the full-length hCNGB1a (NM_001297.4; 3.75 kb) was cloned between the inverted terminal repeats (ITRs) of serotype 2 originating from the pSub201 cis-plasmid (131 bp each) together with the short *hRHO* (194 bp) and a short polyadenylation signal (221 bp). The plasmid backbone used contained a pUC18 (Clontech Laboratories) origin of replication, a kanamycin resistance gene (KanR), and randomized synthetic DNA fragments (pGL2.0; Schön et al., 2017). The plasmid map was designed using the SnapGene Viewer software (GSL Biontech LLC, San Diego, CA, USA).

2.4.1 Polymerase Chain Reaction based cloning of *hRHO194* promoter

In order to amplify the designed *hRHO194* promoter with overhangs containing restriction sites for AflII in 5' and SpeI in 3' a polymerase chain reaction (PCR) was performed using the Q5® high fidelity DNA polymerase (New England Biolabs, Ipswich, MA, USA) according manufacturer's instructions. 1

ng of *pSub-hRHO-hPDE6A-WPRE* (Schön et al., 2017) was used as the template DNA for the 50 µL reaction mix. The PCR reaction was run using the ProFlex PCR system (Thermo Fisher Scientific). Primers used (produced by Eurofins Genomics), the reaction mixture, as well as the reaction protocol are listed below.

Primer name	Sequence 5'-3'	Generated restriction sites
hRHO 194 for	CAT AGC TAG CTT AAG CCT CTC CTC CCT GAC CTC AG	NheI and AflII
hRHO 194 rev	TCA TGG ATC CAC TAG TGA TGA CTC TGG GTT CTG ACC	BamHI and SpeI

PCR reaction mixture	Volume
Template DNA	1 ng
hRHO 194 for (10 µM)	2.5 µL
hRHO 194 rev (10 µM)	2.5 µL
2 × Q5 master mix	25 µL
H$_2$O	ad 50 µL

PCR reaction protocol	Temperature	Duration	Cycles
Initial denaturation	98 °C	30 s	1 cycle
Denaturation	98 °C	10 s	
Annealing	67 °C	20 s	35 cycles
Elongation	72 °C	15 s	
Final elongation	72 °C	2 min	1 cycle

2.4.2 Precipitation of DNA Fragments

In order to precipitate an amplified PCR product, H$_2$O had to be first added to a total volume of 100 µL, followed by 10 µL of 3 M sodium acetate buffer (pH 5.2) and 275 µL of cold ethanol (100 %). After an incubation step for 10 min at -80 °C, the mixture was centrifuged at 20,000 × g at 4 °C for 15 minutes. The pellet was washed with 70 % (v/v) cold ethanol after discarding the supernatant. Subsequently, it was centrifuged at 20 000 × g at 4 °C for 5 min, the supernatant was discarded and the pellet was dried at 50 °C for 20 min. Finally, a suitable volume of H$_2$O was used for resuspension of the purified DNA.

2.4.3   Restriction Digest

FastDigest restriction enzymes purchased from Thermo Fisher Scientific were used in this work according to manufacturer's instructions. For cloning, 3 µg DNA was applied and digested by 0.5 µL of each of the respective enzyme in a total volume of 30 µL.

For the production of the *pGL-hRHO194-hCNGB1a-SV40*, the generated *hRHO194* promoter was first cloned into the *pAAV2.1-mRho-hCNGB1-SV40* plasmid (Michalakis et al., unpublished). Therefore, *hRho194* was digested with AflII and SpeI while the *mRho* promoter was cut out using the same enzymes. To subclone the resulting ligation product into the *pGL2.0*-backbone, *pAAV2.1-hRHO194-hCNGB1a-SV40* and *pGL2.0-hRHO-PDE6A-SV40* (Schön et al., 2017) were digested using AflII and XhoI.

2.4.4   Gel Electrophoresis and Fragment Isolation

To obtain the DNA fragments, the restriction digest was applied to a 0.7 % agarose gel. In order to load the whole 30 µL to the gel, it was made of 60 mL 1× TBE and allowed to become solid in a specialized chamber to create larger pockets. For cloning, the DNA was separated at about 120 V and the desired DNA bands were excised from the gel. DNA isolation was performed using the QIAquick Gel Extraction Kit (Qiagen) according to the manufacturer's instructions.

2.4.5   Dephosphorylation and Ligation

Prior to ligation, it is important to ensure that the DNA fragments generated by the digestion do not re-ligate themselves. For that reason, the DNA to be ligated was dephosphorylated in advance using the Rapid DNA Dephosphorylation Kit (Roche, Basel, Switzerland) in accordance with the manufacturer's protocol. The mixture (see below) was mixed by pipetting and then incubated first for 10 min at RT prior to a second incubation step at 75 °C for 2 min. The dephosphorylated fragments had to be run on the gel and to be isolated again using the QIAquick Gel Extraction Kit (Qiagen, Venlo, The Netherlands).

The T4 DNA Ligase (Thermo Fisher Scientific) was used for ligation according manufacturer's manual. 60-80 ng of vector DNA was applied and the molar ratios of vector and insert were 1:3, respectively. The mixture was either incubated at 16 °C over-night, or for 1.5 h at RT.

Dephosphorylation mixture	Volume
Vector DNA	<1 µg
10 × Phosphate buffer	2 µL
Phosphatase	1 µL
H_2O	ad 20 µL

Ligation mixture	Volume
Vector DNA	60-80 ng
Insert DNA	1:3 of the vector mass
T_4 10 × Ligase buffer	1 µL
T_4 Ligase	1 µL
H_2O	ad 10 µL

2.4.6   Transformation

To produce plasmid DNA in a larger-scale, chemically competent *E.coli* cells (beta-10 competent, K12 strain, NEB, Ipswich, MA, USA) were used to perform DNA transformation. Therefore, a 100 µL aliquot of the corresponding cell suspension was thawed on ice and received 2-5 µL of the ligation mixture (about 1-10 ng of plasmid DNA). After they were gently mixed and incubated on ice for 30 min, the cells were heat shocked at 42 °C for 45 s and rested on ice for at least 2 minutes before being plated on LB(+) agar plates with either 100 µg mL^{-1} ampicillin or 200 µg mL^{-1} kanamycin, depending on the antibiotic resistance gene in the plasmid. In the case of kanamycin, the transformed cell suspension had to be diluted in 900 µL LB(+) and was shaken at 300 rpm for 1 h at 37 °C. Either, 100 µL of the grown cell suspension was directly plated, or it was first centrifuged for 2 min at 3500 rpm (at RT), and the pellet was resuspended in only 100 µL of the supernatant. The agar plate was then incubated overnight at 37 °C in a reversed position.

LB(+) medium	
Peptone	10 g
Yeast extract	5 g
NaCL	5 g
D-(+)-glucose	1 g
H_2O	ad 1 L
Adjust pH to 7.2-7.5 and autoclave	

LB(+) agar	
Agar	15 g
LB(+) medium	ad 1 L
Let the solution cool down to 50 °C and add 100 mg ampicillin or 150 mg kanamycin	

2.4.7   Inoculation of Bacterial Cells and Alkaline Lysis

Individual bacterial colonies were taken from the overnight incubated selection plate and transferred to 13 ml tubes (Sarstedt, Nümbrecht, Germany) containing 5 ml LB (+) medium and ampicillin (100 µg mL^{-1}) or kanamycin (150 µg mL^{-1}). The suspension was incubated overnight in a thermoshaker at 37 °C and 225 rpm. Bacterial clones carrying the kanamycin resistance gene were incubated for 1 h at 37 °C before the antibiotic was added to the tubes. The next day, the suspension was centrifuged for 10 min at

3500 rpm. After removing the supernatant, the bacterial cells were resuspended in 250 μL resuspension buffer and transferred to a 2 mL tube (Eppendorf, Hamburg, Germany). Subsequently, 250 μL lysis buffer were added and the resultant suspension was mixed by inverting (5-6 times) prior to a 5-min incubation step at RT. Afterwards, 250 μL of a neutralization buffer were added and inverted 5-6 times before incubating on ice for 15 min. The suspension was then centrifuged for 15 minutes at 20,000 × g and 4 °C and the resulting supernatant was transferred to a new 1.5 mL Eppendorf tube. For precipitation, 525 μL cold isopropanol (100 %) was added to the DNA. Then, the samples were thoroughly mixed and centrifuged at 20,000 × g for 15 minutes at 4 °C. After removing the supernatant and adding 700 μL 70 % (v/v) ethanol, the solution was centrifuged at 20 000 × g and 4 °C for 5 minutes and the resulting supernatant was discarded. The pellet was allowed to dry at 50 °C before being resuspended in 20 μL H_2O. By using a Nanodrop 2000c spectrophotometer (Thermo Fisher Scientific) the DNA concentration as well as the purity were determined. Before being used, the constructs were first undergone restriction analysis and if the bands were at the right position on the gel, the modified parts of the plasmids were sequenced at Eurofins Genomics. In case of a correct sequence, the PureLink HiPure Plasmid Maxiprep Kit (Invitrogen, Carlsbad, CA, USA) was used for large scale and high purity plasmid isolation. This involved inoculating 200 ml LB(+) medium with single colonies according to the manufacturer's instructions.

Resuspension buffer	
Tris	6.06 g
EDTA	3.72 g
RNase A	100 mg
H_2O	ad 1 L
Adjust pH to 8.0	

Lysis buffer	
NaOH	8.0 g
10 % (w/v) SDS solution	100 mL
H_2O	ad 1 L

Neutralization buffer	Volume
3 M Potassium acetate pH 5.5	500 mL
H_2O	ad 1 L

2.5   Production of rAAV Particles via Triple Transfection In-House

2.5.1   Cultivation of Mammalian Cell Lines

For in-house rAAV production the HEK293T cell line (LentiX 293 T cell line, Clontech Laboratories) was used. These adherent cells were cultivated in T75 cell culture flasks (CELLSTAR®; Greiner Bio-One, Kremsmünster, Austria) in DMEM + GlutaMAX™-I medium ((+) 4.5 g/l glucose, (-) pyruvate, (+) 10

% FBS, (+) 1 % penicillin/streptomycin (Thermo Fisher Scientific)) at 37 °C and 10 % CO_2. Cells were passaged every 3-4 days by washing once with pre-warmed $1 \times$ phosphate buffered saline (PBS) before detaching them by incubating with 2 mL of Trypsin-EDTA (0.05 %; Thermo Fisher Scientific) for 5 min at 37 °C. Trypsinization was stopped by adding 16 mL of the cell culture medium. After segregating cells by pipetting up and down, 1.5 mL of the cell suspension was transferred into a new T75 cell culture flask that was already filled with 13 mL of cell culture medium. For transfection, the HEK293T cells were seeded in 15×15-cm plates in a volume of 16 mL and were allowed to grow at 37 °C and 10 % CO_2.

$1 \times$ PBS	Volume
NaCl	8 g
KCl	0.2 g
Na_2HPO_4	1.42 g
KH_2PO_4	0.27 g
H_2O	ad 1 L

Adjust to pH 7.4 and autoclave

2.5.2 Triple Transfection

The triple transfection included the recombinant plasmid carrying the respective transgene (e.g. *hCNGB1*), the AAV plasmid consisting of R*ep* and *Cap* gene (e.g. pAAV2/5), and the pAd helper plasmid containing the necessary adenoviral genes (E2A, E4, VA). When the HEK293T cells were 50-70 % confluent, they were transfected using the calcium phosphate technique (Graham and van der Eb, 1973). Dextran 500 (Sigma) and polybrene (hexadimethrine bromide, Sigma) were added to the conventional transfection mixture to increase gene transfer efficiency (Wu and Lu, 2007).

Transfection mixture	Volume
Recombinant vector	270 μg
pAd helper	x_1 μg
AAV plasmid	x_2 μg
Polybrene (8 mg mL^{-1})	15 μL
Dextran 500 (10 mg mL^{-1})	1.5 mL
2.5 M $CaCl_2$	1.5 mL
H_2O	ad 15 mL

The quantities of the pAd helper and pAAV2.1 were calculated using the following equations:

x_1: $$\mu g = \frac{270\ \mu g \times MM\ of\ pAd\ helper}{MM\ of\ recombinant\ vector}$$

x_2: $$\mu g = \frac{270\ \mu g \times MM\ of\ AAV\ plasmid}{MM\ of\ recombinant\ vector}$$

MM = molar mass of the double stranded plasmid

The transfection mixture was prepared by pipetting and vortexing the DNA, Polybrene, and Dextran 500. After adding $CaCl_2$ (dropwise) and H_2O, the mixture was vortexed under dropwise addition of 15 mL 2 × BBS before it was incubated at RT for 12 min to allow the formation of homogeneous DNA complexes. Afterwards, 2 mL of the solution was homogeneously distributed on each of the 15 culture dishes and the cells were then incubated overnight at 37 °C and 5 % CO_2. The next morning, the medium was removed and 18 mL of fresh cell culture medium was added to the cells, which were then incubated overnight at 10 % CO_2 and 37 °C.

2 × BBS	Volume
BES (Sigma)	8 g
NaCl	13.08 g
NaH2PO4	0.17 g
H_2O	ad 800 mL

Adjust to pH 6.95, sterile filtrate and autoclave

2.5.3 Harvesting

<u>Cell Harvesting</u>

For cell harvesting, the cells of each dish were scraped off with a cell scraper and collected with the medium in a 500 mL-centrifuge tube and were then centrifuged for 15 min at 4000 rpm at 4 °C (JA-10 rotor, J2-MC high-speed centrifuge; Beckman Coulter, Brea, CA, USA). The rAAVs were either obtained from the harvested cells or via isolation from the supernatant. Whether an rAAV is more likely to be found in the cell pellet or released into the supernatant depends on the capsid being produced.

<u>rAAV Isolation from the Cell Pellet</u>

In order to isolate the rAAV from the cell pellet, the supernatant was removed after the centrifugation step and the pellet was resuspended in 7.5 mL lysis buffer. Subsequently, the cells were treated by three cycles of shock freezing in liquid nitrogen and thawing at 37 °C in a water bath to disrupt the lysed cells. The samples are stored at -80 °C.

Lysis buffer	Volume
NaCl	150 mM
Tris-HCl pH 8.5	50 mM
H_2O	ad 50 mL
Sterile filtrate	

rAAV Isolation from the Supernatant

For an isolation from the cell culture medium, the supernatant was sterile filtered and subsequently precipitated with 8 % polyethylene glycol (PEG 8000, sterile filtered) over night at 4 °C. After centrifuging the next day at 4000 rpm for 15 min, the resulting pellet was resuspended in 7.5 mL of 1× PBS and stored at -80 °C.

2.5.4 Iodixanol Gradient Ultracentrifugation

Both the lysed cell pellet and the precipitated medium were mixed with benzonase (VWR, Radnor, PA, USA) to a final concentration of 50 U mL^{-1} and incubated at 37 °C for 30 min. The digested pellet was centrifuged for 25 min at 4000 rpm and 4 °C and the resulting supernatant was transferred to a Quick-Seal polypropylene tube (39 mL, Beckman Coulter). The pellet was discarded. A gradient was then generated in the tube in a way that the virus-containing supernatant was underlaid with 7 mL of 15 %, 5 mL of 25 %, 5 mL of 40 % and 6 mL of 60 % iodixanol using a long glass pipette and a Gilson MINIPULS3 pump (Hermens et al., 1999). The tube was then sealed with a Tube Topper (Beckman Coulter) and centrifuged at 70 000 rpm at 18 °C for 105 minutes in an ultracentrifuge (Optima L-80K with a 70 Ti rotor; Beckman Coulter). The virus accumulated in the 40 % iodixanol layer. To remove it from the tube, the tube cap was first perforated several times to equalize the pressure. Subsequently, the tube was pricked laterally with a 21-gauge needle at the lower limit of the 40 % phase and the entire layer (approx. 5 mL), up to the level immediately below the 25 % phase, was extracted with a syringe (shown in figure 13). The collected 40 % phase was frozen at -80 °C.
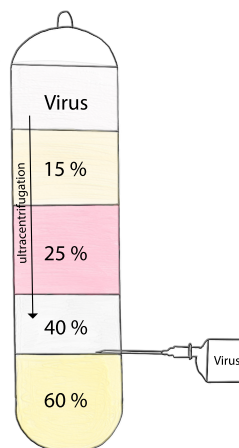
Figure 13: Extraction of the virus-containing phase from the Quick-Seal tube after density gradient ultracentrifugation. Because of the generated gradient (7 mL 15 %, 5 mL 25 %, 5 mL 40 % and 6 mL 60 % iodixanol), the virus is accumulating in the 40 % iodixanol phase during ultracentrifugation. For extraction, the tube is pricked laterally at the lower limit of the 40 % phase and the entire layer can be collected with a syringe.

15 % Iodixanol	Volume
10× PBS	5 mL
1 M MgCl$_2$	50 µL
2.5 M KCl	50 µL
5 M NaCl	10 mL
Optiprep (Progen)	12.5 mL
1 % Phenol red	37.5 µL
H$_2$O	ad 50 mL
Sterile filtrate	

25 % Iodixanol	Volume
10× PBS	5 mL
1 M MgCl$_2$	50 µL
2.5 M KCl	50 µL
Optiprep (Progen)	20.9 mL
1 % Phenol red	50 µL
H$_2$O	ad 50 mL
Sterile filtrate	

40 % Iodixanol	Volume
10× PBS	5 mL
1 M MgCl$_2$	50 µL
2.5 M KCl	50 µL
5 M NaCl	10 mL
Optiprep (Progen)	33.3 mL
H$_2$O	ad 50 mL
Sterile filtrate	

60 % Iodixanol	Volume
1 M MgCl$_2$	50 µL
2.5 M KCl	50 µL
Optiprep (Progen)	33.3 mL
1 % Phenol red	37.5 µL
H$_2$O	ad 50 mL
Sterile filtrate	

2.5.5 Anion Exchange Chromatography

For further purification of the virus particles, anion exchange chromatography was performed using the chromatography system ÄKTAprime plus (GE Healthcare, Chicago, IL, USA) connected to a HiTrap Q FF Sepharose column (GE Healthcare). Prior to this, the column had to be equilibrated with 30 ml buffer A (10 mL min^{-1} flow rate). The virus-containing solution collected from the Quick-Seal tube was diluted 1:1 in buffer A and loaded onto the Sepharose column using a loop injector (Superloop, 50 mL, GE Healthcare). The flow rate was adjusted to 1 mL min and the resulting fractions (fraction size: 1 mL) were collected in 1.5 mL tubes. UV and conductance curves were recorded by using the PrimeView 5.31 software (GE Healthcare). As soon as the conductance curve returned to baseline, the system was first loaded with Buffer B and then with double-distilled water (ddH$_2$O) to eliminate residual virus particles and remaining salt from the column. Cleaning was carried out until the conductance curve reached the value 0 and then extended for another 20 min. The fractions collected at the peak of the conductance curve were pooled in a 15 mL falcon.

Buffer A	Volume
Tris	20 mM
NaCl	15 mM
H$_2$O	add to 1 L

Adjust pH to 8.5 and sterile filtrate

Buffer B	Volume
NaCl	2.5 M
H$_2$O	add to 1 L

Adjust pH to 8.5 and sterile filtrate

2.5.6   Concentration and Salination of the rAAVs

To increase the virus concentration, the fractions obtained during the ion exchange chromatography were transferred to an Amicon column (Amicon® Ultra-4 Centrifugal Filter Units, 100 kDa, Millipore) and centrifuged several times at 20 °C and 4000 rpm (JA-10 rotor, J2-MC High speed centrifuge; Beckman Coulter) until the volume was reduced to 500 µL. The flow-through was discarded. A washing step was performed by adding 1 mL of 0.014 % Tween/PBS-MK solution, thoroughly mixing, and centrifuging again under the previous conditions until the virus suspension was concentrated to a volume of about 100 µL. Due to its molecular mass, the virus suspension had not passed the pores of the filter. Finally, 10 µL aliquots were prepared and stored at -80 °C.

Tween/PBS-MK solution	Volume
10 × PBS	50 mL
1 M MgCl$_2$	500 µL
2.5 M KCl	500 µL
PS20 (Tween 20)	0.014 %
H$_2$O	ad 500 mL

Sterile filtrate

2.5.7   rAAV Titer Determination using Quantitative Real-Time PCR

The genomic titer of the produced batches of rAAVs was determined by quantitative real-time PCR (qPCR). Basically, a standard curve was generated from a dilution series of an amplified fragment which was present in the vector plasmid to be measured. For this work, two different primer pairs were used. Primers to amplify the AAV2-ITRs were applicable to determine the vector genome concentration of all rAAVs containing the ITRs of AAV2. Primer pair 2 was used for all vectors containing the *hRHO194-hCNGB1a-SV40* plasmid. Both titer determinations showed similar results.

Primer pair 1 - AAV2-ITR:

ITR2 for: GCCGAGGACTTGCATTTCTG

ITR2 rev1: TCGGCCAAAGCCATTCTC

Primer pair 2 - hCNGB1-SV40:

hCNGB1a for: AGATCCTGTCGGTGAAGATGC

SV40 rev: TCAATGTATCTTATCATGTCTGCGG

The amplified elements were purified form the agarose gel as described before and the concentration was determined by Nanodrop (Thermo Fisher). To calculate the concentration of the standard for 10^{10} copies of viral genome per 5 μL, the following equation was used:

$$c = \frac{10^{10} \times 660 \times 10^{12}\ pg\ mol^{-1} \times fragment\ size}{6.022 \times 10^{23} mol^{-1} \times 5\ \text{μL}}$$

660×10^{12} pg mol^{-1} = mean molar mass of one base pair

6.022×10^{23} mol^{-1} = Avogadro constant

A 10-fold serial dilution was prepared, whereby the first dilution usually consisted of 10^{10} copies per 5 μL and the last one contained 10^{4} copies per 5 μL. The qPCR was performed using the SYBR^{TM} Select Master Mix (Thermo Fisher Scientific) and the StepOnePlus real-time PCR system (Thermo Fisher Scientific) according manufacturer's instructions. The rAAVs to be measured were diluted 1:100 in H$_2$O. Afterwards, the standard curve as well as the diluted rAAVs were pipetted as triplicates in a 96-well plate and the master mix was added subsequently as shown below. The fluorescent dye (SYBR Green) bound to the DNA and for each sample the fluorescence was measured throughout each PCR cycle. To analyze the virus concentrations, the standard curve was first generated by plotting the resulting C_t values (cycle threshold) against the logarithm of the dilution factors. The genomic titers were then calculated from the C_t values and the corresponding values of the standard curve.

qPCR reaction mixture 1	Volume		qPCR reaction mixture 2	Volume
SYBR Select Master Mix	10 μL		SYBR Select Master Mix	10 μL
ITR for (10 μM)	1 μL		hCNGB1 for (10 μM)	1 μL
ITR rev (10 μM)	1 μL		SV40 rev (10 μM)	1 μL
Template DNA	5 μL		Template DNA	5 μL
H$_2$O	ad 20 μL		H$_2$O	ad 20 μL

qPCR reaction protocol	Temperature	Duration	Cycles
Initial denaturation	95 °C	10 min	1 cycle
Denaturation	95 °C	10 s	
Annealing	60 °C	5 s	40 cycles
Elongation	72 °C	20 s	
Final elongation	72 °C	5 min	1 cycle

2.6   Production of rAAV Particles at Sanofi Genzyme

The production of all vectors used for the preclinical animal studies was conducted by Sanofi Genzyme (Framingham, MA, USA). They used two different manufacturing processes, the triple transfection technique using HEK293 cells as well as a large-scale vector production using a producer cell line. Lot#X17044A and Lot#X17044B were produced by triple transfection of HEK293 cells using polyethyleneimine. The detailed process is described elsewhere (Xiao and Samulski, 1998; Nass et al., 2018). Lot#R18026 was manufactured using a producer cell line. The whole process is described elsewhere in detail (Martin et al., 2013). Briefly, HeLaS3 cells (ATCC CCL-2.2) were transfected with a single plasmid containing the AAV2 *Rep* genes as well as the *Cap* genes of the desired serotype (e.g. AAV2/5), the vector genome flanked by AAV2 ITRs (e.g. *pGL2.0-hRHO194-CNGB1-SV40*), and a puromycin resistance gene. Stable clones were obtained by culturing the cells in the presence of puromycin. After screening the generated cell line for AAV productivity it was infected with wtAd5 virus. For both manufacturing platforms, a two-column vector purification was conducted using an AVB Sepharose HP column (GE Healthcare) followed by an anion exchange chromatography (Qu et al., 2007). Virus particle concentration was determined by TaqMan PCR assay (Nass et al., 2018). The three vectors produced by Sanofi Genzyme are listed below (vector diluent: BSS + 0.014 % Tween20).

Table 1: rAAV vectors produced by Sanofi Genzyme, that were used in this work. #. number, n.d. not determined, ad. Adenovirus, EU. endotoxin units

rAAV	Production technique	Lot #	Full capsid titer	Full capsid ratio	Endotoxin level	Residual infectious Ad
rAAV5.hCNGB1	triple transfection	X17044A	8.9×10^{12} vg mL^{-1}	n.d.	n.d.	n.d.
rAAV5.eGFP	triple transfection	X17044B	1×10^{13} vg mL^{-1}	n.d.	n.d.	n.d.
rAAV5.hCNGB1	producer cell line	R18026	9.7×10^{12} vg mL^{-1}	81 % full	<0.1 EU* mL^{-1}	none detected

BSS + 0.014 % Tween20	Volume
$C_2H_3NaO_2$	29 mM
$C_6H_8O_7$	6 mM
NaCl	110 mM
KCl	10 mM
$CaCl_2$	3 mM
$MgCl_2$	1 mM
PS20 (Tween 20)	0.014 %
pH 7.0	

2.7 Mouse *In Vivo* Experiments

2.7.1 Subretinal Injections

All *in vivo* interventions were performed under anesthesia evoked by intraperitoneal injection of a combination of ketamine (100 mg kg^{-1} body weight; Medistar GmbH, Ascheberg, Germany) and xylazine (10 mg kg^{-1} body weight, Xylariem®; Ecuphar GmbH, Greifswald, Germany), diluted in 0.9 % sodium chloride (NaCl 0.9 %, B. Braun, Melsungen, Germany).

Prior to an *in vivo* intervention, mice were anaesthetized and pupils were dilated by tropicamide eye drops (Mydriaticum Stulln, Pharma Stulln GmbH, Stulln, Germany). All used tools and surfaces were thoroughly cleaned using 70 % ethanol and ddH_2O. The procedure of rAAV subretinal injection was performed using a 34-gauge bevelled needle manually operated with a NanoFil syringe (World Precision Instruments, Sarasota, Fl, USA). The process was controlled by a surgical microscope (OPMI 1 FR Pro, Zeiss, Oberkochen, Germany). With the bevelled side facing up, the needle was carefully inserted from the *ora serrata* into the subretinal space at an angle of approximately 60 degrees. 1.0 μL of diluted viral particles were slowly delivered into the subretinal space (see figure 14). An injection was considered to be successful if, as a result, the formation of a bleb was visible, indicating a temporal subretinal detachment of the retina. To confirm the observed result, a further fundus and retinal monitoring was performed using spectral domain optical coherence tomography and fundus imaging using the Spectralis™ HRA + OCT diagnostic imaging platform (Heidelberg Engineering, Heidelberg, Germany; described in detail below). Mice showing any sign of retinal damage or no subretinal bleb were excluded from further analysis. Afterwards, all injected eyes were treated with dexamethasone and gentamicin ointment (Dexamytrex®, Bausch and Lomb, Berlin, Germany) for prevention of infection as well as for eye moisturization. Finally, mice were allowed to wake up on a 37 °C heat plate.
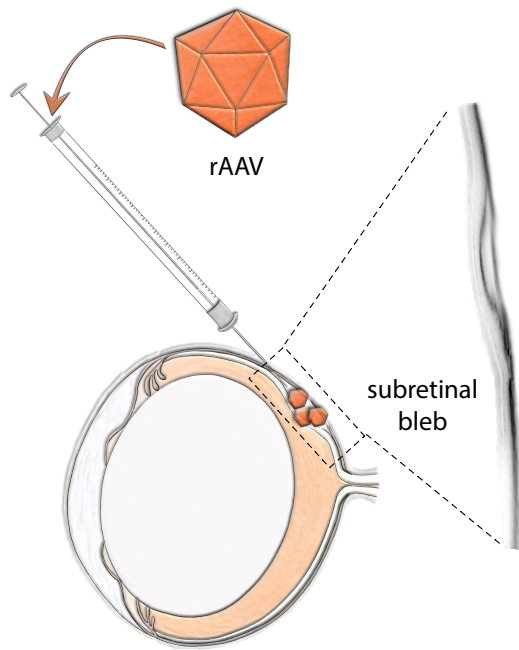
Figure 14: Subretinal injection of rAAVs into the mouse eye. The procedure of rAAV subretinal injection was performed using a 34-gauge bevelled needle manually operated with a NanoFil syringe (World Precision instruments). With the bevelled side facing up, the needle was carefully inserted from the *ora serrata* into the subretinal space at an angle of approximately 60 degrees. If the needle was visible beneath the retina, 1.0 µL of diluted viral particles were slowly delivered into the subretinal space. A temporal subretinal detachment seen as a subretinal bleb of the retina indicated a successful injection, which was confirmed spectral domain optical coherence tomography and fundus imaging using the Spectralis™ HRA + OCT.

2.7.2 Fluorescent Fundus Imaging

Fundus images were recorded using the Micron IV retinal imaging microscope (Phoenix Technology Group, Pasadena, CA, USA). Mice were anaesthetized and pupils were dilated as stated before. The eyes were moistened with 2 % hydroxypropyl methylcellulose (Methocel™, Santa Clara, CA, USA) and positioned in front of the retinal image lens. Bright field (450 nm) and fluorescent fundus images were obtained using the Streampix 6 software (Norpix, Montreal, QC, Canada). Mice were allowed to wake up as indicated above.

2.7.3 Monitoring the Retinal Morphology using Spectral Domain Optical Coherence Tomography

In case of mice, spectral domain optical coherence tomography measurements were conducted using an adapted Spectralis™ HRA + OCT diagnostic imaging platform (Heidelberg Engineering, Dossenheim, Germany) in combination with optic lenses as described previously (Schön et al., 2012). Mice were sedated and pupils were dilated as indicated above. Mice were placed on a platform and the light emitter and receiving unit (head) were positioned in front of the measured eye receiving one drop of Methocel™ and a corneal contact lens. OCT scans were obtained using a 12 ° circular scan mode. Following this procedure, it was taking care of mice as described above. Data was analyzed via the Heidelberg Eye explorer software (Heidelberg Engineering).

2.7.4 Functional Analysis of the Photoreceptors using Electroretinography (ERG)

Full field electroretinography measurements were conducted using the Celeris Fullfield ERG (Diagnosys LLC, Lowell, MA, USA). The following ERG measurements took place under scotopic (dark-adapted) conditions to assess rod-dominated activity. Before measuring, the animals had to be dark adapted overnight (>12 h). Animals were sedated and pupils were dilated as describe before. After completion of mydriasis, eyes were prevented from drying using Methocel^{TM} which also provides the corneal contact to the electrode. Both eyes are measured alternating for each light luminance level: while one eye was measured the other eye served as the reference, respectively. Flashes of varying luminance were directed towards the eyes and the responses were recorded by the ERG machine. For single-flash measurements, 7 different stimuli from 0.01 to 10 cd s m^{-2} were used (see below), based on the ISCEV standardized protocol for clinical dark-adapted ERG recordings (Marmor et al., 1989; regularly updated). All stimuli consisted of white light with a colour temperature of 6500 K. The time between the results as well as the inter sweep delays increased with increasing luminance level (from 10 to 22 s and from 5000 to 10000, respectively), whereas the 1st sweep delay was maintained constant (6000 ms). One result was generated by averaging 5 sweeps. 50 ms were recorded prior to one sweep, while post-trigger time was 300 ms. To ensure moisturization, all mouse eyes receive dexpanthenol eye and nose ointment (Bepanthen®, Bayer) after the *in vivo* experiment. Caretaking of mice was done as described before. Data was analysed by the Espion software (Diagnosys LLC).

Table 2: Scotopic single-flash ERG protocol used in this work. 7 different stimuli from 0.01 to 10 cd s m^{-2} were used, based on the ISCEV standardized protocol for clinical dark-adapted ERG recordings.

Step	Luminance	Results per run	Time between results / s	Sweep pre-trigger time / ms	Sweep post-trigger time / ms	Sweeps per result	1st sweep delay / ms	Inter sweep delay / ms	Pulse color
2	0.01 cd. cd s m^{-2}	1	10	50	300	5	6000	5000	white – 6500 K
3	0.03 cd s m^{-2}	1	10	50	300	5	6000	5000	white – 6500 K
4	0.1 cd s m^{-2}	1	17	50	300	5	6000	10000	white – 6500 K
5	0.3 cd s m^{-2}	1	17	50	300	5	6000	10000	white – 6500 K
6	0.1 cd s m^{-2}	1	22	50	300	5	6000	10000	white – 6500 K
7	0.3 cd s m^{-2}	1	22	50	300	5	6000	10000	white – 6500 K
8	10 cd s m^{-2}	1	22	50	300	5	6000	10000	white – 6500 K

2.7.5 Visual Water Maze Task

A modified Morris Water Maze (Morris, 1984) was previously implemented as a test for vision-guided behavior (Koch et al., 2012). In this work, the published protocol was carried out in a modified version without landmarks. In a circular swimming pool (120 cm in diameter, 70 cm high, white plastic; TSE Systems, Bad Homburg, Germany) mice had to locate a floating platform (10 cm in diameter). Since mice are shy of water, they try to search for a place where they can escape the pool. Therefore, this task has a high motivational factor, which encourages the mice to swim until they find the floating platform. The swimming route of each mouse was recorded by a camera and monitored using the VideoMot2 software by TSE Systems. The design of the visual Water Maze task is shown in figure 15. The experiment was conducted for two days at dim light conditions of 0.32 cd m^{-2} (red light; the luminance was determined using the LS-100 luminance meter by Minolta, Marunouchi, Japan) to observe rod-mediated vision-guided behavior. Therefore, mice had to be dark adapted prior to each task for at least 12 h. Lastly, one day was performed under bright light conditions (82.8 cd m^{-2}) to test cone-specific vision. From trial to trial (6 trials a day) the starting position of the mouse was changed in a pseudorandom order, whereas the platform was kept in a constant location for one day. Each day, the platform was placed at a new position. One trial ended either if the mouse climbed onto the platform or if it had been swimming for 120 seconds. If the mouse did not find the platform, it was gently placed on it. After each trial, the mouse was allowed to sit undisturbed (for 10 s) on the platform, before warmed by a heating lamp and transferred to its home cage. The experiment was performed and analyzed blindly to the animal genotype.
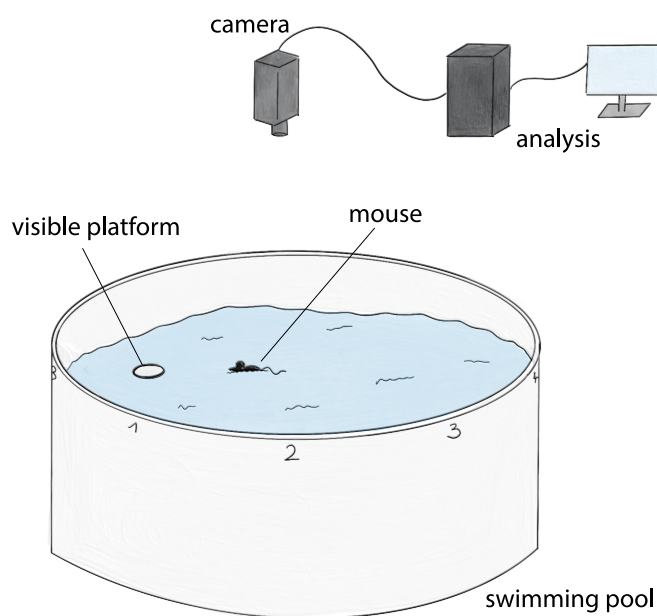
Figure 15: Experimental design of the visual Water Maze task. Mice were put into a circular swimming pool (120 cm in diameter) to locate a stable platform (10 cm in diameter) without the help of any landmarks. The swimming route of each mouse was recorded by a camera and monitored using the VideoMot2 software by TSE Systems. The experiment was conducted for two days at dim light conditions of 0.32 cd m^{-2} (red light) and one day under bright light conditions (82.8 cd m^{-2}). From trial to trial (6 trials a day) the starting position of the mouse was changed, whereas the platform was kept in a constant location for one day. One trial ended either if the mouse climbed onto the platform or if it had been swimming for 120 seconds.

2.8   Dog *In Vivo* Experiments

Dog housing, subretinal injections, all *in vivo* experiments, as well as tissue dissections were conducted at the College of Veterinary Medicine at the Michigan State University, MA, USA, by the work group of Prof. Simon Petersen-Jones.

2.8.1   Subretinal Injection

Anesthesia was performed by standard veterinary techniques. Acepromazine served as premedication, anesthesia was induced by IV propofol, and intubation and maintenance were performed using isoflurane. Pupils were dilated with tropicamide eye drops. Subretinal injections were performed as previously described (Petersen-Jones et al., 2009). Briefly, the subretinal injection was performed under direct observation through an ophthalmic surgical microscope (Opmi6. Carl Zeiss Meditech Inc., Dublin, CA, USA) and a Machemer vitrectomy lens (Ocular Instruments, Bellevue, WA, USA) using a subretinal injector (RetinaJect. SurModics Inc., Irvine, CA, USA) (Komaromy et al., 2006). The injector (equipped with a 39-gauge needle) was inserted through the pars plana and pushed through the vitreous cavity towards the retinal surface. Each dog received two injections containing 100 µL volume into the subretinal space. The formation of a subretinal detachment was recorded.

2.8.2   Electroretinography

Full-field bilateral ERGs were performed as previously described (Annear et al., 2011; Winkler et al., 2013). Dark-adapted responses to a luminance series (15 flash stimuli ranging in luminance from -3.7 to 3.6 log cd s m^{-2}) were simultaneously recorded using an Espion E2 electrophysiology unit (ColorDome Ganzfeld; Diagnosys LLC).

2.8.3   Vision Testing

For investigation of visual acuity of a dog, the four-choice vision testing device was used (Gearhart et al., 2008). Briefly, a dog was placed in a non-transparent box with four tube-shaped exits. Three of these tubes were blocked at the external side, leaving only one tube that allowed access to the outside. With a camera, the behaviour of the dog was recorded. After each trial a different tube was opened, so that the dog had to find the exit again each time and the learning factor was excluded. The time it took a dog to find the exit was measured, as well as the number of attempts a dog needed to find the right exit. Seven

levels of lighting were measured, ranging from scotopic to mesopic to photopic light levels. Each eye was tested separately by covering the contralateral eye with an opaque contact lens.

2.8.4   Immunohistochemistry

For retinal dissection, the mouse eyes were enucleated and temporarily inserted into ice cold 0.1 M PB. Using a stereomicroscope (Stemi 2000, Zeiss), the eye was pierced with a cannula (21G, Sterican, B. Braun) at the *ora serrata* and then fixed in 4 % paraformaldehyde (PFA) for 5 min on ice. Using micro scissors (Vannas Spring Scissor – 2.5 mm Cutting Edge, Fine Science Tools, Heidelberg, Germany) and micro forceps (Dumont #55, Fine Science Tools) the eye was cut along the *ora serrata* to remove cornea, vitreous, and lens. The remaining eye cup was fixed in 4 % PFA for 45 min on ice. Afterwards, the eyes were washed three times with 0.1 M PB and then incubated in 30 % sucrose (in 0.1 M PB) overnight at 4 °C for cryoprotection. Finally, the eyecup was embedded in tissue freezing medium (Tissue-Tek® O.C.T.™ Compound, Sakura Finetek™), frozen on dry ice, and stored at -80 °C until use.

0.1 M PB	Volume
$Na_2HPO_4 \times 2H_2O$	28.48 g
$NaHPO_4 \times H_2O$	5.52 g
H_2O	ad 2 L
Adjust pH to 7.4 and sterile filtrate	

4 % PFA	Volume
Paraformaldehyde	6 g
0.1 M PB	ad 150 mL
Dissolve at 60 °C and sterile filtrate	

Euthanasia of the dogs was performed by an overdose of pentobarbital. Eye removal, fixation, and embedding were performed as described earlier (Mowat et al., 2012). After fixation in 4 % paraformaldehyde (paraformaldehyde powder 95 % in PBS) and embedding in OCT (TissueTek OCT, Electron Microscopy Sciences, Hatfield, PA, USA), the eyes were frozen on dry ice and shipped to the LMU for slicing.

Cryosections were obtained using a cryostat (Leica CM3050 S, Leica, Wetzlar, Germany). The embedded mouse tissue was sliced into 10 µm sections while the thickness of the dog tissue sections was 14 µm. After mounting the tissue on coated glass object slides (Super Frost Plus, Menzel, Thermo Fisher Scientific), it was dried at RT and stored at -20 °C.

Immunohistochemistry staining for mouse and dog retinal tissue was performed in a similar way. First, the cryosections were thawed at RT followed by generating a hydrophobic barrier using a liquid blocker pen (Super PAP Pen Liquid Blocker, Science Services) by surrounding the individual tissues with the pen. After rehydrating the tissue with 0.1 M PB for 5 min, the cryosections were fixed with 4 % PFA in

0.1 M PB for 10 min. Afterwards, the tissue was washed three times with 0.1 M PB and then incubated overnight at 4 °C with the primary antibodies (see table 3) diluted in 0.1 M PB with 5 % ChemiBlocker (CB, Millipore) and 0.3 % Triton X-100. The next day, the tissue was washed thrice with 0.1 M PB followed by a 1.5 h-incubation at RT with the secondary antibodies (table 3), that were diluted in 0.1 M PB with 3 % CB. After the sections were washed again three times with 0.1 M PB, the nuclei were stained for 5 min with Hoechst 33342 solution (Invitrogen, 10 µg mL^{-1} in 0.1 M PB). After a final washing step with 0.1 M PB for 5 min the tissue was mounted using Fluoromount-G medium (Thermo Fisher Scientific, Waltham, MA, USA) and a cover slip (#1.5; Menzel, Thermo Fisher Scientific) and stored at 4 °C.

Table 3: Primary antibodies used for immunohistochemistry.

Primary antibody	Host	Working dilution	Source	Target
Anti-cone arrestin	rabbit	1:300	Kindly provided by Prof. Wolfgang Baehr, University of Utah; stored at -20 °C (Zhang et al., 2012)	cone photoreceptors
Anti-cGMP	sheep	1:3000	Dr. HWM Steinbusch, Maastricht University Medical Center; stored at -20 °C (Tanaka et al., 1997)	rod and cone photoreceptors
Anti-GFAP, Cy3-conjugated, # C9205	mouse monoclonal	1:1000	Sigma-Aldrich, MO, USA; stored at 4 °C, Michalakis et al., 2005)	Müller glia
Anti-Iba-1, #019-19741	rabbit	1:500	Wako, Richmond, VA, USA; stored at -20 °C	microglia
PNA, FITC-conjugated #L7381	lectin	1:100	Sigma-Aldrich, MO, USA; stored at 4 °C	cone photoreceptors
Anti-CNGB1, #HPA039159	rabbit	1:2000	Sigma-Aldrich, MO, USA; stored at -20 °C	rod photoreceptors
Anti-CNGA1, Pmc2G11	mouse	1:30	kindly provided by Prof. Robert Molday; University of British Columbia; Vancouver; stored at 4 °C (Molday et al., 1991)	rod photoreceptors

Table 4: Secondary antibodies used for immunohistochemistry.

Secondary antibody	Host	Working dilution	Source	Target
Alexa488-conjugated anti-mouse, #1397999	goat	1:800	Life Technologies; CA, USA; stored at 4 ℃	mouse
Cy3-conjugated anti-rabbit #711-165-152	donkey	1:400	Jackson Immuno Research, PA, USA; stored at 4 ℃	rabbit
Alexa488-conjugated anti-rabbit	goat	1:800	Life Technologies; CA, USA; stored at 4 ℃	rabbit
Cy2-conjugated anti-sheep, #713-225-147	donkey	1:200	Jackson Immuno Research, PA, USA; stored at 4 ℃	sheep

2.8.5 Laser Scanning Confocal Microscopy

Laser scanning confocal microscope images were obtained using a Leica SP8 confocal system (Leica) equipped with the following lasers: 405, 448, 514, and 552. Images were acquired as confocal z stacks using the LAS X software (Leica) and deconvolved by the Huygens software Suite (Scientific Volume Imaging B.V., The Netherlands) using a signal to noise ratio of 5. Maximum projection (merging of all z stacks) and background subtraction (value of 30) was conducted via the Fiji ImageJ software.

2.9 Statistics

Statistical significance was evaluated via the GraphPad Prism software (version 8). As statistical tests, either paired, or unpaired Two-way analysis of variance (ANOVA) tests have been conducted followed by Sidak's *post-hoc* test for multiple comparison. All values are given as mean ± standard error of the mean (SEM). n is the number of independent measurements and measured values were considered to be statistically significant if the p-value was less than or equal to 0.05. It is defined precisely as follows: *, $p \leq 0.05$, **, $p < 0.01$. ***, $p < 0.001$.

2.10 Software Used in this Work

Table 5: Software used in this work.

Application	Software	Company
Cloning	SnapGene Viewer	GSL Biontech LLC, San Diego, CA, USA
Vector purification	PrimeView 5.31	GE Healthcare, Chicago, IL, USA
qPCR	StepOnePlus	Thermo Fisher Scientific, Waltham MA, USA
Fundus imaging	Streampix 6	Norpix, Montreal, QC, Canada
ERG analysis	Espion	Diagnosys LLC, Lowell, MA, USA
OCT analysis	Spectralis diagnostic imaging	Heidelberg Engineering, Heidelberg, Germany
Behavioral analysis	VideoMot2	TSE Systems, Bad Homburg, Germany
Confocal imaging	LasX	Leica, Wetzlar, Germany
Image processing	Huygens Essential	Scientific Volume Imaging B.V., Hilversum, The Netherlands
	Image J Fiji	
	Affinity Photo	Serif (Europe) Ltd., Nottingham, UK
Statistical analysis and graphics	Prism 8	GraphPad, San Diego, CA, USA
Illustration	Procreate	Savage Interactive Pty Ltd.
	Affinity Designer	Serif (Europe) Ltd., Nottingham, UK

3   Results

In this work, the biological efficacy of a recombinant AAV carrying a human *CNGB1*, which expression is controlled by a shortened and optimized human rhodopsin promoter, was assessed using a *Cngb1* KO mouse model as well as a *Cngb1* KO dog model aiming to evaluate it as a potential candidate for a gene supplementation therapy in humans.

3.1   Design and Production of rAAV5.hCNGB1

In addition to its numerous advantages as a vector, the adeno-associated virus (AAV) only has a low cloning capacity of maximum 5.2 kb (from 5'ITR to 3'ITR), while the production yield is markedly decreased for transgenes exceeding the AAV genome size of 4.7 kb (Grieger and Samulski, 2005; Wu et al., 2010; Dong et al., 2010; Lai et al., 2010). However, the transcripts of the majority of genes expressed in photoreceptors, which mutations are known to lead to hereditary degenerative diseases, have almost this or even a larger size. The cDNA of the human *CNGB1* gene has a size of about 3.7 kb, so the regulatory elements had to be incorporated into the plasmid within 1.5 kb. Therefore, shortened *cis*-regulatory elements were used in order to obtain an AAV plasmid harboring the full-length gene precisely fitting into the AAV vector together with the necessary regulatory elements in *cis*. To achieve a rod-specific expression, the human rhodopsin promoter (*hRHO*) was chosen, as it is known to be a suitable promoter to ensure strong target gene expression in rod photoreceptors (Lem et al., 1991; Zack et al., 1991; Flannery et al., 1997). In addition, the murine rhodopsin promoter (*mRho*) already showed specific gene expression in *Cngb1* KO mice (Koch et al., 2012). However, combining the coding sequence of the full-length *hCNGB1* together with a full-length *hRHO* and an additional terminator, would lead to package capacity excision. Hence, this condition made the intended construct consisting of a *hCNGB1* coding sequence under the control of a *hRHO* a reasonable candidate for the design of a shortened *hRHO* without any loss of its efficiency and specificity.

In the past, the conserved sequences for the binding of transcription factors (TFs) were already identified in the rhodopsin promoter. Using the example of *mRho*, it was shown that within the last 200 base pairs three binding sites for CRX are present, as well as one for NRL, which are sufficient to ensure efficient rod-specific expression of the downstream gene (Lee et al., 2010). The *Crx* gene encodes for the cone-rod homeobox protein and is expressed in both rods and cones (Chen et al., 1997), whereas the neural retina-specific leucine zipper protein, encoded by the *Nrl* gene, is exclusively expressed in rod photoreceptors (Swaroop et al., 1992; Swain et al., 2001; Mears et al., 2001). Both transcription factors

interact with each other in order to regulate the expression of rhodopsin and thus largely contribute to rod cell development (Rehemtulla et al., 1996; Mitton et al., 2000; Mears et al., 2001; Hennig et al., 2008; Reks et al., 2014). In order to design the short human *RHO*, the same binding sites for CRX and NRL were searched within the full-length *hRHO* since they are highly conserved within mammals. By taking into account the conserved TF binding sites, a sequence over 194 bp (figure 16; from bp 617 to bp 810 of the full-length *hRHO* promoter) was defined as the optimal shortened *hRHO* promoter.
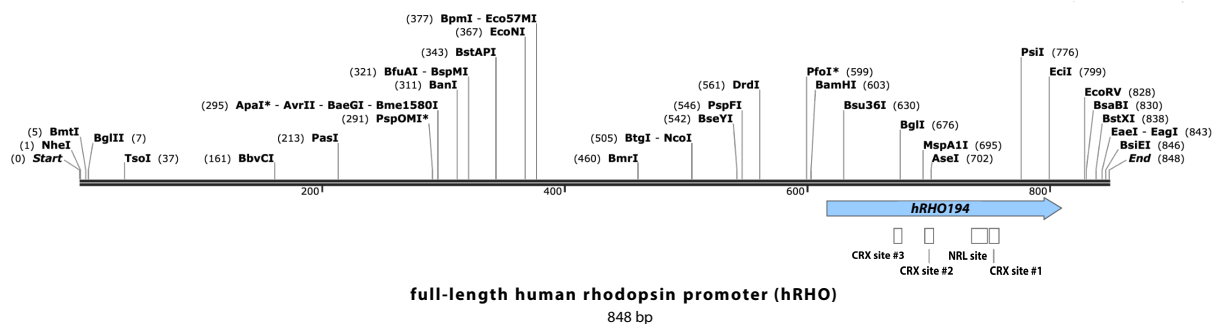
Figure 16: The short human rhodopsin promoter (*hRHO194*). The transcription factor binding sites (conserved motifs) necessary for efficient and rod specific transgene expression are located within the 3' region of the human rhodopsin promoter. The short *hRHO* was designed with a sequence over 194 bp from position 617 to 810 of the full-length *hRHO* containing three CRX sites and one NRL motif.

The short *hRHO* (194 bp) was placed upstream of the full-length transcription variant 1 of *hCNGB1* (NM_001297.4; 3.75 kb) to produce the recombinant vector plasmid. Together with a previously used short polyadenylation signal (*Sv40*; 221 bp; Koch et al., 2012), acting as an effective termination and polyadenylation enhancer (Schambach et al., 2007), the promoter and the transgene were inserted between the inverted terminal repeats (ITRs) of serotype 2 originating from the pSub201 cis-plasmid (131 bp each; Samulski et al., 1987; Schön et al., 2017). Finally, the size of the recombinant vector was 4.66 kb from 5'ITR to 3'ITR and thus did not exceed the packaging capacity of rAAV vectors.

To guarantee a photoreceptor-targeted transgene expression, the recombinant plasmid was packaged in AAV2/5, due to its well-proven ability to transduce postmitotic photoreceptors following subretinal injection in various animal models (Yang et al. 2002; Lotery et al., 2003; Mancuso et al., 2009; Beltran et al., 2010; Boye et al., 2012; Banin et al., 2015). For the first proof-of-concept experiments, the vector was produced in-house by triple transfection using HEK293T cells. For the preclinical animal studies, two vector batches carrying this construct were produced at Sanofi Genzyme at the Framingham facility, MA, USA. For one batch, the rAAV was produced as a triple transfection vector in HEK293 cells (Lot #X17044A; see figure 4A) to primarily assess biological efficacy in the *Cngb1* KO mouse model. This batch was also used for the large animal dose escalation study conducted in a *Cngb1* KO dog model. A

second vector batch was obtained through a HeLaS3-based producer cell line (PCL; Lot#R18026; figure 4B) for a further assessment of dose dependency and long-term efficacy in the *Cngb1* KO mouse model.

3.2 The *hRHO194* Promoter has Driven Efficient, Specific, and Stable Transgene Expression in Rod Photoreceptors

Before both hCNGB1-vectors were used for preclinical animal studies, the designed *hRHO194* promoter was tested for specificity and efficiency. Therefore, a control vector (Lot#X17044B; the transgene expression cassette is illustrated in figure 17A) was applied carrying the same plasmid as Lot#X17044A and Lot#R18026, but possesses the cDNA encoding the enhanced green fluorescent protein (eGFP) instead of the *hCNGB1* gene. Due to the fluorescent characteristics of the eGFP, it was possible to monitor the expression level *in vivo*. In order to do this, 10^{10} vector genomes (vg) of Lot#X17044B (1 µL volume) were injected subretinally into the eyes of adult wildtype mice (*Cngb1* wildtype) and the expression of eGFP was recorded by fundus fluorescence imaging using the Micron IV retinal imaging microscope (Phoenix Technology Group). Pictures were collected at 2, 4, and 6 weeks post injection (*pi*) and are illustrated in figure 17A. At 2 weeks *pi*, eGFP fluorescence was already measurable while intensifying at 4 weeks and further at 6 weeks *pi*. The eGFP expression was seen across approximately 30 % of the retina. This range increased only marginally in size over time, indicating that only minimal lateral spreading occurred. This showed, that the area of target gene expression was restricted to the area of the subretinal bleb covering about 30 % of the retina (highlighted by the grid line in the bright field image). In order to test the vector for rod-specificity, mouse retinas were dissected at 8 weeks *pi* and immunohistochemistry of the respective cryosections was performed. Cones were visualized using an antibody against murine cone arrestin (CAR), which is a marker for cone cells (Zhang et al., 2012). The respective confocal images (figure 17A, upper pictures) showed a distinct native eGFP expression within the photoreceptor layer. The green fluorescence was mainly visible in the outer nuclear layer (ONL) and in the inner segments (IS) of the photoreceptors. Furthermore, a faint signal was seen in the outer segments (OS). The staining with anti-CAR revealed no overlap of the green eGFP fluorescence and the red signal representing the cone marker expression. This indicated, that eGFP was not expressed in cones and consequently, the *hRHO194* promoter provoked an expression restricted to rod photoreceptors.

Previous studies demonstrated a lack of the murine CNGB1 protein in the *Cngb1* KO mouse model due to a non-functional expression caused by a mutation in exon 26 (Hüttl et al., 2005, see sections 1.6.3 and 2.2). Furthermore, an efficient and stable mCNGB1 expression was already achieved in the *Cngb1* KO mouse after introducing mCNGB1 using AAVs (Koch et al., 2012). To investigate whether it is possible

to also achieve a human CNGB1 expression in rod cells of this mouse model, 4-week-old *Cngb1* KO mice were injected into the subretinal space (see figure 14) with 10^{10} vg (1 µL) of rAAV5.hCNGB1 (Lot#X17044A; displayed in figure 17B). The contralateral eyes received the same volume of PBS-MK (sham-injected eyes).

The retinas were dissected 9 months *postnatal* (*pn*) and immunohistochemistry was performed using an antibody against CNGB1 (#HPA039159, Sigma-Aldrich) binding the carboxyterminal region of the human as well as of the murine and the canine CNGB1 protein. Figure 17B illustrates confocal images displaying the CNGB1 expression as a red signal and the nuclei in blue using Hoechst 33342. The treated area of the *Cngb1* KO retina represented the part of the retina covered by the subretinal bleb (up to 30 % of the retina – closer to the injection site), while the untreated area showed a cross section outside of the treated part (more far from the injection site). The treated area revealed a distinct expression of the CNGB1 (red) in the photoreceptor layer (figure 17B, upper pictures), whereas there was no red signal visible in the untreated part of the same retina (figure 17B, lower pictures). This demonstrates, that the human *CNGB1* gene under the control of the human *RHO194* promoter was expressed in mouse rod photoreceptors leading to the production of the human CNGB1 subunit. It further points out, that the forced transgene expression was stable until at least 8 months post treatment.

It is known that native rod CNG channel subunits (CNGB1 and CNGA1) are formed to heterotetrametric channels in the inner segments of rods, but are subsequently transported to the ROS. Therefore, rod CNG channels are natively localized in the plasma membrane of the ROS (Kaupp and Seifert, 2002; Zheng et al., 2002; Biel et al., 2009). However, the human CNGB1 protein was not strictly localized in the ROS, but was also found in the inner segments of these cells (figure 17B, upper left picture). This suggested, that not all AAV-born CNGB1 subunits were able assemble with the three required CNGA1 subunits to form a wildtype-like heterotetrameric CNG channel complex. Only heterotetrameric channels are transported to the OS. Thus, CNGB1 signal in the inner segment might suggest that the vector was overdosed, or the human CNGB1 subunit was not efficiently forming a functional CNG channel together with the murine CNGA1.

In addition, Hoechst 33342 staining revealed a presence of about 9 layers of photoreceptor nuclei in the treated part of the retina (figure 17B, upper pictures), whereas only 2 layers were left in the untreated *Cngb1* KO retina (figure 17B, lower pictures). This suggests, that the rAAV5.hCNGB1 treatment (Lot#X17044A) at 4 weeks of age achieved a rescue of the photoreceptor cells from degeneration at least until the *Cngb1* KO mouse was 9 months old.
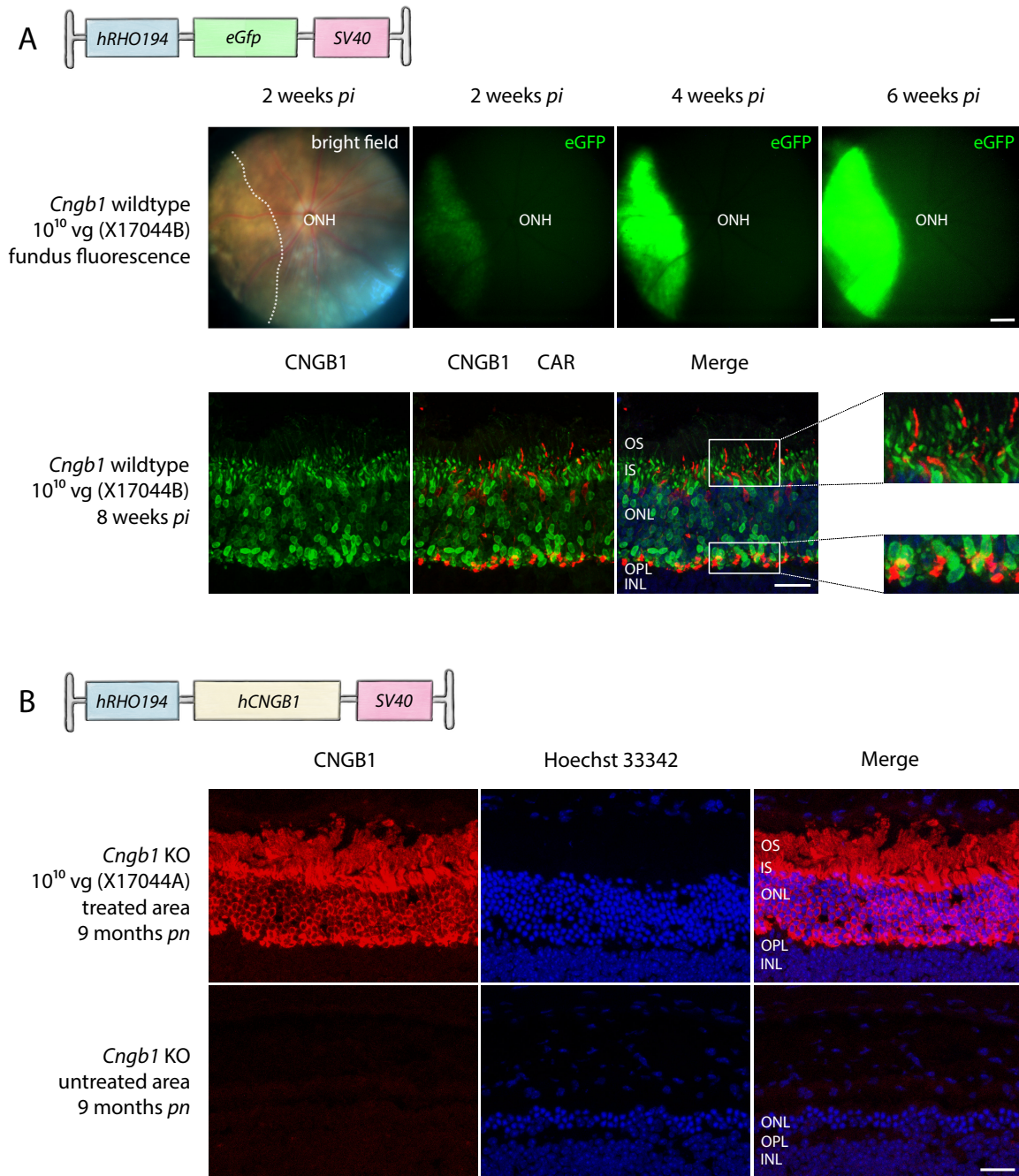
Figure 17: The *hRHO194* promoter has driven efficient, specific, and stable transgene expression in rod photoreceptors.
A. Native eGFP florescence in a wildtype mouse after a subretinal injection of 10^{10} vg (1 µL) of rAAV5.eGFP (Lot#X17044B). Representative fundus fluorescence images (upper pictures) showing eGFP fluorescence at 2, 4, and 6 weeks *pi* revealed transgene expression starting about 2 weeks after injection and reaching the plateau about 6 weeks *pi*. The grid line shows the subretinal bleb. Scale bar marks 200 µm. In the lower pictures, representative confocal images of a retinal cross section showing native eGFP fluorescence (green signal), cone arrestin expression (red signal), and Hoechst (blue signal), are illustrated. Merging revealed no overlap of the green and the red signal indicating a rod-specific expression. Scale bar marks 25 µm. B. Representative confocal images of human CNGB1 expression in cross sections of a *Cngb1* KO mouse retina treated with rAAV5.hCNGB1 (Lot#X17044A – 10^{10} vg) at 9 months (8 months *pi*). The treated area displayed a distinct expression of the *hCNGB1* gene (red signal, upper left picture) in the ONL as well as in the photoreceptor OS whereas there was no red signal visible in the untreated part of the same retina (lower left picture). Hoechst 33342 staining revealed 8 lines of photoreceptor nuclei (shown in blue) in the treated part of the retina (upper middle picture) whereas only 2 layers were left in the untreated area (lower middle picture). Both pictures at the right side (merge) show the combination of CNGB1 and Hoechst 33342. Scale

bar marks 25 μm. ONH. Optic nerve head, OS. outer segments, IS. inner segments, ONL. outer nuclear layer, OPL. outer plexiform layer, INL. inner nuclear layer

3.3 Design of the Preclinical Mouse Dose Escalation Study

To investigate, whether the vector was overdosed by applying 10^{10} vg of X17044A to the *Cngb1* KO mouse model, or whether there was a poor compatibility of murine and human CNG subunits, preclinical dose escalation studies were designed using *Cngb1* KO mice as well as *Cngb1* KO dogs to also further assess the vector efficacy in a large animal model. For the preclinical mouse study, a producer cell line vector was used (Lot#R18026) and injected as 3 different dosages (10^8, 10^9, and 10^{10} vg; 1 μL volume) into 4-week-old *Cngb1* KO mice (twelve mice for each group). The contralateral eyes received 1 μL of the respective vector diluent (BSS + 0.014 % Tween20). 2 and 8 months after the treatment visual function was analyzed by fullfield electroretinography and the process of retinal degeneration was monitored 2, 4, and 8 months *pi* by spectral-domain optical coherence tomography (SD-OCT). Additionally, spatial navigation was observed by visual Water Maze (WM) at 8 months *pi* to get information about the processing of the visual information in treated mice. Transgene expression as well as cell morphology and physiology were investigated by immunohistology at 10 months *postnatal (pn)*. The design of the dose escalation study using the PCL-vector is shown in figure 18.
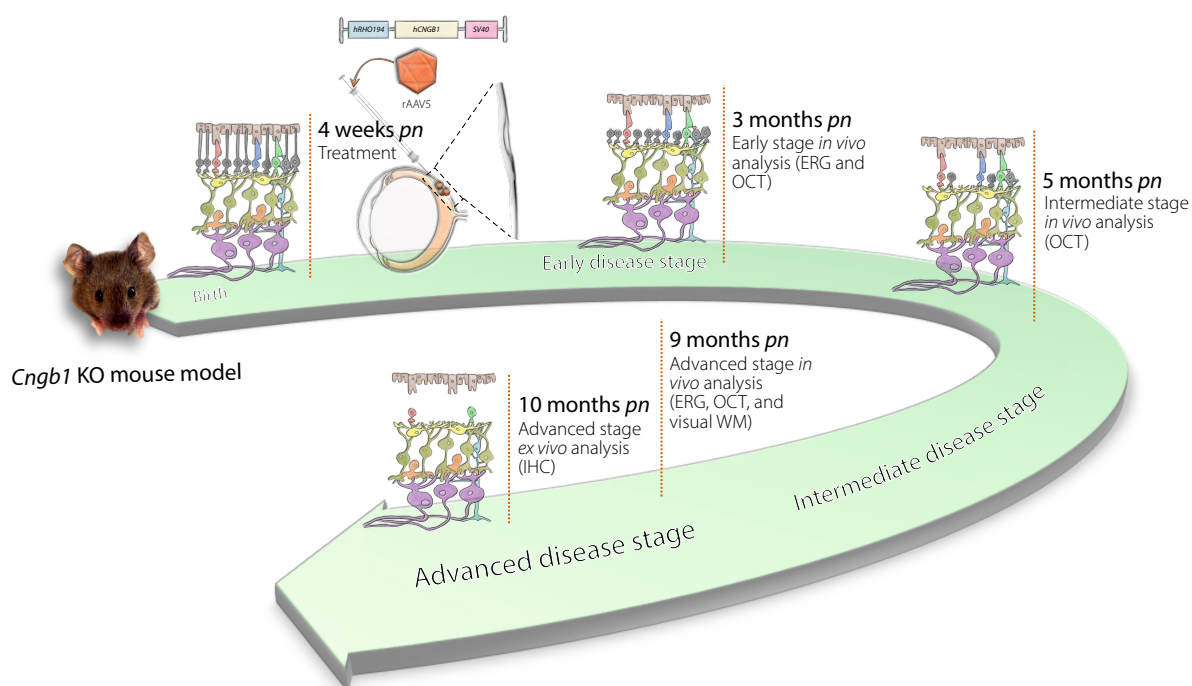
Figure 18: Design of the preclinical mouse dose escalation study. For the preclinical evaluation of rAAV5.hCNGB1 the *Cngb1* KO mouse model was used. In this mouse line the degeneration of the ROS starts at the age of about 2 weeks. By the age of 3 months the outer segments are almost completely degenerated. At this time, the rod cell bodies have also started to degenerate

(starting at approximately 2 months *pn*), resulting in a considerably thinner ONL 2 months later (5 months *pn*). The cone cells are almost not affected until this time. In the advanced phase of the disease, the cones also degenerate (mutation-independent), so that at the age of 10 months only one row of cell nuclei remains in the ONL, consisting of a few non-functional cone cell nuclei. For gene supplementation rAAV5.hCNGB1 was injected subretinally to 4-week-old *Cngb1* KO mice. 2, 4, and 8 months after the treatment visual function was measured by ERG and retinal morphology was monitored by OCT. Spatial navigation was investigated by visual Water Maze at 9 months *pn*. At 10 months *pn*, retinas were dissected in order to perform immunohistochemistry. *pn. postnatal.* rAAV5. Recombinant AAV serotype 5. ERG. Electroretinography. OCT. Optical coherence tomography. WM. Water Maze. IHC. Immunohistochemistry

Table 6 points out the number of mice of each mouse group that performed within the dose escalation study using the PCL vector (Lot#R18026). Mice were defined as non-responders, if they did not show any difference to control in all *in vivo* experiments (the Water Maze was excluded from this evaluation) and in addition revealed a lack of the transgene shown by immunohistochemistry at the end of the study (or if the IHC could not be performed for the respective mouse). Non-responders were excluded from the entire evaluation of the study. In most cases, non-response was correlated with an incorrect subretinal injection, so that either a slight penetration of the retina led to an incomplete virus application, or a damage occurred, which manifested itself as a cataract later in the study. Other causes or remarks were listed specifically for each mouse. Lists for all responders and non-responders with the respective comments as well as an overview of the results can be read in the appendix (tables S1-S6).

Table 6: Number of mice used for the mouse dose escalation study using the PCL vector (R18026). Vector Lot and dose are listed for each mouse group as well as the number of dead mice and non-responders. *pn. postnatal, pn. post injection,* w. week/weeks, m. month/months

Group	Initial number of Animals	Vector	Vector Dose (total vg per eye)	Dead mice	Non-responders	Number of animals used for the study
1	12	AAV5.hCNGB1 (R18026)	1.0×10^8	1 dead mouse (excluded) 1 mouse developed a cataract (excluded)	3 (excluded)	7
2	12	AAV5.hCNGB1 (R18026)	1.0×10^9	1 dead mouse (excluded) 1 mouse developed a cataract (excluded)	3 (excluded)	7
3	12	AAV5.hCNGB1 (R18026)	1.0×10^{10}	-	2 (excluded)	10

3.4 Transgene Expression and Biological Efficacy of rAAV5.hCNGB1 in *Cngb1* KO Mice was Dose Dependent

In order to assess dose dependency of rAAV5.hCNGB1, the Lot#R18026 was injected as 3 different vector doses to 4-week-old *Cngb1* KO mice. Mouse group 1 received 10^8 vg (low dose), 10^9 vg were applied to mouse group 2 (mid dose), and 10^{10} vg were administered to mouse group 3 (high dose). At the end of the study (at 10 months *pn*), the mouse eyes were enucleated and the transgene expression was analyzed in retinal cryosections by immunohistology. Figure 19A demonstrates the expression of hCNGB1 in all three mouse groups 9 months after the injection with Lot#R18026 and thus, the long-term persistence of rAAV5.hCNGB1 and therefore also the long-term expression of hCNGB1 was confirmed by a large-scale vector. However, an obvious dose dependency was also disclosed for Lot#R18026 in the *Cngb1* KO mouse model (figure 19A).

Representative confocal images of mouse group 2 revealed a rescue of about 8 layers of photoreceptor cells at 10 months of age, whereas there were only 1 row remaining in the untreated *Cngb1* KO retina. Thus, the results of the mid-dose treatment with R18026 (10^9 vg) were similar to what was achieved by application of 10^{10} vg of X17044A. This indicated that it was possible to reduce the vector concentration by a factor of 10 while still generating similar results. However, in both mouse groups 1 and 3, only 3-4 layers of photoreceptors have survived to the 10-month time point. Furthermore, the red signal (hCNGB1) was faint in case of group 1 suggesting that 10^8 vg were too less to achieve a sufficient level of transgene expression. 10^{10} vg, however, resulted in a distinct and high-level hCNGB1 expression of Lot#R18026, but the lower number of survived photoreceptor cells indicated that the high vector concentration of 10^{10} vg might have induced photoreceptor death. This was not the case for the treatment with the same vector dose using Lot#X17044A (figure 17B), suggesting toxic side effects of the PCL vector batch.

By comparison of the mid-dosed retinas with the wildtype tissue it was evident that not all photoreceptors were rescued from degeneration in the *Cngb1* KO mouse model. Hoechst 33342 staining displayed 13-14 lines of photoreceptors in the *Cngb1* wildtype retina while about 8 rows were found for the mid-dosed mouse group (group 2; figure 19A). Furthermore, treatment with R18026 also led to CNGB1 localization to the IS. The native CNGB1 localization in the ROS is shown in the cross section of the *Cngb1* wildtype retina (figure 19A).

In the past, it was shown that the CNGA1 subunit, although being capable of forming homomeric functional channels *in vitro*, is not detectable in the *Cngb1* KO mouse retina (Hüttl et al., 2005). Furthermore, it was demonstrated, that in response of supplementing mCNGB1, the endogenous *Cnga1*

gene expression was rescued and mouse CNGA1 protein became detectable in this mouse model (Koch et al., 2012). Confocal images of an untreated *Cngb1* KO mouse are shown in figure 19B confirming that CNGA1 (green signal) was not present in the retina at the age of 10 months. After treatment with rAAV5.hCNGB1 using vector Lot#R18026, the amount of CNGA1 within the ROS was distinctly increased, although the signal was lower compared to the wildtype (figure 19B). The green background staining, which was visible in the extracellular spaces within the RPE and in the OPL of the untreated *Cngb1* KO retina, resulted from the fact that the anti-CNGA1 antibody was produced in the mouse. The anti-mouse secondary antibody used for the IHC did not distinguish between endogenous mouse immunoglobulins within the sample tissue and the mouse primary antibody (CNGA1). Merging revealed in the treated retina only an overlap of the red (CNGB1 expression) and the green signal (CNGA1) demonstrating heterotetrametric channel formation consisting of human CNGB1 and murine CNGA1 and transport of the properly assembled chimeric (mouse CNGA1/human CNGB1) heterotetrameric channels to the ROS. In addition, there were no CNGA1 proteins detectable in the inner segments of the rods, confirming that the endogenous CNGA1 protein level represented the limiting factor for heterotetrameric CNG channel formation.

A

| CNGB1 | Hoechst 33342 | Merge |

Cngb1 KO
10^8 vg (R18026)
treated area
10 months *pn*

OS
IS
ONL
OPL
INL

Cngb1 KO
10^9 vg (R18026)
treated area
10 months *pn*

OS
IS
ONL
OPL
INL

Cngb1 KO
10^{10} vg (R18026)
treated area
10 months *pn*

OS
IS
ONL
OPL
INL

Cngb1 KO
10 months *pn*
untreated area

ONL
OPL
INL

Cngb1 wildtype
untreated

OS
IS
ONL
OPL
INL

B

| CNGB1 | CNGB1 | CNGA1 | Merge |

Cngb1 KO
10^9 vg (R18026)
treated area
10 months *pn*

OS
IS
ONL
OPL
INL
IPL
GCL

OS
IS
ONL
OPL

Cngb1 KO
untreated area
10 months *pn*

ONL
OPL
INL
IPL
GCL

ONL
OPL
INL

Cngb1 wildtype
untreated

OS
IS
ONL
OPL
INL
IPL
GCL

OS
IS
ONL

Figure 19: rAAV5.hCNGB1 treatment was dose dependent in the *Cngb1* KO mouse. Representative confocal images of retinal cross sections of *Cngb1* KO and wildtype mice. *Cngb1* KO mice were injected at 4-weeks of age with different doses of the PCL rAAV5.hCNGB1 (Lot#R18026). Immunohistochemistry staining was conducted at 10 months *pn*. A. Hoechst 33342 staining (blue signal) in retinas injected with 10^8 vg, 10^9 vg, and 10^{10} vg revealed an obvious dose dependency of the treatment demonstrated by 7-8 lines of nuclei that were rescued by applying 10^9 vg , whereas only a few lines were left in mouse groups 1 and 3. The untreated part of the KO exhibited only 1-2 lines of nuclei, while the wildtype possessed 14-15. The CNGB1 expression (red signal) was found in the photoreceptor layer of all treated mouse groups. CNGB1 was distinctly expressed 9 months after treatment with 10^9 vg, localizing in the OS as well as in the IS and the ONL. However, the red signal was faint and the ROS were degenerated after the low-dose treatment. CNGB1 was extensively expressed in the high-dose group, but the outer segments were scarcely existent. Scale bar marks 25 μm. B. Human CNGB1 (red) and murine CNGA1 (green) expression in a wildtype retina and in a mid-dose-treated *Cngb1* KO retina. There was a distinct green signal in the OS of the wildtype retina, while the protein was absent in the untreated area of the *Cngb1* KO. CNGA1 was found to be localized in the OS of the treated area, although the signal was less intense compared to the WT. For both WT and treated KO, merging revealed an overlap of hCNGB1 and mCNGA1 demonstrating the formation of channels consisting of hCNGB1 and mCNGA1 and their trafficking to the ROS. Scale bars mark 50 μm and 15 μm (zoom-in). OS. outer segments, IS. inner segments, ONL. outer nuclear layer, OPL. outer plexiform layer, INL. inner nuclear layer

3.5 Preservation of Rod Outer Segment Structure and Prolonged Survival of Cone Photoreceptors was Achieved by rAAV5.hCNGB1

Since in *Retinitis pigmentosa* photoreceptors degenerate over time, that often results in legal blindness (Hartong et al., 2006), a successful gene supplementation therapy includes an early deceleration of the degradation. In the *Cngb1* KO mouse model, shrinking of the rod outer segments already starts at *postnatal* day 15 (Hüttl et al., 2005). With progression of the disease, the outer nuclear layer (ONL) thickness continuously decreases, resulting in an almost absent ONL at the age of 10 months. This end stage of the degeneration as well as the final outcome of the photoreceptor rescue by the treatment with rAAV5.hCNGB1 has already been demonstrated via immunohistology (figures 17B and 19). In order to also monitor the pathological changes accompanying the degeneration, the retinal morphology was examined *in vivo* by means of spectral-domain optical coherence tomography (SD-OCT). With a weak laser light, the retina was scanned *in vivo* and the light reflections on the different retinal structures were measured (Fujimoto, 2003). Two-dimensional images were reconstructed displaying the different retinal layers in different shades of grey depending on the tissue density.

Figure 20A illustrates a representative OCT image of a *Cngb1* KO retina at the age of 9 months. At 4 weeks of age, the mouse was treated with 10^9 vg of vector Lot#R18026. The image shows the retinal area around the injection site (treated area) and also the distinctly thinner and obviously disorganized untreated part. The zoom-in highlights the border region displaying the transition from the untreated to the treated part. In the untreated area, the ONL was thin and the OS have been disappeared. In the treated area, however, the ONL (see labeling) was distinctly visible as well as the OS of the

photoreceptors (the bright layer directly below the RPE). The photoreceptor layer was about 3-fold thicker than the untreated part revealing a marked preservation of photoreceptors by the treatment. The INL, GCL, as well as the RPE were not visibly altered by the photoreceptor degeneration and were also not affected by the treatment.

Figure 20B shows the quantification of the photoreceptor layer thicknesses of sham-injected *Cngb1* KO retinas (the contralateral eyes of mouse group 1, 2, and 3 that received the vehicle) compared to untreated wildtype retinas. The data confirmed the unchanged thickness of the photoreceptor layer in wildtype retinas (about 110 μm), whereas in *Cngb1* KO retinas photoreceptors degenerated over time resulting in a significantly decreased photoreceptor layer thickness (p-value<0.001). At 3 months of age, the averaged thickness was 68.31 ± 1.30 μm, that was further reduced to 58.06 ± 1.43 μm at 5 months *pn* and to 36.06 ± 1.57 μm at 9 months *pn*.

The averaged photoreceptor layer thicknesses of *Cngb1* KO mouse retinas injected with 10^{10} vg of vector Lot#17044A are displayed in figure 20C. The conditions had been the same as for the other mouse groups, except for the sham injection of the contralateral eye, which contained PBS-MK. The means of the sham-injected photoreceptor layer thicknesses at 3, 5, and 9 months *pn* were 62.08 ± 1.51 μm, 53.91 ± 1.35 μm, and 37.56 ± 2.39 μm, respectively, while the treated retinas had a thickness of 74.58 ± 1.76 μm at the 3-months-time point, 65.46 ± 2.19 μm at 5 months *pn*, and 49.67 ± 2.87 μm at the long-term-time-point (9 months *pn*). Paired two-way ANOVA revealed a significantly thicker photoreceptor layer for the rAAV-treated eye compared to the buffer-treated contralateral eyes (1.2-fold at 3 and 5 months *pn* and up to 1.3-fold at long-term; p<0.001).

Figure 20D illustrates averaged photoreceptor layer thicknesses of treated and sham injected retinas of all mouse groups injected with vector Lot#R18026 (mouse group 1: 10^8 vg, mouse group 2: 10^9 vg, and mouse group 3: 10^{10} vg). There were slight differences between the sham-injected retinas of the three mouse groups, revealing that the course of degeneration was slightly different between the individual mice. Therefore, it was decided to perform a paired two-way ANOVA. For the 3, 5, and 9-months-time point, mouse group 1 revealed photoreceptor layer thicknesses of 75.29 ± 3.15 μm, 62.71 ± 2.31 μm, and 45.14 ± 3.85 μm, respectively. For mouse group 2, thicknesses of 77.86 ± 1.60 μm, 70.86 ± 2.75 μm, and 50.57 ± 4.40 μm were measured and the values determined for mouse group 3 were 71.38 ± 2.02 μm, 60.33 ± 2.77 μm, and 40.78 ± 3.42 μm. Hence, a significant rescue of photoreceptors was achieved for all three mouse groups, although the extent of photoreceptor survival varied greatly from group to group. The treated eyes of mouse group 1 revealed an overall 1.2-fold increase in the photoreceptor layer thickness (p<0.001), the mid-dosed retinas were 1.3-fold thicker (p<0.001), and eyes of mouse group 3 showed only a modest difference (1.1-fold; p=0.002). At the 3-months-time point, the amount of the

rescued photoreceptor layers was similar between the 3 mouse groups. At the 5-months-time point, the effect of the treatment was most obvious for mouse group 2 (14.43 µm of the photoreceptor layer were rescued), whereas this distinct difference was not achieved by applying the high (difference of 5.02 µm; equivalent to about one row of photoreceptor nuclei) or the low dose (9.00 µm difference; equivalent to about two rows of nuclei). After 8 months, the morphological preservation accounted for 13.43 µm for mouse group 1 and 14.29 µm in case of group 2. However, mouse group 3 revealed a smaller difference of 5.30 µm at this time point.

The OCT data showed, that a deceleration of the degeneration was achieved with both virus batches used as well as with all virus concentrations applied. The treatment with 10^9 vg of R18026 and 10^{10} vg of X17044A achieved the highest preservation rate of photoreceptors, whereas the application of the low dose (10^8 vg) of R18026 resulted in a lower photoreceptor rescue. The high dose (10^{10} vg) of R18026 did not have a distinct effect on the degeneration process, suggesting a potential toxic side effect leading to photoreceptor death that counteracted the beneficial effect of the treatment. Together, these data revealed a substantial, dose-dependent preservation of the photoreceptor morphology in the *Cngb1* KO mouse by gene therapy with rAAV5.hCNGB1.

Figure 20: The treatment with rAAV5.hCNGB1 achieved preservation of rod outer segment structure. A. Representative SD-OCT image of a *Cngb1* KO retina at 9 months *pn*, injected with 10^9 total vg (early stage) of rAAV.hCNGB1 (Lot#R18026), demonstrating an obvious rescue of the photoreceptor layer thickness in the treated part of the retina. The black arrows mark the photoreceptor layer. B. Quantification of the photoreceptor layer thicknesses (μm) of sham injected *Cngb1* KO vs wildtype retinas analyzed at 3, 5, and 9 months of age, that show a dramatic decrease of the photoreceptor layer thickness in the *Cngb1* KO mouse model, whereas the photoreceptor layer of the wildtype mice remains unchanged. Wildtype. n=3; sham injected *Cngb1* KO. n=35 (contralateral eyes of mouse group 1, 2, and 3 were used). C. *Cngb1* KO retinas treated with 10^{10} vg of vector Lot#X17044A displayed a significant increase in photoreceptor layer thickness (μm) compared to the respective sham injected contralateral eyes at 3, 5, and 9 months *pn* (p<0.001). 3 months *pn*: n=12; 5 months *pn*: n=11; 9 months *pn*: n=9. D. *Cngb1* KO retinas treated with 10^8 vg (mouse group 1), 10^9 vg (mouse group 2), and 10^{10} vg (mouse group 3) using vector Lot#R18026 compared to their respective sham injected contralateral eyes at 3, 5, and 9 months *pn* demonstrate a dose dependency of the treatment. Although all tested mouse groups revealed a significant rescue of photoreceptors, 10^9 vg was found to be the most efficient vector dose. 10^8 vg, however, provided less distinct results, while 10^{10} vg showed only a marginal benefit. Mouse group 1: n=7; mouse group 2: n=7; mouse group 3: n=10. (3 months *pn*: n=8; two eyes were not analyzable at this time point due to transient opacity of the eye). Values are given as mean ± SEM. Statistics. Two-way ANOVA paired with Sidak's post-hoc test (*: p≤0.05; **: p≤0.01; ***: p≤0.001).

Secondary to the loss of rod photoreceptors, also cone photoreceptors degenerate at later stages of RP. Although their cell nuclei and spherical cell bodies persist much longer in the retina, a loss of native morphology and functionality has been reported ("dormant cones"; Lin et al., 2009; Busskamp et al., 2010 and 2012, Sahel et al., 2013; Wong and Kwok, 2016; Schön et al., 2017). Therefore, an important long-term aim of the *CNGB1* gene therapy was to prevent cone photoreceptors from dying off in order to preserve high acuity daylight vision. In the *Cngb1* KO mouse model, cone degeneration usually starts at about 6 months of age (Hüttl et al., 2005). However, this is not visualizable by OCT due to the fact that cones make up only 2.8 % of the photoreceptors in the retina of a pigmented mouse (Carter-Dawson and Lavail, 1979; Jeon et al., 1998; Ortín-Martínez et al., 2014). Therefore, immunohistochemistry was performed in treated *Cngb1* KO mice using the cone arrestin (CAR) antibody in order to investigate the cone cell shape at the advanced disease stage. Figure 21 shows representative confocal images of mouse CAR expression in cross sections of a *Cngb1* KO mouse injected with 10^9 vg of Lot#R18026 at 10 months of age. The treated part of the *Cngb1* KO retina (area covered by the subretinal bleb) was compared to the untreated area (outside of the subretinal bleb) and a wildtype retina served as a control. In the wildtype retina, the staining visualized IS and OS as well as cell bodies, inner fibers, and the synaptic terminals of the cones, demonstrating the morphology of healthy cone cells within a wildtype retina. In the untreated area of the *Cngb1* KO mouse retina, no intact cones were found. IS and OS had completely disappeared, merely the spherical cell bodies and remnants of synapses were still visible, representing the remaining dormant cones of a *Cngb1* KO retina in the advanced stage of RP45. In the rAAV5.hCNGB1 treated area, the cone cells were completely intact and possessed a wildtype-like morphology including IS, OS, inner fibers, and synapses. The shorter inner fibers (compared to the wild type) most likely resulted from the lower number of remaining rod cells and corresponding thinner ONL. The number of healthy appearing cones was similar to that of the wildtype, demonstrating that the cone cells in the treated *Cngb1* KO retina were not affected by the disease. Since cones degenerate mutation-independently and secondarily to rods, these data suggest that the progression of the disease was arrested by the one-time rAAV5.hCNGB1 treatment and successfully treated photoreceptor cells escaped further degeneration even at this late disease stage. Together, these data showed that treatment with rAAV5.hCNGB1 preserved the morphology of cone cells, thus providing the basis for maintained daylight vision.
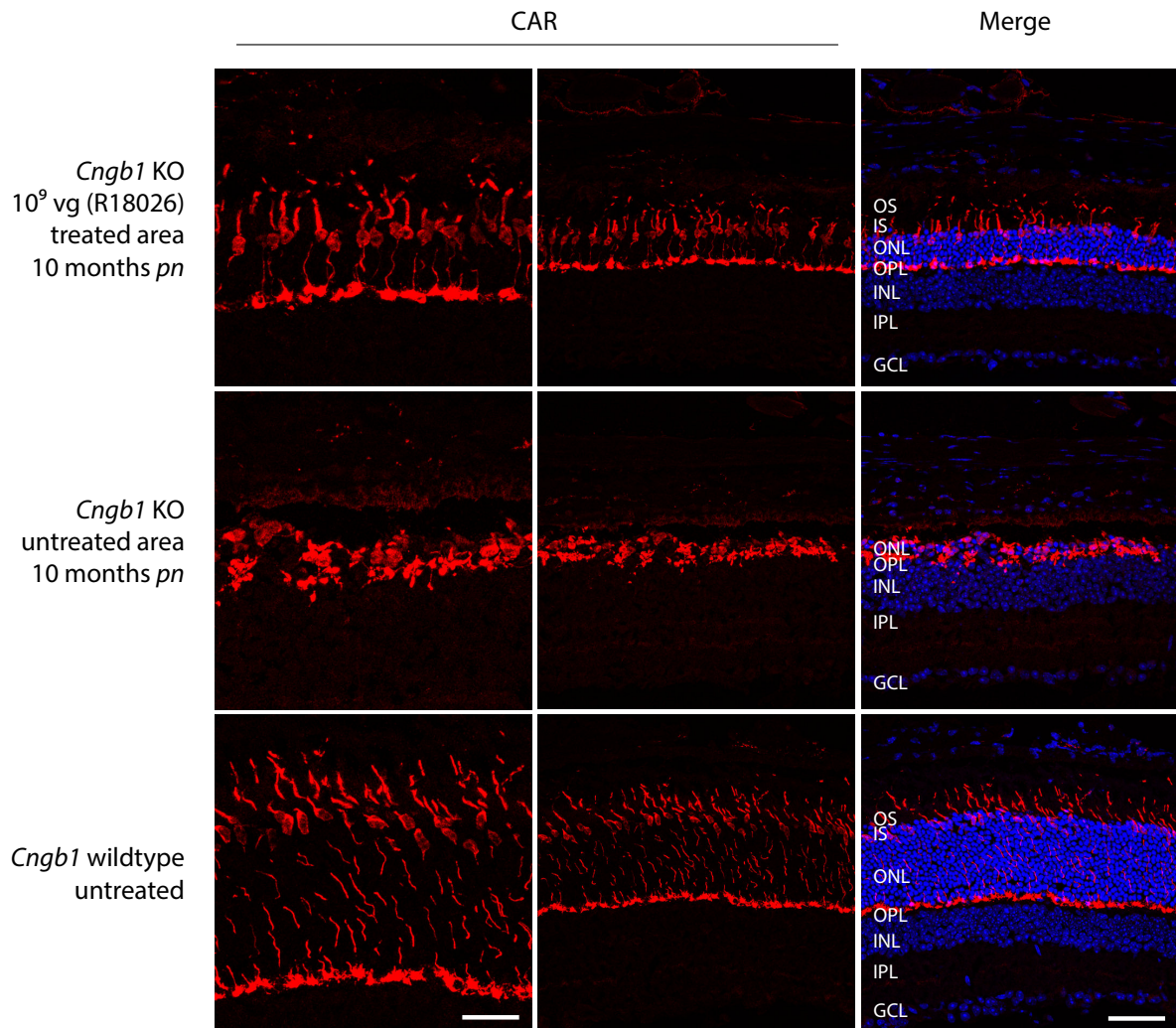
Figure 21: The treatment with rAAV5.hCNGB1 led to prolonged survival of cone photoreceptors. Representative confocal images of murine cone arrestin (CAR) expression in cross sections of a *Cngb1* KO retina (treated and untreated part) at the age of 10 months that received 10^9 vg of rAAV.hCNGB1 (Lot#R18026). A cross section through a wildtype mouse retina served as a control. The treated area revealed a wildtype-like shape of cones with intact IS and OS, whereas only spherical cone cell bodies and cell residues remained in the untreated part. Scale bars mark 25 µm (left pictures) and 50 µm (right pictures). OS. outer segments, IS. inner segments, ONL. outer nuclear layer, OPL. outer plexiform layer, INL. inner nuclear layer, IPL. inner plexiform layer, GCL. ganglion cell layer

3.6 rAAV5.hCNGB1 Achieved Long-Term CNGB1 Expression and Photoreceptor Preservation in the *Cngb1* KO Dog Model

To investigate the efficacy of rAAV5.hCNGB1 in a large animal model, a *Cngb1* KO dog model closely resembling the *Cngb1* KO mouse model but possessing human-sized eyes (Winkler et al., 2013) was used to design a dog dose escalation study for efficacy testing of rAAV5.hCNGB1 (using vector Lot#X17044A). Breeding, surgeries, and *in vivo* examinations were conducted at the College of Veterinary Medicine at the Michigan State University by Prof. Simon Petersen-Jones and his group. At

3 months of age, each dog eye received two subretinal injections of 100 μL volume. 4 different viral doses were administered to the dog eyes (1×10^{12} vg, 2×10^{11} vg, 1×10^{11} vg, and 2×10^{10} vg). The numbers of eyes per dose are listed in table 7. After euthanasia, the dissected retinas were sent to the LMU for cryo-sectioning, immunohistochemistry, and confocal imaging.

To test transgene expression in the *Cngb1* KO dog model, immunohistochemistry was performed using the CNGB1 antibody already used for the mouse study. The eye of a dog that received a high vector dose of 1×10^{12} vg was removed at 12 months *pi*. An overview of about 30 % of the treated retina was obtained by tile scan imaging (multiple individual pictures were captured and assembled into one image covering a larger area using the LasX software). The representative confocal image (figure 22) displayed an obvious CNGB1 expression in the treated part of the retina (the area covered by the subretinal bleb), whereas no signal was observed outside in the untreated area thereby also confirming the absence of the endogenous CNGB1 protein in untreated *Cngb1* KO dog retina. Furthermore, the image illustrated the transition zone from treated to untreated where the red signal disappeared accompanied with a clearly evident thinning of the ONL (shown by Hoechst 33342; blue signal). This data demonstrated the expression of the rAAV-introduced human *CNGB1* gene in the dog retina at more than one year after injection, confirming the long-term persistence of rAAV5.hCNGB1 in a large animal model. It further revealed a substantial preservation of the ONL as a result of the treatment.
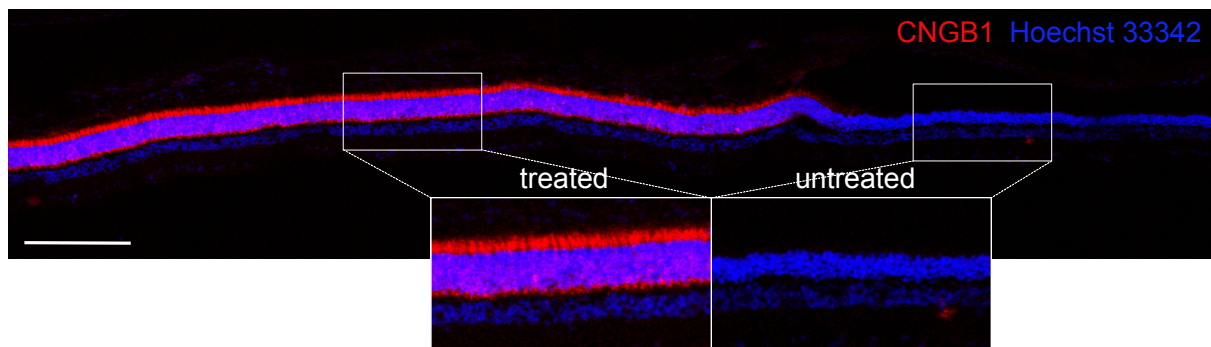
Figure 22: rAAV5.hCNGB1 was efficient in the *Cngb1* KO dog model. Representative confocal image of about 30 % of a cross section of a *Cngb1* KO dog retina, that received two injections (100 μL each) of rAAV5.hCNGB1 (1×10^{12} vg; Lot#X17044A). The dog was treated at the age of 3 months and the immunohistochemistry was performed at 12 months *pi*. The image was obtained by tile scan imaging using the LasX software and depicted both treated (within the subretinal bleb) and untreated part of the retina (outside of the bleb). No CNGB1 protein (red signal) was found in the untreated *Cngb1* KO dog retina, whereas it was distinctly visible in the treated part, leading to a substantial rescue of the photoreceptor layer (nuclei were stained using Hoechst 33342; blue signal). Scale bar marks 200 μm.

In order to examine the vector specificity in the canine model, cross sections of treated *Cngb1* KO dog retina were co-stained with peanut agglutinin (PNA), a lectin from *Arachis hypogaea* characterized by a high affinity for galactose-galactosamine disaccharide residues, which can be used as a marker for cones

(Michalakis et al., 2005). Representative confocal images are shown in figure 23. The red signal in the treated area revealed a distinct CNGB1 expression in the whole photoreceptor layer. CNGB1 was localized to the ROS as well as to the IS, cell bodies, and synapses, a pattern similar to what was seen in the *Cngb1* KO mouse model. This implied that, as already seen for the mouse, chimeric CNG channel heterotetramers with canine CNGA1 and human CNGB1 are formed *in vivo*. Aberrant subcellular IS localization of hCNGB1 was most likely due to an overdose. The PNA staining (green signal) revealed partly broken or truncated cone OS in the untreated area of the *Cngb1* KO dog retina, whereas the morphology of the cone OS within the treated part was regular, well-organized, and intact, indicating preservation of the cone cells. By merging the red and the green channel, there was no overlap visible (highlighted by the zoom-in), indicating a rod-restricted CNGB1 expression by the rAAV5.hCNGB1 vector. Hoechst 33342 revealed 13 rows of photoreceptor nuclei (blue signal) in the treated retina, whereas only 8 layers remained in the untreated part, demonstrating a marked preservation of photoreceptors as a result of the treatment with rAAV5.hCNGB1. It also revealed, that in the dog model not many photoreceptors were degenerated at the age of about 15 months, demonstrating that the disease had not progressed to an advanced phase in the treated *Cngb1* KO dog until this age.
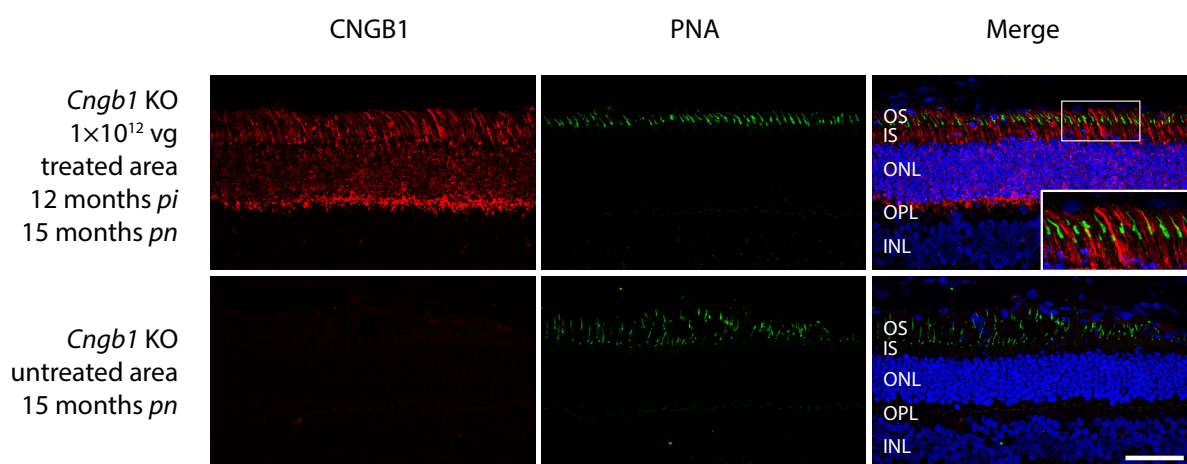
Figure 23: The hCNGB1 expression was restricted to rod photoreceptors in the *Cngb1* KO dog model. Representative confocal images of a cross section of a *Cngb1* KO dog retina, that was harvested at the age of 15 months. The dog was subretinally injected with 1×10^{12} vg of rAAV5.hCNGB1 (Lot#X17044A) at 3 months of age. The cross section through the treated part of the retina shows the CNGB1 protein (red), co-stained with the cone-marker peanut agglutinin (PNA, green). Nuclei were stained with Hoechst 33342 (blue). The treatment resulted in a distinct expression of hCNGB1 in the photoreceptor layer. CNGB1 protein was found in the photoreceptor OS, in the IS as well as in the ONL. Merging revealed no overlap of the green (PNA) and the red channel (hCNGB1) demonstrating a rod-specific hCNGB1 expression in the *Cngb1* KO dog model. Scale bar marks 50 μm. OS. outer segments, IS. inner segments, ONL. outer nuclear layer, OPL. outer plexiform layer, INL. inner nuclear layer

3.7   The Efficacy of rAAV5.hCNGB1 was Dose Dependent in *Cngb1* KO Dogs

To determine the optimal dose range for a *hCngb1* gene supplementation therapy, *Cngb1* KO dogs were treated with 4 different doses of Lot#X17044A by subretinal injection (1×10^{12} vg, 2×10^{11} vg, 1×10^{11} vg, and 2×10^{10} vg). In each dog, both eyes were injected with different doses. The dogs were sacrificed either after about half a year, or after approximately one year to harvest the retina, perform cryosections, and to perform immunohistochemistry for transgene expression analysis. Figure 24 illustrates representative confocal images of *Cngb1* KO dogs injected with different vector doses, stained with anti-CNGB1 (red signal) and anti-CNGA1 (green signal). The untreated part of *Cngb1* KO dogs showed a lack of hCNGB1 expression, whereas the respective protein was distinctly visible in all tested dog eyes (all vector doses). However, a dose dependency of rAAV5.hCNGB1 was also evident in the dog model, shown by a decrease of the hCNGB1 expression along with dose reduction.

The eyes that received 1×10^{12} vg and 2×10^{11} vg were harvested at 12 months *pi*. The respective confocal images revealed a high expression of hCNGB1 in the whole ONL as well as intact rod photoreceptors (figure 24). In the retinas treated with 1×10^{11} vg, CNGB1 expression was still present (at 6 months *pi*), although the signal intensity was lower compared to the higher doses. CNGB1 expression was also found in the eyes that received the low dose (2×10^{10} vg; 6 months *pi*). However, the expression level was markedly lower compared to the higher doses, which on the one hand led to the fact that in this retina the localization of the corresponding protein was limited to the outer segments, but on the other hand resulted in an accumulation of the protein in the uppermost parts of the ROS. This suggested, that the expression level of hCNGB1 decreased after about half a year when administered in a low dose, resulting in a no longer homogeneously distribution of the protein throughout the OS. The ROS of the retinas treated with 2×10^{10} vg were still largely intact, but Hoechst 33342 staining revealed, that the ONL was substantially thinner than in its contralateral eye, which received 1×10^{11} vg (13 lines of nuclei). This indicated, that a treatment with the low dose (2×10^{10} vg) resulted in a substantially lower biological efficacy at 6 months *pi* as it was seen for the higher doses of rAAV5.hCNGB1. 12 rows of nuclei were counted for the retinas treated with 1×10^{12} vg and 2×10^{11} vg (histology at about one year after treatment). Considering that the retina treated with 10^{11} vg was harvested 6 months earlier than the eyes treated with 1×10^{12} vg and 2×10^{11} vg, it can nevertheless be assumed a similar long-term treatment efficiency for the three doses. The untreated *Cngb1* KO dog retina showed 7 lines of cell bodies, indicating that about 5 rows of photoreceptors were rescued by the high- and mid-dose treatments, whereas only one row was rescued by the low dose. This clearly confirmed the dose dependency of the gene supplementation using rAAV5.hCNGB1.

Furthermore, CNGA1 was not found in the untreated *Cngb1* KO retina (figure 24), but *hCNGB1* gene supplementation led to a recurrence of CNGA1 in the ROS. The signal of CNGA1 was dose-dependent similar to the signal of CNGB1, but CNGA1 signals were visible in all treated dog retinas. Merging of the channels resulted in an overlap of the red and green signal, suggesting a colocalization of the two subunits and chimeric CNG channel formation in the *Cngb1* KO dog model. Furthermore, in all dog retinas, the CNGA1 localization was restricted to the ROS, suggesting that also in the dog model CNGA1 was the limiting factor for CNG channel formation and trafficking to the ROS, as it was previously seen in the *Cngb1* KO mouse model.

Together, all vector doses achieved long-term expression of human CNGB1, but the treatment with the lowest dose (2×10^{10}) resulted in a markedly lower transgene expression and in more degenerated photoreceptors compared to the eyes treated with the higher doses. Between the doses of 1×10^{11}, 2×10^{11}, and 1×10^{12} vg only minor differences in transgene expression and photoreceptor rescue were visible, suggesting a lower threshold for sufficient gene expression and a plateau for rAAV5.hCNGB1 in the *Cngb1* KO dog model from a dose of about 1×10^{11} vg upwards.
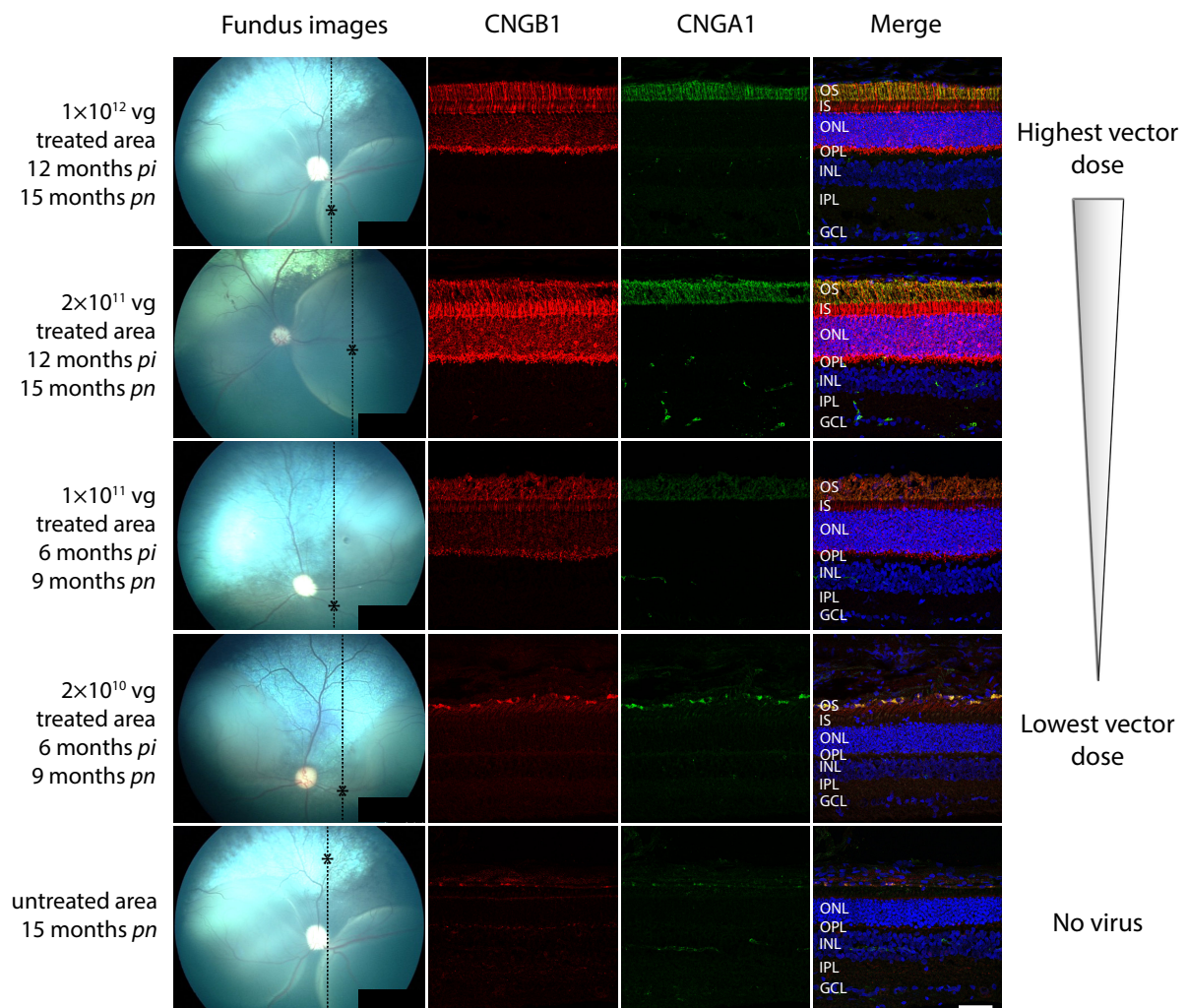
Figure 24: The treatment with rAAV5.hCNGB1 was dose dependent in *Cngb1* KO dogs. Representative confocal images of retinal cross sections of *Cngb1* KO dogs, that were subretinally injected with different doses (1×10^{12} vg, 2×10^{11} vg, 1×10^{11} vg, and 2×10^{10} vg) of AAV5.hCNGB1 (Lot#X17044A) at 3 months of age. Retinas were dissected after either about half a year or after about one year (as indicated) and immunohistochemistry was performed using CNGB1 (red signal) and CNGA1 (green) antibodies, as well as Hoechst 33342 for nucleus staining (blue). The untreated retinal area showed a lack of the CNGB1 protein, while in response to all tested vector doses an expression of the supplemented gene was visible. However, the images displayed an obvious dose dependency of rAAV5.hCNGB1 administered to the *Cngb1* KO dog model. A decreasing of the red signal intensity is seen by reducing the vector dose. Furthermore, CNGB1 protein was found in the whole ONL after applying 1×10^{12} vg, 2×10^{11} vg, or 1×10^{11} vg, whereas the lowest dose (2×10^{10} vg) caused a substantially lower gene expression resulting in a localization restricted to the OS and in a partial accumulation in the uppermost parts of the OS. The treatment also caused CNGA1 to reappear in the OS. Merging showed an overlap of the red and the green signal demonstrating the formation of heterotetrametric channels consisting of human CNGB1 and canine CNGA1, that was transported to the ROS. Staining with Hoechst 33342 showed that the higher the dose, the more photoreceptor cells were preserved from dying off, demonstrating that the highest dose had the most beneficial effect. Furthermore, a markedly reduced photoreceptor preservation was observed for the low-dosed retinas (2×10^{10} vg) compared to the higher doses. Grid lines within the fundus images mark the positions of the cross sections within the dog retinas and the star (*) marks the locations shown by the confocal images. Scale bar marks 50 μm. OS. outer segments, IS. inner segments, ONL. outer nuclear layer, OPL. outer plexiform layer, INL. inner nuclear layer, IPL. inner plexiform layer, GCL. ganglion cell layer

The border regions (transition zone between treated and untreated) of treated *Cngb1* KO dog retinas (figure 25; left picture: 1×10^{11} vg; right pictures: 2×10^{11} vg; shown) provided further evidence for the existence of an optimal vector dose by revealing a wildtype-like CNGB1 localization to the ROS within the peripheral part of the treated area, where the protein was localized strictly to the ROS. Furthermore, the number of photoreceptor nuclei was similar to that of the central treated part of 1×10^{11} vg and 2×10^{11} vg-treated retinas, indicating the optimal dose range for rAAV5.hCNGB1 slightly lower than 1×10^{11} vg.
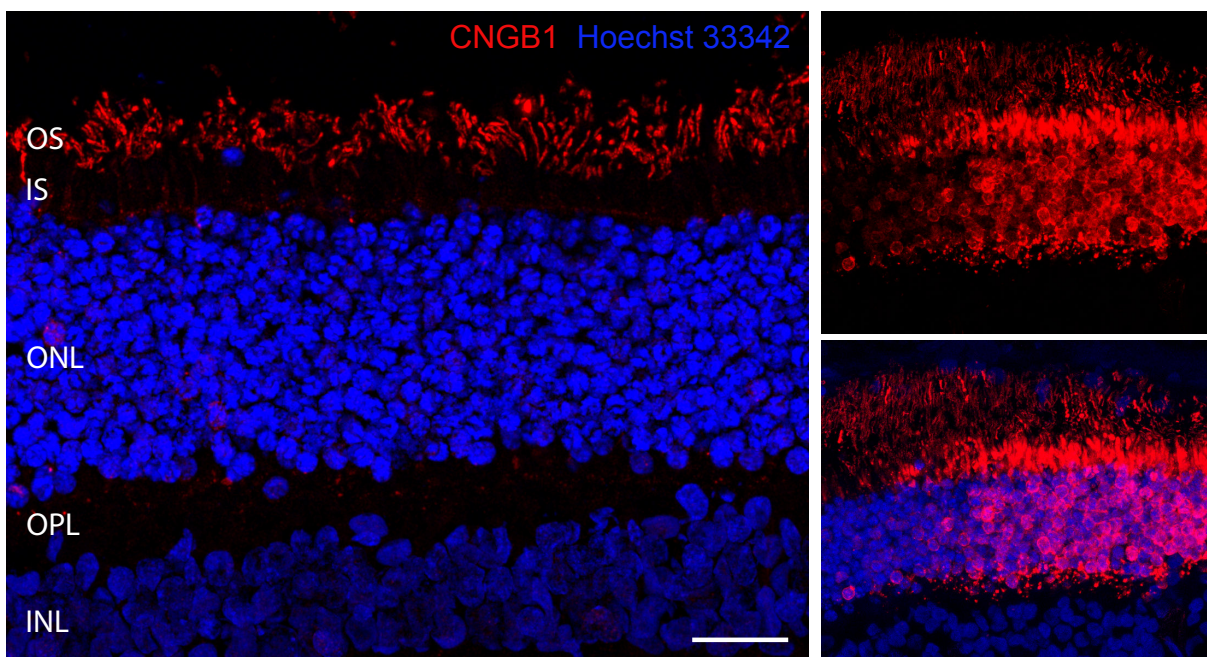
Figure 25: Wildtype-like localization of hCNGB1 at the border region of the treated area in the *Cngb1* KO dog model. Representative confocal images of transition zones between treated and untreated areas of *Cngb1* KO dogs. The dogs were treated at 3 months of age receiving 1×10^{11} vg of rAAV5.hCNGB1 (Lot#X17044A; left picture) and 2×10^{11} vg of

rAAV5.hCNGB1 (Lot#X17044A; right pictures). They were sacrificed about one year *pi*. Left. In the border region, the hCNGB1 localization was restricted to the ROS similar to the native location of CNGB1. Right. Transition from a CNGB1 localization in the entire photoreceptor layer to a localization restricted to the outer segments of the photoreceptors. Scale bar marks 30 μm. OS. outer segments, IS. inner segments, ONL. outer nuclear layer, OPL. outer plexiform layer, INL. inner nuclear layer

3.8 The Introduced Human CNGB1 Subunits were Capable of Forming Functional CNG channels Together with Murine or Canine CNGA1 Subunits

It was already shown, that the supplemented human *CNGB1* gene was translated to a protein that formed a rod specific CNG channel together with murine or canine CNGA1 subunits resulting in CNG channel trafficking to the ROS (figures 17, 19, 23, and 24). However, the question about the physiological functionality of these chimeric protein complexes has still remained open. In order to investigate this, the amount of the second messenger cyclic guanosine monophosphate (cGMP) was examined. In a healthy retina, the CNG channel is open within darkness due to the binding of cGMP that leads to the maintenance of an inward current (for details see figure 10). During daylight conditions cGMP is hydrolyzed by the activated PDE6A resulting in CNG channel closing and therefore to a hyperpolarization of the cell. In the case of RP45, the CNG channel is missing and therefore cGMP cannot bind to the channel resulting in an accumulation inside the cell. Due to a low calcium level within the cell, the guanylyl cyclase (GC) is constantly producing cGMP, leading to a further increase in cGMP concentration. This pathological high level of intracellular cGMP was shown in multiple mouse models for retinal degeneration (Farber and Lolley, 1974; Paquet-Durand et al., 2009; Michalakis et al., 2010; Trifunovic et al., 2010; Paquet-Durand et al., 2011; Xu et al., 2013; Schön et al., 2017) and was reported to contribute to photoreceptor death (Paquet-Durand, 2011; Xu et al., 2013). The *Cngb1* KO mouse model also showed a disordered cGMP metabolism, which was normalized by gene supplementation of *mCngb1* (Koch et al., 2012).

In order to evaluate, whether this could also be achieved by introducing *hCNGB1*, the cGMP level of the *Cngb1* KO mice treated with 10^{10} vg of Lot#X17044A was tested by IHC using an anti-cGMP antibody. The same experiment was performed using a high-dose-treated (1×10^{12} vg) *Cngb1* KO dog retina to further investigate, whether cGMP was also accumulating in the canine model and if this could be prevented by the treatment. Figure 26 shows representative co-stainings using anti-cGMP and anti-CNGB1 in retinal cross sections of a treated *Cngb1* KO mouse (figure 26A) and of a treated *Cngb1* KO dog (26B). Within the untreated area of both retinas, cGMP was distinctly visible in the rod IS and OS indicating intracellular cGMP accumulation in both the mouse and the dog model. However, there was no cGMP found in the treated parts of both retinas demonstrating a normalization of the cGMP

metabolism by the treatment with rAAV5.hCNGB1. The weaker signal of cGMP in the untreated part of the *Cngb1* KO mouse retina resulted from the small number of photoreceptors that remained until this late disease stage (9 months *pn*).

These data indicated that the chimeric CNG channels formed by human CNGB1 and either murine or canine CNGA1 had an intact cGMP-binding CNBD and were also capable of opening.
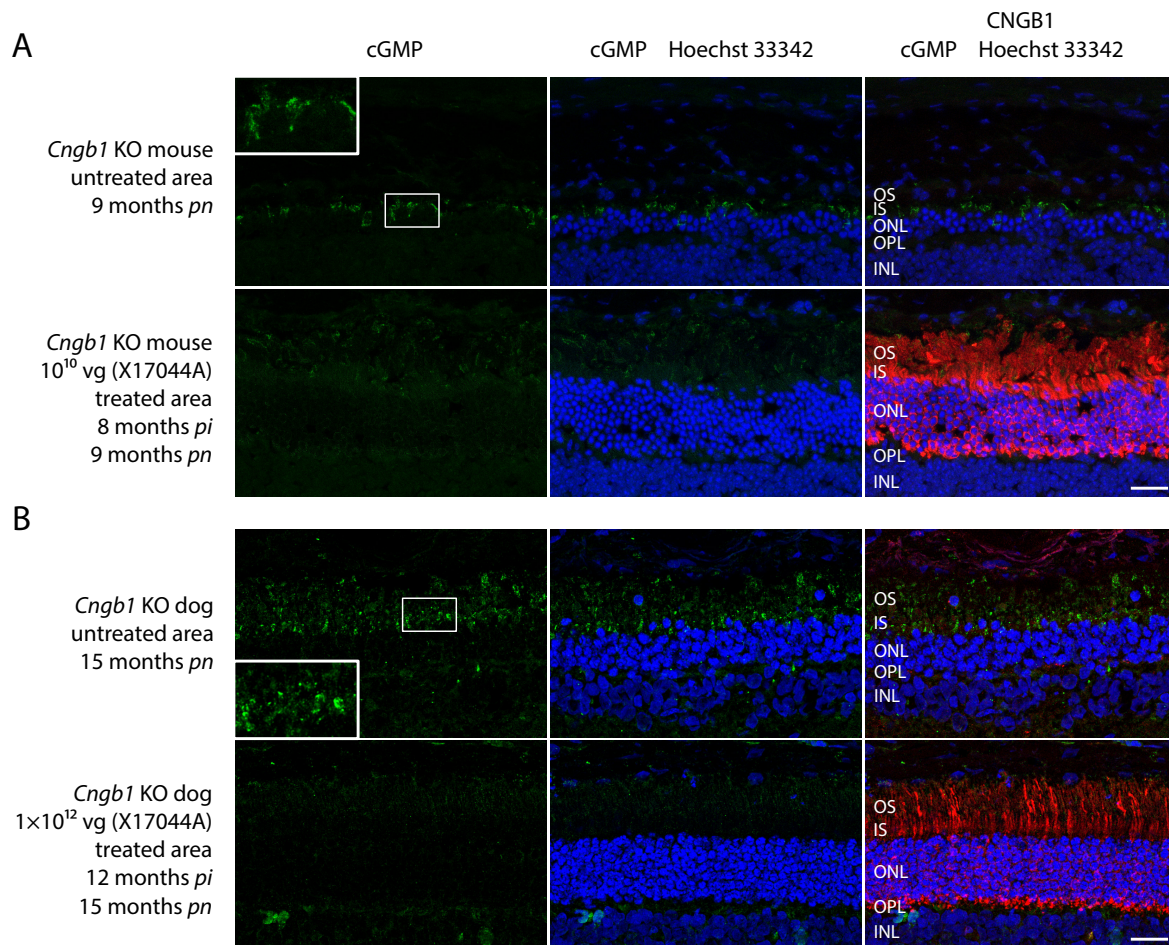
Figure 26: The human CNGB1 protein formed a functional CNG channel together with the murine or canine CNGA1. Representative confocal images of cross sections from *Cngb1* KO mouse and dog retinas. Immunohistochemistry stainings using anti-cGMP (green signal), anti-CNGB1 (red) and Hoechst 33342 (blue) demonstrated an accumulation of cGMP in the OS of the untreated photoreceptors. This was prevented by the rAAV5.hCNGB1 treatment in both mouse and dog demonstrating a normalization of the cGMP metabolism in the *Cngb1* KO. A. Cross sections of one treated and one untreated part of a *Cngb1* KO mouse retina at the age of 9 months that received 10^{10} vg of #X17044A (group X) at 4 weeks of age. B. Cross sections of treated and untreated retinal parts of a *Cngb1* KO dog at 12 months *pi*. The dog was treated with 1×10^{12} vg of #X17044A at the age of 3 months. Scale bar marks 25 µm. OS. outer segments, IS. inner segments, ONL. outer nuclear layer, OPL. outer plexiform layer, INL. inner nuclear layer

3.9   rAAV5.hCNGB1 had a Beneficial Effect on the Rod Function in *Cngb1* KO Mice

Immunohistochemistry already demonstrated a normalization of the cGMP metabolism trough *hCNGB1* gene supplementation (see figure 26). The resulting chimeric CNG channels have proven to be functional in the *Cngb1* KO mouse model as well as in the *Cngb1* KO dog model. However, it remained to be investigated, whether this restored molecular function also leads to recovery of rod cell response to light and consequently to a restoration of retinal function. In order to measure the function of rod photoreceptors as well as of the whole retina in mice, electroretinography measurements have been performed. For this purpose, so called Ganzfeld electroretinograms were recorded. In particular, the back of the eyes received light flashes of varying luminance and the light-induced electric signals were measured using corneal electrodes and amplified for analysis. For obtaining the retinal signal from the rod cells, mice had to be adapted to the dark for at least 12 h and the measurements had to be conducted under scotopic conditions (under exclusion of light). Every mouse received a luminance spectrum from 0.01 cd s m^{-2} up to 10 cd s m^{-2}, based on the ISCEV standardized protocol for clinical dark-adapted ERG recordings (Marmor et al., 1989; regularly updated). The voltage potential was recorded showing a waveform that reflected the whole (illuminated) retina response. A typical scotopic single-flash ERG signal generally consists of an a-wave and a b-wave. The a-wave is the initial negative deflection of the cornea, which originates directly from the photoreceptors. It reflects the hyperpolarization of the photoreceptors caused by the closure of the CNG channels. This reduces the amount of neurotransmitter released from the synapses, leading to depolarization of the post-synaptic bipolar cells. The resulting transretinal current further depolarizes the Müller cells culminating in a positive deflection of the cornea referred to as the b-wave (Stockton and Slaughter, 1989; Dong and Hare, 2000; Seeliger et al., 2001; Tanimoto et al., 2009; Young et al., 2012; McCulloch et al., 2015). To evaluate retinal functions in treated and untreated *Cngb1* KO mice, the b-wave amplitude is usually analyzed, which is counted from maximum negative to maximum positive deflection. Although the b-wave is generated by the bipolar cells, it also indirectly mirrors the activity of photoreceptors, since the generation of a b-wave requires the function of photoreceptors.

A typical signal of a *Cngb1* wildtype mouse at the age of 3 months is shown in figure 27A (grey line). At the lowest light level of 0.01 cd s m^{-2}, there was only a b-wave present. It increased with ascending luminance and beginning from a stimulus of 0.03 cd s m^{-2}, the negative deflection (a-wave) was seen prior to the b-wave. At a flash of about 3 cd s m^{-2} the cone response was partly interfering into the signal and oscillatory potentials (OPs) emerged (McCulloch et al., 2015). OPs are discussed to arise mainly from interactions of bipolar, amacrine, and ganglion cells (Wachtmeister, 1998). The rod response of a *Cngb1*-linked RP patient differs markedly from the wild-type signal and similar changes are also observed in the *Cngb1* KO mouse (Hüttl et al., 2005) and dog model (Winkler et al, 2013; Petersen-Jones

et al., 2018). The black lines in figure 27A depict three typical ERG signals of sham-injected (BSS+0.014 % Tween20) *Cngb1* KO mouse retinas at 3 months of age, mirroring the signal of an RP45 patient at the early stage of the disease. At the luminance of 0.01 cd s m^{-2}, achieving the most rod specific response according to the ISCEV standard, neither a-waves, nor b-waves could be measured. In response to brighter luminance values, b-waves occurred, although they were substantially decreased compared to the wildtype. At the brighter stimuli, small b-waves were measurable, which is most probably due to the massive signal amplification during the electric transmission to the inner retinal cells (Doly, 1994) as well as by the stimulation of cone cells, which in this early phase of the disease are still fully functional.

Figure 27A further illustrates representative rod functions of treated *Cngb1* KO mouse retinas (low, mid, and high dose using Lot#R18026). The retinal response of the mid-dose group (mouse group 2; green line; central graph) demonstrated a distinct increase of the b-wave amplitude compared to the sham-injected contralateral eye (black line). At the rod-specific light intensities (0.01 cd s m^{-2} and 0.03 cd s m^{-2}) a clear signal was seen for the green line whereas the control showed no explicit electric responses. At the brighter light stimuli, the b-wave amplitude of the treated eye was 2-3-fold higher than the amplitudes of the sham-injected control. Furthermore, a small a-wave was also recovered by the mid-dose-treatment seen from a luminance level of 0.01 cd s m^{-2}, upwards. However, the a-wave of the 10^9 vg-treated *Cngb1* KO was much smaller, compared to the wildtype (grey line). The remaining area was not treated, resulting in at least 70 % of non-functional photoreceptors. Since the ERG measured the total retinal signal, it showed the sum of all treated but also all non-treated photoreceptors, resulting in a reduced signal. The ERG measurements of the low-dosed *Cngb1* KO retina (blue line; left graph) also showed increased responses to the different light stimuli, but the signals measured for the rod-specific stimuli (0.01 cd s m^{-2} and 0.03 cd s m^{-2}) were much smaller compared to the mid-dosed eyes. The high-dosed retina (pink line; right graph) showed almost no differences in the electric signals compared to the control at all luminance levels.

These findings were confirmed by the quantification of the b-wave amplitudes of all rAAV5.hCNGB1 (R18026) treated and sham-injected retinas at the 3-months-time-point (figure 27B). The mean b-wave amplitudes were also evaluated for the 9-months-time point (figure 27C). At 3 months *pn*, an averaged amplitude of 27.35 ± 3.57 μV was calculated for the rod-system response (0.01 cd s m^{-2}) of all sham-injected eyes (black line) and a mean of 111.46 ± 9.78 μV was measured for combined rod- and cone-system responses (3 cd s m^{-2}). The mid-dose treatment (10^9 vg; mouse group 2; green line) revealed a significant increase (p<0.001) in the b-wave amplitudes at all light intensities compared to the control. In response to low light flashes, the injected eyes exhibited an averaged b-wave amplitude of 48.51 ± 16.22 μV (0.01 cd s m^{-2}) and after bright light stimuli (3 cd s m^{-2}) 187.54 ± 42.55 μV were measured, revealing an overall increase of about 1.5-2-fold to the control. The treated eyes of mouse group 1 (low

vector dose; 10^8 vg; blue line) showed values of 42.89 ± 10.76 μV in response to 0.01 cd s m^{-2} and of 134.91 ± 24.92 μV at a luminance of 3 cd s m^{-2}. Consequently, there was a less distinct, but still significant increase in the b-wave amplitudes (p=0.004). No increased b-wave amplitudes were detected for the high-dose treatment (10^{10} vg; mouse group 3). For these retinas (pink line), averaged b-wave amplitudes of 25.01 ± 7.70 μV (0.01 cd s m^{-2}) and 105.44 ± 27.49 μV (3 cd s m^{-2}) were measured.

The 9 months follow-up data (figure 27C) showed 2-fold higher b-wave amplitudes (p<0.001) for the mid-dose retinas (10^9 vg) compared to the controls, demonstrating a long-term beneficial effect of the rAAV5.hCNGB1 treatment on the rod function until an advanced stage of the disease. However, the averaged b-wave amplitudes of the treated retinas of mouse group 2 had decreased since the 3-month time point. This decay might be caused by the large untreated area within the treated retina leading to a high number of degenerating photoreceptor cells even within the treated retina. Furthermore, it was already shown by confocal imaging of retinal cross sections (see figure 19), that with a treatment of 10^9 vg of rAAV5.hCNGB1 still about 6 lines of photoreceptors had degenerated until the long-term time point, which might be another reason for the ERG signal reduction. The long-term data for mouse group 1 illustrated a reduction of the treatment effect to a level indistinguishable from control (p=0.22) suggesting that the low dose was not sufficient to achieve a long-term beneficial effect on the retinal function. This further confirmed the immunohistochemistry findings showing a rather low CNGB1 expression level at 10 months *pn*. In addition, no differences in the b-wave amplitudes were determined by comparing treated and untreated eyes of the high-dose-mouse group (p=0.71). Since neither short-term nor long-term beneficial effects of the high-dose treatment were observed on retinal function, even though a strong CNGB1 expression was visible in the IHC, this was a further evidence for a toxic side effect of the high vector dose. Paired comparisons of the treated and the respective contralateral eyes of each mouse group at both time points are shown in figure S2 in the appendix (representative examples and quantification). The averaged ERG signal differences between treated and contralateral eye of each individual mouse (shown as % of control) are listed in tables S1-S3 in the appendix.

Taken together, this dose-ranging study identified an optimal dose for the rAAV5.hCNGB1 treatment which was able to achieve sustained restoration of photoreceptor function in the *Cngb1* KO mouse model without inducing toxic effects. A long-term restoration of photoreceptor function was only seen in the mid-dose group. The low dose group only showed a functional improvement at 3 months , but not at 9 months. Furthermore, treatment at high-dose did not result in rescue of photoreceptor function providing further evidence for toxic side effects of the vector when applied as the high dose.

A
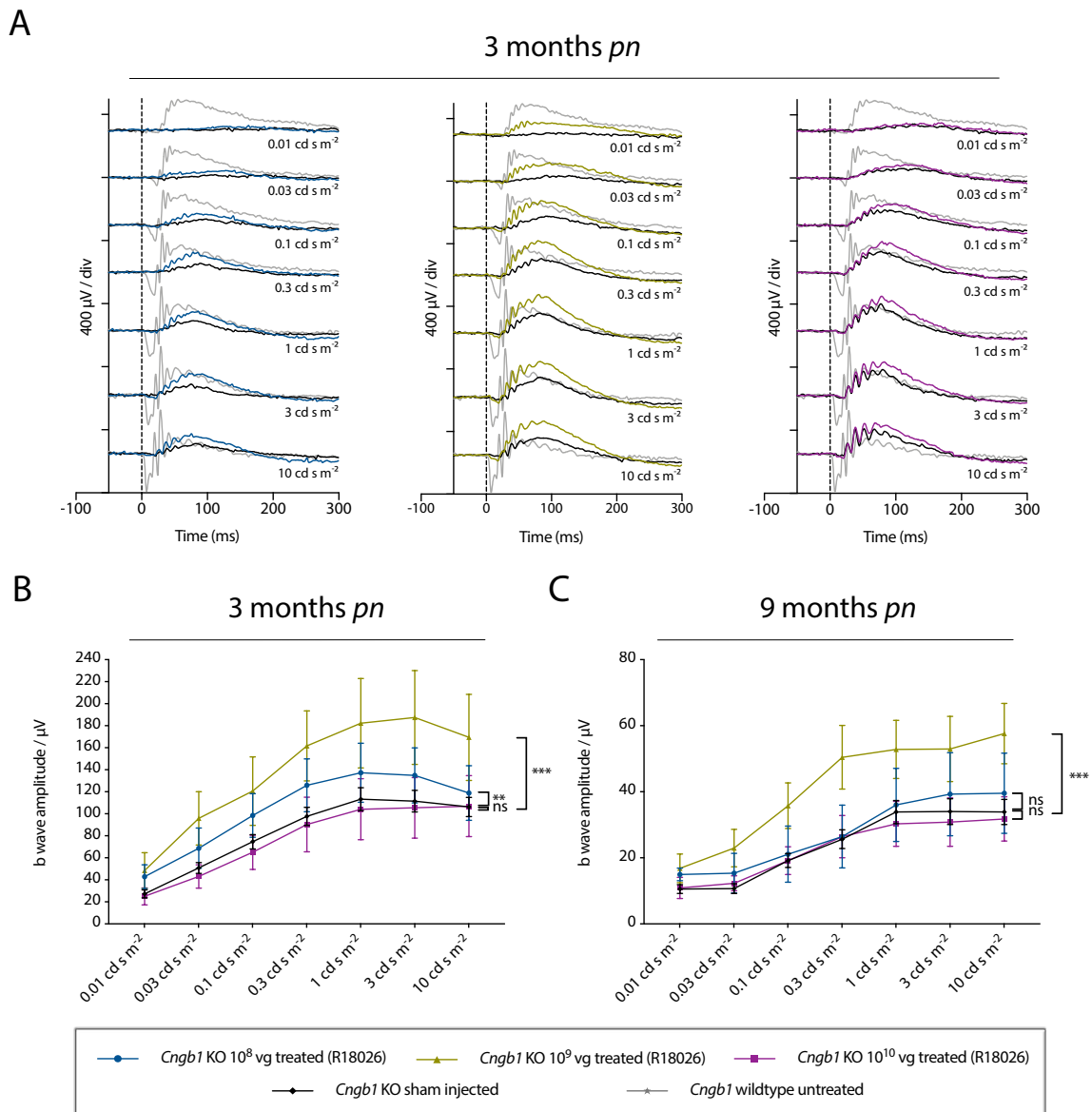
Figure 27: Scotopic electroretinography measurements of *Cngb1* KO and wildtype mice. A. Overlays of representative ERG signals obtained from a wildtype mouse (3 months *pn*) and 3-months-old *Cngb1* KO mice injected with 10^8 vg, 10^9 vg, and 10^{10} vg of rAAV5.hCNGB1 (Lot#R18026). The respective sham-injected contralateral eyes served as controls showing almost no response at the low light intensities of 0.01 and 0.03 cd s m^{-2} and a small b-wave at the brighter luminance levels. In case of mouse group 1 (left graph) there was a slight increase in photoreceptor function in the 10^8 vg-treated-eye compared to the control (black line). In response to all light stimuli, the b-wave was much more prominent in the 10^9 vg-treated-eye (central graph, green line), than in the sham-injected control (black line). At the very low light intensities of 0.01 and 0.03 cd s m^{-2}, an obvious signal was seen in the 10^9 vg-treated-retina (about one third (0.01 cd s m^{-2}) and a half (0.03 cd s m^{-2}) of the wildtype signal). A small a-wave was also recovered by the 10^9 vg of rAAV5.hCNGB1, that was not existent in the sham-injected KO. With the high vector dose (10^{10} vg; right graph; pink line) no obvious differences in the ERG signal were measured compared to the control. B and C. B-wave amplitudes of treated (10^8 vg, 10^9 vg, and 10^{10} vg; Lot#R18026) and sham injected *Cngb1* KO eyes at 3 and 9 months *pn* demonstrated a dose dependent beneficial effect on the retinal function. The injection of 10^9 vg resulted in a significantly increased b-wave amplitude at the 8-months-time point, whereas this could not be achieved by the low or high dose. Values are given as mean ± SEM. Group1: n=7; group 2: n=7; group3: n=10; sham injected: n=34 (mouse group 2: at 2 months *pi*, the measurement of mouse number 7 was excluded due to a fluctuating signal caused by a high background that could not be reduced. Therefore, n=6 at this time point). Statistics: Unpaired two-way ANOVA with Sidak's post hoc test (*: p≤0.05; **: p≤0.01; ***: p≤0.001). A paired comparison to the contralateral eyes of each mouse group is shown in figure S2 in the appendix.

3.10 Treatment with rAAV5.hCNGB1 resulted in Improved Vision-Guided Behavior

ERG measurements revealed that the originally functionless rods of the *Cngb1* KO mice regained the ability to respond to light stimuli after gene supplementation. However, the visual cortex had never received regular visual information from the rods due to lack of functional rods from birth. In order to investigate whether the brain of a treated mouse was able to process the restored retinal function, the visual acuities of *Cngb1* KO and wildtype mice were analyzed at 9 months *pn* by observing the navigation in a visual Water Maze task (figure 28). In a circular swimming pool, mice had to locate a floating escape platform. Since they were water-shy, the mice were highly motivated to swim until they found the platform. The mice were trained for three days and the position of the platform was changed every day to minimize the learning factor. The swimming routes were recorded by a camera and monitored using the VideoMot2 software by TSE Systems. Mice had been swimming on two days in the dark to monitor rod-mediated behavior. Therefore, they had to be dark adapted prior to each day for at least 12 h. Subsequently, one day under daylight conditions was performed to investigate cone-driven vision. Figure 28A shows representative routes of an untreated and an rAAV5.hCNGB1 treated (10^9 vg) *Cngb1* KO mouse at the age of 9 months together with an age matched wildtype mouse at the second day under scotopic conditions. The wildtype had been swimming directly from the starting point in the right direction and thus quickly found the platform. However, the knockout mouse was unable to locate the platform from the other side of the basin and therefore had to explore the main part of the pool until it found the platform. The rAAV5.hCNGB1-treated *Cngb1* KO mouse, however, was considerably more directed and was therefore able to reach the platform much faster than the untreated *Cngb1* KO. Figure 28B displays the latency in seconds (s) illustrating how long a mouse needed to reach the visible platform. At the first day, mice that showed a wildtype-like behavior usually needed one or two trials to habituate causing a slightly prolonged latency and consequently an improvement from day 1 to day 2. Averaged, wildtype mice reached the platform in 11.23 ± 4.40 s at day 1 and improved themselves to day 2 to a latency of 6.23 ± 1.06 s, whereas untreated *Cngb1* KO mice could not improve themselves from day 1 to day 2 and had been swimming for 65.28 ± 11.88 s (day 1) and 66.61 ± 11.12 s (day 2) until they had contact with the platform. Thus, the *Cngb1* KO mice navigated significantly slower through the pool than the wildtype mice (p-value<0.001; Two-way ANOVA). Mice treated with the low dose (mouse group 1 - 10^8 vg) spent 51.06 ± 15.23 s in the pool at day 1 until they reached the platform. At day 2, their performance was even declined (64.08 ± 8.79 s). Mouse group 2 climbed the platform after an averaged latency of 45.29 ± 6.99 s at day 1 that could even be optimized at the second day to 31.60 ± 3.32 s. Thus, mice treated with the mid dose (10^9 vg) navigated significantly faster in the pool than the untreated control mice (p value = 0.02; Two-way ANOVA). When comparing the individual mice (see figure S3 in the appendix), it became evident that all mid-dosed mice (10^9 vg) needed less than 60 s at both days and improved themselves from day 1 to day 2 (except for one mouse). However, in mouse

group 1 and in the untreated control group, most of the individuals needed considerably longer (usually more than 80 s) to find the platform on at least one of the two days and no overall improvement from day 1 to day 2 was observed (figure S3). This indicated that mice treated with 10^9 vg of Lot#R18026 gained the ability to navigate using information provided by the rod visual system and this behavior was preserved until the age of 9 months. The differences in the latencies between mouse group 1 and the untreated control (p-value=0.52; Two-way ANOVA) as well as differences between mouse group 1 and 2 (p-value=0.06; Two-way ANOVA) were not significant.

Under daylight conditions, all mice were able to find the platform with a latency of less than 20 s showing that cone function was still sufficiently preserved to navigate under bright light. A directed navigation at bright light conditions also confirmed that the tested mice behaved normally. Mice that showed abnormal behavior during daylight such as floating in water, swimming in small circles or not moving away from the border of the pool were excluded from the evaluation of the experiment. Figure 28C shows how many individuals of a mouse group were able to find the platform within 1 min. Almost all wildtype mice reached the platform within 1 min (day 1: 95.83 ± 4.17 %; day 2: 100 %) whereas significantly less (p-value=0.001; Two-way ANOVA) untreated *Cngb1* KO mice managed to do so (day 1: 53.70 ± 12.96 %; day 2: 48.15 ± 10.19 %). In 70 ± 15.28 % of the swimming iterations of mouse group 1 the platform was found within 1 min at day 1 and in 46.67 ± 9.72 % at day 2 revealing no significant improvement compared to the untreated control (p-value=0.57; Two-way ANOVA). However, the mid-dosed group (group 2) was significantly more successful than the control group (p-value=0.03; Two-way ANOVA). 73.33 ± 11.30 % (day 1) and 86.67 ± 6.24 % (day 2) of the swimming iterations of mouse group 2 were able to find the platform within 1 min. Again, the difference between mouse group 1 and 2 was not significant (p-value=0.07; Two-way ANOVA), which confirmed the latency data.

Taken together, these data showed that *Cngb1* KO mice treated with rAAV5.hCNGB1, depending on the vector dose, regained the ability to orientate in a room and that this behavior was maintained at least until 9 months of age. Thus, it was proven that the treated mice were able to process the recovered photoreceptor function.
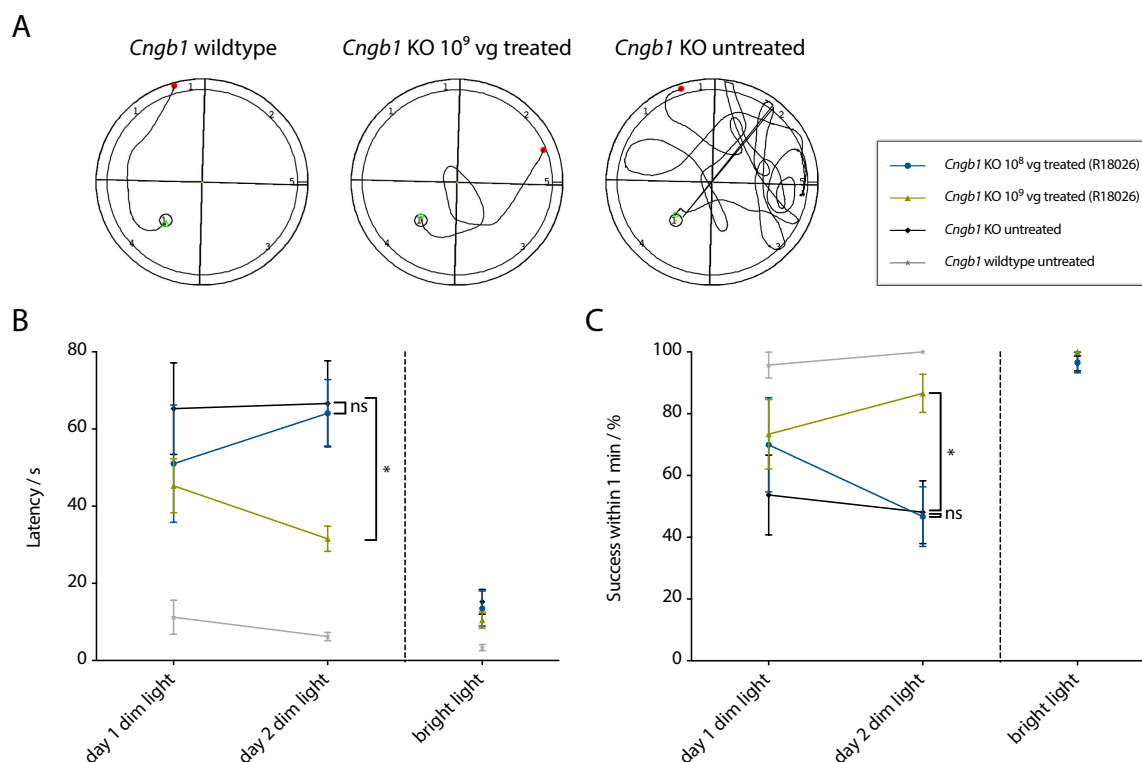
Figure 28: The preserved retinal function of rAAV5.hCNGB1-treated *Cngb1* KO mice was processed by the mouse brains resulting in improved spatial navigation. Navigation of *Cngb1* KO (rAAV5.hCNGB1-treated and untreated; R18026; 10^8 vg and 10^9 vg) and wildtype mice in a visual Water Maze task at the age of 9 months. In a circular swimming pool, mice had to locate a floating escape platform and their swimming routes were recorded. Mice had been swimming on two days in the dark for monitoring rod-mediated behavior and additionally, one day was performed under daylight conditions to investigate cone-driven vision. A. Representative routes of a wildtype mouse, a 10^9 vg-treated *Cngb1* KO mouse, and an untreated control at the second day of the task under dim light conditions. The wildtype located the platform from the other end of the pool and therefore immediately navigated in the right direction. The untreated *Cngb1* KO did not perceive the platform and therefore had to search most of the pool until it encountered the platform, whereas the mid-dose-treated KO (mouse group 2) regained the ability to visually locate the platform resulting in a more rapidly approaching to the destination, as seen for the untreated control. B. Latencies, describing the time until the platform was reached, demonstrated the incompetence of the untreated *Cngb1* KO mice to quickly find the platform, whereas the averaged latency of the wildtype mice was lower than 10 s. Mouse group 1 (10^8 vg) was not able to find the platform significantly faster than the control group, as both groups needed more than 60 s to reach the destination at day 2. However, a significantly faster navigation compared to the control group was discovered for mouse group 2 (10^9 vg-treated), manifesting in a mean latency of about 30 s at day 2. C. Success within 1 min, describing, how often a mouse group climbed the platform within 1 min (% of total trials). The wildtype mice were 100 % successful at day 2, whereas at this day only about half of the trials were successful in case of the untreated *Cngb1* KO mice and mouse group 1. Mouse group 2 was capable to reach the platform in 80 % of the swimming iterations (day 2), and thus showed a significant improvement compared to the control. Values are given as mean ± SEM. 10^8 vg: n=5; 10^9 vg: n=5; untreated: n=9; wildtype: n=4. Statistics: Unpaired two-way ANOVA with Sidak's post hoc test (*: $p \leq 0.05$; **: $p \leq 0.01$; ***: $p \leq 0.001$).

3.11 Addressing the Time Window for a Therapeutic Option

In this work it was shown, that by supplementing hCNGB1, the degeneration of the photoreceptors can be halted. However, with this therapy, it is not possible to restore cells that are already degenerated. Therefore, it will be important to treat RP45 patients as early as possible before substantial photoreceptor degeneration has started. RP45 is characterized by a slow disease progression, so that the degeneration of rod photoreceptors does not begin until adulthood (Hull et al., 2017), thereby providing a large time window for a treatment of human patients. However, the human brain is able to compensate a malfunction of the rod cells over a long period of time, so that patients often do not notice symptoms until the visual field is already constricted due to rod death. Therefore, it is important to also obtain information about the treatment efficacy of rAAV5.hCNGB1 when administered at later disease stages.

Therefore, 6-month-old *Cngb1* KO mice were treated with high doses of rAAV5.hCNGB1 (10^{10} vg, X17044A and R18026). At this age, about 50 % of the rod photoreceptors have been already lost, while cones remain most widely unaffected until this age (Hüttl et al., 2005). The progression of retinal degeneration was assessed using OCT. At 4 months *pi* (10 months *pn*) a high variation in the photoreceptor layer thicknesses was observed among the measured retinas (figure 29B). Two retinas (out of 10 injected eyes) were detected (one for each vector lot) that showed a delayed photoreceptor degeneration in response to the treatment with rAAV5.hCNGB1 at 4 months *pi*. Within these two retinas, a preservation of the photoreceptor outer segments was observed (figure 29A), which were not seen in untreated control retinas (10 months *pn*). OS rescue resulted in markedly thicker photoreceptor layers (differences of 17 μm (X17044A) and 14 μm (R18026) compared to the respective contralateral eyes; figure 29B). For the other tested eyes, however, only a marginal preservation of photoreceptors was observed, suggesting that a substantial amount of photoreceptors were already in state of degeneration which precluded a treatment effect. This high variability of disease progression was also obvious by comparing the individual control eyes. Furthermore, the number of already degenerating cones might have played a role in this variance, as well as the number of cells being already in the stage of apoptosis leading to differences in retinal stress (discussed in section 4.2). Nevertheless, the data also showed that a prevention of disease progression could be achieved by rAAV5.hCNGB1 at this late disease stage. Furthermore, no obvious differences were visible between the different vector lots, indicating no toxic side effect for R18026, when applied to 6-months-old mice.
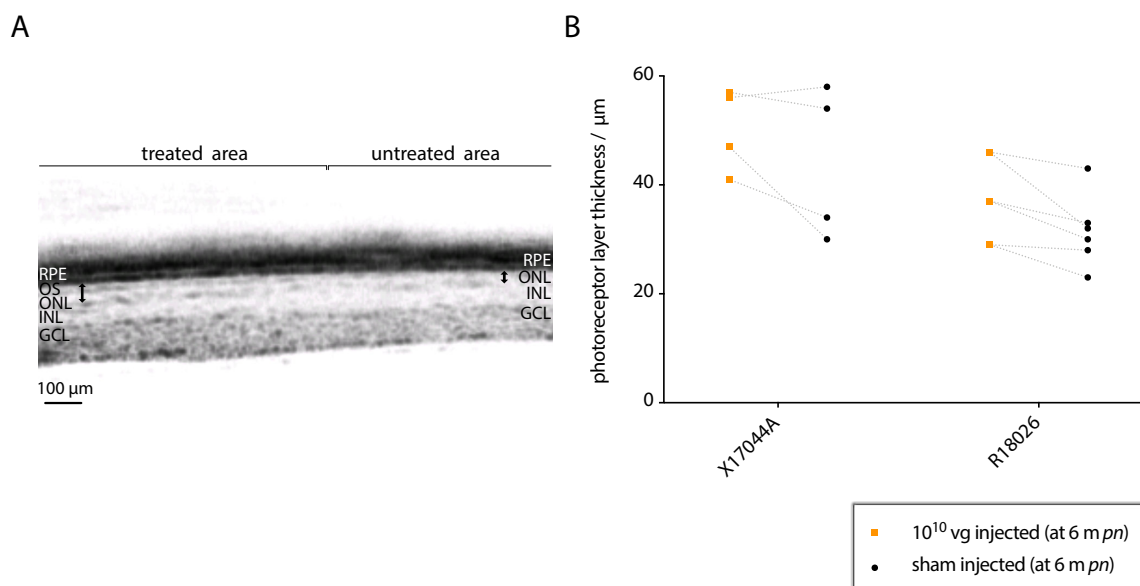
Figure 29: Addressing the time window for a treatment option. *Cngb1* KO mice were injected with 10^{10} vg of rAAV5.hCNGB1 (X17044A and R18026) and OCT measurements were performed at 4 months *pi* (10 months *pn*). In case of two retinas, photoreceptor OS were saved, while in the other retinas, no distinct treatment effect was visible. A. OCT image depicting the rescued OS in the treated part of a 10-months-old murine retina (*Cngb1* KO), that was injected with 10^{10} vg of R18026. Within untreated part, no OS were present, which demonstrated the photoreceptor preservation through the treatment with rAAV5.hCNGB1. B. Photoreceptor layer thicknesses of rAAV5.hCNGB1 treated (10^{10} vg; X17044A and R18026) compared to the respective sham-injected contralateral eyes at 10 months of age, revealing the marked rescue of photoreceptor layer observed in two mice, while in the other eyes, no obvious differences between the contralateral eyes were detectable. Furthermore, no clear difference was observed between vector lot X17044A and R18026. X17044A. n=4. R18026. n=6

3.12 The rAAV5.hCNGB1 Treatment Resulted in Reduced Müller Cell Gliosis

Müller glia cells respond to retinal stress by changing their morphology, biochemistry and physiology (Bringmann et al., 2009). This reaction is termed reactive gliosis (or Müller cell gliosis) and describes a cellular process intended to protect retinal tissue for example by structural stabilization, by encouraging repair mechanisms and restricting tissue remodeling, as well as through modulation of immune- and inflammatory responses (Bringmann and Wiedemann, 2012). One early and sensitive indicator for retinal stress is the upregulation of the glial fibrillary acidic protein (GFAP) showing the induction of intermediate fibers by glial cells (Bignami and Dahl, 1979; Bringmann and Reichenbach, 2001; Lewis and Fisher, 2003). It was shown, that photoreceptor degeneration led to upregulation of GFAP expression in mice (Ekström et al., 1988; Hippert et al., 2015; Roche et al., 2016) and also in humans (Fariss et al., 2000). However, retinal injury as well as retinal detachment can also lead to an increased GFAP level (Lewis and Fisher, 2003; Lewis et al., 2010). In the *Cngb1* KO mouse model, an upregulation of GFAP expression starts 21 days after birth as a consequence of the degeneration process (Hüttl et al.,

2005). A reduction of the GFAP level as a result of murine *Cngb1* gene supplementation has already been demonstrated (Koch et al., 2012).

To prove whether this can also be achieved by supplementation of the human *CNGB1* gene, immunohistochemistry was performed with retinal cross sections of rAAV5.hCNGB1-treated *Cngb1* KO mice with an antibody against GFAP. The CNGB1 antibody served as a positive control for human CNGB1 expression (treated region of the retina). Figure 30 shows GFAP (green signal) and CNGB1 expression, as well as Hoechst 33342 staining in retinal cross sections of treated *Cngb1* KO (Lot#R18026) and wildtype mice at 10 months *pn*. In the wildtype (pictures at the bottom), only the end feet of the Müller glia were GFAP positive (green signal) and no GFAP expression was found in the intermediate fibers, indicating lack of retinal stress in this mouse. Within the untreated part of the mid-dosed *Cngb1* KO retina (10^9 vg), a distinct GFAP upregulation was visible, demonstrating enhanced glial cell activity (images in the upper part of the figure). By the treatment with 10^9 vg of Lot#R18026 (treated area; mouse group 2; top panels in figure 30), a reduction of the Müller cell gliosis was achieved manifesting as a decreased GFAP expression at the age of 10 months compared to the untreated part of this retina. The data indicated a reduced retinal stress as a consequence of a degeneration that was substantially decelerated by the treatment. However, GFAP levels were markedly higher in the 10^8 vg and 10^{10} vg treated retinas (figure 30; central images) compared to both treated and untreated part of the mid-dosed retina (10^9 vg). Furthermore, there was no visible difference between the treated and the untreated part of the low-dosed retina (10^8 vg), indicating, that a treatment with 10^8 vg or 10^{10} vg did not reduce the reactive gliosis. This confirms the assumption, that the degeneration process was neither halted by the low dose, nor by the high dose. The data further suggested, that the reduced Müller cell activity seen in mouse group 2 (10^9 vg) was not restricted to the treated part, but the treatment with rAAV5.hCNGB1 even achieved a reduction of retinal stress in the whole retina.

Combined, these data demonstrated that Müller cell gliosis could be dose-dependently reduced by rAAV5.hCNGB1, showing that therapy led to a significant downregulation of retinal stress. Since a degeneration progression is associated with retinal stress, these data indicated that the treatment with rAAV5.hCNGB1 had the potential to arrest retinal degeneration in the *Cngb1* KO mouse model even after a long period of time.
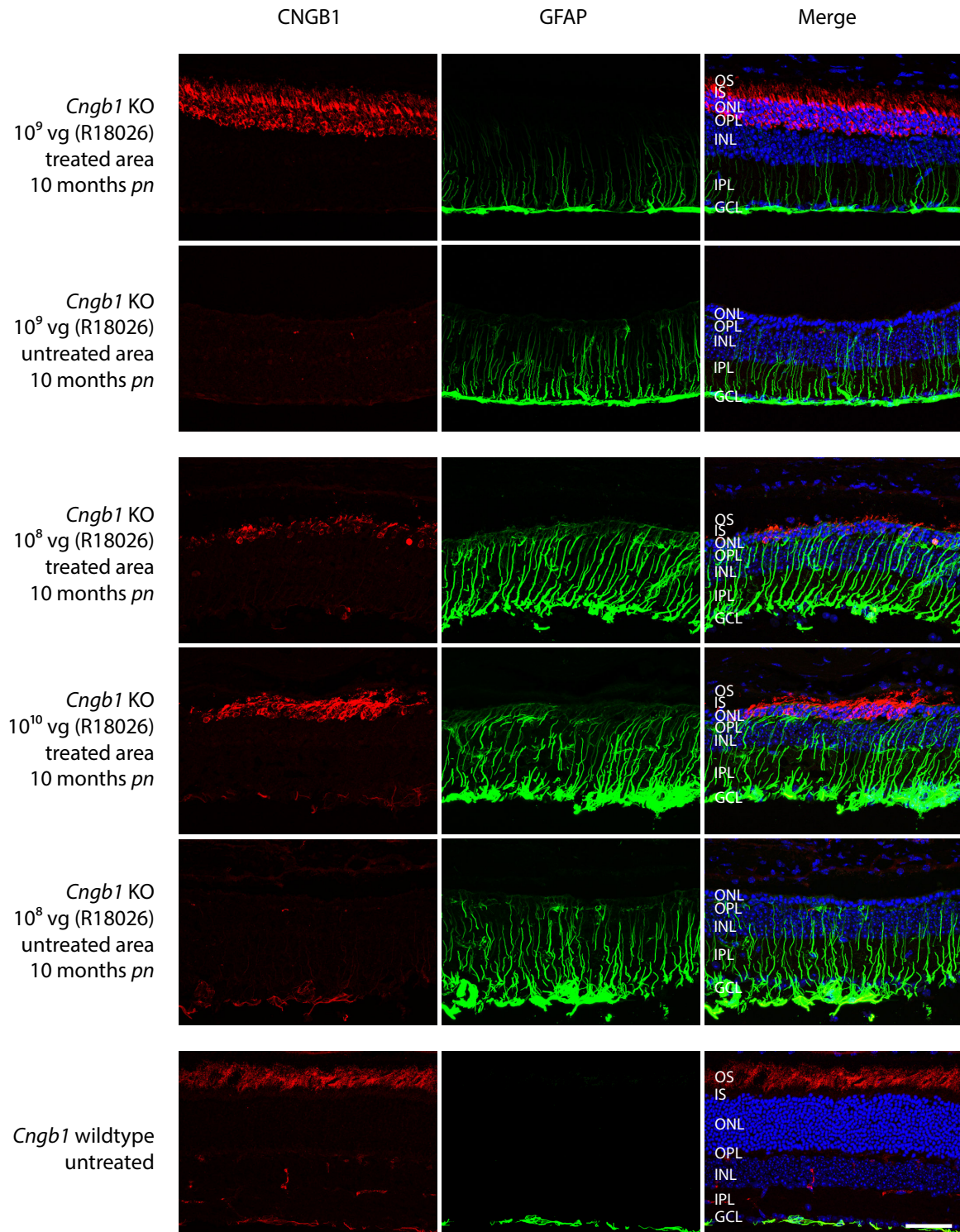
Figure 30: rAAV5.hCNGB1 treatment resulted in reduced Müller cell gliosis. Representative confocal images of retinal cross sections of a wildtype mouse compared with *Cngb1* KO mice, subretinally injected with different doses of AAV5.hCNGB1 (Lot#R18026) at 4 weeks of age. All retinas were dissected at 10 months *pn* and immunohistochemistry was performed using anti-CNGB1 (red signal) and anti-GFAP (green) antibodies, as well as Hoechst 33342 for nucleus staining (blue). The injection of 10^9 vg achieved a decreasing of the GFAP expression in the treated area, compared to the untreated part (outside the subretinal bleb) of the same retina, indicating reduced Müller cell gliosis due to the treatment. The remaining intermediate fibers in the treated *Cngb1* KO retina suggested that mild retinal stress was still present. However, the GFAP levels in mouse group 1(treated and untreated) and 3 (treated) were markedly higher than in both treated and untreated part of mouse group 2, underlining the strength of the reduction of gliosis by the treatment with 10^9 vg but also proving that a treatment with the

high- or low dose did not achieve a decreasing of Müller cell activity. It further suggested that the mid-dose treatment decreased the level of Müller cell gliosis beyond the borders of the treated part. Scale bar marks 50 µm. OS. outer segments, IS. inner segments, ONL. outer nuclear layer, OPL. outer plexiform layer, INL. inner nuclear layer

3.13 The Biological Efficacy of rAAV5.hCNGB1 in the *Cngb1* KO Dog Model

To further evaluate the biological efficacy of rAAV5.hCNGB1 in the *Cngb1* KO dog model, photoreceptor function was measured by scotopic ERG and visual acuity was assessed by performing a four-choice-vision-test under dim-light conditions. Table 7 gives a short summary of the *in vivo* biological efficacy testing at 6 months post injection. The calculated differences of the b-wave amplitudes at a luminance level of 0.01 cd s m^{-2} (rod-specific stimulus) in relation to the untreated *Cngb1* KO control eyes demonstrated a substantial increase in photoreceptor function for all dog groups. The lowest dose of rAAV5.hCNGB1 resulted in a 2.4-fold higher b-wave amplitude than the untreated control. The dog groups injected with 1×10^{11} vg or 2×10^{11} vg showed an increase in retinal function of about 3 fold to the control, and with the highest dose even a beneficial effect of 5.7 fold of the control was recorded. For investigation of the dim light vision the four-choice vision testing system was used (Gearhart et al., 2008). The experiment started by placing a dog in a non-transparent box with four tube-shaped exits. Only one tube was open, allowing the dog to exit the box, while the other tubes were blocked at the external side. With a camera, the behavior of the dog was recorded until it found the exit. After each trial a different tube was opened, so that the dog had to find the exit again each time and the learning factor was excluded. The covering of the respective contralateral eye allowed the assessment of every eye separately. Table 7 gives information about the number of attempts a dog needed to find the exit (mean correct exit choice / % of total trials) as well as about the time it took a dog to find the exit (mean time to exit / s). All trials shown were performed at a low luminance level of 0.01 cd s m^{-2}. The data showed that with rAAV5.hCNGB1-treatment, the *Cngb1* KO dogs chose the right exit in almost 100 % of all trials already at the first attempt, whereas the dogs with untreated eyes only found the correct exit in about 50 % of all trials. By evaluating the time, it took each dog to find the correct exit, it was observed that the dogs with an rAAV5.hCNGB1-treated eye, regardless of the vector dose, found the correct exit in much less time than the control dogs. With a treated eye the dogs were about 4-5 times faster than with an untreated eye. Thus, it could be shown that administration of even the smallest vector dose of rAAV5.hCNGB1 resulted in the ability of the *Cngb1* KO dogs to orient and navigate in the dark in a wild-type-like manner.

Taken together, these data showed that photoreceptor function in *Cngb1* KO dogs was markedly restored with each virus dose of rAAV5.hCNGB1 and the higher the dose, the more function was

recovered. It was also demonstrated that even the smallest amount of virus was sufficient to ensure wild-type-like behavior in the dark.

Table 7: *In vivo* biological efficacy testing of rAAV5.hCNGB1 treated and untreated *Cngb1* KO dogs at 6 months *pi*. At a luminance level of 0.01 cd s m^{-2} the b-wave amplitudes of all treated dog retinas recorded in the ERG, demonstrated a substantial increase in photoreceptor function compared to the untreated *Cngb1* KO control retinas in a dose dependent manner (rod response /mean b-wave amplitude / fold change). Vision testing revealed that with rAAV5.hCNGB1-treatment, the *Cngb1* KO dogs passed the four-choice test much faster (mean time to exit / s) and more accurately (mean correct exit choice / % of total trials) than the untreated control dogs, revealing a dose-independent, wildtype-like behavior for all dogs.

Dose group	Number of dog eyes	Biological efficacy at 6 months *pi*		
		Rod response - mean b-wave amplitude / fold-change	Vision testing - mean correct exit choice / % of total trials	Vision testing - mean time to exit /s
1×10^{12} vg	5	5.7	100	3.4
2×10^{11} vg	4	2.9	98.6	4.6
1×10^{11} vg	5	3.3	100	5.8
2×10^{10} vg	3	2.4	100	4.6
untreated	2	-	53.5	23.7

3.14 Degeneration-Induced Microglia Activation was Prevented by rAAV5.hCNGB1 in *Cngb1* KO Dogs

Retinal degenerative diseases often go along with a chronic pro-inflammatory environment. Microglia represent the immune cell population present in the retina and thus mediate the inflammatory reactions within this tissue. Under acute conditions, inflammatory processes protect the retina (Karlstetter et al., 2010; Gupta et al., 2018). But under chronic conditions, as in degenerative retinal diseases, microglia get pathologically activated. When photoreceptors degenerate, microglia migrate to the outer retina towards the photoreceptors and change their morphology from filopodial-like to amoeboid, leading them to release excessive amounts of inflammatory mediators and to randomly phagocytize stressed but living photoreceptors (Zhao et al., 2015). Both result in tissue damage and deterioration of the disease (Gupta et al., 2003, Rashid et al., 2019). An increased number of activated microglia was also found in 4-week-old *Cngb1* KO mice (Blank et al., 2017).

In order to investigate whether the degeneration progress in the *Cngb1* KO dog model comes along with amoeboid microglia, an immunohistochemistry staining was performed using an antibody against the ionized calcium-binding adapter molecule 1 (IBA-1), which is a marker for microglia in the retina. Furthermore, the staining was intended to clarify whether a prevention of the pathological microglia activation by *CNGB1* gene supplementation can be achieved. The anti-CNGA1 identified the treated regions within one section. By investigating the untreated area (shown by CNGA1 absence) of a *Cngb1*

KO dog retina (figure 31A), filopodial-shaped IBA-1-positive cells were found in the inner retina indicating persisting microglia. Additionally, a few microglia were found in the outer retina that had already been transformed into an amoeboid form. This suggested an immune reaction in the untreated *Cngb1* KO dog eye at the age of 15 months and revealed that also in the large animal model of RP45, inflammation was a side effect of photoreceptor degeneration. By analyzing the treated part of a *Cngb1* KO dog retina (injected with 1×10^{12} vg of rAAV5.hCNGB1), no activated microglia were found in the ONL or the subretinal space, confirmed by the strict localization of IBA-1 to the inner retina. Therefore, it is suggested that the inflammatory reaction in the retina could be prevented by the treatment with rAAV5.hCNGB1 using vector Lot#X17044A.

Throughout the *in vivo* experiments of the dog dose escalation study, patchy areas of retinal thinning were detected within fundus imaging of one eye of a *Cngb1* KO dog that was treated with 2×10^{11} vg of rAAV5.hCNGB1. Furthermore, despite no differences in vision-guided behavior compared to the other dogs treated with 2×10^{11} vg (100 % correct exit choice; mean correct exit choice of the respective dog group: 98.6 %; see table 7), a reduced treatment efficacy of rAAV5.hCNGB1 was observed in case of that dog eye, reflecting as reduced electric potentials in the ERG (no increased rod-specific b-wave amplitudes compared to the untreated *Cngb1* KO eyes at 6 months *pi*; data not shown) and as smaller numbers of rescued photoreceptors at 15 months of age (12 months *pi*; figure 31B; upper panels). Only 7 rows of photoreceptors were counted in the treated retinal area of the eye showing the adverse effects (figure 31B), whereas 12 lines were still present in other *Cngb1* KO dog eyes treated with the same vector dose (see figure 24). CNGA1 staining revealed a localization of CNGA1 to the ROS, indicating CNGB1 expression and intact OS in the treated retina. By examination of this retina for inflammatory processes by IBA-1 staining, a high number of activated microglia was found and this was only slightly reduced in the treated area (figure 31B; upper panels). This suggested that the affected dog had developed an immune response in its eye manifesting as migrating microglia, which further contributed to the death of photoreceptors. The green signal seen within the GCL of the treated area of the affected retina resulted from unspecific staining of the secondary antibody due to the close location of the cross section to the optic nerve. Based on recent findings of inflammatory processes that spread to the contralateral eye (Tribble et al., 2019), the contralateral eye of the affected dog (treated with 1×10^{12} vg) was investigated (figure 31B; lower panels). The untreated retina of the contralateral eye showed a high amount of amoeboid microglia, but less microglia were found compared to the affected eye. With rAAV5.hCNGB1-treatment, inflammation process was marginally reduced. Hoechst 33342 staining revealed a slightly thicker ONL compared to the affected eye, but still considerably less photoreceptors had remained (8 rows) than in other high-dosed retinas (12 rows of photoreceptors; figure 24). This indicated, that the immune reaction had spread to the contralateral eye where it manifested in a slightly attenuated form.

Taken together, the data shown in figure 31 demonstrated that, less prominent than in the *Cngb1* KO mouse model, inflammation was also occurring in the *Cngb1* KO dog model and that this immune reaction could be prevented by *CNGB1* gene supplementation evoked by rAAV5.hCNGB1-treatment. However, in exceptional cases, the treatment using rAAV5.hCNGB1 can lead to intensified inflammation as it was seen one *Cngb1* KO dog eye within the dog dose escalation study.
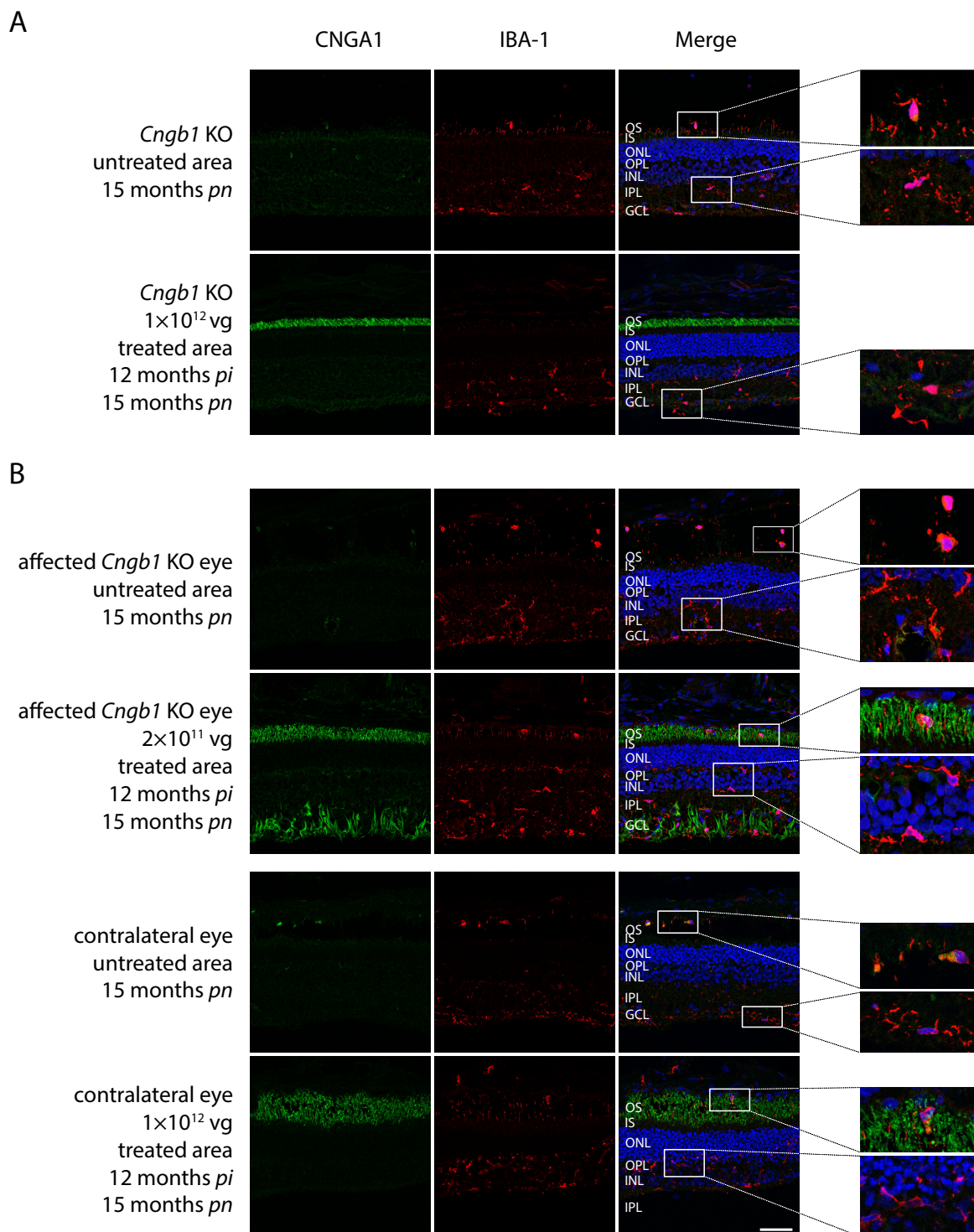
Figure 31: Degeneration-induced immune reaction of *Cngb1* KO dogs could be prevented by rAAV5.hCNGB1, while one dog showed an inflammatory response to the treatment. A. Representative confocal images of retinal cross sections of a *Cngb1* KO dog, treated with 1×10^{12} vg of Lot#X17044A. Immunohistochemistry was performed at 12 months *pi* using anti-IBA-1 (red signal) and anti-CNGA1 (green) and Hoechst 33342 (blue). The untreated area (shown by CNGA1 absence) revealed filopodial-shaped IBA-1-positive cells in the inner retina indicating persisting microglia. Additionally, a few amoeboid microglia were found in the outer retina, suggesting an immune reaction in the *Cngb1* KO dog eye in response to retinal degeneration. In the treated part of the retina, no activated microglia were found in the photoreceptor layer or within the subretinal space implying a prevention of microglia activation by the treatment. B. Upper panels. Immunohistochemistry of retinal cross sections of a *Cngb1* KO dog eye that showed adverse events throughout the *in vivo* experiments. The eye was treated with 2×10^{11} vg of X17044A and the retina was harvested at 12 months *pi*. Anti-IBA-1 staining revealed a high number of activated microglia within both treated and untreated part of the retina. Furthermore, Hoechst 33342 staining displayed a markedly thinner ONL in the treated retinal part compared to other retinas treated with the same vector dose, indicating an immune response in that eye which resulted in migrating microglia leading to photoreceptor death. Compared to the affected eye, its contralateral eye, which was treated with 1×10^{12} vg, showed a slightly reduced amount of amoeboid microglia in both treated and untreated retinal parts. The ONL thickness was considerably lower as within the other retinas treated with the high vector dose, indicating a spreading of the inflammation to the contralateral eye where it manifested in a slightly attenuated form.

4   Discussion

Loss-of-function mutations in the cyclic nucleotide-gated channel beta 1 subunit (*Cngb1*) gene are known to cause *Retinitis pigmentosa* type 45 (RP45) – a hereditary blinding disease. In this study a novel recombinant AAV vector for an efficient expression of human CNGB1 in rod cells was developed and its efficacy treating RP45 was investigated in two different *Cngb1* KO animal models.

The study demonstrated efficient, specific, and long-term hCNGB1 expression in murine and canine rod photoreceptors driven by the shortened human rhodopsin promoter (*hRHO194*). By treatment with rAAV5.hCNGB1, a substantial preservation of rod and cone photoreceptors was achieved in both *Cngb1* KO mice and dogs. Furthermore, the efficacy of rAAV5.hCNGB1 was dose-dependent manifesting itself as an increasing expression level with ascending dose, resulting in enhanced biological efficacy in both animal models. However, a toxic side effect was identified for the vector lot produced in a producer cell line, emerging in a dose-dependent manner, which was not observed for the vector lot produced by triple-transfection. It was further shown, that the introduced human CNGB1 subunit was capable of forming functional chimeric rod-specific CNG channels together with murine as well as with canine CNGA1 subunits leading to a recovery of rod photoreceptor function in both animal models. Both animal models were also able to process the regained retinal function, resulting in a significantly improved navigation in the dark in the case of the mouse model and even in a wild-type-like rod mediated behavior of the treated dogs. Furthermore, retinal stress in the *Cngb1* KO mouse, manifesting as Müller cell gliosis, was reduced by rAAV5.hCNGB1, even beyond the treated region of the retina. Finally, it was shown that a degeneration-induced inflammation was diminished by the treatment, shown as reduced microglia activation. However, one dog developed an immune reaction against the applied virus seen as migrating microglia to the ONL.

These results demonstrated the efficacy of the *hCNGB1* gene supplementation therapy in small and large animals and thus showed the transferability of this approach to human application. Thereby, the work covered a major part of the preclinical drug development phase and proved to be a suitable candidate for a clinical application. In addition, this work served as a basis for a design of preclinical toxicology studies as well as for early-phase clinical application of this vector. A subsequent toxicological study in mice, dogs, and non-human primates (NHP) would complete the preclinical phase using the definitive AAV vector produced under good laboratory practice (GLP) conditions. Finally, the data obtained here provided important information for new and innovative approaches towards future therapies.

4.1 *hRHO194* and AAV2/5 Enabled Efficient and Long-Term Transgene Expression in Rod Photoreceptors

4.1.1 AAV5 as Suitable Capsid for Photoreceptor-Targeted Gene Expression

First subretinal injections of AAV5.eGFP (X17044B; expression was driven by *hRHO194*) into a wildtype mouse showed initiation of target gene expression, visualized by eGFP fluorescence, at about 2 weeks after vector administration (figure 17A). A delay of 2-4 weeks was also observed previously for both AAV2/5 as well as for AAV2/2 (Auricchio et al., 2001), reflecting the time required for the vector DNA to enter the cell nucleus and become transcriptionally active. It is assumed that the process of viral uncoating plays a significant role in the kinetics of transgene expression, and this depends on the type of capsid (Thomas et al., 2004; Natkunarajah et al., 2008). Although the AAV5 serotype has slower kinetics and also a lower photoreceptor transduction efficiency than AAV8 (Allocca et al., 2007; Natkunarajah et al., 2008; Mussolino et al., 2011; Vandenberghe and Auriccho, 2012), it has been shown to be a suitable vector for targeting photoreceptors in several *in vivo* studies even outperforming the well-established AAV2 (Auricchio et al., 2001; Yang et al., 2002; Lotery et al., 2003; Pang et al., 2007; Li et al., 2009; Vandenberghe and Auriccho, 2012). In addition, AAV5 has been shown to effectively target photoreceptors in canine and NHPs and has been successfully used to restore retinal function and maintain retinal structure in models of various retinal diseases (Min et al, 2005; Alexander et al, 2007; Mancuso et al, 2007; Pang et al, 2008; Mancuso et al., 2009; Komaromy et al, 2010; Gorbatyuk et al, 2010; Beltran et al., 2010; Boye et al, 2010; Pang et al, 2010; Li et al, 2011; Mao et al, 2011; Pang et al, 2012; Boye et al., 2012; Lopes et al., 2013; Lhériteau et al., 2014; Banin et al., 2015; Ye et al., 2017; Deng et al., 2019).

4.1.2 Pros and Cons of the Subretinal Injection – Emerging Alternatives

In the presented mouse study, approximately 30 % of the retina were covered by one single subretinal injection of 1 µL volume, which was already observed in previous studies using other AAV serotypes (Michalakis et al., 2010; Schön et al., 2017). Due to the marginal lateral spreading of this virus, the area did not increase noticeably beyond the area of the subretinal bleb over the weeks. This was further indicated by the sharp transition zone from the treated to the untreated part. Therefore, only 30 % of the retinal tissue was treated. The low lateral spreading of AAV5 has also been demonstrated in dogs (Bruewer et al., 2013). Other AAV serotypes showed greater lateral spreading in the retina, but the area, that can be covered by a subretinal injection, is generally limited. Further disadvantages of subretinal injections (SR) include the retinal detachment, creating a gap between the photoreceptor layer and the

RPE, which can cause several harmful macromolecular and structural modifications in the retina. In case of a degenerating retina, there is also the risk of retinal thinning or even holes, as the retina is already very fragile. Adverse side effects can also include choroidal effusion or ocular hypo- or hypertension (Fisher et al., 2005; Maguire et al., 2008; Dalkara et al., 2009; Jacobson et al., 2012; Vandenberghe et al., 2013; Bainbridge et al, 2015; Reid et al., 2017; Takahashi et al., 2018). Therefore, many scientists work on alternative delivery methods. Promising results have been achieved by the less invasive intravitreal (IV) injection, where the drug is administered into the vitreous, leading to the distribution of the applied rAAV over the entire retina. However, most of the natural AAV serotypes are trapped in the inner limiting membrane (ILM) at the vitreoretinal junction. It contains a number of extracellular matrix proteins and some are recognized by the AAVs as receptors, preventing virus passaging (Candiello et al., 2007; Halfter et al., 2008; Dalkara et al., 2009). For this reason, there have been approaches to surgically remove the ILM prior to intravitreal AAV injection (Takahashi et al., 2018; Teo et al., 2018). Other researchers are instead focusing on the development of novel mutant capsid variants. By generating capsid libraries, novel AAV variants are currently being developed, which are intended to no longer recognize the receptors of the ILM and are therefore be able to reach the outer retinal cells as well as the RPE (see section 4.7.1; Dalkara et al., 2013; Kay et al., 2013; Weinmann and Grimm, 2017; Hickey et al., 2017; Reid et al., 2017; Büning and Srivastava, 2019). However, a large portion of the vector is already eliminated within the anterior route following an intravitreal injection (Park et al., 2016). Furthermore, IV injections carry an elevated risk of immune responses to the rAAV. Based on several preclinical studies it is assumed that neutralizing antibodies (NAbs) are more likely to be produced after IV injections than after SR injections (Li et al., 2008; Amado et al., 2010, Vandenberghe et al., 2011). A large number of neutralizing antibodies has the potential to inhibit gene transfer efficiency, which becomes even more relevant for vector re-administrations or a time-shifted injection of the contralateral eye (see section 4.7.2; Kotterman et al., 2015; Bennett et al., 2016; Seitz et al., 2017; Reichel et al., 2017 and 2018; Lee et al., 2019). Due to these hurdles, the field of retinal gene therapy is currently still dominated by subretinal injections, as in the preclinical mouse and dog study presented herein. However, in future, the intravitreal injection may become an emerging application method for this field.

4.2 Preservation of Photoreceptors by rAAV5.hCNGB1 Therapy - the Relevance of the Animal Model and the Timing of Treatment

In the *Cngb1* KO mouse model, hCNGB1 was stably expressed at least up to 9 months post injection accompanied by a rescue of about 8 lines of photoreceptor nuclei, whereas only one line remained in the untreated part of the retina. Thus, it is assumed that the degeneration was stopped in a great number of cells once the *CNGB1* gene was expressed. However, still considerably fewer photoreceptors survived

compared to a wildtype of the same age, which, on the one hand, was caused by the fact that not every rod cell was infected by an rAAV and also not every infection resulted in episomal persistence of the recombinant DNA, since it is estimated that only about 30 % of all rAAVs reaches the nucleus of an infected cell (Zhong et al., 2008; Xiao et al., 2012). There are several host-cell mechanisms to prevent rAAV infection during the different steps including cellular uptake, post-entry trafficking, nuclear import, second-strand synthesis, and transgene expression (see section 1.2.2). One important host-mechanism preventing efficient AAV transduction is the ubiquitin-dependent proteasomal degradation, which is currently also a target for rAAV transduction improvements (see section 4.7.2; Duan et al., 2000; Zhong et al., 2008; Nathwani et al., 2009; Mitchell and Samulski, 2013; Gabriel et al., 2013; Berry and Asokan, 2016). On the other hand, progressing degeneration within the treated part of the retina might be also due to the rod outer segment (ROS) shortening, which had already started before the injection time point (age of 4 weeks). In the *Cngb1* KO mouse model, the degeneration of the ROS already begins at the age of 15 days while the maximum of dying photoreceptor cells is already reached on day 23 (Hüttl et al., 2005; Paquet-Durand et al., 2011). Since additional two weeks passed between injection and the start of transgene expression (see section 4.1.1), a considerably large number of ROS was already affected by degeneration resulting in the death of the respective photoreceptors. So far, only sporadic studies demonstrated that degeneration can be halted even in advanced stages of RP (Koch et al., 2015). More often, data from preclinical and clinical studies showed that only a limited time window exists in which an RP patient can be treated. If a certain time point (point of no return) is exceeded, the treatment no longer prevents the progression of degeneration (Cideciyan et al., 2013; Cepko and Vandenberghe, 2013). It is known, that already degenerated cells cannot be restored, but it is not yet known whether a cell that is already in a state of apoptosis can be saved from complete death. There are already approaches that aim to target apoptosis in photoreceptors for the therapy of RP (Marigo, 2007). Oxidative stress, capable of leading cells to a state of apoptosis, is known to play a key role in retinal degeneration (Sanvicens et al., 2004; Trachsel-Moncho et al., 2018). There is also a hypothesis that attributes the mutation-independent cone degeneration to the oxidative stress emerging during rod death (Usui et al., 2009). The administration of antioxidants could therefore help to reduce cone degeneration (Komeima et al., 2007; Sanz et al., 2007; Drack et al., 2012). Therapeutically relieving stress from cells prior to treatment might be a solution to extend the effectiveness of gene therapy beyond the point of no return. Improvements in transduction efficiencies could also be helpful to address this issue (Petit et al., 2016).

After treatment with rAAV5.hCNGB1 many rod cells still died in the mouse retina, but it was demonstrated that the cone cells in the treated part of the retina were completely intact even after a long time period (age of 10 months; 9 months after injection; figure 21). At this late RP stage, the cones in the untreated retina were only visible as sleeping cell bodies. In addition, a long-term beneficial effect

on photoreceptor function was demonstrated (figure 27), as well as a substantial restoration of vision (figure 28). Furthermore, it was shown that retinal stress, manifesting as Müller cell gliosis, was very pronounced in untreated *Cngb1* KO retinas, but was only marginally present within the retinal parts that were treated with rAAV.hCNGB1 (figure 30). Together, this suggests that visual function was restored and disease progression was prevented in the treated mouse retina even over a long time period, proving that the rAAV5.hCNGB1-therapy was efficient in the *Cngb1* KO mouse model.

However, treatment with rAAV5.hCNGB1 showed an even more positive effect in the dog study. In the treated *Cngb1* KO dog retinas, only very few photoreceptors were degenerated until the long-term time point (see figure 24) and also photoreceptor function (see table 7) was restored more markedly compared to the mouse model. Several factors might play a role in the differences of the therapeutic outcome between the mouse and the dog study, mainly involving the differences in the eye morphology allowing more precise subretinal injections into canine eyes than into murine eyes (see section 1.3). Since it is known that the dog eye is much more similar to a human eye than a mouse eye, the canine study mimics the clinical situation much more closely. The mouse eye has a size of only 3.5 mm, whereas the eyes of dog and human are both larger than 20 mm (see section 1.3). In addition, the eye to lens ratio in dogs and humans is very similar, both possess a small lens providing a large space for the vitreous. In the mouse eye, however, the lens occupies almost the entire vitreous area, so it has to be injected from posterior. Dog and human eyes allow the anterior approach, offering the possibility of a safer and more precise injection (see section 1.3). In addition, the large size of the human and dog eye allows for permanent monitoring during surgery. Consequently, usually a larger amount of virus reaches the subretinal space resulting in a higher transduction efficiency. In addition, less damage is caused during the injection. The higher biological efficacy of rAAV5.hCNGB1 observed in the dog study was most likely due to the fact that each dog retina received two injections (à 100 μL), resulting in not only one third (in case of the mouse; see figure 17A) but two thirds of the retina being transduced (see fundus images in figure 24). Another factor to consider is the longer lifespan of the dog leading to a later onset of the disease and slower progression of retinal degeneration, allowing to interfere earlier in the degeneration process when treating at 3 months *pn* (Casal and Haskins, 2006; Wolfe, 2009; Winkler et al., 2013; Volland et al, 2015). In order to achieve the optimal therapeutic effect, intervention in the course of the disease should begin as early in life as possible. This is regardless of the subject, whether it is an animal model or a human patient. However, for the mouse model it has to be considered that the younger the mouse is, the smaller the eye to be injected, which means that a subretinal injection is more likely to result in greater collateral damage, sometimes even becoming devastating over time (e.g. as cataract). For a long-term mouse study, it is therefore a risk to inject prematurely. Although human RP45 has an early onset, it progresses slowly, so that the degeneration of rod photoreceptors usually does not start before adult age (Hull et al., 2017). This effectively provides a large time window for a treatment

of human patients before photoreceptors get lost. However, the human brain is able to compensate a rod cell dysfunction over a long time period, and thus patients often do not recognize any symptoms until the visual field begins to constrict due to rod cell degradation (usually at about 20-30 years of age; Hull et al., 2017). In the future, it will be therefore important to make diagnostic and sequencing techniques more cost-effective, so that the specific type of RP can be defined the respective gene therapy can be applied as soon as possible after photoreceptor loss is recognized by the patient.

Furthermore, it will be important to investigate the efficiencies of ocular gene therapy dugs applied at later disease stages when photoreceptor degeneration is already ongoing. Therefore, further preclinical studies are needed, applying the vector at various later time points to determine the pathological stage at which it is no longer possible to intervene in the course of degeneration (point of no return). Initial experiments in *Cngb1* KO mice, in which the virus was injected at the age of 6 months, showed a high variation of the treatment outcome at 4 months. *pi* (10 months *pn*; see figure 29). At 6 months of age, about 50 % of the rod photoreceptors have been already died in a *Cngb1* KO mouse, while cones are usually still most widely unaffected (Hüttl et al., 2005). In very few instances, a delayed photoreceptor degeneration could be achieved at 4 months *pi* through rAAV5.hCNGB1 treatment. In these retinas, even the photoreceptor outer segments were preserved, which were virtually not existent in untreated retinas at this age (10 months *pn*). However, in most of the treated retinas, only a marginal rescue of photoreceptors was achieved indicating that the number of cells being already in the stage of apoptosis and the number of already degenerating cones were too high at the injection time point, leading to retinal stress resulting in an earlier passing of the point of no return and a closing of the time window for therapeutic intervention.

4.3   The Localization of the Human CNGB1 Protein – Finding the Optimal Dose Range

In both *Cngb1* KO mouse and dog models the human CNGB1 protein was found to be not strictly localized to the ROS (figures 17B, 19, and 24), indicating, that not all produced human CNGB1 molecules were transported to the ROS. Since only heterotetrametric channels are transported to the photoreceptor OS, the data demonstrated, that not every CNGB1 subunit could form a functional CNG channel complex together with the three required CNGA1 subunits. This result either suggests an excess of CNGB1 regarding to CNGA1 implying that the vector was overdosed, or an inefficient chimeric CNG channel formation of a human CNGB1 and a murine or canine CNGA1. The CNGB1 localization within the inner segments of the ROS was found in mouse for both vector lots (X17044A and for R18026), negating a possible influence of the vector production method on the CNGB1 protein localization. Furthermore, the efficiencies of cross-species CNG channel formation of the introduced human CNGB1

and canine or murine CNGA1 did not differ in efficiency and there was also no CNGA1 found in the rod IS of mice and dogs (figures 19B and 24) indicating the availability of the entire number of CNGA1 molecules for CNG channel formation. The localization of CNGA1 to the ROS further demonstrated the role of CNGA1 as a limiting factor for the amount of CNG channels transported to the ROS further proving that unphysiologically high amounts of CNGB1 in the ROS were not caused by the treatment (Kaupp and Seifert, 2002, Zheng et al., 2002, Biel et al., 2009). Summarizing, these data indicated that the efficiency in CNG channel formation was not impaired due to the origin of the subunits from different species. A further indication of a virus overdosing was provided by the dose escalation study using the dog model. Within this study, a wild-type-like CNGB1 localization (restricted to the ROS) was found at the border region (transition zone between treated and untreated area) of a mid-dosed *Cngb1* KO dog retina (1×10^{11} vg; see figure 25).

The dog dose escalation study also revealed a considerably higher hCNGB1 expression for the dose of 1×10^{11} vg as for the lower dose of 2×10^{10} vg, as well as a higher biological efficacy observed by ERG and vision testing (table 7) as well as by examination of the rescued photoreceptors (figure 24). In contrast, there were only marginal differences in transgene expression and biological efficacy between 1×10^{11} vg and the next higher dose (2×10^{11}). The highest vector dose (1×10^{12} vg) achieved the highest photoreceptor function of the rAAV5.hCNGB1 treated dogs (table 7), but not more cells were saved from degeneration compared to 1×10^{11} vg and 2×10^{11} vg (figure 24), indicating that with the highest dose a plateau was reached in the *Cngb1* KO dog model. Furthermore, the analysis of the behavioral experiment demonstrated that all doses applied led to a wild-type-like capability of the animals to navigate in the dark, demonstrating that even the smallest dose of rAAV5.hCNGB1 was sufficient to restore the vision of a *Cngb1* KO dog treated. In order to determine the optimal dose for a clinical application, dose-dependent risks must also be considered (dose-dependent immune reactions or toxic side effects; see section 4.7.2). Therefore, the highest dose is not necessarily the preferred dose, even if it achieves the highest therapeutic effect. Since the dose of 1×10^{11} vg resulted in a therapeutic outcome similar to the higher doses and since the transition zone between treated and untreated area of the respective dog eyes revealed a wild-type-like CNGB1 localization, the optimal virus genome dosage for the rAAV5.hCNGB1 therapy in dogs is expected to be slightly lower than 1×10^{11} vg. However, the viral dose should be chosen higher than 2×10^{10} vg, as the dose of 2×10^{10} showed considerably lower transgene expression (figure 24) and biological efficiency (figure 24 and table 7). Since the dog eye has a similar morphology as the human eye (see sections 1.3), the dose range determined for the dog will be roughly transferable to humans. For comparison, the FDA and EMA approved dose of voretigene neparvovec-rzyl (LUXTURNA™) is 1.5×10^{11} vg per eye (Maguire et al., 2009 and 2019). Therefore, the viral genome dosage of rAAV5.hCNGB1 in humans is probably in a similar range to LUXTURNA™. For finally

transferring the optimal dose of rAAV5.hCNGB1 to humans, the estimated vector dose should also be confirmed in NHP eyes before applying the vector to the clinic.

4.4 Different Results were Obtained Using the High Dose of the Two Vectors from Lot#X17044A and Lot#R18026

In the *Cngb1* KO mouse model, rAAV5.hCNGB1 efficacy was evaluated by injection of the vector produced via two different techniques. During the examination it became obvious, that different results (*in vivo* and *ex vivo*) were obtained using vector Lot#X17044A (produced by triple transfection in HEK293 cells) and Lot#R18026 (produced in a HeLaS3-based producer cell line). With the dose of 10^{10} vg, a marked therapeutic effect was achieved with X17044A manifesting as a distinct hCNGB1 expression and in 8 rows of preserved photoreceptors (figure 17B). Treatment with 10^{10} vg of R18026 also resulted in a high-level hCNGB1 expression, but only about 4 rows of cell nuclei remained within the ONL after 9 months (figure 19A). These data were also confirmed by OCT (figure 20) showing a decelerated degeneration after administration of X17044A (high dose), whereas only marginally effects were achieved with the high dose of R18026. Instead, results similar to those of X17044A were obtained using a 10-fold lower virus dose (mid dose; 10^9 vg), seen by OCT (figure 20) and immunohistology (figure 19A). The less survived photoreceptor cells in case of the high-dose of R18026 indicated an induced photoreceptor death probably due to toxic side effects of the treatment using the PCL vector batch. No toxic side effects were found for the triple-transfection vector, neither in mouse, nor in dog. This suggests that either more toxic contaminants or more disturbing empty capsids were present in R18026 (see section 4.7.2). Harmful adenoviral residues might have also played a role in the toxic side effect, since the PCL-based AAV production is induced by adenoviral infection (Penaud-Budloo et al., 2018). Furthermore, HeLa cells contain human papilloma viral (HPV) sequences, known to be a cause for cervical cancer, which might also be responsible for toxic effects. HPV genes within HeLa cells are thought to contribute to efficient packaging of rAAV due to helper functions provided by these genes (Ogston et al., 2000; Hermonat et al., 2000; You et al., 2006; Cao et al., 2012), but also raised safety concerns associated with these sequences (Schwarz et al., 1985; Gao et al., 2002; Martin et al., 2013). These concerns led to the generation of alternative producer cell lines for example based on the A549 cell line (Gao et al., 2002; Farson et al., 2004; Martin et al., 2013). Other causative factors for AAV toxicity are discussed in section 4.7.2.

4.5 Degeneration-Induced Retinal Stress and Inflammation can be Reduced by rAAV5.hCNGB1

In this work it was demonstrated, that Müller cell gliosis, which is elevated within degeneration (Bringmann and Wiedemann, 2012), was reduced in *Cngb1* KO mouse retina by the treatment with rAAV5.hCNGB1 (figure 30). It was further shown, that the glial activity was not only decreased within the treated part, but a slight decrease of reactive gliosis was also seen in the untreated part of that retina, suggesting that the degeneration-induced retinal stress of the entire retina can be influenced by CNGB1 gene supplementation. Nevertheless, there were still a few intermediate fibers visible in the treated part of the mid-dosed retina, despite being faint and not reaching the ONL. This indicated that mitigated retinal stress was still present which might be caused by the dying photoreceptors that were not infected by rAAVs (see section 4.2). However, retinal stress can be also attributed to injury resulting from the subretinal injection. The treated area was much closer to the injection site than the untreated part and was located within the subretinal bleb. Both, the injection itself and the following retinal detachment led to retinal injury resulting in reactive gliosis (Lewis and Fisher, 2003; Lewis et al., 2010). In addition, the rAAV itself might also have been a causative factor for reactive gliosis, since immunogenicity and genotoxicity can be induced by rAAVs (see section 4.7.2).

An increased microglia activation was found in untreated *Cngb1* KO dog eyes (figure 31), revealing that inflammation is a side effect of the photoreceptor degeneration in the canine model of RP45, as it was previously shown in the *Cngb1* KO mouse model (Blank et al., 2017). It was further demonstrated by treatment with rAAV5.CNGB1, that the pathological activation of microglia can be prevented in *Cngb1* KO dogs resulting in a reduced immune reaction (Figure 31A; Gupta et al., 2003; Zhao et al., 2015; Rashid et al., 2019). However, one dog eye treated by injection with 2×10^{11} vg of rAAV5.hCNGB1 developed an immune response, resulting in an increased photoreceptor death and in activated microglia which migrated to the ONL (figure31B). An immune response was not detected in any other eye (except for the contralateral eye to which the inflammation had spread), such that one eye out of 17 treated eyes was affected. 3 other eyes were injected with the same dose (2×10^{11} vg) and 5 others with even a higher dose (1×10^{12} vg). Since the affected dog eye was not treated with the highest dose, it can be assumed that the immune response was not caused dose-dependently by rAAV5.hCNGB1. Consequently, and since only one single eye was affected, this suggests, that the dog was either predisposed for cell-based immune reactions (see section 4.7.2), or a damage was provoked during injection which contributed to microglia activation.

4.6 Clinical Perspectives for RP – the Current Status of Gene Therapy

4.6.1 Pharmacological Treatment

Today, there is a growing number of treatment approaches for RP patients, all aiming to prevent the progression of the disease and to restore visual function (Musarella and McDonald, 2011; Lin et al., 2015; Dias et al., 2018). Various approaches rather focus on minimizing the symptoms and slowing down the progression of the disease by continuous administration of medication including neuroprotective agents such as neurotrophic or growth factors (Harvey et al., 2006; Buch et al., 2007; Trifunovic et al., 2012), anti-apoptotic agents (Doonan et al., 2011; Fernandez-Sanchez et al., 2012; Cuenca et al., 2014; Guadagni et al., 2015), or anti-inflammatory agents (Glybina et al., 2009; Yoshida et al., 2013a and b). In addition, the administration of antioxidants, such as vitamin A palmitate, fish oil (docosahexaenoic acid (DHA)), and lutein (Cuenca et al., 2014; Guadagni et al., 2015) is a common method of slowing disease progression and relieving symptoms. The pharmacological treatment approach is well tolerated but significant effects have rarely been proven so far. One promising therapeutic option for types of RP caused by mutations affecting the retinoid cycle is the continuous oral administration of 9 cis-retinyl acetate (QLT091001), which was shown to achieve a significant visual benefit even in advanced RP patients (Koenekoop et al., 2014; Scholl et al., 2015; Kenna et al., 2020). Nevertheless, retinal degenerative diseases cannot be cured in this way and further disease progression is still unavoidable despite any pharmacological treatment. However, the administration of neuroprotective drugs or antioxidants will certainly always be an accompanying treatment for the novel therapeutic approaches.

4.6.2 Gene Therapy

Viral and Non-Viral Vectors

Due to its ease of manipulation, the widely confirmed safety, and the high number of serotypes possessing a tropism for retinal tissue, AAV is currently the preferred vector for retinal gene therapy. A large number of clinical trials using AAVs are currently ongoing and many more are already in the process of recruitment or being planned (ClinicalTrials.gov). However, it still has to compete with other viral vectors, such as lentiviruses (LV) and adenoviruses (Ad), as well as with non-viral vectors. LVs have the advantage of a large cargo capacity (up to 10 kb). Long-term expression can even be achieved in dividing cells due to its ability to integrate its genome into the host cell. However, this can also be a disadvantage, posing the risk of insertional mutagenesis. Furthermore, LV production is much more complex (Trapani et al., 2014; Dias et al., 2018). Adenoviruses have the largest capacity (up to 37 kb), have a low risk of mutagenesis, and show a high transduction efficiency (Trapani et al., 2014; Dias et al.,

2018). However, they can elicit strong immune responses within the host organism, since adenoviral genes are expressed in the transduced cells (Kafri et al., 1998; Ziccardi et al., 2019). Preclinical studies with non-viral vectors such as liposome, polypeptide or polymer-based nanoparticles or physical methods such as electroporation have already been conducted (Conley et al., 2008; Ziccardi et al., 2019). These techniques are associated with a lower risk of immunogenicity than viral vectors. Furthermore, there is no mutagenic potential and large quantities of these vectors can be produced. However, there are also some limitations, such as the low transfection efficiency due to inefficient core penetration, and also the lack of long-term gene expression (Andrieu-Soler et al., 2006; Han et al., 2012; Dalkara et al., 2016; Trapani et al., 2014; Dias et al., 2018).

<u>Finding Ways to Extend the Applicability of One Treatment Approach to Several Types of RP</u>
In general, gene replacement therapy treats only one specific type of RP at a time, since it is only targeting a specific mutation. As RP is a very heterogeneous disease, the therapy of one mutation usually only reaches a very small number of RP patients (orphan drug). In order to treat several RP variants with a single therapy, scientists are also working on the discovery of downstream pathways and on the identification of potential key genes that might contribute to the survival of retinal cells. The rod-derived cone viability factor (RdCVF; Byrne et al., 2015) and the *Nrl* gene encoding for the neural retina leucine zipper (NRL; Yu et al., 2016) are examples for this approach.

<u>Genome Editing</u>
Generally, gene replacement therapy has conclusively shown to successfully enable the expression of a transfected gene that performs the tasks of a mutated gene. However, this only concerns autosomal recessive forms of RP (arRP), where it is sufficient to extrachromosomally integrate an intact gene in the host cell without eliminating the defective gene in the host genome. In autosomal dominant forms of RP (adRP), however, even a mutation on only one allele causes the phenotypic manifestation of the disease. In order to prevent this, either the mutated gene must be eliminated and an intact gene has to be integrated simultaneously (e.g. RNA interference (RNAi); Cideciyan et al., 2018), or the mutation causing the disease must be corrected (targeted gene editing). For this purpose, an RNA-guided DNA cleavage system recently discovered in bacteria and archaea serves as an excellent tool (Doudna and Charpentier, 2014). The specific clustered regularly interspaced short palindromic repeat (CRISPR)/Cas9 system can efficiently be used for a surgical DNA repair by non-homologous end-joining (NHEJ), which results in insertions and/or deletions at the target site, or by homology directed-repair (HDR), enabling a targeted exchange of specific sequences (Jinek et al, 2012; Cox et al, 2015; Chrenek et al., 2016; Cabral et al., 2017; Yiu, 2018). Promising results have already been achieved (Bakondi et al., 2016) and with this technique, long-term gene therapy would be possible even in dividing cells. But before this approach can be applied to the clinic, hurdles such as off-target effects of

the Cas9 nuclease, the efficiency of the HDR, immunogenicity of the CRISPR/Cas9 components, as well as the diminished fitness of the edited cells still have to be overcome. In addition, Cas9 nucleases usually have long sequences, which often leads to space limitations within the AAV (Dai et al., 2016; Hung et al., 2016; Dias et al., 2018). This issue can for example be addressed by dual vectors (discussed in section 4.7.1). In addition, researchers are currently working on the investigation of alternative Cas variants that require less space, for example the variant of *Staphylococcus aureus* (SaCas9), with a genome editing efficiency similar to that of the well-studied variant of *Streptococcus pyogenes* (SpCas9), while being about 1 kb smaller (Ran et al., 2015; Cebrian-Serrano and Davies, 2017).

Summarizing, the described genetic approaches aim at curing the disease by bypassing the genetic cause, allowing deceleration of disease progression or even prevention of disease manifestation in the best-case scenario. However, photoreceptors, that have already degenerated prior to therapeutic intervention cannot be restored by gene therapy. Therefore, it is necessary to determine the type of disorder at an early stage of the disease to rescue as many cells as possible. If the genetic cause of the retinal degeneration has either been identified too late, or the mutation cannot be identified, or the underlying cause is found to be located in several genes, or if no gene therapy approach exists for the causative gene defect, alternative therapeutic options are available, that allow a recovery of vision even if most of the photoreceptors have already been died (see below under 4.6.3).

4.6.3   Therapeutic Options to Treat RP at an Advanced Stage

<u>Retinal Prosthetic Implants</u>

Using retinal prostheses, visual function is taken over by electronic retinal implants. In this approach, neural activity is induced in the remaining inner retinal cells, so that no RPE or photoreceptor cells need to be present in the diseased retina, making electronic implants an option for RP patients in the terminal stage of the disease (Weiland and Humayun, 2014). Currently two systems are commercially available. The Argus II (Second Sight Medical Products; SSMP; Sylmar, CA, USA), an epiretinal prosthesis (Humayun et al., 2012; Ho et al., 2015), and the Alpha-IMS (Retina Implant AG, Reutlingen, Germany), a wireless subretinal implant (Stingl et al., 2015). Both systems achieve slight improvements in vision of legally blind patients, but the overall outcome is usually very modest (Humayun et al., 2012; Ho et al., 2015; Stingl et al., 2015).

Optogenetics

An additional emerging technique allowing the restoration of vision in advanced retinal degeneration is the use of optogenetics. With this approach, remaining retinal cells that are not light-sensitive, such as bipolar cells, ganglion cells, or the remnant cones are photosensitized by genetically introducing light-sensitive proteins (such as opsins) into these cells (Duebel et al., 2015; Yue et al., 2016; Simunovic et al., 2019). The vision of previously blinded animals was restored in several preclinical experiments, achieving sensitivities that were close to those of cone cells (within 1-2 log units of the threshold for cone vision), but with slower kinetics (Lin et al., 2008; Busskamp et al., 2010; Ivanova et al., 2010; Doroudchi et al., 2011; Cehajic-Kapetanovic et al., 2015; Simunovic et al., 2019). Optogenetics is a causative gene-independent approach, that allows the excitation of the neural apparatus more precisely and over a larger area as electronic retinal implants (Simunovic et al., 2019). In recent years, significant progress has been made in this field, but there are still many open questions to be clarified including the identification of the ideal optogenetic molecule, the ideal vector, and the ideal surgical approach.

Stem Cell Therapy

Within the field of cell therapy, intensive research is currently being conducted on induced pluripotent stem cells (IPSCs) as a source for retinal cell transplants. Although embryonic stem cells (ESCs) have already been transplanted in several animal models and have proven their capacity to differentiate into retinal precursors (Lamba et al., 2009; Gonzalez-Cordero et al., 2013; Assawachananont et al., 2014; Shirai et al., 2016; M'Barek et al., 2017), human ESCs are fraught with social problems of acceptance due to ethical reasons, as donor embryos are needed. It also carries the risk of immunological rejection of these cells. Using induced pluripotent stem cells (IPSCs), that secondarily obtain pluripotency and self-renewal properties (similar to that of ESCs) by means of certain transcription factors, these obstacles can be circumvented as IPSCs are generated from differentiated cells of the patient himself. However, the use of transcription factors carries the risk of malignancies (Bassuk et al., 2016; MacLaren et al., 2016) and, in addition, the underlying genetic defect must be corrected *ex vivo* in advance, as otherwise the retinal cells differentiating from the IPSCs would re-express the patient's disease phenotype. Although the efficiency has not yet been extensively proven, there are currently several preclinical studies that have successfully transplanted IPSCs and thereby been able to restore visual function (Lamba et al., 2010; Tucker et al., 2011; Zhou et al., 2011; Li et al., 2012). If some hurdles can be overcome in the future, such as weak transplantation efficiencies and still inaccurate graft-host synapses, IPSC-based cell therapy will become a promising therapeutic approach to treat RP in advanced stages (Zengh et al., 2015; Singh et al., 2018; Dias et al., 2018; M'Barek and Monville, 2019; Yanai et al., 2019).

4.7 Optimization of AAV-Based Gene Therapy Approaches

In recent years, the number of clinical trials testing AAV-based gene therapeutics has steadily increased. The high transduction efficiency, broad spectrum of target tissues, and an excellent safety profile have established AAV vectors as the platform of choice for *in vivo* gene therapy. However, the clinical translation of novel and effective therapeutic products is a lengthy process, and during preclinical as well as clinical trials, different hurdles are often encountered. Addressing these issues provides the key to broadening opportunities for AAV gene transfer as a therapeutic option for a wide range of human diseases in the future.

4.7.1 AAV Capsid and Genome Engineering

The basic goal in the development of novel synthetic AAVs is to increase the transduction efficiency as well as the specificity of the virus while reducing immune recognition (Colella et al., 2018). Currently, the correlation between capsid structure and function is studied intensively, allowing specific modifications of amino acid residues to generate AAV capsid libraries from which the most suitable capsids can be selected (directed evolution; Dalkara et al., 2013; Kay et al., 2013; Kotterman and Schaffer, 2014; Deverman et al., 2016; Weinmann and Grimm, 2017; Hickey et al., 2017; Reid et al., 2017; Büning and Srivastava, 2019). In parallel, vector engineering is used to bypass humoral immunity to the AAV capsid, which may already exist if the subject has previously been exposed to a wild-type virus (Maheshri et al., 2006; Perabo et al., 2006; Tse et al., 2017; Barnes et al., 2019).

Research is also focused on the vector genome to overcome some of the major limitations, such as the slow onset of gene expression (due to the time required to convert single-stranded DNA into double-stranded DNA). With self-complementary (sc-) AAV vectors, the second synthesis step of AAV transduction can be bypassed. In several animal models it was shown, that sc-AAV vectors drive faster onset and higher levels of transgene expression (McCarty et al., 2001; Yokoi et al., 2007; Nathwani et al., 2006 and 2011; Petersen-Jones et al., 2009; Buie et al., 2010). Many genes to be transferred exceed the capacity of the AAV (approx. 5 kb). This issue can be addressed using "oversized" AAVs (Grieger and Samulski, 2005; Alloca et al., 2008; Monahan et al., 2010; Hirsch et al., 2013) by packaging large genes that are usually be truncated to a size of 5 kb and reconstituted after AAV delivery (Dong et al., 2010). However, this approach limits the transduction efficiency and leads to a heterogeneity of the virus particles during production (Monahan et al., 2010; Wu et al., 2010; Dong et al., 2010; Hirsch et al., 2013). More promising for clinical application is therefore the dual AAV vector approach, whereby a large transgene is split into two separate halves, each half being packaged in a separate AAV vector (of <5 kb).

By co-infecting a cell with the two vectors, the transgene can be reassembled *in vivo*. Several dual AAV vector strategies have been developed including ITR-mediated formation of head-to-tail-concatemers (trans-splicing vectors; Yan et al., 2000), generation of overlapping vectors by homologous recombination (Duan et al., 2001), and the combination of both methods (hybrid dual vectors; Gosh et al., 2008). The therapeutic efficacy of this system, although still lower compared to single vectors, was already demonstrated in several animal models (Lostal et al., 2010; Trapani et al., 2014; Colella et al., 2014; Sondergaard et al., 2015; Potter et al., 2017; Kodippili et al., 2018).

4.7.2   Issues in AAV-Mediated Gene Therapy

<u>Immunogenicity in AAV-target cells</u>

Both the capsid and the genome of the AAV can lead to an immune response of the host organism. In general, the closer these two components resemble those of a wild-type AAV, the lower is the risk of an immune response. Cell-directed immunity against the AAV capsid is a critical factor for the safety and efficiency of gene therapy. Predominantly outside the central nervous system, cytotoxic T-cells can play a major role, when they are activated in a virus dose-dependent manner and mediate the clearance of transduced cells that present viral antigens on their surface (Mingozzi et al., 2007; Mingozzi et al., 2009; Basner-Tscharkajan and Mingozzi, 2014; Kumar et al., 2017; Colella et al., 2018; Rabinowitz et al., 2019; Martino and Markusic, 2020; Verdera et al., 2020). The role of empty capsids (viruses lacking the vector genome and therefore being unable to offer any therapeutic benefit) in this process is not fully understood. However, since they contribute to the increase in the dose of viral capsids, it is assumed that they have the potential to enhance innate or adaptive immune responses and to reduce the transduction efficiency of the respective treatment (Li et al., 2013; Gao et al., 2014; Wright et al., 2014; Hinderer et al., 2018; Rabinowitz et al., 2019). In contrast, other studies have shown that empty capsids can also act as decoys for anti-AAV antibodies, allowing full virions to escape the humoral immunity and thereby increasing transduction efficiency (Mingozzi et al., 2013). In addition, contaminants resulting from the production process (for example plasmid DNA or host cell contaminants) may also affect immunity. In order to minimize immune responses, the knowledge about critical capsid antigens or contaminants must be increased and also an adapted immunosuppression during gene therapy needs to be ensured, as it was already performed in several preclinical as well as in clinical studies (Herzog et al., 2001; Wang et al., 2007; Bainbridge et al., 2008; Mowat et al., 2017; Reichel et al., 2017). However, timing and expression of an immune response can be very individual, making the correct administration of immunosuppressive drugs more difficult (Manno et al., 2006; McIntosh et al., 2012; Mingozzi et al., 2009). It will therefore be important to evaluate safety and efficacy of a gene transfer in combination with the proposed immunosuppression in a relevant disease model to identify the potentially harmful

interactions. Since most individuals are exposed to wild-type AAVs already early in life, causing the production of neutralizing AAV antibodies (NAbs), most patients to be treated with AAV-based gene therapy have already built up humoral immunity to various AAV capsids, resulting in reduced transduction efficiencies (Erles et al., 1999; Boutin et al., 2010; Calcedo et al., 2011; Li et al., 2012; Louis Jeune et al., 2013; Mingozzi et al., 2013; Martino and Markusic, 2020). In addition, animal models, including NHPs and dog models, may also be permanent hosts of wild type AAVs (Gao et al., 2002; Shin et al., 2012; Rapti et al., 2012; Calcedo et al., 2015). Especially in case of systemic AAV administration, the presence of NAbs in the patient group as well as a possible resistance of the vector to an acquired humoral immunity should be thoroughly tested before starting a clinical trial (Mingozzi et al., 2013; Meliani et al., 2015; Guo et al., 2019). Not only the AAV capsid, but also the transgene can provoke an immune response in the host, largely mediated by Toll-like receptors (TLRs; Martino and Markusic, 2020). For example, TLR-specific signaling was shown to be upregulated in response to sc-AAVs (Zhu et al., 2009; Martino et al., 2011; Rogers et al., 2015; Martino and Markusic, 2020) and CpG sequences (Faust et al., 2013).

<u>Potency and Efficacy of AAV Vectors</u>

It is largely known that the transduction efficiency, the duration of viral persistence, and the transgene expression level are in principle dose-dependent. It is always necessary to balance the dose in order to ensure stable expression and maintain a low dose in order to avoid an immune response. Vector optimization (AAV capsid/genome and transgene sequence) can help to increase transgene activity in order to keep the vector dose as low as possible, which is required for long-term therapeutic efficacy. For example, mutations in tyrosine, serine, threonine and lysine residues have already been made in various AAV capsids, which serve to protect the viruses from proteasomal degradation (Zhong et al., 2008; Gabriel et al., 2013). Additionally, new powerful "synthetic" capsid variants can be created by "rational design" or "in silico" molecular reconstruction, as well as via "DNA shuffling" (Cabanes-Creus et al., 2019). AAVs can also be protected from proteasomal degradation by administration of certain proteasome inhibitors (Duan et al., 2000; Nathwani et al., 2009; Mitchell and Samulski, 2013; Wang et al., 2014; Berry and Asokan, 2016). The AAV genome can also be modified, for example by eliminating sequences forming hairpin structures (Xie et al., 2017), and further possibilities to optimize therapeutic efficiency are also offered by the transgene expression cassette. Regulatory elements, including promoter, enhancer, polyadenylation signals, Kozak sequences, UTRs, or introns are of primary importance (Papadakis et al., 2004; Schambach et al., 2007; Lee et al., 2010; Choi et al., 2014). Furthermore, the guanine cytosine (GC) content can be influenced as well as the codon by eliminating alternative open reading frames or cryptic splice sites (Ronzitti et al., 2016; Song et al., 2018).

AAV Genotoxicity

Although AAV is considered a virus with low risk of DNA integration into the host genome, genotoxicity is still an issue that needs to be taken into account, as integration of the AAV genome can cause loss- or gain-of-function mutations that might interfere with homeostasis and functionality of the affected cell, eventually leading to tumor formation (Yang et al., 1997; Russell and Kay, 1999; Hirata et al., 2002; Nakai et al., 2003; Deyle and Russell, 2009; Salganik et al., 2015; Chandler et al., 2016 and 2017; Collella et al., 2018). In several mouse studies, insertional mutagenesis has been documented (Donsante et al., 2007; Chandler et al., 2015), but these concerns have not been confirmed in long-term studies using either large animals (Favre et al., 2001; Niemeyer et al., 2009; Nathwani et al., 2011; Gil-Farina et al., 2016), or humans (Simonelli et al., 2009; Nathwani et al., 2014; Maguire et al., 2019; Al-Zaidy and Mendell, 2019). Nevertheless, it will remain relevant for long-term studies to monitor tumor formation and to identify AAV vector integration sites.

AAV Persistence

Due to the young history of AAV-based gene therapy, no limit of AAV persistence has yet been identified in clinical trials, as long-term studies are still ongoing. However, long-term efficacy of voretigene neparvovec-rzyl (LUXTURNA™) over a duration of 4 years has already been confirmed (Maguire et al., 2019). Furthermore, a 10-year persistence of AAV2 has been demonstrated in the past as part of a haemophilia B gene therapy study (Buchlis et al., 2012). Although the AAV-delivered recombinant DNA is usually converted into highly stable mono- or concatemeric circles (chromatin-like structure; Duan et al., 1998; Penaud-Budloo et al., 2008; see section 1.2.1), a lifelong persistence of AAVs in a patient's organism cannot be guaranteed after one single administration of the drug. At least for dividing tissue (e.g. developing liver) it is known, that the AAV gets lost over time due to its extrachromosomal location within the host cell (see section 1.2.1). It therefore has to be assumed that for some therapies, the virus has to be administered again in order to maintain the therapeutic effect. Since it is known from some preclinical as well as clinical studies that the predisposed immune system is already activated (usually in the form of a high titer of NAbs) when AAV vector re-administration is performed (Amado et al., 2010; Annear et al., 2011; Sun et al., 2018; Weed et al., 2019; Salas et al., 2019), various approaches already exist to prevent this reaction, including capsid switching (Demaster et al., 2012; Majowicz et al., 2017; Bockor et al., 2017), co-delivery of AAV with immunomodulatory molecules (Corti et al., 2015; Meliani et al., 2018), and plasmapheresis (Monteilhet et al., 2011).

4.8   Future Perspectives

Among the strategies that have been developed as a treatment for RP, AAV-based gene therapy has matured as a reliable and by far most robust tool for routine applications, as demonstrated by numerous clinical studies. However, some challenges still need to be overcome to use the system as a universal tool, such as the limited cargo capacity of the AAV, the inability to correct dominant genes, the amount of undiscovered mutations, and the insufficient number of animal models. In addition, the therapeutic efficacy should be further improved, especially in advanced RP cases. In order to avoid re-administration, one goal should be to maintain vision over the entire lifetime of a patient with a single treatment. In the future, attempts should also be made to depart from subretinal injections, which are carried out with vitrectomy surgery and are also very unlikely to be repeated as the retinal detachment can lead to irreversible retinal damage. To achieve this, it will be necessary to develop further novel vectors that are able to overcome the ILM and do not trigger an immune reaction. In future, genotyping should be more cost-efficient and more RP patients should have access to it in order to enable earlier treatment. It will be further important to develop therapies treating a broader spectrum of inherited diseases, requiring a high understanding of the respective downstream pathways. In combination with the CRISPR/Cas system, it will be possible to correct dominant mutations and also to achieve long-term maintenance of treatment success. Finally, costs and the time required for preclinical and clinical studies, that are necessary for a successful drug approval, are enormous. These costs are a substantial burden on the society and generate a difficult situation to industrial decision makers for the development of new gene therapeutics.

5   References

Acland, G.M., Aguirre, G.D., Ray, J., Zhang, Q., Aleman, T.S., Cideciyan, A.V., Pearce-Kelling, S.E., Anand, V., Zeng, Y., Maguire, A.M.*, et al.* (2001). Gene therapy restores vision in a canine model of childhood blindness. Nat Genet *28*, 92-95.

Afshar, F., Arno, G., Ba-Abbad, R., Esposti, S.D., Michaelides, M., Webster, A.R., and Mahroo, O.A. (2020). Awareness of olfactory impairment in a cohort of patients with CNGB1-associated retinitis pigmentosa. Eye (Lond) *34*, 783-784.

Ahnelt, P.K., and Kolb, H. (2000). The mammalian photoreceptor mosaic-adaptive design. Prog Retin Eye Res *19*, 711-777.

Al-Zaidy, S.A., and Mendell, J.R. (2019). From Clinical Trials to Clinical Practice: Practical Considerations for Gene Replacement Therapy in SMA Type 1. Pediatr Neurol *100*, 3-11.

Alazard-Dany, N., Nicolas, A., Ploquin, A., Strasser, R., Greco, A., Epstein, A.L., Fraefel, C., and Salvetti, A. (2009). Definition of herpes simplex virus type 1 helper activities for adeno-associated virus early replication events. PLoS Pathog *5*, e1000340.

Alexander, J.J., Umino, Y., Everhart, D., Chang, B., Min, S.H., Li, Q., Timmers, A.M., Hawes, N.L., Pang, J.J., Barlow, R.B.*, et al.* (2007). Restoration of cone vision in a mouse model of achromatopsia. Nat Med *13*, 685-687.

Allocca, M., Doria, M., Petrillo, M., Colella, P., Garcia-Hoyos, M., Gibbs, D., Kim, S.R., Maguire, A., Rex, T.S., Di Vicino, U.*, et al.* (2008). Serotype-dependent packaging of large genes in adeno-associated viral vectors results in effective gene delivery in mice. J Clin Invest *118*, 1955-1964.

Allocca, M., Mussolino, C., Garcia-Hoyos, M., Sanges, D., Iodice, C., Petrillo, M., Vandenberghe, L.H., Wilson, J.M., Marigo, V., Surace, E.M.*, et al.* (2007). Novel adeno-associated virus serotypes efficiently transduce murine photoreceptors. J Virol *81*, 11372-11380.

Amado, D., Mingozzi, F., Hui, D., Bennicelli, J.L., Wei, Z., Chen, Y., Bote, E., Grant, R.L., Golden, J.A., Narfstrom, K.*, et al.* (2010). Safety and efficacy of subretinal readministration of a viral vector in large animals to treat congenital blindness. Sci Transl Med *2*, 21ra16.

Ammann, F., Klein, D., and Franceschetti, A. (1965). Genetic and epidemiological investigations on pigmentary degeneration of the retina and allied disorders in Switzerland. J Neurol Sci *2*, 183-196.

Andrieu-Soler, C., Bejjani, R.A., de Bizemont, T., Normand, N., BenEzra, D., and Behar-Cohen, F. (2006). Ocular gene therapy: a review of nonviral strategies. Mol Vis *12*, 1334-1347.

Annear, M.J., Bartoe, J.T., Barker, S.E., Smith, A.J., Curran, P.G., Bainbridge, J.W., Ali, R.R., and Petersen-Jones, S.M. (2011). Gene therapy in the second eye of RPE65-deficient dogs improves retinal function. Gene Ther *18*, 53-61.

Ardell, M.D., Aragon, I., Oliviera, L., Porche, G.E., Burke, E., and Pittler, S.J. (1996). The beta subunit of human rod photoreceptor cGMP-gated cation channel is generated from a complex transcription unit. FEBS Letters *389*, 213-218.

Ardell, M.D., Bedsole, D.L., Schoborg, R.V., and Pittler, S.J. (2000). Genomic organization of the human rod photoreceptor cGMP-gated cation channel beta-subunit gene. Gene *245*, 311-318.

Arshavsky, V.Y., and Burns, M.E. (2012). Photoreceptor signaling: supporting vision across a wide range of light intensities. J Biol Chem *287*, 1620-1626.

Arshavsky, V.Y., and Burns, M.E. (2014). Current understanding of signal amplification in phototransduction. Cell Logist *4*, e29390.

Assawachananont, J., Mandai, M., Okamoto, S., Yamada, C., Eiraku, M., Yonemura, S., Sasai, Y., and Takahashi, M. (2014). Transplantation of embryonic and induced pluripotent stem cell-derived 3D retinal sheets into retinal degenerative mice. Stem Cell Reports *2*, 662-674.

Atchison, R.W., Casto, B.C., and Hammon, W.M. (1965). Adenovirus-Associated Defective Virus Particles. Science *149*, 754-756.

Auricchio, A. (2003). Pseudotyped AAV vectors for constitutive and regulated gene expression in the eye. Vision Res *43*, 913-918.

References

Auricchio, A., Kobinger, G., Anand, V., Hildinger, M., O'Connor, E., Maguire, A.M., Wilson, J.M., and Bennett, J. (2001). Exchange of surface proteins impacts on viral vector cellular specificity and transduction characteristics: the retina as a model. Hum Mol Genet *10*, 3075-3081.

Ayuso, C., and Millan, J.M. (2010). Retinitis pigmentosa and allied conditions today: a paradigm of translational research. Genome Med *2*, 34.

Ayuso, E., Mingozzi, F., and Bosch, F. (2010). Production, purification and characterization of adeno-associated vectors. Curr Gene Ther *10*, 423-436.

Azam, M., Collin, R.W., Malik, A., Khan, M.I., Shah, S.T., Shah, A.A., Hussain, A., Sadeque, A., Arimadyo, K., Ajmal, M., *et al.* (2011). Identification of novel mutations in Pakistani families with autosomal recessive retinitis pigmentosa. Arch Ophthalmol *129*, 1377-1378.

Ba-Abbad, R., Holder, G.E., Robson, A.G., Neveu, M.M., Waseem, N., Arno, G., and Webster, A.R. (2019). Isolated rod dysfunction associated with a novel genotype of CNGB1. Am J Ophthalmol Case Rep *14*, 83-86.

Baden, T., and Osorio, D. (2019). The Retinal Basis of Vertebrate Color Vision. Annu Rev Vis Sci *5*, 177-200.

Bainbridge, J.W., Mehat, M.S., Sundaram, V., Robbie, S.J., Barker, S.E., Ripamonti, C., Georgiadis, A., Mowat, F.M., Beattie, S.G., Gardner, P.J., *et al.* (2015). Long-term effect of gene therapy on Leber's congenital amaurosis. N Engl J Med *372*, 1887-1897.

Bainbridge, J.W., Smith, A.J., Barker, S.S., Robbie, S., Henderson, R., Balaggan, K., Viswanathan, A., Holder, G.E., Stockman, A., Tyler, N., *et al.* (2008). Effect of gene therapy on visual function in Leber's congenital amaurosis. N Engl J Med *358*, 2231-2239.

Bakondi, B., Lv, W., Lu, B., Jones, M.K., Tsai, Y., Kim, K.J., Levy, R., Akhtar, A.A., Breunig, J.J., Svendsen, C.N., *et al.* (2016). In Vivo CRISPR/Cas9 Gene Editing Corrects Retinal Dystrophy in the S334ter-3 Rat Model of Autosomal Dominant Retinitis Pigmentosa. Mol Ther *24*, 556-563.

Balakrishnan, B., and Jayandharan, G.R. (2014). Basic biology of adeno-associated virus (AAV) vectors used in gene therapy. Curr Gene Ther *14*, 86-100.

Banerjee, S., Yao, J., Zhang, X., Niu, J., and Chen, Z. (2017). Next generation sequencing identified novel heterozygous nonsense mutation in CNGB1 gene associated with retinitis pigmentosa in a Chinese patient. Oncotarget *8*, 88345-88350.

Banin, E., Gootwine, E., Obolensky, A., Ezra-Elia, R., Ejzenberg, A., Zelinger, L., Honig, H., Rosov, A., Yamin, E., Sharon, D., *et al.* (2015). Gene Augmentation Therapy Restores Retinal Function and Visual Behavior in a Sheep Model of CNGA3 Achromatopsia. Mol Ther *23*, 1423-1433.

Bareil, C., Hamel, C.P., Delague, V., Arnaud, B., Demaille, J., and Claustres, M. (2001). Segregation of a mutation in CNGB1 encoding the beta-subunit of the rod cGMP-gated channel in a family with autosomal recessive retinitis pigmentosa. Hum Genet *108*, 328-334.

Barnes, C., Scheideler, O., and Schaffer, D. (2019). Engineering the AAV capsid to evade immune responses. Curr Opin Biotechnol *60*, 99-103.

Bartlett, J.S., Wilcher, R., and Samulski, R.J. (2000). Infectious entry pathway of adeno-associated virus and adeno-associated virus vectors. J Virol *74*, 2777-2785.

Basner-Tschakarjan, E., Bijjiga, E., and Martino, A.T. (2014). Pre-Clinical Assessment of Immune Responses to Adeno-Associated Virus (AAV) Vectors. Front Immunol *5*, 28.

Basner-Tschakarjan, E., and Mingozzi, F. (2014). Cell-Mediated Immunity to AAV Vectors, Evolving Concepts and Potential Solutions. Front Immunol *5*, 350.

Bassuk, A.G., Zheng, A., Li, Y., Tsang, S.H., and Mahajan, V.B. (2016). Precision Medicine: Genetic Repair of Retinitis Pigmentosa in Patient-Derived Stem Cells. Sci Rep *6*, 19969.

Beltran, W.A., Boye, S.L., Boye, S.E., Chiodo, V.A., Lewin, A.S., Hauswirth, W.W., and Aguirre, G.D. (2010). rAAV2/5 gene-targeting to rods: dose-dependent efficiency and complications associated with different promoters. Gene Ther *17*, 1162-1174.

Beltran, W.A., Cideciyan, A.V., Guziewicz, K.E., Iwabe, S., Swider, M., Scott, E.M., Savina, S.V., Ruthel, G., Stefano, F., Zhang, L., *et al.* (2014). Canine retina has a primate fovea-like bouquet of cone photoreceptors which is affected by inherited macular degenerations. PLoS One *9*, e90390.

Beltran, W.A., Cideciyan, A.V., Lewin, A.S., Iwabe, S., Khanna, H., Sumaroka, A., Chiodo, V.A., Fajardo, D.S., Roman, A.J., Deng, W.T., *et al.* (2012). Gene therapy rescues photoreceptor blindness in dogs and paves the way for treating human X-linked retinitis pigmentosa. Proc Natl Acad Sci U S A *109*, 2132-2137.

Ben M'Barek, K., Habeler, W., Plancheron, A., Jarraya, M., Regent, F., Terray, A., Yang, Y., Chatrousse, L., Domingues, S., Masson, Y., *et al.* (2017). Human ESC-derived retinal epithelial cell sheets potentiate rescue of photoreceptor cell loss in rats with retinal degeneration. Sci Transl Med *9*.

Ben M'Barek, K., and Monville, C. (2019). Cell Therapy for Retinal Dystrophies: From Cell Suspension Formulation to Complex Retinal Tissue Bioengineering. Stem Cells Int *2019*, 4568979.

Bennett, J., Chung, D.C., and Maguire, A. (2012). Gene delivery to the retina: from mouse to man. Methods Enzymol *507*, 255-274.

Bennett, J., Maguire, A.M., Cideciyan, A.V., Schnell, M., Glover, E., Anand, V., Aleman, T.S., Chirmule, N., Gupta, A.R., Huang, Y., *et al.* (1999). Stable transgene expression in rod photoreceptors after recombinant adeno-associated virus-mediated gene transfer to monkey retina. Proc Natl Acad Sci U S A *96*, 9920-9925.

Bennett, J., Tanabe, T., Sun, D., Zeng, Y., Kjeldbye, H., Gouras, P., and Maguire, A.M. (1996). Photoreceptor cell rescue in retinal degeneration (rd) mice by in vivo gene therapy. Nat Med *2*, 649-654.

Bennett, J., Wellman, J., Marshall, K.A., McCague, S., Ashtari, M., DiStefano-Pappas, J., Elci, O.U., Chung, D.C., Sun, J., Wright, J.F., *et al.* (2016). Safety and durability of effect of contralateral-eye administration of AAV2 gene therapy in patients with childhood-onset blindness caused by RPE65 mutations: a follow-on phase 1 trial. Lancet *388*, 661-672.

Berry, G.E., and Asokan, A. (2016). Cellular transduction mechanisms of adeno-associated viral vectors. Curr Opin Virol *21*, 54-60.

Berson, E.L., Gouras, P., Gunkel, R.D., and Myrianthopoulos, N.C. (1969). Rod and cone responses in sex-linked retinitis pigmentosa. Arch Ophthalmol *81*, 215-225.

Berson, E.L., Rosner, B., Sandberg, M.A., Hayes, K.C., Nicholson, B.W., Weigel-DiFranco, C., and Willett, W. (1993). A randomized trial of vitamin A and vitamin E supplementation for retinitis pigmentosa. Arch Ophthalmol *111*, 761-772.

Berson, E.L., Rosner, B., and Simonoff, E. (1980). Risk factors for genetic typing and detection in retinitis pigmentosa. Am J Ophthalmol *89*, 763-775.

Bertran, J., Miller, J.L., Yang, Y., Fenimore-Justman, A., Rueda, F., Vanin, E.F., and Nienhuis, A.W. (1996). Recombinant adeno-associated virus-mediated high-efficiency, transient expression of the murine cationic amino acid transporter (ecotropic retroviral receptor) permits stable transduction of human HeLa cells by ecotropic retroviral vectors. J Virol *70*, 6759-6766.

Biel, M., and Michalakis, S. (2009). Cyclic nucleotide-gated channels. Handb Exp Pharmacol, 111-136.

Biel, M., Michalakis, S., Ludwig, A., and Hofmann, F. (2009). Cyclic Nucleotide-Gated and Hyperpolarization-Activated Channels. In Encyclopedia of Neuroscience, L.R. Squire, ed. (Oxford: Academic Press), pp. 279-284.

Biel, M., Zong, X., Ludwig, A., Sautter, A., and Hofmann, F. (1999). Structure and function of cyclic nucleotide-gated channels. Rev Physiol Biochem Pharmacol *135*, 151-171.

Bignami, A., and Dahl, D. (1979). The radial glia of Muller in the rat retina and their response to injury. An immunofluorescence study with antibodies to the glial fibrillary acidic (GFA) protein. Exp Eye Res *28*, 63-69.

Birtel, J., Gliem, M., Mangold, E., Muller, P.L., Holz, F.G., Neuhaus, C., Lenzner, S., Zahnleiter, D., Betz, C., Eisenberger, T., *et al.* (2018). Next-generation sequencing identifies unexpected genotype-phenotype correlations in patients with retinitis pigmentosa. PLoS One *13*, e0207958.

Blaese, R.M. (1993). Development of gene therapy for immunodeficiency: adenosine deaminase deficiency. Pediatr Res *33*, S49-53; discussion S53-45.

Blank, T., Goldmann, T., Koch, M., Amann, L., Schon, C., Bonin, M., Pang, S., Prinz, M., Burnet, M., Wagner, J.E., *et al.* (2017). Early Microglia Activation Precedes Photoreceptor Degeneration in a Mouse Model of CNGB1-Linked Retinitis Pigmentosa. Front Immunol *8*, 1930.

References

Bockor, L., Bortolussi, G., Iaconcig, A., Chiaruttini, G., Tiribelli, C., Giacca, M., Benvenuti, F., Zentilin, L., and Muro, A.F. (2017). Repeated AAV-mediated gene transfer by serotype switching enables long-lasting therapeutic levels of hUgt1a1 enzyme in a mouse model of Crigler-Najjar Syndrome Type I. Gene Ther *24*, 649-660.

Bocquet, B., Marzouka, N.A., Hebrard, M., Manes, G., Senechal, A., Meunier, I., and Hamel, C.P. (2013). Homozygosity mapping in autosomal recessive retinitis pigmentosa families detects novel mutations. Mol Vis *19*, 2487-2500.

Bonigk, W., Bradley, J., Muller, F., Sesti, F., Boekhoff, I., Ronnett, G.V., Kaupp, U.B., and Frings, S. (1999). The native rat olfactory cyclic nucleotide-gated channel is composed of three distinct subunits. J Neurosci *19*, 5332-5347.

Boughman, J.A., Conneally, P.M., and Nance, W.E. (1980). Population genetic studies of retinitis pigmentosa. Am J Hum Genet *32*, 223-235.

Boughman, J.A., Vernon, M., and Shaver, K.A. (1983). Usher syndrome: definition and estimate of prevalence from two high-risk populations. J Chronic Dis *36*, 595-603.

Boutin, S., Monteilhet, V., Veron, P., Leborgne, C., Benveniste, O., Montus, M.F., and Masurier, C. (2010). Prevalence of serum IgG and neutralizing factors against adeno-associated virus (AAV) types 1, 2, 5, 6, 8, and 9 in the healthy population: implications for gene therapy using AAV vectors. Hum Gene Ther *21*, 704-712.

Bowmaker, J.K., Dartnall, H.J., and Mollon, J.D. (1979). The violet-sensitive receptors of primate retinae [proceedings]. J Physiol *292*, 31P.

Boye, S.E., Alexander, J.J., Boye, S.L., Witherspoon, C.D., Sandefer, K.J., Conlon, T.J., Erger, K., Sun, J., Ryals, R., Chiodo, V.A., *et al.* (2012). The human rhodopsin kinase promoter in an AAV5 vector confers rod- and cone-specific expression in the primate retina. Hum Gene Ther *23*, 1101-1115.

Boye, S.E., Boye, S.L., Pang, J., Ryals, R., Everhart, D., Umino, Y., Neeley, A.W., Besharse, J., Barlow, R., and Hauswirth, W.W. (2010). Functional and behavioral restoration of vision by gene therapy in the guanylate cyclase-1 (GC1) knockout mouse. PLoS One *5*, e11306.

Bradley, J., Reisert, J., and Frings, S. (2005). Regulation of cyclic nucleotide-gated channels. Curr Opin Neurobiol *15*, 343-349.
Branca, M.A. (2005). Gene therapy: cursed or inching towards credibility? Nat Biotechnol *23*, 519-521.

Bravo-Gil, N., Gonzalez-Del Pozo, M., Martin-Sanchez, M., Mendez-Vidal, C., Rodriguez-de la Rua, E., Borrego, S., and Antinolo, G. (2017). Unravelling the genetic basis of simplex Retinitis Pigmentosa cases. Sci Rep *7*, 41937.

Bringmann, A., Iandiev, I., Pannicke, T., Wurm, A., Hollborn, M., Wiedemann, P., Osborne, N.N., and Reichenbach, A. (2009). Cellular signaling and factors involved in Muller cell gliosis: neuroprotective and detrimental effects. Prog Retin Eye Res *28*, 423-451.

Bringmann, A., and Reichenbach, A. (2001). Role of Muller cells in retinal degenerations. Front Biosci *6*, E72-92.

Bringmann, A., and Wiedemann, P. (2012). Muller glial cells in retinal disease. Ophthalmologica *227*, 1-19.

Bruewer, A.R., Mowat, F.M., Bartoe, J.T., Boye, S.L., Hauswirth, W.W., and Petersen-Jones, S.M. (2013). Evaluation of lateral spread of transgene expression following subretinal AAV-mediated gene delivery in dogs. PLoS One *8*, e60218.

Bryant, L.M., Christopher, D.M., Giles, A.R., Hinderer, C., Rodriguez, J.L., Smith, J.B., Traxler, E.A., Tycko, J., Wojno, A.P., and Wilson, J.M. (2013). Lessons learned from the clinical development and market authorization of Glybera. Hum Gene Ther Clin Dev *24*, 55-64.

Buch, P.K., Bainbridge, J.W., and Ali, R.R. (2008). AAV-mediated gene therapy for retinal disorders: from mouse to man. Gene Ther *15*, 849-857.

Buch, P.K., MacLaren, R.E., and Ali, R.R. (2007). Neuroprotective gene therapy for the treatment of inherited retinal degeneration. Curr Gene Ther *7*, 434-445.

Buchlis, G., Podsakoff, G.M., Radu, A., Hawk, S.M., Flake, A.W., Mingozzi, F., and High, K.A. (2012). Factor IX expression in skeletal muscle of a severe hemophilia B patient 10 years after AAV-mediated gene transfer. Blood *119*, 3038-3041.

Buie, L.K., Rasmussen, C.A., Porterfield, E.C., Ramgolam, V.S., Choi, V.W., Markovic-Plese, S., Samulski, R.J., Kaufman, P.L., and Borras, T. (2010). Self-complementary AAV virus (scAAV) safe and long-term gene transfer in the trabecular meshwork of living rats and monkeys. Invest Ophthalmol Vis Sci *51*, 236-248.

Buller, R.M., Janik, J.E., Sebring, E.D., and Rose, J.A. (1981). Herpes simplex virus types 1 and 2 completely help adenovirus-associated virus replication. J Virol *40*, 241-247.

Buning, H., and Srivastava, A. (2019). Capsid Modifications for Targeting and Improving the Efficacy of AAV Vectors. Mol Ther Methods Clin Dev *12*, 248-265.

Bunker, C.H., Berson, E.L., Bromley, W.C., Hayes, R.P., and Roderick, T.H. (1984). Prevalence of retinitis pigmentosa in Maine. Am J Ophthalmol *97*, 357-365.

Burger, C., Gorbatyuk, O.S., Velardo, M.J., Peden, C.S., Williams, P., Zolotukhin, S., Reier, P.J., Mandel, R.J., and Muzyczka, N. (2004). Recombinant AAV viral vectors pseudotyped with viral capsids from serotypes 1, 2, and 5 display differential efficiency and cell tropism after delivery to different regions of the central nervous system. Mol Ther *10*, 302-317.

Busskamp, V., Duebel, J., Balya, D., Fradot, M., Viney, T.J., Siegert, S., Groner, A.C., Cabuy, E., Forster, V., Seeliger, M., *et al.* (2010). Genetic reactivation of cone photoreceptors restores visual responses in retinitis pigmentosa. Science *329*, 413-417.

Busskamp, V., Picaud, S., Sahel, J.A., and Roska, B. (2012). Optogenetic therapy for retinitis pigmentosa. Gene Ther *19*, 169-175.

Byrne, L.C., Dalkara, D., Luna, G., Fisher, S.K., Clérin, E., Sahel, J.A., Léveillard, T., and Flannery, J.G. (2015). Viral-mediated RdCVF and RdCVFL expression protects cone and rod photoreceptors in retinal degeneration. J Clin Invest *125*, 105-116.

Cabanes-Creus, M., Ginn, S.L., Amaya, A.K., Liao, S.H.Y., Westhaus, A., Hallwirth, C.V., Wilmott, P., Ward, J., Dilworth, K.L., Santilli, G., *et al.* (2019). Codon-Optimization of Wild-Type Adeno-Associated Virus Capsid Sequences Enhances DNA Family Shuffling while Conserving Functionality. Mol Ther Methods Clin Dev *12*, 71-84.

Cabral, T., DiCarlo, J.E., Justus, S., Sengillo, J.D., Xu, Y., and Tsang, S.H. (2017). CRISPR applications in ophthalmologic genome surgery. Curr Opin Ophthalmol *28*, 252-259.

Calcedo, R., Franco, J., Qin, Q., Richardson, D.W., Mason, J.B., Boyd, S., and Wilson, J.M. (2015). Preexisting Neutralizing Antibodies to Adeno-Associated Virus Capsids in Large Animals Other Than Monkeys May Confound In Vivo Gene Therapy Studies. Hum Gene Ther Methods *26*, 103-105.

Calcedo, R., Morizono, H., Wang, L., McCarter, R., He, J., Jones, D., Batshaw, M.L., and Wilson, J.M. (2011). Adeno-associated virus antibody profiles in newborns, children, and adolescents. Clin Vaccine Immunol *18*, 1586-1588.

Candiello, J., Balasubramani, M., Schreiber, E.M., Cole, G.J., Mayer, U., Halfter, W., and Lin, H. (2007). Biomechanical properties of native basement membranes. FEBS J *274*, 2897-2908.

Cao, M., You, H., and Hermonat, P.L. (2014). The X gene of adeno-associated virus 2 (AAV2) is involved in viral DNA replication. PLoS One *9*, e104596.

Cao, M., Zhu, H., Bandyopadhyay, S., You, H., and Hermonat, P.L. (2012). HPV-16 E1, E2 and E6 each complement the Ad5 helper gene set, increasing rAAV2 and wt AAV2 production. Gene Ther *19*, 418-424.

Carter-Dawson, L.D., and LaVail, M.M. (1979). Rods and cones in the mouse retina. I. Structural analysis using light and electron microscopy. J Comp Neurol *188*, 245-262.

Casal, M., and Haskins, M. (2006). Large animal models and gene therapy. Eur J Hum Genet *14*, 266-272.

Caspi, R.R. (2006). Ocular autoimmunity: the price of privilege? Immunol Rev *213*, 23-35.

Cebrian-Serrano, A., and Davies, B. (2017). CRISPR-Cas orthologues and variants: optimizing the repertoire, specificity and delivery of genome engineering tools. Mamm Genome *28*, 247-261.

Cehajic-Kapetanovic, J., Eleftheriou, C., Allen, A.E., Milosavljevic, N., Pienaar, A., Bedford, R., Davis, K.E., Bishop, P.N., and Lucas, R.J. (2015). Restoration of Vision with Ectopic Expression of Human Rod Opsin. Curr Biol *25*, 2111-2122.

Cepko, C.L., and Vandenberghe, L.H. (2013). Retinal gene therapy coming of age. Hum Gene Ther *24*, 242-244.

Chader, G.J. (2002). Animal models in research on retinal degenerations: past progress and future hope. Vision Research *42*, 393-399.

Chandler, R.J., LaFave, M.C., Varshney, G.K., Burgess, S.M., and Venditti, C.P. (2016). Genotoxicity in Mice Following AAV Gene Delivery: A Safety Concern for Human Gene Therapy? Mol Ther *24*, 198-201.

References

Chandler, R.J., LaFave, M.C., Varshney, G.K., Trivedi, N.S., Carrillo-Carrasco, N., Senac, J.S., Wu, W., Hoffmann, V., Elkahloun, A.G., Burgess, S.M.*, et al.* (2015). Vector design influences hepatic genotoxicity after adeno-associated virus gene therapy. J Clin Invest *125*, 870-880.

Chandler, R.J., Sands, M.S., and Venditti, C.P. (2017). Recombinant Adeno-Associated Viral Integration and Genotoxicity: Insights from Animal Models. Hum Gene Ther *28*, 314-322.

Charbel Issa, P., Reuter, P., Kühlewein, L., Birtel, J., Gliem, M., Tropitzsch, A., Whitcroft, K.L., Bolz, H.J., Ishihara, K., MacLaren, R.E.*, et al.* (2018). Olfactory Dysfunction in Patients With CNGB1-Associated Retinitis Pigmentosa. JAMA ophthalmology *136*, 761-769.

Chen, S., Wang, Q.L., Nie, Z., Sun, H., Lennon, G., Copeland, N.G., Gilbert, D.J., Jenkins, N.A., and Zack, D.J. (1997). Crx, a novel Otx-like paired-homeodomain protein, binds to and transactivates photoreceptor cell-specific genes. Neuron *19*, 1017-1030.

Chen, T.C., Cense, B., Pierce, M.C., Nassif, N., Park, B.H., Yun, S.H., White, B.R., Bouma, B.E., Tearney, G.J., and de Boer, J.F. (2005). Spectral domain optical coherence tomography: ultra-high speed, ultra-high resolution ophthalmic imaging. Arch Ophthalmol *123*, 1715-1720.

Chen, Y., Moiseyev, G., Takahashi, Y., and Ma, J.X. (2006). RPE65 gene delivery restores isomerohydrolase activity and prevents early cone loss in Rpe65-/- mice. Invest Ophthalmol Vis Sci *47*, 1177-1184.

Choi, J.H., Yu, N.K., Baek, G.C., Bakes, J., Seo, D., Nam, H.J., Baek, S.H., Lim, C.S., Lee, Y.S., and Kaang, B.K. (2014). Optimization of AAV expression cassettes to improve packaging capacity and transgene expression in neurons. Mol Brain *7*, 17.

Chrenek, M.A., Nickerson, J.M., and Boatright, J.H. (2016). Clustered Regularly Interspaced Short Palindromic Repeats: Challenges in Treating Retinal Disease. Asia Pac J Ophthalmol (Phila) *5*, 304-308.

Cideciyan, A.V., Jacobson, S.G., Beltran, W.A., Sumaroka, A., Swider, M., Iwabe, S., Roman, A.J., Olivares, M.B., Schwartz, S.B., Komaromy, A.M.*, et al.* (2013). Human retinal gene therapy for Leber congenital amaurosis shows advancing retinal degeneration despite enduring visual improvement. Proc Natl Acad Sci U S A *110*, E517-525.

Cideciyan, A.V., Sudharsan, R., Dufour, V.L., Massengill, M.T., Iwabe, S., Swider, M., Lisi, B., Sumaroka, A., Marinho, L.F., Appelbaum, T.*, et al.* (2018). Mutation-independent rhodopsin gene therapy by knockdown and replacement with a single AAV vector. Proc Natl Acad Sci U S A *115*, E8547-E8556.

Clark, K.R., Voulgaropoulou, F., Fraley, D.M., and Johnson, P.R. (1995). Cell lines for the production of recombinant adeno-associated virus. Hum Gene Ther *6*, 1329-1341.

Clement, N., and Grieger, J.C. (2016). Manufacturing of recombinant adeno-associated viral vectors for clinical trials. Mol Ther Methods Clin Dev *3*, 16002.

Clement, N., Knop, D.R., and Byrne, B.J. (2009). Large-scale adeno-associated viral vector production using a herpesvirus-based system enables manufacturing for clinical studies. Hum Gene Ther *20*, 796-806.

Cohen, A.I. (1961). The fine structure of the extrafoveal receptors of the Rhesus monkey. Exp Eye Res *1*, 128-136.

Colella, P., Ronzitti, G., and Mingozzi, F. (2018). Emerging Issues in AAV-Mediated In Vivo Gene Therapy. Mol Ther Methods Clin Dev *8*, 87-104.

Colella, P., Trapani, I., Cesi, G., Sommella, A., Manfredi, A., Puppo, A., Iodice, C., Rossi, S., Simonelli, F., Giunti, M.*, et al.* (2014). Efficient gene delivery to the cone-enriched pig retina by dual AAV vectors. Gene Ther *21*, 450-456.

Conley, S.M., Cai, X., and Naash, M.I. (2008). Nonviral ocular gene therapy: assessment and future directions. Curr Opin Mol Ther *10*, 456-463.

Corti, M., Cleaver, B., Clément, N., Conlon, T.J., Faris, K.J., Wang, G., Benson, J., Tarantal, A.F., Fuller, D., Herzog, R.W.*, et al.* (2015). Evaluation of Readministration of a Recombinant Adeno-Associated Virus Vector Expressing Acid Alpha-Glucosidase in Pompe Disease: Preclinical to Clinical Planning. Hum Gene Ther Clin Dev *26*, 185-193.

Cox, D.B., Platt, R.J., and Zhang, F. (2015). Therapeutic genome editing: prospects and challenges. Nat Med *21*, 121-131.

Cuenca, N., Fernández-Sánchez, L., Campello, L., Maneu, V., De la Villa, P., Lax, P., and Pinilla, I. (2014). Cellular responses following retinal injuries and therapeutic approaches for neurodegenerative diseases. Prog Retin Eye Res *43*, 17-75.

Dai, W.J., Zhu, L.Y., Yan, Z.Y., Xu, Y., Wang, Q.L., and Lu, X.J. (2016). CRISPR-Cas9 for in vivo Gene Therapy: Promise and Hurdles. Mol Ther Nucleic Acids *5*, e349.

Dalkara, D., Byrne, L.C., Klimczak, R.R., Visel, M., Yin, L., Merigan, W.H., Flannery, J.G., and Schaffer, D.V. (2013). In vivo-directed evolution of a new adeno-associated virus for therapeutic outer retinal gene delivery from the vitreous. Sci Transl Med *5*, 189ra176.

Dalkara, D., Goureau, O., Marazova, K., and Sahel, J.A. (2016). Let There Be Light: Gene and Cell Therapy for Blindness. Hum Gene Ther *27*, 134-147.

Dalkara, D., Kolstad, K.D., Caporale, N., Visel, M., Klimczak, R.R., Schaffer, D.V., and Flannery, J.G. (2009). Inner limiting membrane barriers to AAV-mediated retinal transduction from the vitreous. Mol Ther *17*, 2096-2102.

Dan, H., Huang, X., Xing, Y., and Shen, Y. (2020). Application of targeted panel sequencing and whole exome sequencing for 76 Chinese families with retinitis pigmentosa. Mol Genet Genomic Med, e1131.

Daya, S., and Berns, K.I. (2008). Gene therapy using adeno-associated virus vectors. Clin Microbiol Rev *21*, 583-593.

Delori, F.C., Dorey, C.K., Staurenghi, G., Arend, O., Goger, D.G., and Weiter, J.J. (1995). In vivo fluorescence of the ocular fundus exhibits retinal pigment epithelium lipofuscin characteristics. Invest Ophthalmol Vis Sci *36*, 718-729.

Demaster, A., Luo, X., Curtis, S., Williams, K.D., Landau, D.J., Drake, E.J., Kozink, D.M., Bird, A., Crane, B., Sun, F.*, et al.* (2012). Long-term efficacy following readministration of an adeno-associated virus vector in dogs with glycogen storage disease type Ia. Hum Gene Ther *23*, 407-418.

Deng, W.T., Li, J., Zhu, P., Freedman, B., Smith, W.C., Baehr, W., and Hauswirth, W.W. (2019). Rescue of M-cone Function in Aged Opn1mw-/- Mice, a Model for Late-Stage Blue Cone Monochromacy. Invest Ophthalmol Vis Sci *60*, 3644-3651.

Deverman, B.E., Pravdo, P.L., Simpson, B.P., Kumar, S.R., Chan, K.Y., Banerjee, A., Wu, W.-L., Yang, B., Huber, N., Pasca, S.P.*, et al.* (2016). Cre-dependent selection yields AAV variants for widespread gene transfer to the adult brain. Nature biotechnology *34*, 204-209.

Deyle, D.R., and Russell, D.W. (2009). Adeno-associated virus vector integration. Curr Opin Mol Ther *11*, 442-447.

Di Foggia, V., Makwana, P., Ali, R.R., and Sowden, J.C. (2016). Induced Pluripotent Stem Cell Therapies for Degenerative Disease of the Outer Retina: Disease Modeling and Cell Replacement. J Ocul Pharmacol Ther *32*, 240-252.

Di Pasquale, G., Davidson, B.L., Stein, C.S., Martins, I., Scudiero, D., Monks, A., and Chiorini, J.A. (2003). Identification of PDGFR as a receptor for AAV-5 transduction. Nat Med *9*, 1306-1312.

Dias, M.F., Joo, K., Kemp, J.A., Fialho, S.L., da Silva Cunha, A., Jr., Woo, S.J., and Kwon, Y.J. (2018). Molecular genetics and emerging therapies for retinitis pigmentosa: Basic research and clinical perspectives. Prog Retin Eye Res *63*, 107-131.

Dinculescu, A., Glushakova, L., Min, S.H., and Hauswirth, W.W. (2005). Adeno-associated virus-vectored gene therapy for retinal disease. Hum Gene Ther *16*, 649-663.

Ding, W., Zhang, L., Yan, Z., and Engelhardt, J.F. (2005). Intracellular trafficking of adeno-associated viral vectors. Gene Ther *12*, 873-880.

Doly, M. (1994). Transduction of the light message: from the photon to the optic nerve. Fundam Clin Pharmacol *8*, 147-154.
Dong, B., Nakai, H., and Xiao, W. (2010). Characterization of genome integrity for oversized recombinant AAV vector. Mol Ther *18*, 87-92.

Dong, C.J., and Hare, W.A. (2000). Contribution to the kinetics and amplitude of the electroretinogram b-wave by third-order retinal neurons in the rabbit retina. Vision Res *40*, 579-589.

Donsante, A., Miller, D.G., Li, Y., Vogler, C., Brunt, E.M., Russell, D.W., and Sands, M.S. (2007). AAV vector integration sites in mouse hepatocellular carcinoma. Science *317*, 477.

Doonan, F., O'Driscoll, C., Kenna, P., and Cotter, T.G. (2011). Enhancing survival of photoreceptor cells in vivo using the synthetic progestin Norgestrel. J Neurochem *118*, 915-927.

Doroudchi, M.M., Greenberg, K.P., Zorzos, A.N., Hauswirth, W.W., Fonstad, C.G., Horsager, A., and Boyden, E.S. (2011). Towards optogenetic sensory replacement. Conference proceedings: Annual International Conference of the IEEE Engineering in Medicine and Biology Society IEEE Engineering in Medicine and Biology Society Annual Conference *2011*, 3139-3141.

References

Doudna, J.A., and Charpentier, E. (2014). Genome editing. The new frontier of genome engineering with CRISPR-Cas9. Science *346*, 1258096.

Drack, A.V., Dumitrescu, A.V., Bhattarai, S., Gratie, D., Stone, E.M., Mullins, R., and Sheffield, V.C. (2012). TUDCA slows retinal degeneration in two different mouse models of retinitis pigmentosa and prevents obesity in Bardet-Biedl syndrome type 1 mice. Invest Ophthalmol Vis Sci *53*, 100-106.

Duan, D., Li, Q., Kao, A.W., Yue, Y., Pessin, J.E., and Engelhardt, J.F. (1999). Dynamin is required for recombinant adeno-associated virus type 2 infection. J Virol *73*, 10371-10376.

Duan, D., Sharma, P., Yang, J., Yue, Y., Dudus, L., Zhang, Y., Fisher, K.J., and Engelhardt, J.F. (1998). Circular intermediates of recombinant adeno-associated virus have defined structural characteristics responsible for long-term episomal persistence in muscle tissue. J Virol *72*, 8568-8577.

Duan, D., Yue, Y., Yan, Z., Yang, J., and Engelhardt, J.F. (2000). Endosomal processing limits gene transfer to polarized airway epithelia by aden o-associated virus. J Clin Invest *105*, 1573-1587.

Dudek, A.M., Pillay, S., Puschnik, A.S., Nagamine, C.M., Cheng, F., Qiu, J., Carette, J.E., and Vandenberghe, L.H. (2018). An Alternate Route for Adeno-associated Virus (AAV) Entry Independent of AAV Receptor. J Virol *92*.

Duebel, J., Marazova, K., and Sahel, J.-A. (2015). Optogenetics. Current opinion in ophthalmology *26*, 226-232.

Ekstrom, P., Sanyal, S., Narfstrom, K., Chader, G.J., and van Veen, T. (1988). Accumulation of glial fibrillary acidic protein in Muller radial glia during retinal degeneration. Invest Ophthalmol Vis Sci *29*, 1363-1371.

Erles, K., Sebökovà, P., and Schlehofer, J.R. (1999). Update on the prevalence of serum antibodies (IgG and IgM) to adeno-associated virus (AAV). Journal of Medical Virology *59*, 406-411.

Farber, D.B., and Lolley, R.N. (1974). Cyclic guanosine monophosphate: elevation in degenerating photoreceptor cells of the C3H mouse retina. Science *186*, 449-451.

Fariss, R.N., Li, Z.Y., and Milam, A.H. (2000). Abnormalities in rod photoreceptors, amacrine cells, and horizontal cells in human retinas with retinitis pigmentosa. Am J Ophthalmol *129*, 215-223.

Farson, D., Harding, T.C., Tao, L., Liu, J., Powell, S., Vimal, V., Yendluri, S., Koprivnikar, K., Ho, K., Twitty, C., *et al.* (2004). Development and characterization of a cell line for large-scale, serum-free production of recombinant adeno-associated viral vectors. J Gene Med *6*, 1369-1381.

Faust, S.M., Bell, P., Cutler, B.J., Ashley, S.N., Zhu, Y., Rabinowitz, J.E., and Wilson, J.M. (2013). CpG-depleted adeno-associated virus vectors evade immune detection. J Clin Invest *123*, 2994-3001.

Favre, D., Provost, N., Blouin, V., Blancho, G., Chérel, Y., Salvetti, A., and Moullier, P. (2001). Immediate and long-term safety of recombinant adeno-associated virus injection into the nonhuman primate muscle. Mol Ther *4*, 559-566.

Fernández-Sánchez, L., Lax, P., Isiegas, C., Ayuso, E., Ruiz, J.M., de la Villa, P., Bosch, F., de la Rosa, E.J., and Cuenca, N. (2012). Proinsulin slows retinal degeneration and vision loss in the P23H rat model of retinitis pigmentosa. Hum Gene Ther *23*, 1290-1300.

Fischer, A., and Cavazzana-Calvo, M. (2008). Gene therapy of inherited diseases. Lancet *371*, 2044-2047.

Fischer, A.J., Zelinka, C., and Milani-Nejad, N. (2015). Reactive retinal microglia, neuronal survival, and the formation of retinal folds and detachments. Glia *63*, 313-327.

Flannery, J.G., Zolotukhin, S., Vaquero, M.I., LaVail, M.M., Muzyczka, N., and Hauswirth, W.W. (1997). Efficient photoreceptor-targeted gene expression in vivo by recombinant adeno-associated virus. Proc Natl Acad Sci U S A *94*, 6916-6921.

Flotte, T.R., Afione, S.A., and Zeitlin, P.L. (1994). Adeno-associated virus vector gene expression occurs in nondividing cells in the absence of vector DNA integration. Am J Respir Cell Mol Biol *11*, 517-521.

Foltz, L.P., and Clegg, D.O. (2019). Patient-derived induced pluripotent stem cells for modelling genetic retinal dystrophies. Prog Retin Eye Res *68*, 54-66.

Forsythe, E., and Beales, P.L. (2013). Bardet-Biedl syndrome. Eur J Hum Genet *21*, 8-13.

Fradin, M., Colin, E., Hannouche-Bared, D., Audo, I., Sahel, J.A., Biskup, S., Carre, W., Ziegler, A., Wilhelm, C., Guichet, A., *et al.* (2016). Run of homozygosity analysis reveals a novel nonsense variant of the CNGB1 gene involved in retinitis pigmentosa 45. Ophthalmic Genet *37*, 357-359.

Friedmann, T., and Roblin, R. (1972). Gene therapy for human genetic disease? Science *175*, 949-955.

Fu, Q., Wang, F., Wang, H., Xu, F., Zaneveld, J.E., Ren, H., Keser, V., Lopez, I., Tuan, H.F., Salvo, J.S., *et al.* (2013). Next-generation sequencing-based molecular diagnosis of a Chinese patient cohort with autosomal recessive retinitis pigmentosa. Invest Ophthalmol Vis Sci *54*, 4158-4166.

Fujimoto, J.G. (2003). Optical coherence tomography for ultrahigh resolution in vivo imaging. Nat Biotechnol *21*, 1361-1367. Fuster-Garcia, C., Garcia-Garcia, G., Jaijo, T., Blanco-Kelly, F., Tian, L., Hakonarson, H., Ayuso, C., Aller, E., and Millan, J.M. (2019). Expanding the Genetic Landscape of Usher-Like Phenotypes. Invest Ophthalmol Vis Sci *60*, 4701-4710.

Gabriel, N., Hareendran, S., Sen, D., Gadkari, R.A., Sudha, G., Selot, R., Hussain, M., Dhaksnamoorthy, R., Samuel, R., Srinivasan, N., *et al.* (2013). Bioengineering of AAV2 capsid at specific serine, threonine, or lysine residues improves its transduction efficiency in vitro and in vivo. Hum Gene Ther Methods *24*, 80-93.

Gao, G.P., Alvira, M.R., Wang, L., Calcedo, R., Johnston, J., and Wilson, J.M. (2002). Novel adeno-associated viruses from rhesus monkeys as vectors for human gene therapy. Proc Natl Acad Sci U S A *99*, 11854-11859.

Gao, K., Li, M., Zhong, L., Su, Q., Li, J., Li, S., He, R., Zhang, Y., Hendricks, G., Wang, J., *et al.* (2014). Empty Virions In AAV8 Vector Preparations Reduce Transduction Efficiency And May Cause Total Viral Particle Dose-Limiting Side-Effects. Mol Ther Methods Clin Dev *1*, 20139.

Gao, S.S., Jia, Y., Zhang, M., Su, J.P., Liu, G., Hwang, T.S., Bailey, S.T., and Huang, D. (2016). Optical Coherence Tomography Angiography. Invest Ophthalmol Vis Sci *57*, Oct27-36.

Garafalo, A.V., Cideciyan, A.V., Heon, E., Sheplock, R., Pearson, A., WeiYang Yu, C., Sumaroka, A., Aguirre, G.D., and Jacobson, S.G. (2019). Progress in treating inherited retinal diseases: Early subretinal gene therapy clinical trials and candidates for future initiatives. Prog Retin Eye Res, 100827.

Gaudet, D., Methot, J., Dery, S., Brisson, D., Essiembre, C., Tremblay, G., Tremblay, K., de Wal, J., Twisk, J., van den Bulk, N., *et al.* (2013). Efficacy and long-term safety of alipogene tiparvovec (AAV1-LPLS447X) gene therapy for lipoprotein lipase deficiency: an open-label trial. Gene Ther *20*, 361-369.

Gearhart, P.M., Gearhart, C.C., and Petersen-Jones, S.M. (2008). A Novel Method for Objective Vision Testing in Canine Models of Inherited Retinal Disease. Invest Ophthalmol Vis Sci *49*, 3568-3576.

Geller, A.M., and Sieving, P.A. (1993). Assessment of foveal cone photoreceptors in Stargardt's macular dystrophy using a small dot detection task. Vision Res *33*, 1509-1524.

Geoffroy, M.C., and Salvetti, A. (2005). Helper functions required for wild type and recombinant adeno-associated virus growth. Curr Gene Ther *5*, 265-271.

Georgiou, M., Kalitzeos, A., Patterson, E.J., Dubra, A., Carroll, J., and Michaelides, M. (2018). Adaptive optics imaging of inherited retinal diseases. Br J Ophthalmol *102*, 1028-1035.

Ghosh, A., Yue, Y., Lai, Y., and Duan, D. (2008). A hybrid vector system expands adeno-associated viral vector packaging capacity in a transgene-independent manner. Mol Ther *16*, 124-130.

Gil-Farina, I., Fronza, R., Kaeppel, C., Lopez-Franco, E., Ferreira, V., D'Avola, D., Benito, A., Prieto, J., Petry, H., Gonzalez-Aseguinolaza, G., *et al.* (2016). Recombinant AAV Integration Is Not Associated With Hepatic Genotoxicity in Nonhuman Primates and Patients. Mol Ther *24*, 1100-1105.

Glybina, I.V., Kennedy, A., Ashton, P., Abrams, G.W., and Iezzi, R. (2009). Photoreceptor neuroprotection in RCS rats via low-dose intravitreal sustained-delivery of fluocinolone acetonide. Invest Ophthalmol Vis Sci *50*, 4847-4857.

Goldberg, A.F., Moritz, O.L., and Williams, D.S. (2016). Molecular basis for photoreceptor outer segment architecture. Prog Retin Eye Res *55*, 52-81.

Gonzalez-Cordero, A., West, E.L., Pearson, R.A., Duran, Y., Carvalho, L.S., Chu, C.J., Naeem, A., Blackford, S.J.I., Georgiadis, A., Lakowski, J., *et al.* (2013). Photoreceptor precursors derived from three-dimensional embryonic stem cell cultures integrate and mature within adult degenerate retina. Nat Biotechnol *31*, 741-747.

References

Gorbatyuk, M.S., Knox, T., LaVail, M.M., Gorbatyuk, O.S., Noorwez, S.M., Hauswirth, W.W., Lin, J.H., Muzyczka, N., and Lewin, A.S. (2010). Restoration of visual function in P23H rhodopsin transgenic rats by gene delivery of BiP/Grp78. Proc Natl Acad Sci U S A *107*, 5961-5966.

Graham, F.L., and van der Eb, A.J. (1973). A new technique for the assay of infectivity of human adenovirus 5 DNA. Virology *52*, 456-467.

Grieger, J.C., and Samulski, R.J. (2005). Packaging capacity of adeno-associated virus serotypes: impact of larger genomes on infectivity and postentry steps. J Virol *79*, 9933-9944.

Grieger, J.C., Soltys, S.M., and Samulski, R.J. (2016). Production of Recombinant Adeno-associated Virus Vectors Using Suspension HEK293 Cells and Continuous Harvest of Vector From the Culture Media for GMP FIX and FLT1 Clinical Vector. Mol Ther *24*, 287-297.

Grimm, D., Pandey, K., and Kay, M.A. (2005). Adeno-associated virus vectors for short hairpin RNA expression. Methods Enzymol *392*, 381-405.

Grimm, D., Zhou, S., Nakai, H., Thomas, C.E., Storm, T.A., Fuess, S., Matsushita, T., Allen, J., Surosky, R., Lochrie, M.*, et al.* (2003). Preclinical in vivo evaluation of pseudotyped adeno-associated virus vectors for liver gene therapy. Blood *102*, 2412-2419.

Grondahl, J. (1987). Estimation of prognosis and prevalence of retinitis pigmentosa and Usher syndrome in Norway. Clin Genet *31*, 255-264.

Guadagni, V., Novelli, E., Piano, I., Gargini, C., and Strettoi, E. (2015). Pharmacological approaches to retinitis pigmentosa: A laboratory perspective. Prog Retin Eye Res *48*, 62-81.

Guo, P., Zhang, J., Chrzanowski, M., Huang, J., Chew, H., Firrman, J.A., Sang, N., Diao, Y., and Xiao, W. (2019). Rapid AAV-Neutralizing Antibody Determination with a Cell-Binding Assay. Mol Ther Methods Clin Dev *13*, 40-46.

Gupta, N., Brown, K.E., and Milam, A.H. (2003). Activated microglia in human retinitis pigmentosa, late-onset retinal degeneration, and age-related macular degeneration. Exp Eye Res *76*, 463-471.

Gupta, N., Shyamasundar, S., Patnala, R., Karthikeyan, A., Arumugam, T.V., Ling, E.A., and Dheen, S.T. (2018). Recent progress in therapeutic strategies for microglia-mediated neuroinflammation in neuropathologies. Expert Opin Ther Targets *22*, 765-781.

Habibi, I., Chebil, A., Falfoul, Y., Allaman-Pillet, N., Kort, F., Schorderet, D.F., and El Matri, L. (2016). Identifying mutations in Tunisian families with retinal dystrophy. Scientific Reports *6*.

Haim, M. (2002). Epidemiology of retinitis pigmentosa in Denmark. Acta Ophthalmol Scand Suppl, 1-34.

Halfter, W., Dong, S., Dong, A., Eller, A.W., and Nischt, R. (2008). Origin and turnover of ECM proteins from the inner limiting membrane and vitreous body. Eye (Lond) *22*, 1207-1213.

Hamel, C. (2006). Retinitis pigmentosa. Orphanet Journal of Rare Diseases *1*, 40.

Han, Z., Conley, S.M., Makkia, R., Guo, J., Cooper, M.J., and Naash, M.I. (2012). Comparative analysis of DNA nanoparticles and AAVs for ocular gene delivery. PLoS One *7*, e52189.

Hartong, D.T., Berson, E.L., and Dryja, T.P. (2006). Retinitis pigmentosa. The Lancet *368*, 1795-1809.

Harvey, A.R., Hu, Y., Leaver, S.G., Mellough, C.B., Park, K., Verhaagen, J., Plant, G.W., and Cui, Q. (2006). Gene therapy and transplantation in CNS repair: the visual system. Prog Retin Eye Res *25*, 449-489.

Hastie, E., and Samulski, R.J. (2015). Adeno-associated virus at 50: a golden anniversary of discovery, research, and gene therapy success--a personal perspective. Human gene therapy *26*, 257-265.

Haverkamp, S., Wassle, H., Duebel, J., Kuner, T., Augustine, G.J., Feng, G., and Euler, T. (2005). The primordial, blue-cone color system of the mouse retina. J Neurosci *25*, 5438-5445.

Hennig, A.K., Peng, G.H., and Chen, S. (2008). Regulation of photoreceptor gene expression by Crx-associated transcription factor network. Brain Res *1192*, 114-133.

Hensley, S.E., and Amalfitano, A. (2007). Toll-like receptors impact on safety and efficacy of gene transfer vectors. Mol Ther *15*, 1417-1422.

Hermens, W.T., ter Brake, O., Dijkhuizen, P.A., Sonnemans, M.A., Grimm, D., Kleinschmidt, J.A., and Verhaagen, J. (1999). Purification of recombinant adeno-associated virus by iodixanol gradient ultracentrifugation allows rapid and reproducible preparation of vector stocks for gene transfer in the nervous system. Hum Gene Ther *10*, 1885-1891.

Hermonat, P.L., Santin, A.D., and Zhan, D. (2000). Binding of the human papillomavirus type 16 E7 oncoprotein and the adeno-associated virus Rep78 major regulatory protein in vitro and in yeast and the potential for downstream effects. J Hum Virol *3*, 113-124.

Herzog, R.W., Mount, J.D., Arruda, V.R., High, K.A., and Lothrop, C.D., Jr. (2001). Muscle-directed gene transfer and transient immune suppression result in sustained partial correction of canine hemophilia B caused by a null mutation. Mol Ther *4*, 192-200.

Hickey, D.G., Edwards, T.L., Barnard, A.R., Singh, M.S., de Silva, S.R., McClements, M.E., Flannery, J.G., Hankins, M.W., and MacLaren, R.E. (2017). Tropism of engineered and evolved recombinant AAV serotypes in the rd1 mouse and ex vivo primate retina. Gene Ther *24*, 787-800.

Hinderer, C., Katz, N., Buza, E.L., Dyer, C., Goode, T., Bell, P., Richman, L.K., and Wilson, J.M. (2018). Severe Toxicity in Nonhuman Primates and Piglets Following High-Dose Intravenous Administration of an Adeno-Associated Virus Vector Expressing Human SMN. Hum Gene Ther *29*, 285-298.

Hippert, C., Graca, A.B., Barber, A.C., West, E.L., Smith, A.J., Ali, R.R., and Pearson, R.A. (2015). Muller glia activation in response to inherited retinal degeneration is highly varied and disease-specific. PLoS One *10*, e0120415.

Hirata, R., Chamberlain, J., Dong, R., and Russell, D.W. (2002). Targeted transgene insertion into human chromosomes by adeno-associated virus vectors. Nat Biotechnol *20*, 735-738.

Hirsch, M.L., Li, C., Bellon, I., Yin, C., Chavala, S., Pryadkina, M., Richard, I., and Samulski, R.J. (2013). Oversized AAV transductifon is mediated via a DNA-PKcs-independent, Rad51C-dependent repair pathway. Mol Ther *21*, 2205-2216.

Ho, A.C., Humayun, M.S., Dorn, J.D., da Cruz, L., Dagnelie, G., Handa, J., Barale, P.O., Sahel, J.A., Stanga, P.E., Hafezi, F.*, et al.* (2015). Long-Term Results from an Epiretinal Prosthesis to Restore Sight to the Blind. Ophthalmology *122*, 1547-1554.

Hodgkin, A.L., McNaughton, P.A., and Nunn, B.J. (1985). The ionic selectivity and calcium dependence of the light-sensitive pathway in toad rods. J Physiol *358*, 447-468.

Holopigian, K., Greenstein, V., Seiple, W., and Carr, R.E. (1996). Rates of change differ among measures of visual function in patients with retinitis pigmentosa. Ophthalmology *103*, 398-405.

Hood, D.C., Lazow, M.A., Locke, K.G., Greenstein, V.C., and Birch, D.G. (2011). The transition zone between healthy and diseased retina in patients with retinitis pigmentosa. Invest Ophthalmol Vis Sci *52*, 101-108.

Hoon, M., Okawa, H., Della Santina, L., and Wong, R.O. (2014). Functional architecture of the retina: development and disease. Prog Retin Eye Res *42*, 44-84.

Hosel, M., Broxtermann, M., Janicki, H., Esser, K., Arzberger, S., Hartmann, P., Gillen, S., Kleeff, J., Stabenow, D., Odenthal, M.*, et al.* (2012). Toll-like receptor 2-mediated innate immune response in human nonparenchymal liver cells toward adeno-associated viral vectors. Hepatology *55*, 287-297.

Huang, D., Swanson, E.A., Lin, C.P., Schuman, J.S., Stinson, W.G., Chang, W., Hee, M.R., Flotte, T., Gregory, K., Puliafito, C.A.*, et al.* (1991). Optical coherence tomography. Science *254*, 1178-1181.

Huang, L., Zhang, Q., Huang, X., Qu, C., Ma, S., Mao, Y., Yang, J., Li, Y., Li, Y., Tan, C.*, et al.* (2017). Mutation screening in genes known to be responsible for Retinitis Pigmentosa in 98 Small Han Chinese Families. Sci Rep *7*, 1948.

Hull, S., Attanasio, M., Arno, G., Carss, K., Robson, A.G., Thompson, D.A., Plagnol, V., Michaelides, M., Holder, G.E., Henderson, R.H.*, et al.* (2017). Clinical Characterization of CNGB1-Related Autosomal Recessive Retinitis Pigmentosa. JAMA Ophthalmol *135*, 137-144.

Humayun, M.S., Dorn, J.D., da Cruz, L., Dagnelie, G., Sahel, J.A., Stanga, P.E., Cideciyan, A.V., Duncan, J.L., Eliott, D., Filley, E.*, et al.* (2012). Interim results from the international trial of Second Sight's visual prosthesis. Ophthalmology *119*, 779-788.

Hung, S.S., Chrysostomou, V., Li, F., Lim, J.K., Wang, J.H., Powell, J.E., Tu, L., Daniszewski, M., Lo, C., Wong, R.C.*, et al.* (2016). AAV-Mediated CRISPR/Cas Gene Editing of Retinal Cells In Vivo. Invest Ophthalmol Vis Sci *57*, 3470-3476.

References

Huttl, S., Michalakis, S., Seeliger, M., Luo, D.G., Acar, N., Geiger, H., Hudl, K., Mader, R., Haverkamp, S., Moser, M., *et al.* (2005). Impaired channel targeting and retinal degeneration in mice lacking the cyclic nucleotide-gated channel subunit CNGB1. J Neurosci *25*, 130-138.

Hwang, Y.H., Kim, S.W., Kim, Y.Y., Na, J.H., Kim, H.K., and Sohn, Y.H. (2012). Optic nerve head, retinal nerve fiber layer, and macular thickness measurements in young patients with retinitis pigmentosa. Curr Eye Res *37*, 914-920.

Iannaccone, A., Rispoli, E., Vingolo, E.M., Onori, P., Steindl, K., Rispoli, D., and Pannarale, M.R. (1995). Correlation between Goldmann perimetry and maximal electroretinogram response in retinitis pigmentosa. Doc Ophthalmol *90*, 129-142.

Ivanova, E., Hwang, G.-S., Pan, Z.-H., and Troilo, D. (2010). Evaluation of AAV-mediated expression of Chop2-GFP in the marmoset retina. Investigative ophthalmology & visual science *51*, 5288-5296.

Jacobson, S.G., Cideciyan, A.V., Ratnakaram, R., Heon, E., Schwartz, S.B., Roman, A.J., Peden, M.C., Aleman, T.S., Boye, S.L., Sumaroka, A., *et al.* (2012). Gene therapy for leber congenital amaurosis caused by RPE65 mutations: safety and efficacy in 15 children and adults followed up to 3 years. Arch Ophthalmol *130*, 9-24.

Javed, A., and Cayouette, M. (2017). Temporal Progression of Retinal Progenitor Cell Identity: Implications in Cell Replacement Therapies. Front Neural Circuits *11*, 105.

Jay, M. (1982). On the heredity of retinitis pigmentosa. Br J Ophthalmol *66*, 405-416.

Jenkins, P.M., Hurd, T.W., Zhang, L., McEwen, D.P., Brown, R.L., Margolis, B., Verhey, K.J., and Martens, J.R. (2006). Ciliary targeting of olfactory CNG channels requires the CNGB1b subunit and the kinesin-2 motor protein, KIF17. Curr Biol *16*, 1211-1216.

Jenks, S. (2000). Gene therapy death--"everyone has to share in the guilt". J Natl Cancer Inst *92*, 98-100.

Jeon, C.J., Strettoi, E., and Masland, R.H. (1998). The major cell populations of the mouse retina. J Neurosci *18*, 8936-8946.
JH, W. (2009). Gene Therapy in Large Animal Models of Human Genetic Diseases. ILAR J *50*, 107-111.

Jinek, M., Chylinski, K., Fonfara, I., Hauer, M., Doudna, J.A., and Charpentier, E. (2012). A programmable dual-RNA-guided DNA endonuclease in adaptive bacterial immunity. Science *337*, 816-821.

Jones, M.K., Lu, B., Girman, S., and Wang, S. (2017). Cell-based therapeutic strategies for replacement and preservation in retinal degenerative diseases. Prog Retin Eye Res *58*, 1-27.

Kafri, T., Morgan, D., Krahl, T., Sarvetnick, N., Sherman, L., and Verma, I. (1998). Cellular immune response to adenoviral vector infected cells does not require de novo viral gene expression: implications for gene therapy. Proc Natl Acad Sci U S A *95*, 11377-11382.

Karlstetter, M., Ebert, S., and Langmann, T. (2010). Microglia in the healthy and degenerating retina: insights from novel mouse models. Immunobiology *215*, 685-691.

Kaufmann, K.B., Buning, H., Galy, A., Schambach, A., and Grez, M. (2013). Gene therapy on the move. EMBO Mol Med *5*, 1642-1661.

Kaupp, U.B., and Seifert, R. (2002). Cyclic Nucleotide-Gated Ion Channels. Physiol Rev *82*, 769-824.

Kay, C.N., Ryals, R.C., Aslanidi, G.V., Min, S.H., Ruan, Q., Sun, J., Dyka, F.M., Kasuga, D., Ayala, A.E., Van Vliet, K., *et al.* (2013). Targeting photoreceptors via intravitreal delivery using novel, capsid-mutated AAV vectors. PLoS One *8*, e62097.

Keilhauer, C.N., and Delori, F.C. (2006). Near-infrared autofluorescence imaging of the fundus: visualization of ocular melanin. Invest Ophthalmol Vis Sci *47*, 3556-3564.

Kenna, P.F., Humphries, M.M., Kiang, A.S., Brabet, P., Guillou, L., Ozaki, E., Campbell, M., Farrar, G.J., Koenekoop, R., and Humphries, P. (2020). Advanced late-onset retinitis pigmentosa with dominant-acting D477G RPE65 mutation is responsive to oral synthetic retinoid therapy. BMJ Open Ophthalmol *5*, e000462.

Kizhatil, K., Baker, S.A., Arshavsky, V.Y., and Bennett, V. (2009). Ankyrin-G promotes cyclic nucleotide-gated channel transport to rod photoreceptor sensory cilia. Science *323*, 1614-1617.

Koch, S., Sothilingam, V., Garcia Garrido, M., Tanimoto, N., Becirovic, E., Koch, F., Seide, C., Beck, S.C., Seeliger, M.W., Biel, M., *et al.* (2012). Gene therapy restores vision and delays degeneration in the CNGB1(-/-) mouse model of retinitis pigmentosa. Hum Mol Genet *21*, 4486-4496.

Kodippili, K., Hakim, C.H., Pan, X., Yang, H.T., Yue, Y., Zhang, Y., Shin, J.H., Yang, N.N., and Duan, D. (2018). Dual AAV Gene Therapy for Duchenne Muscular Dystrophy with a 7-kb Mini-Dystrophin Gene in the Canine Model. Hum Gene Ther *29*, 299-311.

Koenekoop, R.K., Sui, R., Sallum, J., van den Born, L.I., Ajlan, R., Khan, A., den Hollander, A.I., Cremers, F.P., Mendola, J.D., Bittner, A.K., *et al.* (2014). Oral 9-cis retinoid for childhood blindness due to Leber congenital amaurosis caused by RPE65 or LRAT mutations: an open-label phase 1b trial. Lancet *384*, 1513-1520.

Koenig, R. (2003). Bardet-Biedl syndrome and Usher syndrome. Dev Ophthalmol *37*, 126-140.

Kolb, H. (1995). Simple Anatomy of the Retina. In Webvision: The Organization of the Retina and Visual System, H. Kolb, E. Fernandez, and R. Nelson, eds. (Salt Lake City (UT)).

Komaromy, A.M., Alexander, J.J., Rowlan, J.S., Garcia, M.M., Chiodo, V.A., Kaya, A., Tanaka, J.C., Acland, G.M., Hauswirth, W.W., and Aguirre, G.D. (2010). Gene therapy rescues cone function in congenital achromatopsia. Hum Mol Genet *19*, 2581-2593.

Komaromy, A.M., Varner, S.E., de Juan, E., Acland, G.M., and Aguirre, G.D. (2006). Application of a new subretinal injection device in the dog. Cell Transplant *15*, 511-519.

Komeima, K., Rogers, B.S., and Campochiaro, P.A. (2007). Antioxidants slow photoreceptor cell death in mouse models of retinitis pigmentosa. J Cell Physiol *213*, 809-815.

Kondo, H., Qin, M., Mizota, A., Kondo, M., Hayashi, H., Hayashi, K., Oshima, K., Tahira, T., and Hayashi, K. (2004). A homozygosity-based search for mutations in patients with autosomal recessive retinitis pigmentosa, using microsatellite markers. Invest Ophthalmol Vis Sci *45*, 4433-4439.

Korschen, H.G., Illing, M., Seifert, R., Sesti, F., Williams, A., Gotzes, S., Colville, C., Muller, F., Dose, A., Godde, M., *et al.* (1995). A 240 kDa protein represents the complete beta subunit of the cyclic nucleotide-gated channel from rod photoreceptor. Neuron *15*, 627-636.

Kostic, C., and Arsenijevic, Y. (2016). Animal modelling for inherited central vision loss. J Pathol *238*, 300-310.
Kotterman, M.A., and Schaffer, D.V. (2014). Engineering adeno-associated viruses for clinical gene therapy. Nat Rev Genet *15*, 445-451.

Kotterman, M.A., Yin, L., Strazzeri, J.M., Flannery, J.G., Merigan, W.H., and Schaffer, D.V. (2015). Antibody neutralization poses a barrier to intravitreal adeno-associated viral vector gene delivery to non-human primates. Gene Ther *22*, 116-126.

Kumar, S.R.P., Hoffman, B.E., Terhorst, C., de Jong, Y.P., and Herzog, R.W. (2017). The Balance between CD8(+) T Cell-Mediated Clearance of AAV-Encoded Antigen in the Liver and Tolerance Is Dependent on the Vector Dose. Mol Ther *25*, 880-891.

Kuroda, M., Hirami, Y., Hata, M., Mandai, M., Takahashi, M., and Kurimoto, Y. (2014). Intraretinal hyperreflective foci on spectral-domain optical coherence tomographic images of patients with retinitis pigmentosa. Clin Ophthalmol *8*, 435-440.

Lai, Y., Yue, Y., and Duan, D. (2010). Evidence for the failure of adeno-associated virus serotype 5 to package a viral genome > or = 8.2 kb. Mol Ther *18*, 75-79.

Lamb, T.D., and Pugh, E.N., Jr. (2006). Phototransduction, dark adaptation, and rhodopsin regeneration the proctor lecture. Invest Ophthalmol Vis Sci *47*, 5137-5152.

Lamba, D.A., Gust, J., and Reh, T.A. (2009). Transplantation of human embryonic stem cell-derived photoreceptors restores some visual function in Crx-deficient mice. Cell Stem Cell *4*, 73-79.

Lamba, D.A., McUsic, A., Hirata, R.K., Wang, P.R., Russell, D., and Reh, T.A. (2010). Generation, purification and transplantation of photoreceptors derived from human induced pluripotent stem cells. PLoS One *5*, e8763.

Lebherz, C., Maguire, A., Tang, W., Bennett, J., and Wilson, J.M. (2008). Novel AAV serotypes for improved ocular gene transfer. J Gene Med *10*, 375-382.

Lee, J., Myers, C.A., Williams, N., Abdelaziz, M., and Corbo, J.C. (2010). Quantitative fine-tuning of photoreceptor cis-regulatory elements through affinity modulation of transcription factor binding sites. Gene Ther *17*, 1390-1399.

Lee, S., Kang, I.K., Kim, J.H., Jung, B.K., Park, K., Chang, H., Lee, J.Y., and Lee, H. (2019). Relationship Between Neutralizing Antibodies Against Adeno-Associated Virus in the Vitreous and Serum: Effects on Retinal Gene Therapy. Translational Vision Science & Technology *8*.

References

Lem, J., Applebury, M.L., Falk, J.D., Flannery, J.G., and Simon, M.I. (1991). Tissue-specific and developmental regulation of rod opsin chimeric genes in transgenic mice. Neuron *6*, 201-210.

Lewis, G.P., Chapin, E.A., Luna, G., Linberg, K.A., and Fisher, S.K. (2010). The fate of Muller's glia following experimental retinal detachment: nuclear migration, cell division, and subretinal glial scar formation. Mol Vis *16*, 1361-1372.

Lewis, G.P., and Fisher, S.K. (2003). Up-regulation of glial fibrillary acidic protein in response to retinal injury: its potential role in glial remodeling and a comparison to vimentin expression. Int Rev Cytol *230*, 263-290.

Lhériteau, E., Petit, L., Weber, M., Le Meur, G., Deschamps, J.Y., Libeau, L., Mendes-Madeira, A., Guihal, C., François, A., Guyon, R.*, et al.* (2014). Successful gene therapy in the RPGRIP1-deficient dog: a large model of cone-rod dystrophy. Mol Ther *22*, 265-277.

Li, C., He, Y., Nicolson, S., Hirsch, M., Weinberg, M.S., Zhang, P., Kafri, T., and Samulski, R.J. (2013). Adeno-associated virus capsid antigen presentation is dependent on endosomal escape. J Clin Invest *123*, 1390-1401.

Li, Q., Miller, R., Han, P.Y., Pang, J., Dinculescu, A., Chiodo, V., and Hauswirth, W.W. (2008). Intraocular route of AAV2 vector administration defines humoral immune response and therapeutic potential. Mol Vis *14*, 1760-1769.

Li, W., Zhang, L., Johnson, J.S., Zhijian, W., Grieger, J.C., Ping-Jie, X., Drouin, L.M., Agbandje-McKenna, M., Pickles, R.J., and Samulski, R.J. (2009). Generation of novel AAV variants by directed evolution for improved CFTR delivery to human ciliated airway epithelium. Mol Ther *17*, 2067-2077.

Li, X., Li, W., Dai, X., Kong, F., Zheng, Q., Zhou, X., Lu, F., Chang, B., Rohrer, B., Hauswirth, W.W.*, et al.* (2011). Gene therapy rescues cone structure and function in the 3-month-old rd12 mouse: a model for midcourse RPE65 leber congenital amaurosis. Invest Ophthalmol Vis Sci *52*, 7-15.

Li, Y., Tsai, Y.T., Hsu, C.W., Erol, D., Yang, J., Wu, W.H., Davis, R.J., Egli, D., and Tsang, S.H. (2012). Long-term safety and efficacy of human-induced pluripotent stem cell (iPS) grafts in a preclinical model of retinitis pigmentosa. Mol Med *18*, 1312-1319.

Li, Z.Y., Possin, D.E., and Milam, A.H. (1995). Histopathology of bone spicule pigmentation in retinitis pigmentosa. Ophthalmology *102*, 805-816.

Lin, B., Koizumi, A., Tanaka, N., Panda, S., and Masland, R.H. (2008). Restoration of visual function in retinal degeneration mice by ectopic expression of melanopsin. Proc Natl Acad Sci U S A *105*, 16009-16014.

Lin, J., Calcedo, R., Vandenberghe, L.H., Bell, P., Somanathan, S., and Wilson, J.M. (2009). A new genetic vaccine platform based on an adeno-associated virus isolated from a rhesus macaque. J Virol *83*, 12738-12750.

Lin, M.K.T., Y.-T.; Tsang, S. H. (2015). Emerging Treatments for Retinits Pigmentosa. Retin Physician *12*, 52-55.

Linden, R.M., Winocour, E., and Berns, K.I. (1996). The recombination signals for adeno-associated virus site-specific integration. Proc Natl Acad Sci U S A *93*, 7966-7972.

Lingao, M.D., Ganesh, A., Karthikeyan, A.S., Al Zuhaibi, S., Al-Hosni, A., Al Khayat, A., Capasso, J., Trumler, A.A., Stroh, E., Al Shekaili, H.*, et al.* (2016). Macular cystoid spaces in patients with retinal dystrophy. Ophthalmic Genet *37*, 377-383.

Liu, G., Liu, X., Li, H., Du, Q., and Wang, F. (2016). Optical Coherence Tomographic Analysis of Retina in Retinitis Pigmentosa Patients. Ophthalmic Res *56*, 111-122.

Liu, Y., Chen, S.J., Li, S.Y., Qu, L.H., Meng, X.H., Wang, Y., Xu, H.W., Liang, Z.Q., and Yin, Z.Q. (2017). Long-term safety of human retinal progenitor cell transplantation in retinitis pigmentosa patients. Stem Cell Res Ther *8*, 209.

Lopes, V.S., Boye, S.E., Louie, C.M., Boye, S., Dyka, F., Chiodo, V., Fofo, H., Hauswirth, W.W., and Williams, D.S. (2013). Retinal gene therapy with a large MYO7A cDNA using adeno-associated virus. Gene Ther *20*, 824-833.

Lostal, W., Bartoli, M., Bourg, N., Roudaut, C., Bentaïb, A., Miyake, K., Guerchet, N., Fougerousse, F., McNeil, P., and Richard, I. (2010). Efficient recovery of dysferlin deficiency by dual adeno-associated vector-mediated gene transfer. Hum Mol Genet *19*, 1897-1907.

Lotery, A.J., Yang, G.S., Mullins, R.F., Russell, S.R., Schmidt, M., Stone, E.M., Lindbloom, J.D., Chiorini, J.A., Kotin, R.M., and Davidson, B.L. (2003). Adeno-associated virus type 5: transduction efficiency and cell-type specificity in the primate retina. Hum Gene Ther *14*, 1663-1671.

Louis Jeune, V., Joergensen, J.A., Hajjar, R.J., and Weber, T. (2013). Pre-existing anti-adeno-associated virus antibodies as a challenge in AAV gene therapy. Hum Gene Ther Methods *24*, 59-67.

Luo, D.G., Xue, T., and Yau, K.W. (2008). How vision begins: an odyssey. Proc Natl Acad Sci U S A *105*, 9855-9862.

MacLaren, R.E., Bennett, J., and Schwartz, S.D. (2016). Gene Therapy and Stem Cell Transplantation in Retinal Disease: The New Frontier. Ophthalmology *123*, S98-S106.

Maguire, A.M., High, K.A., Auricchio, A., Wright, J.F., Pierce, E.A., Testa, F., Mingozzi, F., Bennicelli, J.L., Ying, G.S., Rossi, S., *et al.* (2009). Age-dependent effects of RPE65 gene therapy for Leber's congenital amaurosis: a phase 1 dose-escalation trial. Lancet *374*, 1597-1605.

Maguire, A.M., Russell, S., Wellman, J.A., Chung, D.C., Yu, Z.F., Tillman, A., Wittes, J., Pappas, J., Elci, O., Marshall, K.A., *et al.* (2019). Efficacy, Safety, and Durability of Voretigene Neparvovec-rzyl in RPE65 Mutation-Associated Inherited Retinal Dystrophy: Results of Phase 1 and 3 Trials. Ophthalmology *126*, 1273-1285.

Maguire, A.M., Simonelli, F., Pierce, E.A., Pugh, E.N., Jr., Mingozzi, F., Bennicelli, J., Banfi, S., Marshall, K.A., Testa, F., Surace, E.M., *et al.* (2008). Safety and efficacy of gene transfer for Leber's congenital amaurosis. N Engl J Med *358*, 2240-2248.

Maheshri, N., Koerber, J.T., Kaspar, B.K., and Schaffer, D.V. (2006). Directed evolution of adeno-associated virus yields enhanced gene delivery vectors. Nat Biotechnol *24*, 198-204.

Majowicz, A., Salas, D., Zabaleta, N., Rodríguez-Garcia, E., González-Aseguinolaza, G., Petry, H., and Ferreira, V. (2017). Successful Repeated Hepatic Gene Delivery in Mice and Non-human Primates Achieved by Sequential Administration of AAV5(ch) and AAV1. Mol Ther *25*, 1831-1842.

Mancuso, K., Hauswirth, W.W., Li, Q., Connor, T.B., Kuchenbecker, J.A., Mauck, M.C., Neitz, J., and Neitz, M. (2009). Gene therapy for red-green colour blindness in adult primates. Nature *461*, 784-787.

Mancuso, K., Hendrickson, A.E., Connor, T.B., Jr., Mauck, M.C., Kinsella, J.J., Hauswirth, W.W., Neitz, J., and Neitz, M. (2007). Recombinant adeno-associated virus targets passenger gene expression to cones in primate retina. J Opt Soc Am A Opt Image Sci Vis *24*, 1411-1416.

Manno, C.S., Pierce, G.F., Arruda, V.R., Glader, B., Ragni, M., Rasko, J.J., Ozelo, M.C., Hoots, K., Blatt, P., Konkle, B., *et al.* (2006). Successful transduction of liver in hemophilia by AAV-Factor IX and limitations imposed by the host immune response. Nat Med *12*, 342-347.

Mao, H., James, T., Jr., Schwein, A., Shabashvili, A.E., Hauswirth, W.W., Gorbatyuk, M.S., and Lewin, A.S. (2011). AAV delivery of wild-type rhodopsin preserves retinal function in a mouse model of autosomal dominant retinitis pigmentosa. Hum Gene Ther *22*, 567-575.

Maranhao, B., Biswas, P., Gottsch, A.D., Navani, M., Naeem, M.A., Suk, J., Chu, J., Khan, S.N., Poleman, R., Akram, J., *et al.* (2015). Investigating the Molecular Basis of Retinal Degeneration in a Familial Cohort of Pakistani Decent by Exome Sequencing. PLoS One *10*, e0136561.

Maria, M., Ajmal, M., Azam, M., Waheed, N.K., Siddiqui, S.N., Mustafa, B., Ayub, H., Ali, L., Ahmad, S., Micheal, S., *et al.* (2015). Homozygosity mapping and targeted sanger sequencing reveal genetic defects underlying inherited retinal disease in families from pakistan. PLoS One *10*, e0119806.

Marigo, V. (2007). Programmed cell death in retinal degeneration: targeting apoptosis in photoreceptors as potential therapy for retinal degeneration. Cell Cycle *6*, 652-655.

Marmor, M.F. (1979). The electroretinogram in retinitis pigmentosa. Arch Ophthalmol *97*, 1300-1304.

Marmor, M.F. (1989). An international standard for electroretinography. Doc Ophthalmol *73*, 299-302.

Marmor, M.F., Holder, G.E., Porciatti, V., Trick, G.L., and Zrenner, E. (1995). Guidelines for basic pattern electroretinography. Recommendations by the International Society for Clinical Electrophysiology of Vision. Doc Ophthalmol *91*, 291-298.

Martin, J., Frederick, A., Luo, Y., Jackson, R., Joubert, M., Sol, B., Poulin, F., Pastor, E., Armentano, D., Wadsworth, S., *et al.* (2013). Generation and characterization of adeno-associated virus producer cell lines for research and preclinical vector production. Hum Gene Ther Methods *24*, 253-269.

Martino, A.T., and Markusic, D.M. (2020). Immune Response Mechanisms against AAV Vectors in Animal Models. Mol Ther Methods Clin Dev *17*, 198-208.

References

Martino, A.T., Suzuki, M., Markusic, D.M., Zolotukhin, I., Ryals, R.C., Moghimi, B., Ertl, H.C., Muruve, D.A., Lee, B., and Herzog, R.W. (2011). The genome of self-complementary adeno-associated viral vectors increases Toll-like receptor 9-dependent innate immune responses in the liver. Blood *117*, 6459-6468.

Mathebula, S.D. (2012). A review of ocular genetics and inherited eye diseases. S Afr Optom *71*, 178-189

Mattapallil, M.J., Wawrousek, E.F., Chan, C.C., Zhao, H., Roychoudhury, J., Ferguson, T.A., and Caspi, R.R. (2012). The Rd8 mutation of the Crb1 gene is present in vendor lines of C57BL/6N mice and embryonic stem cells, and confounds ocular induced mutant phenotypes. Invest Ophthalmol Vis Sci *53*, 2921-2927.

Matulef, K., and Zagotta, W.N. (2003). Cyclic nucleotide-gated ion channels. Annu Rev Cell Dev Biol *19*, 23-44.

Maurer, A.C., Pacouret, S., Cepeda Diaz, A.K., Blake, J., Andres-Mateos, E., and Vandenberghe, L.H. (2018). The Assembly-Activating Protein Promotes Stability and Interactions between AAV's Viral Proteins to Nucleate Capsid Assembly. Cell Rep *23*, 1817-1830.

Mays, L.E., and Wilson, J.M. (2011). The complex and evolving story of T cell activation to AAV vector-encoded transgene products. Mol Ther *19*, 16-27.

McCarty, D.M., Monahan, P.E., and Samulski, R.J. (2001). Self-complementary recombinant adeno-associated virus (scAAV) vectors promote efficient transduction independently of DNA synthesis. Gene Ther *8*, 1248-1254.

McCarty, D.M., Young, S.M., Jr., and Samulski, R.J. (2004). Integration of adeno-associated virus (AAV) and recombinant AAV vectors. Annu Rev Genet *38*, 819-845.

McCulloch, D.L., Marmor, M.F., Brigell, M.G., Hamilton, R., Holder, G.E., Tzekov, R., and Bach, M. (2015). ISCEV Standard for full-field clinical electroretinography (2015 update). Doc Ophthalmol *130*, 1-12.

McIntosh, J.H., Cochrane, M., Cobbold, S., Waldmann, H., Nathwani, S.A., Davidoff, A.M., and Nathwani, A.C. (2012). Successful attenuation of humoral immunity to viral capsid and transgenic protein following AAV-mediated gene transfer with a non-depleting CD4 antibody and cyclosporine. Gene Ther *19*, 78-85.

McKenna, K.C., and Kapp, J.A. (2004). Ocular immune privilege and CTL tolerance. Immunol Res *29*, 103-112.

Mears, A.J., Kondo, M., Swain, P.K., Takada, Y., Bush, R.A., Saunders, T.L., Sieving, P.A., and Swaroop, A. (2001). Nrl is required for rod photoreceptor development. Nat Genet *29*, 447-452.

Meliani, A., Boisgerault, F., Hardet, R., Marmier, S., Collaud, F., Ronzitti, G., Leborgne, C., Costa Verdera, H., Simon Sola, M., Charles, S.*, et al.* (2018). Antigen-selective modulation of AAV immunogenicity with tolerogenic rapamycin nanoparticles enables successful vector re-administration. Nat Commun *9*, 4098.

Meliani, A., Leborgne, C., Triffault, S., Jeanson-Leh, L., Veron, P., and Mingozzi, F. (2015). Determination of anti-adeno-associated virus vector neutralizing antibody titer with an in vitro reporter system. Human gene therapy methods *26*, 45-53.

Michalakis, S., Becirovic, E., and Biel, M. (2018). Retinal Cyclic Nucleotide-Gated Channels: From Pathophysiology to Therapy. Int J Mol Sci *19*.

Michalakis, S., Geiger, H., Haverkamp, S., Hofmann, F., Gerstner, A., and Biel, M. (2005). Impaired opsin targeting and cone photoreceptor migration in the retina of mice lacking the cyclic nucleotide-gated channel CNGA3. Invest Ophthalmol Vis Sci *46*, 1516-1524.

Michalakis, S., Muhlfriedel, R., Tanimoto, N., Krishnamoorthy, V., Koch, S., Fischer, M.D., Becirovic, E., Bai, L., Huber, G., Beck, S.C.*, et al.* (2010). Restoration of cone vision in the CNGA3-/- mouse model of congenital complete lack of cone photoreceptor function. Mol Ther *18*, 2057-2063.

Michalakis, S., Reisert, J., Geiger, H., Wetzel, C., Zong, X., Bradley, J., Spehr, M., Huttl, S., Gerstner, A., Pfeifer, A.*, et al.* (2006). Loss of CNGB1 protein leads to olfactory dysfunction and subciliary cyclic nucleotide-gated channel trapping. J Biol Chem *281*, 35156-35166.

Milam, A.H., Li, Z.Y., and Fariss, R.N. (1998). Histopathology of the human retina in retinitis pigmentosa. Prog Retin Eye Res *17*, 175-205.

Min, S.H., Molday, L.L., Seeliger, M.W., Dinculescu, A., Timmers, A.M., Janssen, A., Tonagel, F., Tanimoto, N., Weber, B.H., Molday, R.S.*, et al.* (2005). Prolonged recovery of retinal structure/function after gene therapy in an Rs1h-deficient mouse model of x-linked juvenile retinoschisis. Mol Ther *12*, 644-651.

Mingozzi, F., Anguela, X.M., Pavani, G., Chen, Y., Davidson, R.J., Hui, D.J., Yazicioglu, M., Elkouby, L., Hinderer, C.J., Faella, A.*, et al.* (2013). Overcoming preexisting humoral immunity to AAV using capsid decoys. Sci Transl Med *5*, 194ra192.

Mingozzi, F., and High, K.A. (2011). Immune responses to AAV in clinical trials. Curr Gene Ther *11*, 321-330.

Mingozzi, F., Maus, M.V., Hui, D.J., Sabatino, D.E., Murphy, S.L., Rasko, J.E., Ragni, M.V., Manno, C.S., Sommer, J., Jiang, H.*, et al.* (2007). CD8(+) T-cell responses to adeno-associated virus capsid in humans. Nat Med *13*, 419-422.

Mingozzi, F., Meulenberg, J.J., Hui, D.J., Basner-Tschakarjan, E., Hasbrouck, N.C., Edmonson, S.A., Hutnick, N.A., Betts, M.R., Kastelein, J.J., Stroes, E.S.*, et al.* (2009). AAV-1-mediated gene transfer to skeletal muscle in humans results in dose-dependent activation of capsid-specific T cells. Blood *114*, 2077-2086.

Mishra, L., and Rose, J.A. (1990). Adeno-associated virus DNA replication is induced by genes that are essential for HSV-1 DNA synthesis. Virology *179*, 632-639.

Mitchell, A.M., and Samulski, R.J. (2013). Mechanistic insights into the enhancement of adeno-associated virus transduction by proteasome inhibitors. J Virol *87*, 13035-13041.

Mitton, K.P., Swain, P.K., Chen, S., Xu, S., Zack, D.J., and Swaroop, A. (2000). The leucine zipper of NRL interacts with the CRX homeodomain. A possible mechanism of transcriptional synergy in rhodopsin regulation. J Biol Chem *275*, 29794-29799. Molday, R.S., and Moritz, O.L. (2015). Photoreceptors at a glance. J Cell Sci *128*, 4039-4045.

Molday, R.S., Molday, L.L., Dose, A., Clark-Lewis, I., Illing, M., Cook, N.J., Eismann, E., and Kaupp, U.B. (1991). The cGMP-gated channel of the rod photoreceptor cell characterization and orientation of the amino terminus. J Biol Chem *266*, 21917-21922.

Monahan, P.E., Lothrop, C.D., Sun, J., Hirsch, M.L., Kafri, T., Kantor, B., Sarkar, R., Tillson, D.M., Elia, J.R., and Samulski, R.J. (2010). Proteasome inhibitors enhance gene delivery by AAV virus vectors expressing large genomes in hemophilia mouse and dog models: a strategy for broad clinical application. Mol Ther *18*, 1907-1916.

Monteilhet, V., Saheb, S., Boutin, S., Leborgne, C., Veron, P., Montus, M.-F., Moullier, P., Benveniste, O., and Masurier, C. (2011). A 10 patient case report on the impact of plasmapheresis upon neutralizing factors against adeno-associated virus (AAV) types 1, 2, 6, and 8. Molecular therapy : the journal of the American Society of Gene Therapy *19*, 2084-2091.

Morris, R. (1984). Developments of a water-maze procedure for studying spatial learning in the rat. J Neurosci Methods *11*, 47-60.

Mowat, F.M., Occelli, L.M., Bartoe, J.T., Gervais, K.J., Bruewer, A.R., Querubin, J., Dinculescu, A., Boye, S.L., Hauswirth, W.W., and Petersen-Jones, S.M. (2017). Gene Therapy in a Large Animal Model of PDE6A-Retinitis Pigmentosa. Front Neurosci *11*, 342.

Mowat, F.M.P.-J., S. M.; Williamson, H.; Williams, D. L.; Luthert, P. J.; Ali, R. R.; Bainbridge, J. W. (2008). Topographical characterization of cone photoreceptors and the area centralis of the canine retina. Mol Vis *14*, 2518-2527.

Mueller, C., and Flotte, T.R. (2008). Clinical gene therapy using recombinant adeno-associated virus vectors. Gene Ther *15*, 858-863.

Muhlfriedel, R., Michalakis, S., Garcia Garrido, M., Biel, M., and Seeliger, M.W. (2013). Optimized technique for subretinal injections in mice. Methods Mol Biol *935*, 343-349.

Musarella, M.A., and Macdonald, I.M. (2011). Current concepts in the treatment of retinitis pigmentosa. J Ophthalmol *2011*, 753547.

Mussolino, C., della Corte, M., Rossi, S., Viola, F., Di Vicino, U., Marrocco, E., Neglia, S., Doria, M., Testa, F., Giovannoni, R.*, et al.* (2011). AAV-mediated photoreceptor transduction of the pig cone-enriched retina. Gene Ther *18*, 637-645.

Mustafi, D., Engel, A.H., and Palczewski, K. (2009). Structure of cone photoreceptors. Prog Retin Eye Res *28*, 289-302.

Mutti, D.O.Z., K.; Murphy, C. J. (1999). Naturally Occurring Vitreous Chamber-Based Myopia in the Labrador Retriever.

Na, K.H., Kim, H.J., Kim, K.H., Han, S., Kim, P., Hann, H.J., and Ahn, H.S. (2017). Prevalence, Age at Diagnosis, Mortality, and Cause of Death in Retinitis Pigmentosa in Korea-A Nationwide Population-based Study. Am J Ophthalmol *176*, 157-165.

Nagasaka, Y., Ito, Y., Ueno, S., and Terasaki, H. (2018). Number of Hyperreflective Foci in the Outer Retina Correlates with Inflammation and Photoreceptor Degeneration in Retinitis Pigmentosa. Ophthalmol Retina *2*, 726-734.

References

Nakai, H., Montini, E., Fuess, S., Storm, T.A., Grompe, M., and Kay, M.A. (2003). AAV serotype 2 vectors preferentially integrate into active genes in mice. Nat Genet *34*, 297-302.

Nakai, H., Yant, S.R., Storm, T.A., Fuess, S., Meuse, L., and Kay, M.A. (2001). Extrachromosomal recombinant adeno-associated virus vector genomes are primarily responsible for stable liver transduction in vivo. J Virol *75*, 6969-6976.

Nangia, V., Jonas, J.B., Khare, A., and Sinha, A. (2012). Prevalence of retinitis pigmentosa in India: the Central India Eye and Medical Study. Acta Ophthalmol *90*, e649-650.

Naso, M.F., Tomkowicz, B., Perry, W.L., 3rd, and Strohl, W.R. (2017). Adeno-Associated Virus (AAV) as a Vector for Gene Therapy. BioDrugs *31*, 317-334.

Nass, S.A., Mattingly, M.A., Woodcock, D.A., Burnham, B.L., Ardinger, J.A., Osmond, S.E., Frederick, A.M., Scaria, A., Cheng, S.H., and O'Riordan, C.R. (2018). Universal Method for the Purification of Recombinant AAV Vectors of Differing Serotypes. Mol Ther Methods Clin Dev *9*, 33-46.

Nathwani, A.C., Cochrane, M., McIntosh, J., Ng, C.Y., Zhou, J., Gray, J.T., and Davidoff, A.M. (2009). Enhancing transduction of the liver by adeno-associated viral vectors. Gene Ther *16*, 60-69.

Nathwani, A.C., Gray, J.T., Ng, C.Y., Zhou, J., Spence, Y., Waddington, S.N., Tuddenham, E.G., Kemball-Cook, G., McIntosh, J., Boon-Spijker, M., *et al.* (2006). Self-complementary adeno-associated virus vectors containing a novel liver-specific human factor IX expression cassette enable highly efficient transduction of murine and nonhuman primate liver. Blood *107*, 2653-2661.

Nathwani, A.C., Reiss, U.M., Tuddenham, E.G., Rosales, C., Chowdary, P., McIntosh, J., Della Peruta, M., Lheriteau, E., Patel, N., Raj, D., *et al.* (2014). Long-term safety and efficacy of factor IX gene therapy in hemophilia B. N Engl J Med *371*, 1994-2004.

Nathwani, A.C., Rosales, C., McIntosh, J., Rastegarlari, G., Nathwani, D., Raj, D., Nawathe, S., Waddington, S.N., Bronson, R., Jackson, S., *et al.* (2011). Long-term safety and efficacy following systemic administration of a self-complementary AAV vector encoding human FIX pseudotyped with serotype 5 and 8 capsid proteins. Mol Ther *19*, 876-885.

Natkunarajah, M., Trittibach, P., McIntosh, J., Duran, Y., Barker, S.E., Smith, A.J., Nathwani, A.C., and Ali, R.R. (2008). Assessment of ocular transduction using single-stranded and self-complementary recombinant adeno-associated virus serotype 2/8. Gene Ther *15*, 463-467.

Niemeyer, G.P., Herzog, R.W., Mount, J., Arruda, V.R., Tillson, D.M., Hathcock, J., van Ginkel, F.W., High, K.A., and Lothrop, C.D., Jr. (2009). Long-term correction of inhibitor-prone hemophilia B dogs treated with liver-directed AAV2-mediated factor IX gene therapy. Blood *113*, 797-806.

Nikonov, S.S., Kholodenko, R., Lem, J., and Pugh, E.N., Jr. (2006). Physiological features of the S- and M-cone photoreceptors of wild-type mice from single-cell recordings. J Gen Physiol *127*, 359-374.

Nishiguchi, K.M., Tearle, R.G., Liu, Y.P., Oh, E.C., Miyake, N., Benaglio, P., Harper, S., Koskiniemi-Kuendig, H., Venturini, G., Sharon, D., *et al.* (2013). Whole genome sequencing in patients with retinitis pigmentosa reveals pathogenic DNA structural changes and NEK2 as a new disease gene. Proc Natl Acad Sci U S A *110*, 16139-16144.

Nonnenmacher, M., and Weber, T. (2011). Adeno-associated virus 2 infection requires endocytosis through the CLIC/GEEC pathway. Cell Host Microbe *10*, 563-576.

Nonnenmacher, M., and Weber, T. (2012). Intracellular transport of recombinant adeno-associated virus vectors. Gene Ther *19*, 649-658.

Ogden, P.J., Kelsic, E.D., Sinai, S., and Church, G.M. (2019). Comprehensive AAV capsid fitness landscape reveals a viral gene and enables machine-guided design. Science *366*, 1139-1143.

Ogston, P., Raj, K., and Beard, P. (2000). Productive replication of adeno-associated virus can occur in human papillomavirus type 16 (HPV-16) episome-containing keratinocytes and is augmented by the HPV-16 E2 protein. J Virol *74*, 3494-3504.

Ortin-Martinez, A., Nadal-Nicolas, F.M., Jimenez-Lopez, M., Alburquerque-Bejar, J.J., Nieto-Lopez, L., Garcia-Ayuso, D., Villegas-Perez, M.P., Vidal-Sanz, M., and Agudo-Barriuso, M. (2014). Number and distribution of mouse retinal cone photoreceptors: differences between an albino (Swiss) and a pigmented (C57/BL6) strain. PLoS One *9*, e102392.

Pagon, R.A. (1988). Retinitis pigmentosa. Surv Ophthalmol *33*, 137-177.

Palczewski, K. (2014). Chemistry and biology of the initial steps in vision: the Friedenwald lecture. Invest Ophthalmol Vis Sci *55*, 6651-6672.

Palczewski, K., Sokal, I., and Baehr, W. (2004). Guanylate cyclase-activating proteins: structure, function, and diversity. Biochem Biophys Res Commun *322*, 1123-1130.

Pang, J., Boye, S.E., Lei, B., Boye, S.L., Everhart, D., Ryals, R., Umino, Y., Rohrer, B., Alexander, J., Li, J.*, et al.* (2010). Self-complementary AAV-mediated gene therapy restores cone function and prevents cone degeneration in two models of Rpe65 deficiency. Gene Ther *17*, 815-826.

Pang, J., Cheng, M., Stevenson, D., Trousdale, M.D., Dorey, C.K., and Blanks, J.C. (2004). Adenoviral-mediated gene transfer to retinal explants during development and degeneration. Exp Eye Res *79*, 189-201.

Pang, J.J., Deng, W.T., Dai, X., Lei, B., Everhart, D., Umino, Y., Li, J., Zhang, K., Mao, S., Boye, S.L.*, et al.* (2012). AAV-mediated cone rescue in a naturally occurring mouse model of CNGA3-achromatopsia. PLoS One *7*, e35250.

Pang, J.J., Lauramore, A., Deng, W.T., Li, Q., Doyle, T.J., Chiodo, V., Li, J., and Hauswirth, W.W. (2008). Comparative analysis of in vivo and in vitro AAV vector transduction in the neonatal mouse retina: effects of serotype and site of administration. Vision Res *48*, 377-385.

Papadakis, E.D., Nicklin, S.A., Baker, A.H., and White, S.J. (2004). Promoters and control elements: designing expression cassettes for gene therapy. Curr Gene Ther *4*, 89-113.

Paquet-Durand, F., Beck, S., Michalakis, S., Goldmann, T., Huber, G., Muhlfriedel, R., Trifunovic, D., Fischer, M.D., Fahl, E., Duetsch, G.*, et al.* (2011). A key role for cyclic nucleotide gated (CNG) channels in cGMP-related retinitis pigmentosa. Hum Mol Genet *20*, 941-947.

Paquet-Durand, F., Hauck, S.M., van Veen, T., Ueffing, M., and Ekstrom, P. (2009). PKG activity causes photoreceptor cell death in two retinitis pigmentosa models. J Neurochem *108*, 796-810.

Park, S.J., Choi, Y., Na, Y.M., Hong, H.K., Park, J.Y., Park, K.H., Chung, J.Y., and Woo, S.J. (2016). Intraocular Pharmacokinetics of Intravitreal Aflibercept (Eylea) in a Rabbit Model. Invest Ophthalmol Vis Sci *57*, 2612-2617.

Park, S.S., Moisseiev, E., Bauer, G., Anderson, J.D., Grant, M.B., Zam, A., Zawadzki, R.J., Werner, J.S., and Nolta, J.A. (2017). Advances in bone marrow stem cell therapy for retinal dysfunction. Prog Retin Eye Res *56*, 148-165.

Penaud-Budloo, M., Francois, A., Clement, N., and Ayuso, E. (2018). Pharmacology of Recombinant Adeno-associated Virus Production. Mol Ther Methods Clin Dev *8*, 166-180.

Penaud-Budloo, M., Le Guiner, C., Nowrouzi, A., Toromanoff, A., Cherel, Y., Chenuaud, P., Schmidt, M., von Kalle, C., Rolling, F., Moullier, P.*, et al.* (2008). Adeno-associated virus vector genomes persist as episomal chromatin in primate muscle. J Virol *82*, 7875-7885.

Peng, Y., Tang, L., and Zhou, Y. (2017). Subretinal Injection: A Review on the Novel Route of Therapeutic Delivery for Vitreoretinal Diseases. Ophthalmic Res *58*, 217-226.

Perabo, L., Endell, J., King, S., Lux, K., Goldnau, D., Hallek, M., and Büning, H. (2006). Combinatorial engineering of a gene therapy vector: directed evolution of adeno-associated virus. J Gene Med *8*, 155-162.

Perez-Carro, R., Corton, M., Sanchez-Navarro, I., Zurita, O., Sanchez-Bolivar, N., Sanchez-Alcudia, R., Lelieveld, S.H., Aller, E., Lopez-Martinez, M.A., Lopez-Molina, M.I.*, et al.* (2016). Panel-based NGS Reveals Novel Pathogenic Mutations in Autosomal Recessive Retinitis Pigmentosa. Sci Rep *6*, 19531.

Perkins, B.D., and Fadool, J.M. (2010). Photoreceptor structure and development analyses using GFP transgenes. Methods in cell biology *100*, 205-218.

Petersen-Jones, S.M., Bartoe, J.T., Fischer, A.J., Scott, M., Boye, S.L., Chiodo, V., and Hauswirth, W.W. (2009). AAV retinal transduction in a large animal model species: Comparison of a self-complementary AAV2/5 with a single-stranded AAV2/5 vector. Mol Vis *15*, 1835-1842.

Petersen-Jones, S.M., Occelli, L.M., Winkler, P.A., Lee, W., Sparrow, J.R., Tsukikawa, M., Boye, S.L., Chiodo, V., Capasso, J.E., Becirovic, E.*, et al.* (2018). Patients and animal models of CNGbeta1-deficient retinitis pigmentosa support gene augmentation approach. J Clin Invest *128*, 190-206.

Petit, L., Khanna, H., and Punzo, C. (2016). Advances in Gene Therapy for Diseases of the Eye. Hum Gene Ther *27*, 563-579.
Petit, L., Lheriteau, E., Weber, M., Le Meur, G., Deschamps, J.Y., Provost, N., Mendes-Madeira, A., Libeau, L., Guihal, C., Colle, M.A.*, et al.* (2012). Restoration of vision in the pde6beta-deficient dog, a large animal model of rod-cone dystrophy. Mol Ther *20*, 2019-2030.

References

Pichard, V., Provost, N., Mendes-Madeira, A., Libeau, L., Hulin, P., Tshilenge, K.T., Biget, M., Ameline, B., Deschamps, J.Y., Weber, M., *et al.* (2016). AAV-mediated Gene Therapy Halts Retinal Degeneration in PDE6beta-deficient Dogs. Mol Ther *24*, 867-876.

Pillay, S., Meyer, N.L., Puschnik, A.S., Davulcu, O., Diep, J., Ishikawa, Y., Jae, L.T., Wosen, J.E., Nagamine, C.M., Chapman, M.S., *et al.* (2016). An essential receptor for adeno-associated virus infection. Nature *530*, 108-112.

Powell, S.K., Rivera-Soto, R., and Gray, S.J. (2015). Viral expression cassette elements to enhance transgene target specificity and expression in gene therapy. Discov Med *19*, 49-57.

Pugh, E.W., Jaquish, C.E., Sorant, A.J., Doetsch, J.P., Bailey-Wilson, J.E., and Wilson, A.F. (1997). Comparison of sib-pair and variance-components methods for genomic screening. Genet Epidemiol *14*, 867-872.

Qu, G., Bahr-Davidson, J., Prado, J., Tai, A., Cataniag, F., McDonnell, J., Zhou, J., Hauck, B., Luna, J., Sommer, J.M., *et al.* (2007). Separation of adeno-associated virus type 2 empty particles from genome containing vectors by anion-exchange column chromatography. J Virol Methods *140*, 183-192.

Rabinowitz, J., Chan, Y.K., and Samulski, R.J. (2019). Adeno-associated Virus (AAV) versus Immune Response. Viruses *11*.

Rabinowitz, J.E., Rolling, F., Li, C., Conrath, H., Xiao, W., Xiao, X., and Samulski, R.J. (2002). Cross-packaging of a single adeno-associated virus (AAV) type 2 vector genome into multiple AAV serotypes enables transduction with broad specificity. J Virol *76*, 791-801.

Ran, F.A., Cong, L., Yan, W.X., Scott, D.A., Gootenberg, J.S., Kriz, A.J., Zetsche, B., Shalem, O., Wu, X., Makarova, K.S., *et al.* (2015). In vivo genome editing using Staphylococcus aureus Cas9. Nature *520*, 186-191.

Rapti, K., Louis-Jeune, V., Kohlbrenner, E., Ishikawa, K., Ladage, D., Zolotukhin, S., Hajjar, R.J., and Weber, T. (2012). Neutralizing antibodies against AAV serotypes 1, 2, 6, and 9 in sera of commonly used animal models. Mol Ther *20*, 73-83.

Rashid, K., Akhtar-Schaefer, I., and Langmann, T. (2019). Microglia in Retinal Degeneration. Front Immunol *10*, 1975.

Rehemtulla, A., Warwar, R., Kumar, R., Ji, X., Zack, D.J., and Swaroop, A. (1996). The basic motif-leucine zipper transcription factor Nrl can positively regulate rhodopsin gene expression. Proc Natl Acad Sci U S A *93*, 191-195.

Reichel, F.F., Dauletbekov, D.L., Klein, R., Peters, T., Ochakovski, G.A., Seitz, I.P., Wilhelm, B., Ueffing, M., Biel, M., Wissinger, B., *et al.* (2017). AAV8 Can Induce Innate and Adaptive Immune Response in the Primate Eye. Mol Ther *25*, 2648-2660.

Reichel, F.F., Peters, T., Wilhelm, B., Biel, M., Ueffing, M., Wissinger, B., Bartz-Schmidt, K.U., Klein, R., Michalakis, S., Fischer, M.D., *et al.* (2018). Humoral Immune Response After Intravitreal But Not After Subretinal AAV8 in Primates and Patients. Invest Ophthalmol Vis Sci *59*, 1910-1915.

Reid, C.A., Ertel, K.J., and Lipinski, D.M. (2017). Improvement of Photoreceptor Targeting via Intravitreal Delivery in Mouse and Human Retina Using Combinatory rAAV2 Capsid Mutant Vectors. Invest Ophthalmol Vis Sci *58*, 6429-6439.

Reks, S.E., McIlvain, V., Zhuo, X., and Knox, B.E. (2014). Cooperative activation of Xenopus rhodopsin transcription by paired-like transcription factors. BMC Mol Biol *15*, 4.

Rieke, F., and Baylor, D.A. (2000). Origin and functional impact of dark noise in retinal cones. Neuron *26*, 181-186.

Roche, S.L., Wyse-Jackson, A.C., Byrne, A.M., Ruiz-Lopez, A.M., and Cotter, T.G. (2016). Alterations to retinal architecture prior to photoreceptor loss in a mouse model of retinitis pigmentosa. Int J Dev Biol *60*, 127-139.

Rodriguez-Munoz, A., Aller, E., Jaijo, T., Gonzalez-Garcia, E., Cabrera-Peset, A., Gallego-Pinazo, R., Udaondo, P., Salom, D., Garcia-Garcia, G., and Millan, J.M. (2020). Expanding the clinical and molecular heterogeneity of nonsyndromic inherited retinal dystrophies. J Mol Diagn.

Rogers, G.L., Martino, A.T., Aslanidi, G.V., Jayandharan, G.R., Srivastava, A., and Herzog, R.W. (2011). Innate Immune Responses to AAV Vectors. Front Microbiol *2*, 194.

Rogers, G.L., Suzuki, M., Zolotukhin, I., Markusic, D.M., Morel, L.M., Lee, B., Ertl, H.C., and Herzog, R.W. (2015). Unique Roles of TLR9- and MyD88-Dependent and -Independent Pathways in Adaptive Immune Responses to AAV-Mediated Gene Transfer. J Innate Immun *7*, 302-314.

Ronzitti, G., Bortolussi, G., van Dijk, R., Collaud, F., Charles, S., Leborgne, C., Vidal, P., Martin, S., Gjata, B., Sola, M.S., *et al.* (2016). A translationally optimized AAV-UGT1A1 vector drives safe and long-lasting correction of Crigler-Najjar syndrome. Mol Ther Methods Clin Dev *3*, 16049.

Rosenthal, N., and Brown, S. (2007). The mouse ascending: perspectives for human-disease models. Nat Cell Biol *9*, 993-999. Russell, D.W., and Kay, M.A. (1999). Adeno-associated virus vectors and hematology. Blood *94*, 864-874.

Russell, S., Bennett, J., Wellman, J.A., Chung, D.C., Yu, Z.-F., Tillman, A., Wittes, J., Pappas, J., Elci, O., McCague, S., *et al.* (2017). Efficacy and safety of voretigene neparvovec (AAV2-hRPE65v2) in patients with RPE65 -mediated inherited retinal dystrophy: a randomised, controlled, open-label, phase 3 trial. The Lancet *390*, 849-860.

Rutledge, E.A., and Russell, D.W. (1997). Adeno-associated virus vector integration junctions. J Virol *71*, 8429-8436.

Sahel, J., Bonnel, S., Mrejen, S., and Paques, M. (2010). Retinitis pigmentosa and other dystrophies. Dev Ophthalmol *47*, 160-167.

Sahel, J.A., Leveillard, T., Picaud, S., Dalkara, D., Marazova, K., Safran, A., Paques, M., Duebel, J., Roska, B., and Mohand-Said, S. (2013). Functional rescue of cone photoreceptors in retinitis pigmentosa. Graefes Arch Clin Exp Ophthalmol *251*, 1669-1677.

Salas, D., Kwikkers, K.L., Zabaleta, N., Bazo, A., Petry, H., van Deventer, S.J., Aseguinolaza, G.G., and Ferreira, V. (2019). Immunoadsorption enables successful rAAV5-mediated repeated hepatic gene delivery in nonhuman primates. Blood Adv *3*, 2632-2641.

Salganik, M., Hirsch, M.L., and Samulski, R.J. (2015). Adeno-associated Virus as a Mammalian DNA Vector. Microbiol Spectr *3*.

Samulski, R.J., Chang, L.S., and Shenk, T. (1987). A recombinant plasmid from which an infectious adeno-associated virus genome can be excised in vitro and its use to study viral replication. J Virol *61*, 3096-3101.

Samulski, R.J., and Muzyczka, N. (2014). AAV-Mediated Gene Therapy for Research and Therapeutic Purposes. Annu Rev Virol *1*, 427-451.

Sandberg, M.A., Weigel-DiFranco, C., Rosner, B., and Berson, E.L. (1996). The relationship between visual field size and electroretinogram amplitude in retinitis pigmentosa. Invest Ophthalmol Vis Sci *37*, 1693-1698.

Sandro, Q., Relizani, K., and Benchaouir, R. (2019). AAV Production Using Baculovirus Expression Vector System. Methods Mol Biol *1937*, 91-99.

Sanlioglu, S., Benson, P.K., Yang, J., Atkinson, E.M., Reynolds, T., and Engelhardt, J.F. (2000). Endocytosis and nuclear trafficking of adeno-associated virus type 2 are controlled by rac1 and phosphatidylinositol-3 kinase activation. J Virol *74*, 9184-9196.

Sanvicens, N., Gomez-Vicente, V., Masip, I., Messeguer, A., and Cotter, T.G. (2004). Oxidative stress-induced apoptosis in retinal photoreceptor cells is mediated by calpains and caspases and blocked by the oxygen radical scavenger CR-6. J Biol Chem *279*, 39268-39278.

Sanz, M.M., Johnson, L.E., Ahuja, S., Ekström, P.A., Romero, J., and van Veen, T. (2007). Significant photoreceptor rescue by treatment with a combination of antioxidants in an animal model for retinal degeneration. Neuroscience *145*, 1120-1129.

Saqib, M.A., Nikopoulos, K., Ullah, E., Sher Khan, F., Iqbal, J., Bibi, R., Jarral, A., Sajid, S., Nishiguchi, K.M., Venturini, G., *et al.* (2015). Homozygosity mapping reveals novel and known mutations in Pakistani families with inherited retinal dystrophies. Sci Rep *5*, 9965.

Sautter, A., Zong, X., Hofmann, F., and Biel, M. (1998). An isoform of the rod photoreceptor cyclic nucleotide-gated channel beta subunit expressed in olfactory neurons. Proc Natl Acad Sci U S A *95*, 4696-4701.

Schambach, A., Galla, M., Maetzig, T., Loew, R., and Baum, C. (2007). Improving transcriptional termination of self-inactivating gamma-retroviral and lentiviral vectors. Mol Ther *15*, 1167-1173.

Schmitz, L., and Motani, R. (2010). Morphological differences between the eyeballs of nocturnal and diurnal amniotes revisited from optical perspectives of visual environments. Vision Res *50*, 936-946.

Scholl, H.P.N., Moore, A.T., Koenekoop, R.K., Wen, Y., Fishman, G.A., van den Born, L.I., Bittner, A., Bowles, K., Fletcher, E.C., Collison, F.T., *et al.* (2015). Safety and Proof-of-Concept Study of Oral QLT091001 in Retinitis Pigmentosa Due to Inherited Deficiencies of Retinal Pigment Epithelial 65 Protein (RPE65) or Lecithin:Retinol Acyltransferase (LRAT). PloS One *10*, e0143846-e0143846.

References

Schon, C., Hoffmann, N.A., Ochs, S.M., Burgold, S., Filser, S., Steinbach, S., Seeliger, M.W., Arzberger, T., Goedert, M., Kretzschmar, H.A.*, et al.* (2012). Long-term in vivo imaging of fibrillar tau in the retina of P301S transgenic mice. PLoS One *7*, e53547.

Schon, C., Sothilingam, V., Muhlfriedel, R., Garcia Garrido, M., Beck, S.C., Tanimoto, N., Wissinger, B., Paquet-Durand, F., Biel, M., Michalakis, S.*, et al.* (2017). Gene therapy successfully delays degeneration in a mouse model of PDE6A-linked retinitis pigmentosa (RP 43). Hum Gene Ther.

Schorderet, D.F., Iouranova, A., Favez, T., Tiab, L., and Escher, P. (2013). IROme, a new high-throughput molecular tool for the diagnosis of inherited retinal dystrophies. Biomed Res Int *2013*, 198089.

Schwarz, E., Freese, U.K., Gissmann, L., Mayer, W., Roggenbuck, B., Stremlau, A., and zur Hausen, H. (1985). Structure and transcription of human papillomavirus sequences in cervical carcinoma cells. Nature *314*, 111-114.

Seeliger, M.W., Zrenner, E., Apfelstedt-Sylla, E., and Jaissle, G.B. (2001). Identification of Usher syndrome subtypes by ERG implicit time. Invest Ophthalmol Vis Sci *42*, 3066-3071.

Seitz, I.P., Michalakis, S., Wilhelm, B., Reichel, F.F., Ochakovski, G.A., Zrenner, E., Ueffing, M., Biel, M., Wissinger, B., Bartz-Schmidt, K.U.*, et al.* (2017). Superior Retinal Gene Transfer and Biodistribution Profile of Subretinal Versus Intravitreal Delivery of AAV8 in Nonhuman Primates. Invest Ophthalmol Vis Sci *58*, 5792-5801.

Seok, J., Warren, H.S., Cuenca, A.G., Mindrinos, M.N., Baker, H.V., Xu, W., Richards, D.R., McDonald-Smith, G.P., Gao, H., Hennessy, L.*, et al.* (2013). Genomic responses in mouse models poorly mimic human inflammatory diseases. Proc Natl Acad Sci U S A *110*, 3507-3512.

Shin, J.-H., Yue, Y., Smith, B., and Duan, D. (2012). Humoral immunity to AAV-6, 8, and 9 in normal and dystrophic dogs. Human gene therapy *23*, 287-294.

Shirai, H., Mandai, M., Matsushita, K., Kuwahara, A., Yonemura, S., Nakano, T., Assawachananont, J., Kimura, T., Saito, K., Terasaki, H.*, et al.* (2016). Transplantation of human embryonic stem cell-derived retinal tissue in two primate models of retinal degeneration. Proc Natl Acad Sci U S A *113*, E81-90.

Simonelli, F., Maguire, A.M., Testa, F., Pierce, E.A., Mingozzi, F., Bennicelli, J.L., Rossi, S., Marshall, K., Banfi, S., Surace, E.M.*, et al.* (2010). Gene therapy for Leber's congenital amaurosis is safe and effective through 1.5 years after vector administration. Mol Ther *18*, 643-650.

Simpson, D.A., Clark, G.R., Alexander, S., Silvestri, G., and Willoughby, C.E. (2011). Molecular diagnosis for heterogeneous genetic diseases with targeted high-throughput DNA sequencing applied to retinitis pigmentosa. J Med Genet *48*, 145-151.

Simunovic, M.P., Shen, W., Lin, J.Y., Protti, D.A., Lisowski, L., and Gillies, M.C. (2019). Optogenetic approaches to vision restoration. Exp Eye Res *178*, 15-26.

Singh, M.S., and MacLaren, R.E. (2018). Stem Cell Treatment for Age-Related Macular Degeneration: the Challenges. Invest Ophthalmol Vis Sci *59*, AMD78-AMD82.

Singh, M.S., Park, S.S., Albini, T.A., Canto-Soler, M.V., Klassen, H., MacLaren, R.E., Takahashi, M., Nagiel, A., Schwartz, S.D., and Bharti, K. (2020). Retinal stem cell transplantation: Balancing safety and potential. Prog Retin Eye Res *75*, 100779.

Singh, R.K., Occelli, L.M., Binette, F., Petersen-Jones, S.M., and Nasonkin, I.O. (2019). Transplantation of Human Embryonic Stem Cell-Derived Retinal Tissue in the Subretinal Space of the Cat Eye. Stem Cells Dev *28*, 1151-1166.

Sjostrand, F.S. (1953). The ultrastructure of the outer segments of rods and cones of the eye as revealed by the electron microscope. J Cell Comp Physiol *42*, 15-44.

Sondergaard, P.C., Griffin, D.A., Pozsgai, E.R., Johnson, R.W., Grose, W.E., Heller, K.N., Shontz, K.M., Montgomery, C.L., Liu, J., Clark, K.R.*, et al.* (2015). AAV.Dysferlin Overlap Vectors Restore Function in Dysferlinopathy Animal Models. Ann Clin Transl Neurol *2*, 256-270.

Song, C., Conlon, T.J., Deng, W.T., Coleman, K.E., Zhu, P., Plummer, C., Mandapati, S., Van Hoosear, M., Green, K.B., Sonnentag, P.*, et al.* (2018). Toxicology and Pharmacology of an AAV Vector Expressing Codon-Optimized RPGR in RPGR-Deficient Rd9 Mice. Hum Gene Ther Clin Dev *29*, 188-197.

Song, J., Smaoui, N., Ayyagari, R., Stiles, D., Benhamed, S., MacDonald, I.M., Daiger, S.P., Tumminia, S.J., Hejtmancik, F., and Wang, X. (2011). High-throughput retina-array for screening 93 genes involved in inherited retinal dystrophy. Invest Ophthalmol Vis Sci *52*, 9053-9060.

Sonntag, F., Bleker, S., Leuchs, B., Fischer, R., and Kleinschmidt, J.A. (2006). Adeno-associated virus type 2 capsids with externalized VP1/VP2 trafficking domains are generated prior to passage through the cytoplasm and are maintained until uncoating occurs in the nucleus. J Virol *80*, 11040-11054.

Sonntag, F., Kother, K., Schmidt, K., Weghofer, M., Raupp, C., Nieto, K., Kuck, A., Gerlach, B., Bottcher, B., Muller, O.J.*, et al.* (2011). The assembly-activating protein promotes capsid assembly of different adeno-associated virus serotypes. J Virol *85*, 12686-12697.

Sorrentino, F.S., Gallenga, C.E., Bonifazzi, C., and Perri, P. (2016). A challenge to the striking genotypic heterogeneity of retinitis pigmentosa: a better understanding of the pathophysiology using the newest genetic strategies. Eye (Lond) *30*, 1542-1548.

Stern, J.H., Tian, Y., Funderburgh, J., Pellegrini, G., Zhang, K., Goldberg, J.L., Ali, R.R., Young, M., Xie, Y., and Temple, S. (2018). Regenerating Eye Tissues to Preserve and Restore Vision. Cell Stem Cell *22*, 834-849.

Stingl, K., Bartz-Schmidt, K.U., Besch, D., Chee, C.K., Cottriall, C.L., Gekeler, F., Groppe, M., Jackson, T.L., MacLaren, R.E., Koitschev, A.*, et al.* (2015). Subretinal Visual Implant Alpha IMS--Clinical trial interim report. Vision Res *111*, 149-160.

Stockton, R.A., and Slaughter, M.M. (1989). B-wave of the electroretinogram. A reflection of ON bipolar cell activity. J Gen Physiol *93*, 101-122.

Summerford, C., and Samulski, R.J. (1998). Membrane-associated heparan sulfate proteoglycan is a receptor for adeno-associated virus type 2 virions. J Virol *72*, 1438-1445.

Sun, J., Shao, W., Chen, X., Merricks, E.P., Wimsey, L., Abajas, Y.L., Niemeyer, G.P., Lothrop, C.D., Monahan, P.E., Samulski, R.J.*, et al.* (2018). An Observational Study from Long-Term AAV Re-administration in Two Hemophilia Dogs. Mol Ther Methods Clin Dev *10*, 257-267.

Sun, J.Y., Anand-Jawa, V., Chatterjee, S., and Wong, K.K. (2003). Immune responses to adeno-associated virus and its recombinant vectors. Gene Ther *10*, 964-976.

Surace, E.M., and Auricchio, A. (2003). Adeno-associated viral vectors for retinal gene transfer. Prog Retin Eye Res *22*, 705-719.

Swain, P.K., Hicks, D., Mears, A.J., Apel, I.J., Smith, J.E., John, S.K., Hendrickson, A., Milam, A.H., and Swaroop, A. (2001). Multiple phosphorylated isoforms of NRL are expressed in rod photoreceptors. J Biol Chem *276*, 36824-36830.

Swaroop, A., Xu, J.Z., Pawar, H., Jackson, A., Skolnick, C., and Agarwal, N. (1992). A conserved retina-specific gene encodes a basic motif/leucine zipper domain. Proc Natl Acad Sci U S A *89*, 266-270.

Szamier, R.B. (1981). Ultrastructure of the preretinal membrane in retinitis pigmentosa. Invest Ophthalmol Vis Sci *21*, 227-236.

Takahashi, K., Morizane, Y., Hisatomi, T., Tachibana, T., Kimura, S., Hosokawa, M.M., Shiode, Y., Hirano, M., Doi, S., Toshima, S.*, et al.* (2018). The influence of subretinal injection pressure on the microstructure of the monkey retina. PLoS One *13*, e0209996.

Tanaka, J., Markerink-van Ittersum, M., Steinbusch, H.W., and De Vente, J. (1997). Nitric oxide-mediated cGMP synthesis in oligodendrocytes in the developing rat brain. Glia *19*, 286-297.

Tanimoto, N., Muehlfriedel, R.L., Fischer, M.D., Fahl, E., Humphries, P., Biel, M., and Seeliger, M.W. (2009). Vision tests in the mouse: Functional phenotyping with electroretinography. Front Biosci (Landmark Ed) *14*, 2730-2737.

Teo, K.Y.C., Lee, S.Y., Barathi, A.V., Tun, S.B.B., Tan, L., and Constable, I.J. (2018). Surgical Removal of Internal Limiting Membrane and Layering of AAV Vector on the Retina Under Air Enhances Gene Transfection in a Nonhuman Primate. Invest Ophthalmol Vis Sci *59*, 3574-3583.

Thomas, C.E., Storm, T.A., Huang, Z., and Kay, M.A. (2004). Rapid uncoating of vector genomes is the key to efficient liver transduction with pseudotyped adeno-associated virus vectors. J Virol *78*, 3110-3122.

Thorne, B.A., Takeya, R.K., and Peluso, R.W. (2009). Manufacturing recombinant adeno-associated viral vectors from producer cell clones. Hum Gene Ther *20*, 707-714.

Tolone, A., Belhadj, S., Rentsch, A., Schwede, F., and Paquet-Durand, F. (2019). The cGMP Pathway and Inherited Photoreceptor Degeneration: Targets, Compounds, and Biomarkers. Genes (Basel) *10*.

References

Trachsel-Moncho, L., Benlloch-Navarro, S., Fernandez-Carbonell, A., Ramirez-Lamelas, D.T., Olivar, T., Silvestre, D., Poch, E., and Miranda, M. (2018). Oxidative stress and autophagy-related changes during retinal degeneration and development. Cell Death Dis *9*, 812.

Trapani, I., Puppo, A., and Auricchio, A. (2014). Vector platforms for gene therapy of inherited retinopathies. Prog Retin Eye Res *43*, 108-128.

Trifunovic, D., Dengler, K., Michalakis, S., Zrenner, E., Wissinger, B., and Paquet-Durand, F. (2010). cGMP-dependent cone photoreceptor degeneration in the cpfl1 mouse retina. J Comp Neurol *518*, 3604-3617.

Trifunović, D., Sahaboglu, A., Kaur, J., Mencl, S., Zrenner, E., Ueffing, M., Arango-Gonzalez, B., and Paquet-Durand, F. (2012). Neuroprotective strategies for the treatment of inherited photoreceptor degeneration. Curr Mol Med *12*, 598-612.

Trudeau, M.C., and Zagotta, W.N. (2002). An Intersubunit Interaction Regulates Trafficking of Rod Cyclic Nucleotide-Gated Channels and Is Disrupted in an Inherited Form of Blindness. Neuron *34*, 197-207.

Tschernutter, M., Schlichtenbrede, F.C., Howe, S., Balaggan, K.S., Munro, P.M., Bainbridge, J.W., Thrasher, A.J., Smith, A.J., and Ali, R.R. (2005). Long-term preservation of retinal function in the RCS rat model of retinitis pigmentosa following lentivirus-mediated gene therapy. Gene Ther *12*, 694-701.

Tse, L.V., Klinc, K.A., Madigan, V.J., Castellanos Rivera, R.M., Wells, L.F., Havlik, L.P., Smith, J.K., Agbandje-McKenna, M., and Asokan, A. (2017). Structure-guided evolution of antigenically distinct adeno-associated virus variants for immune evasion. Proc Natl Acad Sci U S A *114*, E4812-e4821.

Tucker, B.A., Park, I.H., Qi, S.D., Klassen, H.J., Jiang, C., Yao, J., Redenti, S., Daley, G.Q., and Young, M.J. (2011). Transplantation of adult mouse iPS cell-derived photoreceptor precursors restores retinal structure and function in degenerative mice. PLoS One *6*, e18992.

Uhrig, S., Coutelle, O., Wiehe, T., Perabo, L., Hallek, M., and Buning, H. (2012). Successful target cell transduction of capsid-engineered rAAV vectors requires clathrin-dependent endocytosis. Gene Ther *19*, 210-218.

Usui, S., Oveson, B.C., Lee, S.Y., Jo, Y.J., Yoshida, T., Miki, A., Miki, K., Iwase, T., Lu, L., and Campochiaro, P.A. (2009). NADPH oxidase plays a central role in cone cell death in retinitis pigmentosa. J Neurochem *110*, 1028-1037.

Vance, M.A., Mitchell, A., and Samulski, R.J. (2015). AAV Biology, Infectivity and Therapeutic Use from Bench to Clinic. In Gene Therapy - Principles and Challenges.

Vandenberghe, L.H., and Auricchio, A. (2012). Novel adeno-associated viral vectors for retinal gene therapy. Gene Ther *19*, 162-168.

Vandenberghe, L.H., Bell, P., Maguire, A.M., Cearley, C.N., Xiao, R., Calcedo, R., Wang, L., Castle, M.J., Maguire, A.C., Grant, R.*, et al.* (2011). Dosage thresholds for AAV2 and AAV8 photoreceptor gene therapy in monkey. Sci Transl Med *3*, 88ra54.

Vandenberghe, L.H., Bell, P., Maguire, A.M., Xiao, R., Hopkins, T.B., Grant, R., Bennett, J., and Wilson, J.M. (2013). AAV9 targets cone photoreceptors in the nonhuman primate retina. PLoS One *8*, e53463.

Van Essen, D.C., Lewis, J.W., Drury, H.A., Hadjikhani, N., Tootell, R.B., Bakircioglu, M., and Miller, M.I. (2001). Mapping visual cortex in monkeys and humans using surface-based atlases. Vision Res *41*, 1359-1378.

Verbakel, S.K., van Huet, R.A.C., Boon, C.J.F., den Hollander, A.I., Collin, R.W.J., Klaver, C.C.W., Hoyng, C.B., Roepman, R., and Klevering, B.J. (2018). Non-syndromic retinitis pigmentosa. Prog Retin Eye Res *66*, 157-186.

Verdera, H.C., Kuranda, K., and Mingozzi, F. (2020). AAV Vector Immunogenicity in Humans: A Long Journey to Successful Gene Transfer. Mol Ther *28*, 723-746.

Vinberg, F., Wang, T., De Maria, A., Zhao, H., Bassnett, S., Chen, J., and Kefalov, V.J. (2017). The Na(+)/Ca(2+), K(+) exchanger NCKX4 is required for efficient cone-mediated vision. Elife *6*.

Volland, S., Esteve-Rudd, J., Hoo, J., Yee, C., and Williams, D.S. (2015). A comparison of some organizational characteristics of the mouse central retina and the human macula. PLoS One *10*, e0125631.

Vollrath, D., Feng, W., Duncan, J.L., Yasumura, D., D'Cruz, P.M., Chappelow, A., Matthes, M.T., Kay, M.A., and LaVail, M.M. (2001). Correction of the retinal dystrophy phenotype of the RCS rat by viral gene transfer of Mertk. Proc Natl Acad Sci U S A *98*, 12584-12589.

Wachtmeister, L. (1998). Oscillatory potentials in the retina: what do they reveal. Prog Retin Eye Res *17*, 485-521.

Walters, R.W., Yi, S.M., Keshavjee, S., Brown, K.E., Welsh, M.J., Chiorini, J.A., and Zabner, J. (2001). Binding of adeno-associated virus type 5 to 2,3-linked sialic acid is required for gene transfer. J Biol Chem *276*, 20610-20616.

Wang, X., Stafford, W., Mazurkiewicz, M., Fryknäs, M., Brjnic, S., Zhang, X., Gullbo, J., Larsson, R., Arnér, E.S., D'Arcy, P.*, et al.* (2014). The 19S Deubiquitinase inhibitor b-AP15 is enriched in cells and elicits rapid commitment to cell death. Mol Pharmacol *85*, 932-945.

Wang, Z., Allen, J.M., Riddell, S.R., Gregorevic, P., Storb, R., Tapscott, S.J., Chamberlain, J.S., and Kuhr, C.S. (2007). Immunity to adeno-associated virus-mediated gene transfer in a random-bred canine model of Duchenne muscular dystrophy. Hum Gene Ther *18*, 18-26.

Wassle, H. (2004). Parallel processing in the mammalian retina. Nat Rev Neurosci *5*, 747-757.

Weber, M., Rabinowitz, J., Provost, N., Conrath, H., Folliot, S., Briot, D., Chérel, Y., Chenuaud, P., Samulski, J., Moullier, P.*, et al.* (2003). Recombinant adeno-associated virus serotype 4 mediates unique and exclusive long-term transduction of retinal pigmented epithelium in rat, dog, and nonhuman primate after subretinal delivery. Mol Ther *7*, 774-781.

Weed, L., Ammar, M.J., Zhou, S., Wei, Z., Serrano, L.W., Sun, J., Lee, V., Maguire, A.M., Bennett, J., and Aleman, T.S. (2019). Safety of Same-Eye Subretinal Sequential Readministration of AAV2-hRPE65v2 in Non-human Primates. Mol Ther Methods Clin Dev *15*, 133-148.

Weiland, J.D., and Humayun, M.S. (2014). Retinal prosthesis. IEEE Trans Biomed Eng *61*, 1412-1424.

Weinmann, J., and Grimm, D. (2017). Next-generation AAV vectors for clinical use: an ever-accelerating race. Virus Genes *53*, 707-713.

Weinstein, R. (1999). Phytanic acid storage disease (Refsum's disease): clinical characteristics, pathophysiology and the role of therapeutic apheresis in its management. J Clin Apher *14*, 181-184.

Weitz, D., Zoche, M., Muller, F., Beyermann, M., Korschen, H.G., Kaupp, U.B., and Koch, K.W. (1998). Calmodulin controls the rod photoreceptor CNG channel through an unconventional binding site in the N-terminus of the beta-subunit. EMBO J *17*, 2273-2284.

Willett, K., and Bennett, J. (2013). Immunology of AAV-Mediated Gene Transfer in the Eye. Front Immunol *4*, 261.

Wilson, J.M. (2009). Lessons learned from the gene therapy trial for ornithine transcarbamylase deficiency. Mol Genet Metab *96*, 151-157.

Winkler, P.A., Ekenstedt, K.J., Occelli, L.M., Frattaroli, A.V., Bartoe, J.T., Venta, P.J., and Petersen-Jones, S.M. (2013). A large animal model for CNGB1 autosomal recessive retinitis pigmentosa. PLoS One *8*, e72229.

Witmer, M.T., and Kiss, S. (2013). Wide-field imaging of the retina. Surv Ophthalmol *58*, 143-154.

Wong, F., and Kwok, S.Y. (2016). The Survival of Cone Photoreceptors in Retinitis Pigmentosa. JAMA Ophthalmol *134*, 249-250.

Wright, J.F. (2009). Transient transfection methods for clinical adeno-associated viral vector production. Hum Gene Ther *20*, 698-706.

Wright, J.F. (2014). Product-Related Impurities in Clinical-Grade Recombinant AAV Vectors: Characterization and Risk Assessment. Biomedicines *2*, 80-97.

Wu, C., and Lu, Y. (2007). Inclusion of high molecular weight dextran in calcium phosphate-mediated transfection significantly improves gene transfer efficiency. Cell Mol Biol (Noisy-le-grand) *53*, 67-74.

Wu, Z., Asokan, A., and Samulski, R.J. (2006). Adeno-associated virus serotypes: vector toolkit for human gene therapy. Mol Ther *14*, 316-327.

Wu, Z., Yang, H., and Colosi, P. (2010). Effect of genome size on AAV vector packaging. Mol Ther *18*, 80-86.

Xiang, Q., Guo, Y., Cao, Y., Xiong, W., Deng, X., Xu, H., Li, Y., Du, D., and Deng, H. (2018). Identification of a CNGB1 Frameshift Mutation in a Han Chinese Family with Retinitis Pigmentosa. Optom Vis Sci *95*, 1155-1161.

References

Xiao, P.J., Li, C., Neumann, A., and Samulski, R.J. (2012). Quantitative 3D tracing of gene-delivery viral vectors in human cells and animal tissues. Mol Ther *20*, 317-328.

Xiao, P.J., and Samulski, R.J. (2012). Cytoplasmic trafficking, endosomal escape, and perinuclear accumulation of adeno-associated virus type 2 particles are facilitated by microtubule network. J Virol *86*, 10462-10473.

Xiao, X., Li, J., and Samulski, R.J. (1998). Production of high-titer recombinant adeno-associated virus vectors in the absence of helper adenovirus. J Virol *72*, 2224-2232.

Xiao, X., Li, J., and Samulski, R.J. (1998). Production of high-titer recombinant adeno-associated virus vectors in the absence of helper adenovirus. J Virol *72*, 2224-2232.

Xie, J., Mao, Q., Tai, P.W.L., He, R., Ai, J., Su, Q., Zhu, Y., Ma, H., Li, J., Gong, S., *et al.* (2017). Short DNA Hairpins Compromise Recombinant Adeno-Associated Virus Genome Homogeneity. Mol Ther *25*, 1363-1374.

Xu, J., Morris, L., Thapa, A., Ma, H., Michalakis, S., Biel, M., Baehr, W., Peshenko, I.V., Dizhoor, A.M., and Ding, X.Q. (2013). cGMP accumulation causes photoreceptor degeneration in CNG channel deficiency: evidence of cGMP cytotoxicity independently of enhanced CNG channel function. J Neurosci *33*, 14939-14948.

Yan, Z., Zhang, Y., Duan, D., and Engelhardt, J.F. (2000). Trans-splicing vectors expand the utility of adeno-associated virus for gene therapy. Proceedings of the National Academy of Sciences *97*, 6716.

Yanai, A., McNab, P., and Gregory-Evans, K. (2019). Retinal therapy with induced pluripotent stem cells; leading the way to human clinical trials. Expert Review of Ophthalmology *14*, 53-59.

Yang, C.C., Xiao, X., Zhu, X., Ansardi, D.C., Epstein, N.D., Frey, M.R., Matera, A.G., and Samulski, R.J. (1997). Cellular recombination pathways and viral terminal repeat hairpin structures are sufficient for adeno-associated virus integration in vivo and in vitro. J Virol *71*, 9231-9247.

Yang, G.S., Schmidt, M., Yan, Z., Lindbloom, J.D., Harding, T.C., Donahue, B.A., Engelhardt, J.F., Kotin, R., and Davidson, B.L. (2002). Virus-mediated transduction of murine retina with adeno-associated virus: effects of viral capsid and genome size. J Virol *76*, 7651-7660.

Yaqoob, Z., Wu, J., and Yang, C. (2005). Spectral domain optical coherence tomography: a better OCT imaging strategy. Biotechniques *39*, S6-13.

Yau, K.W. (1994). Cyclic nucleotide-gated channels: an expanding new family of ion channels. Proc Natl Acad Sci U S A *91*, 3481-3483.

Yau, K.W., and Nakatani, K. (1985). Light-induced reduction of cytoplasmic free calcium in retinal rod outer segment. Nature *313*, 579-582.

Ye, G.J., Komaromy, A.M., Zeiss, C., Calcedo, R., Harman, C.D., Koehl, K.L., Stewart, G.A., Iwabe, S., Chiodo, V.A., Hauswirth, W.W., *et al.* (2017). Safety and Efficacy of AAV5 Vectors Expressing Human or Canine CNGB3 in CNGB3-Mutant Dogs. Hum Gene Ther Clin Dev *28*, 197-207.

Yiu, G. (2018). Genome Editing in Retinal Diseases using CRISPR Technology. Ophthalmol Retina *2*, 1-3.

Yokoi, K., Kachi, S., Zhang, H.S., Gregory, P.D., Spratt, S.K., Samulski, R.J., and Campochiaro, P.A. (2007). Ocular gene transfer with self-complementary AAV vectors. Invest Ophthalmol Vis Sci *48*, 3324-3328.

Yokoyama, S. (2000). Phylogenetic analysis and experimental approaches to study color vision in vertebrates. Methods Enzymol *315*, 312-325.

Yoshida, N., Ikeda, Y., Notomi, S., Ishikawa, K., Murakami, Y., Hisatomi, T., Enaida, H., and Ishibashi, T. (2013). Clinical evidence of sustained chronic inflammatory reaction in retinitis pigmentosa. Ophthalmology *120*, 100-105.

Yoshida, N., Ikeda, Y., Notomi, S., Ishikawa, K., Murakami, Y., Hisatomi, T., Enaida, H., and Ishibashi, T. (2013). Laboratory evidence of sustained chronic inflammatory reaction in retinitis pigmentosa. Ophthalmology *120*, e5-12.

You, H., Liu, Y., Prasad, C.K., Agrawal, N., Zhang, D., Bandyopadhyay, S., Liu, H., Kay, H.H., Mehta, J.L., and Hermonat, P.L. (2006). Multiple human papillomavirus genes affect the adeno-associated virus life cycle. Virology *344*, 532-540.

Young, B., Eggenberger, E., and Kaufman, D. (2012). Current electrophysiology in ophthalmology: a review. Curr Opin Ophthalmol *23*, 497-505.

Yu, W., Mookherjee, S., Chaitankar, V., Hiriyanna, S., Kim, J.W., Brooks, M., Ataeijannati, Y., Sun, X., Dong, L., Li, T., *et al.* (2017). Nrl knockdown by AAV-delivered CRISPR/Cas9 prevents retinal degeneration in mice. Nat Commun *8*, 14716.

Yue, L., Weiland, J.D., Roska, B., and Humayun, M.S. (2016). Retinal stimulation strategies to restore vision: Fundamentals and systems. Prog Retin Eye Res *53*, 21-47.

Zack, D.J., Bennett, J., Wang, Y., Davenport, C., Klaunberg, B., Gearhart, J., and Nathans, J. (1991). Unusual topography of bovine rhodopsin promoter-lacZ fusion gene expression in transgenic mouse retinas. Neuron *6*, 187-199.

Zhang, T., Baehr, W., and Fu, Y. (2012). Chemical chaperone TUDCA preserves cone photoreceptors in a mouse model of Leber congenital amaurosis. Invest Ophthalmol Vis Sci *53*, 3349-3356.

Zhang, Y., Molday, L.L., Molday, R.S., Sarfare, S.S., Woodruff, M.L., Fain, G.L., Kraft, T.W., and Pittler, S.J. (2009). Knockout of GARPs and the beta-subunit of the rod cGMP-gated channel disrupts disk morphogenesis and rod outer segment structural integrity. J Cell Sci *122*, 1192-1200.

Zhao, L., Zabel, M.K., Wang, X., Ma, W., Shah, P., Fariss, R.N., Qian, H., Parkhurst, C.N., Gan, W.B., and Wong, W.T. (2015). Microglial phagocytosis of living photoreceptors contributes to inherited retinal degeneration. EMBO Mol Med *7*, 1179-1197.
Zheng, A., Li, Y., and Tsang, S.H. (2015). Personalized therapeutic strategies for patients with retinitis pigmentosa. Expert Opin Biol Ther *15*, 391-402.

Zheng, J., Trudeau, M.C., and Zagotta, W.N. (2002). Rod Cyclic Nucleotide-Gated Channels Have a Stoichiometry of Three CNGA1 Subunits and One CNGB1 Subunit. Neuron *36*, 891-896.

Zhong, H., Molday, L.L., Molday, R.S., and Yau, K.W. (2002). The heteromeric cyclic nucleotide-gated channel adopts a 3A:1B stoichiometry. Nature *420*, 193-198.

Zhong, L., Li, B., Jayandharan, G., Mah, C.S., Govindasamy, L., Agbandje-McKenna, M., Herzog, R.W., Weigel-Van Aken, K.A., Hobbs, J.A., Zolotukhin, S., *et al.* (2008). Tyrosine-phosphorylation of AAV2 vectors and its consequences on viral intracellular trafficking and transgene expression. Virology *381*, 194-202.

Zhou, L., Wang, W., Liu, Y., Fernandez de Castro, J., Ezashi, T., Telugu, B.P., Roberts, R.M., Kaplan, H.J., and Dean, D.C. (2011). Differentiation of induced pluripotent stem cells of swine into rod photoreceptors and their integration into the retina. Stem Cells *29*, 972-980.

Zhu, J., Huang, X., and Yang, Y. (2009). The TLR9-MyD88 pathway is critical for adaptive immune responses to adeno-associated virus gene therapy vectors in mice. J Clin Invest *119*, 2388-2398.

Ziccardi, L., Cordeddu, V., Gaddini, L., Matteucci, A., Parravano, M., Malchiodi-Albedi, F., and Varano, M. (2019). Gene Therapy in Retinal Dystrophies. Int J Mol Sci *20*.

6   Appendix

Table S1: Mouse group 1 responder – low dose: 10^8 total vg. Detailed list of bleb size, b-wave amplitude, photoreceptor layer thickness, latency, and transgene expression. For both ERG and OCT, the percentage of the treated eye of the contralateral eye is calculated. The values of the b-wave amplitude result from the average of all b-wave-amplitudes of a whole protocol (luminance 0.01-10 cd s m^{-2}). The Water Maze values show the latency of a treated mouse at day 2 in relation to the mean value of all untreated mice. Bleb size, transgene expression area, and area of rescued photoreceptors were divided into small, medium, and large. Transgene expression level was divided in low, medium, and high. The number of lines of nuclei represents the total number of lines but not only the rescued ones. The intact OS are divided into no, partly, and yes. A rescue (highlighted in green) is identified if the increase of average ERG signal is 20 µV or higher. A negative effect of the treatment (labeled in red) is displayed in red if the value is decreased by 20 µV or more. In case of the OCT, the threshold is ± 10 µm. m. month/months; *pn. postnatal*

Mouse number	bleb size	ERG: average b-wave amplitude in µV (% of control)			OCT: photoreceptor layer thickness in µm (% of control)			WM: Latency at day 2 in s (% of control mean)	Immunohistochemistry					
									Transgene expression		Rescued photoreceptors			comment
		3 m pn	5 m pn	9 m pn	3 m pn	5 m pn	9 m pn		area	level	area	lines of nuclei	intact OS	
1	small	197	143	200	121	109	131	86	no expression		medium	2-3	no	-
5	medium	86	195	99	113	110	152	126	no expression		medium	2-3	no	-
6	large	317	140	188	119	109	138	61	large	low	large	3	partly	-
8	large	196	214	250	116	112	178	128	large	low	large	3	partly	-
9	medium	189	88	164	105	106	138	131	no expression		small	3	partly	-
10	large	75	127	212	105	90	130	80	large	low	large	2-3	partly	-
12	medium	64	71	69	117	122	141	18	small	low	small	3	partly	-

Table S2: Mouse group 2 responder – mid dose: 10^9 vg. Detailed list of bleb size, b-wave amplitude, photoreceptor layer thickness, latency, and transgene expression. For both, ERG and OCT, the percentage of the treated eye of the contralateral eye is calculated. The values of the b-wave amplitude result from the average of all b-wave-amplitudes of a whole protocol (luminance 0.01-10 cd s m^{-2}). The Water Maze values show the latency of a treated mouse at day 2 in relation to the mean value of all untreated mice. Bleb size, transgene expression area, and area of rescued photoreceptors were divided into small, medium, and large. Transgene expression level was divided in low, medium, and high. The number of lines of nuclei represents the total number of lines but not only the rescued ones. The intact OS are divided into no, partly, and yes. A rescue (highlighted in green) is identified if the increase of average ERG signal is 20 µV or higher. A negative effect of the treatment (labeled in red) is displayed in red if the value is decreased by 20 µV or more. In case of the OCT, the threshold is ± 10 µm. m. month/months; *pn. postnatal*

Mouse number	bleb size	ERG: average b-wave amplitude in µV (% of control)			OCT: photoreceptor layer thickness in µm (% of control)			WM: Latency at day 2 in s (% of control mean)	Immunohistochemistry Transgene expression		Rescued photoreceptors			comment
		3 m *pn*	5 m *pn*	9 m *pn*	3 m *pn*	5 m *pn*	9 m *pn*		area	level	area	lines of nuclei	intact OS	
1	small	-	108	183	104	119	100	62	small	low	small	3	no	slight prick during injection
4	small	160	200	103	108	114	102	50	large	low	large	4-5	partly	slight prick during injection
5	medium	92	70	300	108	145	190	34	-		-			eye was lost during preparation
7	small	75	198	128	101	121	146	53	no expression		small	3	no	weak ERG signal for both OD and OS
9	large	140	138	266	116	120	131	39	large	high	large	7	yes	-
10	large	67	91	160	113	112	116	99	small	medium	medium	4-5	partly	weak ERG signal for both OD and OS
12	large	216	162	253	126	156	231	-	large	high	large	8-12	yes	floater in the WM

Table S3: Mouse group 3 responder – high dose: 10^{10} total vg. Detailed list of bleb size, b-wave amplitude, photoreceptor layer thickness, latency, and transgene expression. For both, ERG and OCT, the percentage of the treated eye of the contralateral eye is calculated. The values of the b-wave amplitude result from the average of all b-wave-amplitudes of a whole protocol (luminance 0.01-10 cd s m^{-2}). The Water Maze values show the latency of a treated mouse at day 2 in relation to the mean value of all untreated mice. Bleb size, transgene expression area, and area of rescued photoreceptors were divided into small, medium, and large. Transgene expression level was divided in low, medium, and high. The number of lines of nuclei represents the total number of lines but not only the rescued ones. The intact OS are divided into no, partly, and yes. A rescue (highlighted in green) is identified if the increase of average ERG signal is 20 µV or higher. A negative effect of the treatment (labeled in red) is displayed in red if the value is decreased by 20 µV or more. In case of the OCT, the threshold is ± 10 µm. m. month/months; *pn. postnatal*

Mouse number	bleb size	ERG: average b-wave amplitude in µV (% of control)			OCT: photoreceptor layer thickness in µm (% of control)			WM: Latency at day 2 in s (% of control mean)	Transgene expression		Rescued photo-receptors			comment
		3 m pn	5 m pn	9 m pn	3 m pn	5 m pn	9 m pn		area	level	area	lines of nuclei	intact OS	
1	small	-	116	156	-	90	116	-	small	low	small	3	partly	slight prick during injection
2	small	-	182	45	103	109	114	-	no expression		small	2	no	-
3	medium	-	121	88	103	97	121	-	no expression		small	2	no	-
4	small	-	178	123	135	115	150	-	small	medium	large	3	no	-
5	large	115	109	141	100	104	118	-	large	high	large	5-6	partly	-
7	large	103	87	193	133	108	122	-	no expression		no rescue			weak ERG signal for both OD and OS
8	medium	72	119	126	110	106	92	-	large	low	large	2	no	-
9	medium	94	50	53	-	100	104	-	small	low	small	2	no	-
11	large	84	93	95	96	109	100	-	medium	medium	medium	2	no	weak ERG signal for both OD and OS
12	large	132	68	109	95	100	139	-	large	high	large	3	partly	

Table S4: Mouse group 1 non responder and dead mice – low dose: 10^8 total vg. Detailed list of bleb size, b-wave amplitude, photoreceptor layer thickness, latency, and transgene expression. For both, ERG and OCT, the percentage of the treated eye of the contralateral eye is calculated. The values of the b-wave amplitude result from the average of all b-wave-amplitudes of a whole protocol (luminance 0.01-10 cd s m^{-2}). The Water Maze values show the latency of a treated mouse at day 2 in relation to the mean value of all untreated mice. Bleb size, transgene expression area, and area of rescued photoreceptors were divided into small, medium, and large. Transgene expression level was divided in low, medium, and high. The number of lines of nuclei represents the total number of lines but not only the rescued ones. The intact OS are divided into no, partly, and yes. m. month/months; *pn. postnatal*

Mouse number	bleb size	ERG: average b-wave amplitude in µV (% of control)			OCT: photoreceptor layer thickness in µm (% of control)			WM: Latency at day 2 in s (% of control mean)	Immunohistochemistry Transgene expression		Rescued photo-receptors			comment
		3 m *pn*	5 m *pn*	9 m *pn*	3 m *pn*	5 m *pn*	9 m *pn*		area	level	area	lines of nuclei	intact OS	
2	small	95	66	101	102	97	121	72	no expression		no rescue			-
3	small	63	66	72	92	94	109	62	no expression		no rescue			-
4	small	155	129	58	105	135	106	74	-		-			cataract
7	large	-	-	-	-	-	-	-	-		-			died at 3 months *pn*
11	small	121	106	97	103	96	84	92	no expression		no rescue			-

Table S5: Mouse group 2 non responder and dead mice – mid dose: 10^9 total vg. Detailed list of bleb size, b-wave amplitude, photoreceptor layer thickness, latency, and transgene expression. For both, ERG and OCT, the percentage of the treated eye of the contralateral eye is calculated. The values of the b-wave amplitude result from the average of all b-wave-amplitudes of a whole protocol (luminance 0.01-10 cd s m^{-2}). The Water Maze values show the latency of a treated mouse at day 2 in relation to the mean value of all untreated mice. Bleb size, transgene expression area, and area of rescued photoreceptors were divided into small, medium, and large. Transgene expression level was divided in low, medium, and high. The number of lines of nuclei represents the total number of lines but not only the rescued ones. The intact OS are divided into no, partly, and yes. m. month/months; *pn. postnatal*

Mouse number	bleb size	ERG: average b-wave amplitude in µV (% of control)			OCT: photoreceptor layer thickness in µm (% of control)			WM: Latency at day 2 in s (% of control mean)	Immunohistochemistry Transgene expression		Rescued photo-receptors			comment
		3 m *pn*	5 m *pn*	9 m *pn*	3 m *pn*	5 m *pn*	9 m *pn*		area	level	area	lines of nuclei	intact OS	
2	small	-	97	103	96	105	118	13	no expression		no rescue			slight prick
3	small	97	75	95	112	106	92	29	no expression		no rescue			slight prick
6	large	-	-	-	-	-	-	-	-		-			died at 4 m *pn*
8	small	78	94	112	106	105	100	40	no expression		no rescue			no rescued PR
11	small	126	133	54	109	118	173	138	small	low	small	3	no	cataract

Table S6: Mouse group 3 non responder – high dose: 10^{10} total vg. Detailed list of bleb size, b-wave amplitude, photoreceptor layer thickness, latency, and transgene expression. For both, ERG and OCT, the percentage of the treated eye of the contralateral eye is calculated. The values of the b-wave amplitude result from the average of all b-wave-amplitudes of a whole protocol (luminance 0.01-10 cd s m^{-2}). The Water Maze values show the latency of a treated mouse at day 2 in relation to the mean value of all untreated mice. Bleb size, transgene expression area, and area of rescued photoreceptors were divided into small, medium, and large. Transgene expression level was divided in low, medium, and high. The number of lines of nuclei represents the total number of lines but not only the rescued ones. The intact OS are divided into no, partly, and yes. m - month/months; *pn - postnatal*

Mouse number	bleb size	ERG: average b-wave amplitude in µV (% of control)			OCT: photoreceptor layer thickness in µm (% of control)			WM: Latency at day 2 in s (% of control mean)	Transgene expression		Rescued photo-receptors			comment
		3 m *pn*	5 m *pn*	9 m *pn*	3 m *pn*	5 m *pn*	9 m *pn*		area	level	area	lines of nuclei	intact OS	
6	small	86	69	97	100	108	96	-	-			-		eye was lost during preparation weak ERG signal for both OD and OS
10	large	83	64	38	97	100	87	-	-			-		eye was lost during preparation
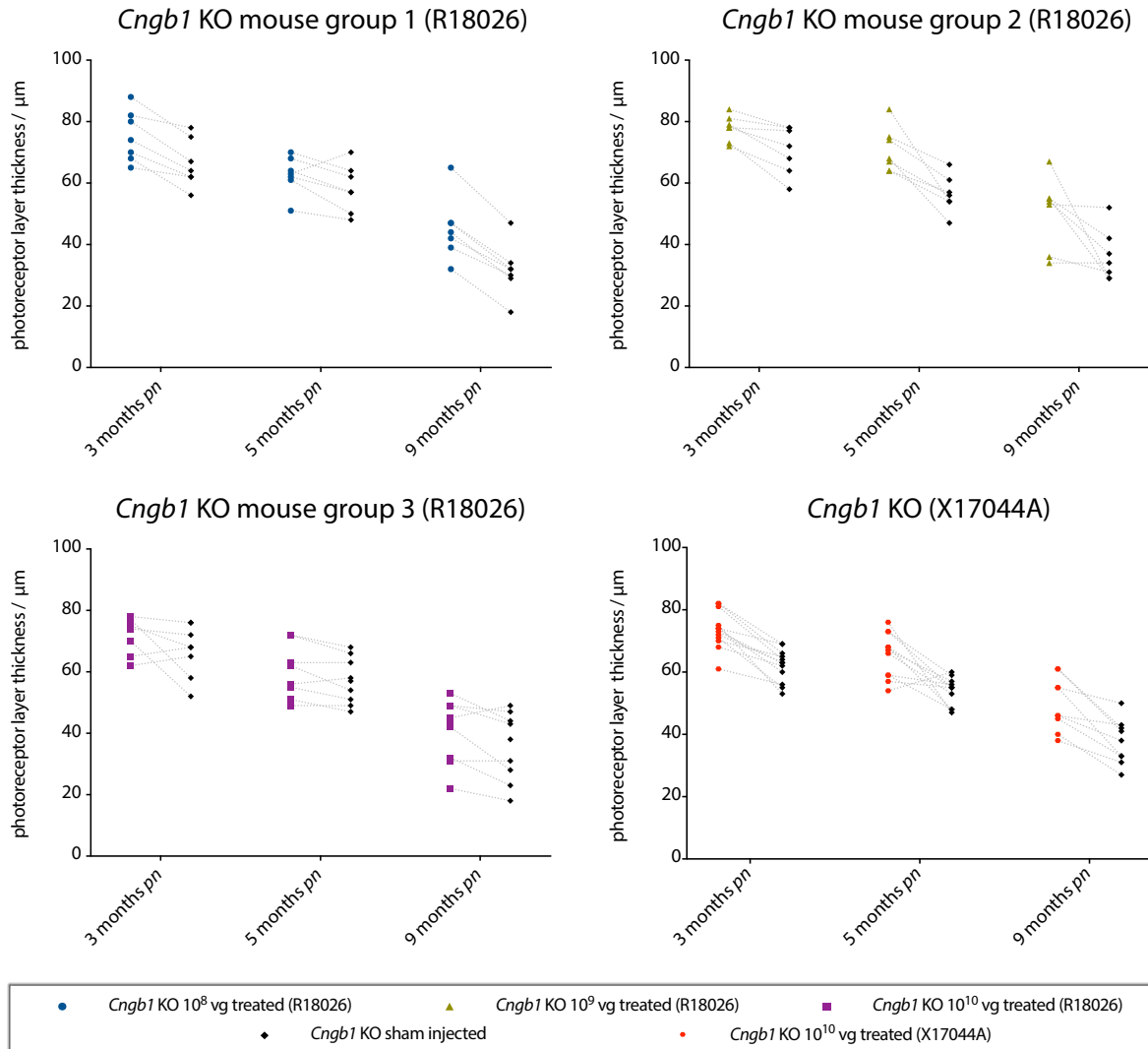
Figure S1: Individual photoreceptor layer thicknesses (μm) of all treated retinas (R18026) compared to the respective sham injected control retinas at 3, 5, and 9 months of age. In case of mouse group 1, an increase in the photoreceptor layer thickness was visible for all 10^8 vg-treated retinas compared to the sham-injected contralateral eyes. The difference was most obvious at the 9-months-time point. The 10^9 vg-treated retinas revealed a more marked photoreceptor rescue at 5 months *pn*, except for two individuals, which showed a strong decrease in the photoreceptor layer thickness from 5 months *pn* towards the 9-months-time point. For mouse group 3, only a marginal benefit of the high-dose treatment was achieved for all individuals. For all mice of the mouse group, that was treated with X17044A, a benefit of the treatment was achieved, which became more obvious at the 9-months-time point. Mouse group 1: n=7; mouse group 2: n=7; mouse group 3: n=10 (3 months *pn*: n=8; 2 eyes were not analyzable at this time point due to transient opacities); mouse group treated with X17044A: 3 and 5 months *pn*: n=11; 9 months *pn*: n=9.
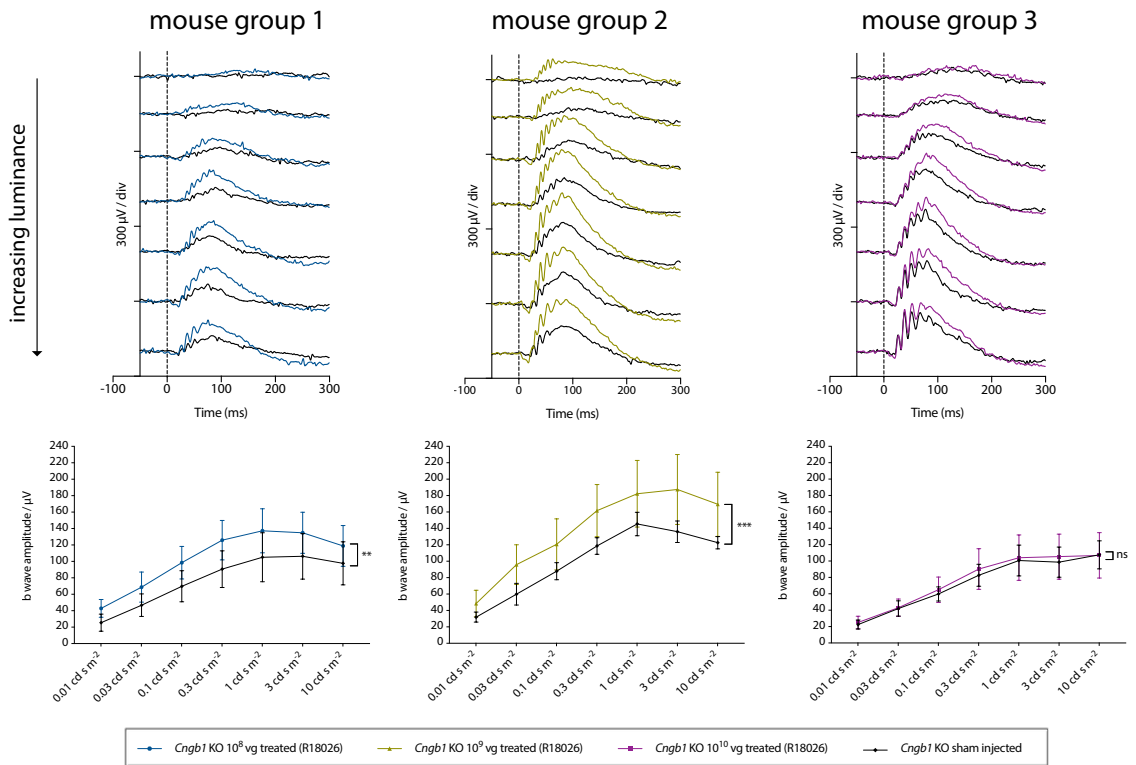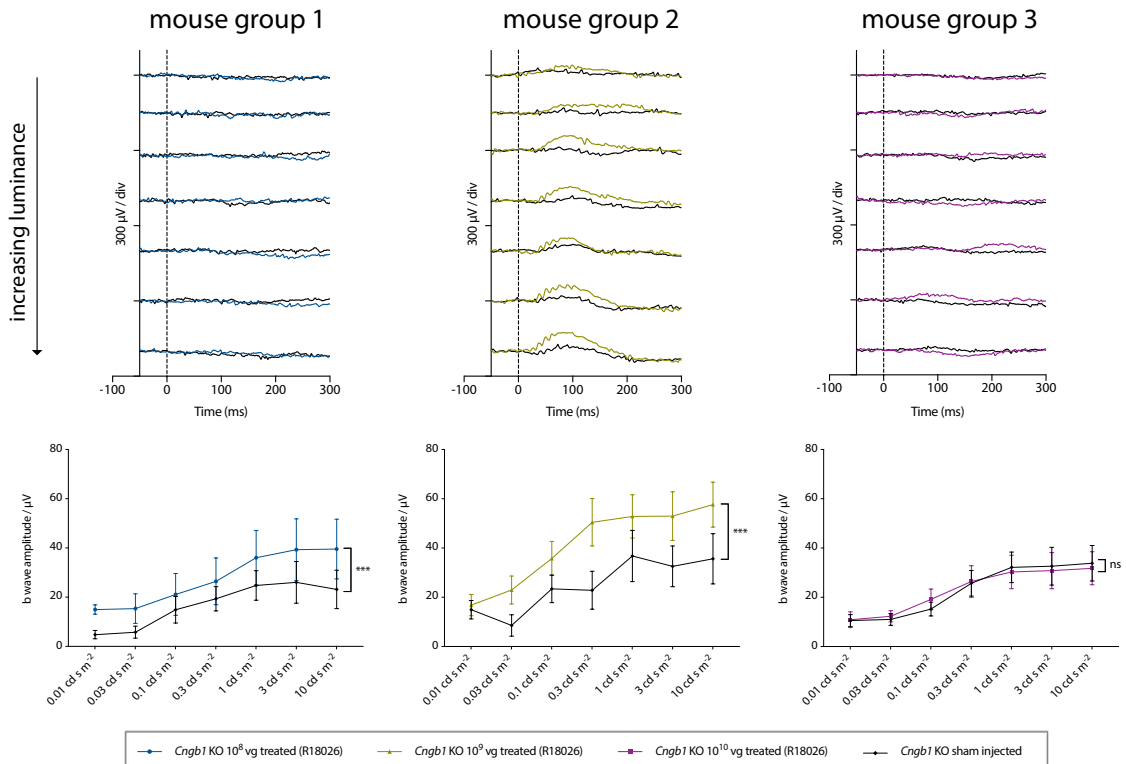
Figure S2: Individual ERG signals of *Cngb1* KO mice treated with rAAV5.hCNGB1 (R18026; mouse group 1 (10⁸ vg), 2 (10⁹ vg), and 3 (10¹⁰ vg)) at 3 and 9 months *pn*. Representative ERG signals and quantification of the respective b-wave amplitudes of each mouse group (paired comparison of the treated and the respective contralateral eyes) at 3 months *pn* (A)

and 9 months *pn* (B). A. A slight, but significant increase in photoreceptor function was visible for the 10^8 vg-treated-eye compared to the control (black line). In the 10^9 vg-treated-eye (central graph, green line), the b-wave was much more prominent in response to all light stimuli (significant), than in the sham-injected control (black line) and a small a-wave was also recovered by 10^9 vg. With the high vector dose (10^{10} vg; right graph; pink line) no obvious differences in the ERG signal were measured compared to the control. B. The injection of 10^9 vg resulted in a significantly increased b-wave amplitude at 9 months *pn*, whereas no electric response was recovered by the high dose. The low dose achieved a slight increase in photoreceptor function in only some of the treated mice, but an overall significant functional rescue was achieved by the low dose. Values are given as mean ± SEM. Group1: n=7; group 2: n=7; group3: n=10 (mouse group 2: at 2 months *pi*, the measurement of mouse number 7 was excluded due to a fluctuating signal caused by a high background that could not be reduced. Therefore, n=6 at this time point). Statistics: Paired two-way ANOVA with Sidak's post hoc test (*: p≤0.05; **: p≤0.01; ***: p≤0.001).
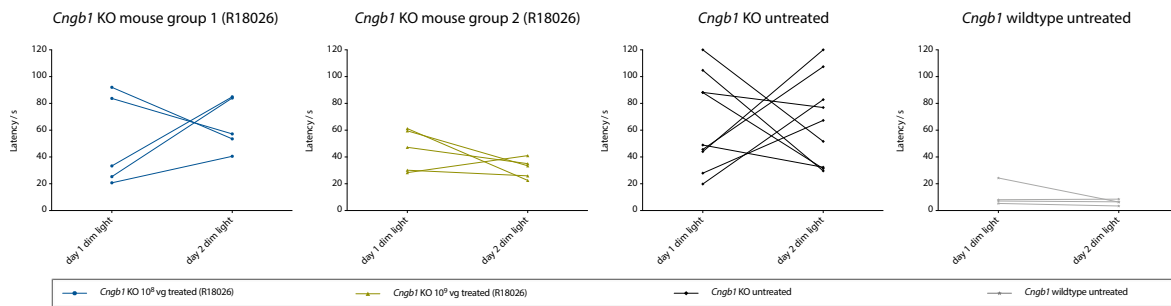
Figure S3: Individual latencies of 9-months-old *Cngb1* KO and wildtype mice at day 1 and 2 of the visual Water Maze task. Mice had been swimming on two days in the dark for monitoring rod-mediated behavior. All *Cngb1* wildtype mice (grey line) were able to find the floating platform within about 10 s at both days. Only one mouse needed 30 s at the first day due to habituation. *Cngb1* KO mice treated with 10^9 vg of R18026 (mouse group 2; green line) reached the platform between 30-60 s, and were all (except for one mouse) able to improve themselves to latencies of 20-40 s. In case of mouse group 1 (10^8 vg) and the untreated *Cngb1* KO mice, most of the individuals needed more than 60 s at least at one of the 2 days and no overall improvement from day 1 to day 2 was observed. 10^8 vg: n=5; 10^9 vg: n=5; untreated: n=9; wildtype: n=4.

Acknowledgments

It is my great pleasure to thank Prof. Dr. Stylianos Michalakis for assigning me this fascinating topic and for welcoming me into his research group. Many thanks Stelio, for your profound scientific input, as well as for your efforts to continuously challenge your PhD students and to always give me the chance to develop scientifically and personally.

A big thank also goes to Prof. Dr. Martin Biel for admitting me to his institute and for his permanent support and scientific input as one of my Thesis Advisory Committee (TAC) members.

I would also like to thank Prof. Dr. Hildegard Büning for her openness to share her vast scientific knowledge with me by being the third TAC member, and also for her kind advice and moral support.

Furthermore, I would like to thank Prof. Dr. Simon Petersen-Jones and his group of the College of Veterinary Medicine at the Michigan State University for a great and fruitful collaboration. Many thanks for giving me the opportunity to work with canine tissue and to be involved in a preclinical study using large animals. Many thanks also to Dr. Catherine O'Riordan for organizing the collaboration with Sanofi Genzyme, for a lot of highly productive discussions and the production of the rAAVs used for the preclinical studies.

I would like to thank the Graduate School of Systemic Neurosciences (GSN) for the opportunity to participate in its doctoral program, for the permanent support during my doctoral studies and for the opportunity to develop both as a scientist and as an individual, as well as for looking outside the box and broadening my horizon.

Special thanks also to Dr. Christian Schön for his availability in all scientific and non-scientific matters, for intensively introducing me to the ophthalmological techniques, for so many fruitful and challenging scientific discussions, and for his friendly and patient attitude. I learned so much from you, Christian! I would also like to thank Lena Zobel for joining our projects with so much enthusiasm and for all those hours we spent together with the mice. I wish you all the best for the CNGB1 project and I am looking forward to celebrate with you the completion of the preclinical phase of rAAV5.hCNGB1.

Many thanks also to all colleagues of the working group, who always ensured a harmonious atmosphere. It was a great pleasure to work together with all of you in the Lab. Particularly, I would like to emphasize Dr. Anna Geserich, Constanze Scheel, Dr. Lisa Riedmayr, Marina Pavlou, Dr. Sybille Böhm, Dr. Verena